The Dissertation Committee for Seongwoo Jo certifies that this is the approved version of the following dissertation:

Seismic Behavior and Design of Low-rise Reinforced Concrete Masonry with Clay Masonry Veneer

Committee:

Richard E. Klingner, Supervisor

Thomas J. Hughes

James O. Jirsa

Loukas F. Kallivokas

Dan L. Wheat

Seismic Behavior and Design of Low-rise Reinforced Concrete Masonry with Clay Masonry Veneer

by

Seongwoo Jo, B.S., M.S.E.

Dissertation

Presented to the Faculty of the Graduate School of

The University of Texas at Austin

in Partial Fulfillment

of the Requirements

for the Degree of

Doctor of Philosophy

The University of Texas at Austin

May 2010

Dedication

To my family who are always with me

Acknowledgements

I would like to express my most sincere thanks and appreciation to Dr. Richard E. Klingner for his advice, criticism, and support throughout the research. Special thanks are given to the staff of Phil M. Ferguson Laboratory and all the people who worked together on the project, “Performance-Based Design of New Masonry Structures”.

I also wish to express my thanks to my friends, especially In Sung Kim, Gun Up Kwon and Hussein Okail, for their help during the research and to Dr. Hong-Gun Park for encouraging me to study for my M.S. and Ph.D.

Last not least, thanks are given to National Science Foundation and masonry industry for having made the research possible

.

Seongwoo Jo

January 2010

Seismic Behavior and Design of Low-rise Reinforced Concrete Masonry with Clay Masonry Veneer

Publication No. _____

Seongwoo Jo, Ph. D.

The University of Texas at Austin, 2010

Supervisor: Richard E. Klingner

The research described here is part of a multi-university project on "Performance-based Design of New Masonry Structures." Within the context of that project, the main objectives of this research was to study the inelastic seismic performance of low-rise concrete masonry structures with clay masonry veneer and veneer connectors; to develop analytical models for those structures and the elements comprising them; and to use the results of the research to propose refinements to current design provisions for concrete masonry with clay masonry veneer.

The experimental work described here includes the design and testing of concrete masonry wall specimens with clay masonry veneer under quasi-static loading. Identical

specimens were subjected to shake-table testing at another university. The experimental work described here also includes the design of a full-scale, one-story concrete masonry building specimen with clay masonry veneer. That building specimen was subjected to shake-table testing at another university.

The analytical work of this research includes the development of nonlinear hysteretic models for concrete masonry walls, clay masonry veneer and veneer connectors. The analytical models for wall specimens were calibrated using the results of the quasi-static and shake-table tests of wall specimens. The analytical model for the building specimen was compared with and refined using shake-table test results for the building specimen. Finally, the calibrated and refined analytical model of the building specimen was used for parameter studies intended to supply general information about the behavior of low-rise reinforced concrete masonry structures with clay masonry veneer.

Based on the these experimental and analytical results, basic concepts of the seismic response and design of low-rise concrete masonry buildings were reaffirmed; most design and construction requirements of the 2008 MSJC Code and Specification were reaffirmed; and several recommendations were made to improve those requirements.

Table of Contents

List of Tables

List of Figures

CHAPTER 1
Introduction

1.1 OUTLINE OF OVERALL PROJECT

From October 2006 through September 2009, the US National Science Foundation's NEES (Network for Earthquake Engineering Simulation) program sponsored a research project "Performance-based Design of New Masonry Structures." In addition to direct funding and equipment support from the NSF NEES program, this project received financial and in-kind support from many segments of the masonry industry. The project focused primarily on new masonry construction rather than existing masonry construction. In the project, the following issues were addressed:

- seismic performance of masonry veneer and its backings (wood-stud frame and concrete masonry);
- seismic performance of masonry veneer connectors;
- inelastic behavior of low-rise concrete masonry shear walls; and
- performance-based design provisions for masonry and masonry veneer.

The project participants include the following:

- The University of Texas at Austin (Richard E. Klingner, Seongwoo Jo);
- The University of California at San Diego (Benson Shing, Hussein Okail);
- Washington State University (David McLean, Katherine Keane, Charlena Grimes); and
- North Carolina A&T State University (W. Mark McGinley, University of Louisville, under contract).

The project included experimental and analytical research, education of the profession and the public, and development of design recommendations for code implementation. The experimental work carried out in this project consisted of the following:

- in-plane, quasi-static tests of wood-stud and concrete masonry walls with clay masonry veneer;
- out-of-plane, quasi-static tests of veneer over wood-stud and over concrete masonry walls;
- shaking-table tests of such walls as in quasi-static tests; and
- shaking-table tests of two prototype buildings (wood-stud building with clay masonry veneer and concrete masonry building with clay masonry veneer).

The analytical work comprised the following:

- to develop analytical models for in-plane wood-stud and concrete masonry walls with clay masonry veneer along with connectors, and calibrate the models using quasi-static and shake table test data;
- to develop analytical models for out-of-plane wood-stud and concrete masonry walls with clay masonry veneer along with connectors, and calibrate the models using quasi-static and shake table test data;
- to develop analytical models for two prototype buildings (wood-stud building with clay masonry veneer and concrete masonry building with clay masonry veneer), and calibrate the models using shake table test data; and
- to conduce parameter study using developed analytical models.

The experimental and analytical work centered around two prototype structures: a wood-stud frame with clay masonry veneer (Figure 1-1) and a reinforced concrete masonry building with clay masonry veneer (Figure 1-2). The clay masonry veneer,

attached to the backing system (wood-stud frames or reinforced concrete masonry) using connectors, enhances esthetics and thermal, acoustic and water-penetration resistance. The connectors used in this project are shown in Figure 1-3 through Figure 1-5, where mortar is not present for clarity.

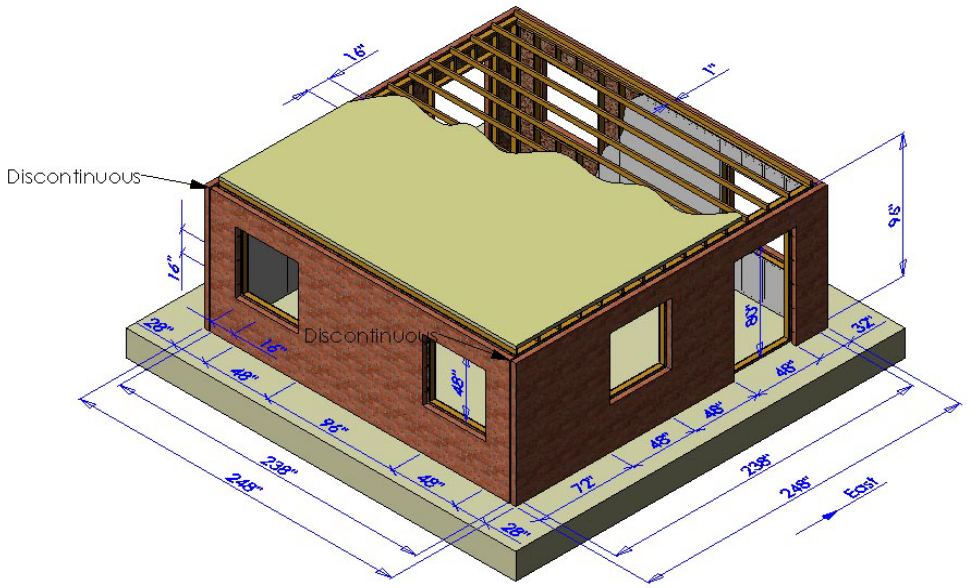

Figure 1-1 Prototype structure, wood-stud frame with clay masonry veneer

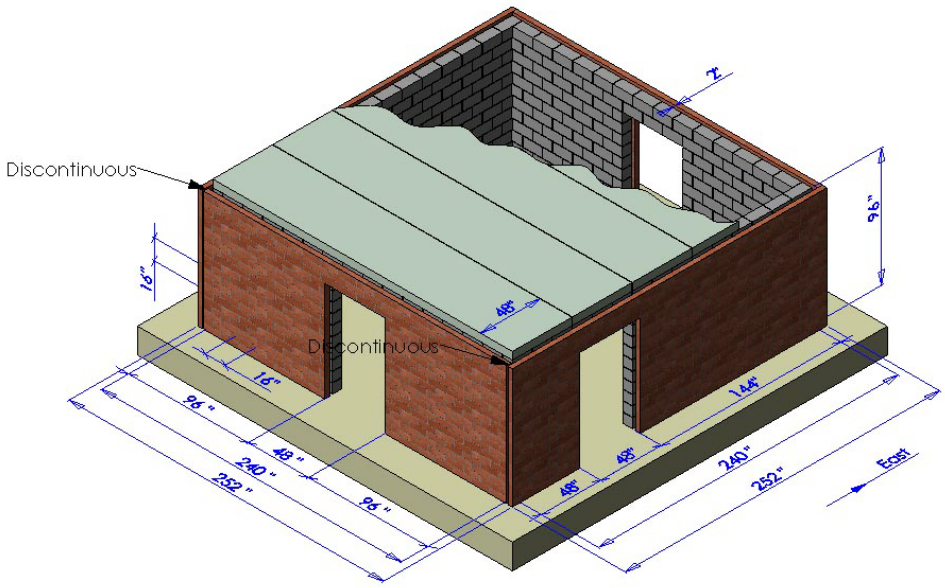

Figure 1-2 Prototype structure, reinforced concrete masonry building with clay masonry veneer

Figure 1-3 Connectors for wood-stud frame backing, corrugated connector (left) and rigid connector (right)

Figure 1-4 Connectors for concrete masonry backing, tri-wire connector

Figure 1-5 Connectors for concrete masonry backing, double eye-and-pintle connector

1.2 OBJECTIVES AND SCOPE OF THIS DISSERTATION WITHIN THE PROJECT

The research described by this dissertation was conducted as part of the project outlined in Section 1.1, and mainly involves concrete masonry with clay masonry veneer: experimental work, analytical work and development of refined performance-based design provisions. Specific objectives of the research described by this dissertation are as follows:

- to study seismic performance of masonry veneer along with connectors for concrete masonry backing;
- to study inelastic behavior of low-rise concrete masonry structures;
- to develop analytical models for concrete masonry with clay masonry veneer and conduct parametric study; and
- to propose refinements to performance-based design provisions for concrete masonry with clay masonry veneer.

Experimental work of this research focused on evaluating seismic performance of concrete masonry walls and masonry veneer over concrete masonry backing along with connectors, and evaluating seismic performance of low-rise concrete masonry buildings with clay masonry veneer. The experimental work included the following:

- design of concrete masonry walls with clay masonry veneer for quasi-static and shake table testing;
- quasi-static testing of concrete masonry walls with clay masonry veneer;
- evaluation of quasi-static tests and shake table tests of concrete masonry walls with clay masonry veneer;
- design of the concrete masonry building with clay masonry veneer; and
- evaluation of shake table tests of the concrete masonry building with clay masonry veneer.

Analytical work of this research was intended to develop analytical models for concrete masonry walls, clay masonry veneer and connectors, and to conduct parametric study using the developed analytical models. The primarily purpose of the analytical models was to catch key seismic behaviors of low-rise concrete masonry buildings with clay masonry veneer. The analytical work included the following:

- development of analytical models for concrete masonry walls (in-plane and out-of-plane), connectors (in-plane and out-of-plane) and clay masonry veneer (in-plane);
- prediction of quasi-static and shake table response of concrete masonry walls with clay masonry veneer;
- prediction of shake-table response of concrete masonry building with clay masonry veneer;
- calibration of the developed analytical models using quasi-static and shake table test data; and
- parameter studies using the developed and calibrated analytical models.

CHAPTER 2
Background

2.1 BACKGROUND ON PERFORMANCE-BASED SEISMIC DESIGN OF BUILDINGS

In this section, the background on performance-based seismic design of buildings is reviewed. The extensive literature on this topic is well summarized by Ghobarah (2001). The traditional approach to structural design of buildings is to define the load applied to the building; to design each element of the building; to analyze the design; and to check if each element, and the entire building, satisfies requirements for stress (or force) and deformation (or displacement). The above steps must be repeated until those requirements are satisfied. The primary objective of this traditional procedure is to ensure strength and serviceability of the building, generally by stress requirements and deformation requirements, respectively (Ghobarah 2001).

Although buildings designed using building codes based on this traditional approach performed well from a life-safety perspective during recent earthquakes such as the 1994 M6.7 Northridge and 1995 M7.2 Hanshin–Awaji (Kobe) earthquakes, the level of damage to structures, economic loss due to loss of use, and cost of repair were unexpectedly high. These resulted in the introduction of performance-based design concept into building codes for seismic design. Even though there have been different interpretations of the term "performance-based design," the most appropriate definition is that performance-based design refers to a methodology in which structural design criteria are expressed in terms of achieving a set of performance objectives. The performance objectives may be a level of stress not to be exceeded, a load, a displacement, a limit state or a target damage state. Accordingly, performance-based objectives can be viewed as an extension of traditional requirements for crack control or deflection limits (Ghobarah 2001).

To develop performance-based seismic design guidelines for new and existing buildings in US, Federal Emergency Management Agency (FEMA) contracted in September 2001 with the Applied Technology Council (ATC) to carry out the ATC-58 Project. That project identifies the following basic steps for the performance-based seismic design:

> . . . establishment of appropriate performance objectives that define expected building performance in future earthquakes; development of a preliminary design, believed capable of providing the desired performance; assessing whether the design is actually capable of providing this performance, through evaluation of the probability of experiencing losses of different types; and finally, adjusting the design until the performance assessment process indicates a risk of loss that is deemed acceptable (FEMA 461).

Unfortunately, sufficient information is not available on common structural materials to implement the basic steps above for the coming generation of performance-based design codes, and considerable research is still being conducted toward that objective.

Current seismic design of masonry building in the US is based mainly on the results of the TCCMAR research program, conducted from 1984 to 1994. The program was intended to provide the technical basis for the development of a limit-state design standard for masonry buildings. In the TCCMAR program, Assis *et al.* (1989) established basic stress-block parameters for flexural behavior of masonry elements. Shing *et al.* (1991) reaffirmed basic design principles for flexure-dominated and shear-dominated masonry shear walls. Leiva and Klingner (1991) addressed performance and design of multi-story masonry walls with openings. He and Priestley (1992) addressed flanged walls. Finally, Seible *et al.* (1992) addressed the behavior and design of building-type assemblages. The TCCMAR program focused on traditional seismic design (rather than performance-based seismic design) of masonry elements and buildings, and did not address masonry veneer.

2.2 CONSTRUCTION PROCEDURE FOR REINFORCED CONCRETE MASONRY WITH CLAY MASONRY VENEER

In this section, construction procedures used for reinforced concrete masonry with clay masonry veneer are briefly described. The purpose of this is to provide background on the construction of such masonry in general, and on the construction of the specimens tested here in particular.

First, the base foundation or floor is built with dowel bars placed in grade beams (Figure 2-1). Hollow concrete masonry units are laid (Figure 2-2), with horizontal reinforcement (Figure 2-3) and connectors (Figure 2-4) placed in specified courses. After finishing the hollow concrete masonry wall, vertical reinforcement (Figure 2-5) is placed and the wall is grouted (Figure 2-6). A shelf angle (Figure 2-7) is bolted to the concrete masonry wall just above the foundation or floor, and flashing (Figure 2-8) is placed on the shelf angle. Finally, clay masonry units are laid (Figure 2-9), and are attached to the CMU wall with connectors (Figure 2-10). In this research, two types of connectors were used: tri-wire connectors and double eye-and-pintle connectors. Those connectors are shown in Figure 2-11 and Figure 2-12, respectively, for comparison.

Figure 2-1 Base foundation with dowel bars

Figure 2-2 Hollow concrete masonry units being laid

Figure 2-3 Detail of horizontal reinforcement and knocked-out webs

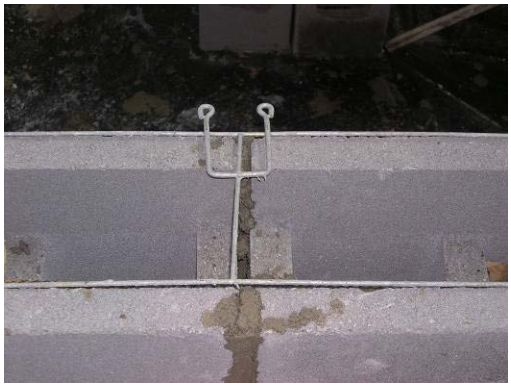

Figure 2-4 Adjustable connectors

Figure 2-5 Placement of vertical reinforcement

Figure 2-6 Grouting of concrete masonry

Figure 2-7 Placement of shelf angle

Figure 2-8 Installation of flashing

Figure 2-9 Laying clay masonry veneer

Figure 2-10 Installing connectors to clay masonry veneer

Figure 2-11 Tri-wire connectors

Figure 2-12 Double eye-and-pintle connectors

2.3 SEISMIC BEHAVIOR OF LOW-RISE CONCRETE MASONRY WITH CLAY MASONRY VENEER

The typical seismic response of the low-rise concrete masonry with clay masonry veneer (Figure 2-13) is shown schematically in Figure 2-14. CMU Walls oriented perpendicular to the direction of ground motion (out-of-plane CMU walls) behave as vertically spanning beams, excited at the bottom by the foundation floor and at the top by the roof diaphragm (Figure 2-15). Their inertial forces contribute to the response of the diaphragm. CMU Walls oriented parallel to the direction of ground motion (in-plane

CMU walls) transmit the diaphragm reactions to the foundation. The in-plane CMU walls respond essentially as rigid bodies, rotating and sliding at their bases (Shing *et al.* 1991 and Merryman *et al.* 1989). A portion of the CMU wall perpendicular to the direction of shaking, if connected to the CMU wall parallel to the direction of shaking, can act as a flange (He and Priestley 1992). The length of flange that can be considered to be effective is given by the MSJC Code (MSJC 2008). If there is an effective flange, the flanged in-plane CMU walls will have asymmetric response in the two opposite directions parallel to the web. When the flange is in tension, the in-plane CMU walls will have higher flexural strength but lower tip displacement capacity. The construction joints present at each end of lintels prevent the coupled behavior of in-plane CMU walls at each side of the lintels. Accordingly, horizontal forces only will be transferred through the lintels between the in-plane CMU walls.

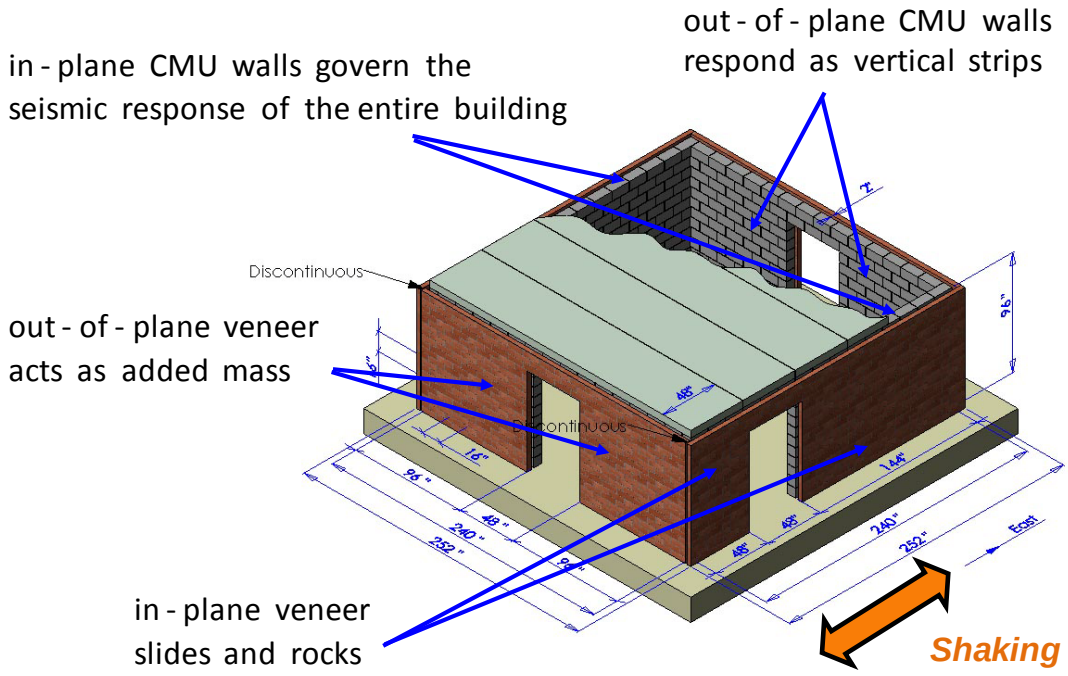

Figure 2-13 Seismic behavior of low-rise concrete masonry with clay masonry veneer

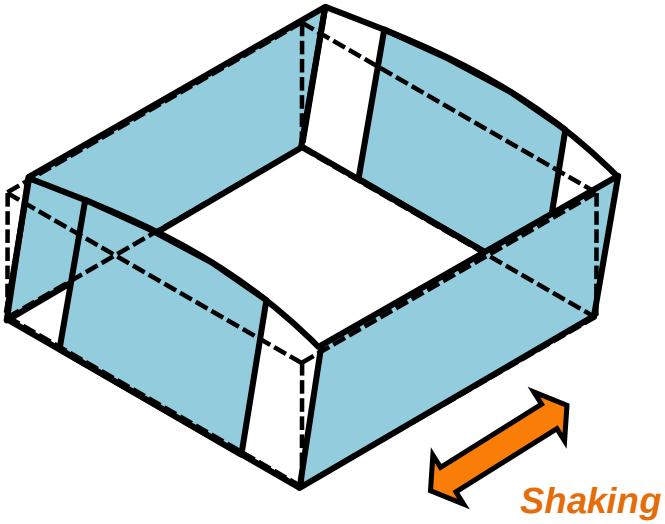

Figure 2-14 Seismic response of low-rise masonry buildings

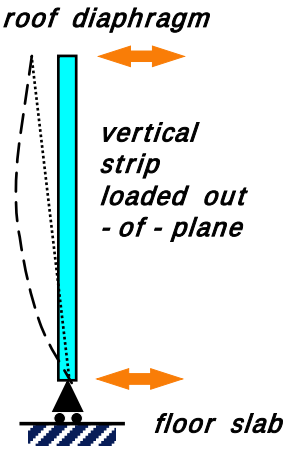

Figure 2-15 Out-of-plane seismic response of concrete masonry walls

The veneer oriented perpendicular to the direction of shaking (out-of-plane veneer) generally responds in out-of-plane flexure. Since the flexural stiffness of the veneer before cracking is small compared to the flexural stiffness of the out-of-plane CMU walls, the out-of-plane veneer essentially acts as attached mass only, provided that the out-of-plane connectors continue to securely connect the veneer to the CMU walls. The flexural resistance of the out-of-plane veneer becomes more negligible once flexural

cracking occurs in bed joints, usually around mid-height. In axial direction, the connectors typically are strong enough to essentially remain elastic up to the maximum considered earthquake (MCE).

The veneer oriented parallel to the direction of shaking (in-plane veneer) generally responds by rocking or sliding depending on the aspect ratio (height to plan length). Most response of the in-plane veneer will come from sliding only for a low aspect ratio, and from rocking only for a high aspect ratio. For an intermediate aspect ratio, rocking and sliding will be combined. The relative movement of the in-plane veneer to the in-plane CMU walls by sliding or rocking produces forces in connectors. The connectors, in horizontal and vertical shear, typically begin to yield around the design basis earthquake (DBE) accompanying rocking or sliding of the veneer. Connectors subjected to many repeated reversed cycles of vertical or horizontal shearing deformations past the elastic limit generally fail by fracture in low-cycle fatigue.

CHAPTER 3
Introduction and Material Properties for Quasi-static CMU Wall Specimens

3.1 INTRODUCTION TO CMU WALL SPECIMENS

As part of the NSF NEES masonry project, six reinforced concrete masonry wall specimens with clay masonry veneer (CMU wall specimens) were tested quasi-statically at The University of Texas at Austin (UT Austin). In this chapter, material properties for those quasi-static CMU wall specimens are presented.

Material tests included the following: sieve analysis of the sand used for the mortar; compressive strength of mortar; compressive strengths of clay and concrete masonry units; compressive strength of grout; compressive strength of clay and concrete masonry prisms; bond-wrench testing of clay masonry prisms; and tensile testing of reinforcement. In this chapter, each of those tests is described, and the corresponding results are presented.

As shown in Figure 3-1, the material specimens were constructed at the same time as the corresponding wall specimens. As shown in Figure 3-2, the clay masonry prisms, CMU prisms, and grout specimens were covered with plastic sheeting and air-cured next to the walls. The mortar cubes were cured in lime-water. The CMU wall specimens were air-cured from 4 months to a year before testing, while the masonry material specimens were cured about a year before testing. The reinforcing bar specimens were taken from the same heats as the bars used for construction.

Figure 3-1 Specimens for material strength testing as constructed

Figure 3-2 Specimens for material strength testing as cured

3.2 SIEVE ANALYSIS OF SAND

The sand was tested by the National Concrete Masonry Association Research and Development Laboratory in accordance with ASTM C136-06. Results of sieve analysis are plotted by a solid line in Figure 3-3, in which the two dotted lines indicate the upper and lower grading limits prescribed by ASTM C144-04. As shown in Figure 3-3, the sand used in quasi-static CMU wall specimens does not satisfy the grading requirements of ASTM C144-04. It could, however, satisfy the "use" requirements of that standard as explained in Section 3.3. The calculated fineness modulus of the sand was 1.76.

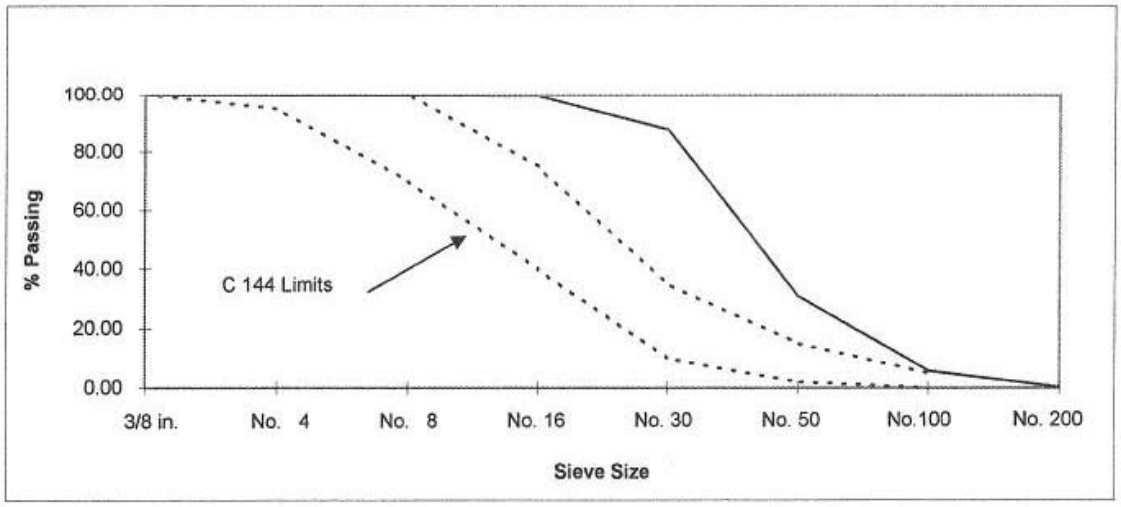

Figure 3-3 Sieve analysis of sand

3.3 COMPRESSIVE STRENGTH OF MORTAR

Compressive strengths of 2-in. mortar cubes were determined according to ASTM C780-07, which refers in turn to ASTM C109-05. Results for cement-lime mortar are summarized in Table 3-1, and results for masonry cement mortar are summarized in Table 3-2. Five sets of three cement-lime mortar cubes and four sets of three masonry cement mortar cubes were prepared, and all cubes but one were tested. One masonry cement mortar cube, representing the CMU wall of Specimen UT CMU 4 MC, was not well constructed and was not tested. Figure 3-4 shows a photo of compressive testing of a typical mortar cube. The average compressive strengths were 2555 psi for cement-lime mortar cubes and 2209 psi for masonry cement mortar cubes.

Even though those strengths were evaluated using job flow rather than the laboratory flow required by the property specification of ASTM C270, because the compressive strengths exceeded the required property-specified strength of 1800 psi, it can be inferred that the sand met the “use” requirements of ASTM C144.

Table 3-1 Compressive strengths of cement-lime mortar cubes

mortar	cement-lime mortar				
corresponding wall specimens	UT CMU 1	UT CMU 2	UT CMU 3, 4	UT CMU 1, 2	UT CMU 3, 4
type of wall	CMU	CMU	CMU	clay	clay
Cube 1 (psi)	3493	2444	1714	1837	3354
Cube 2 (psi)	3474	2511	1706	1869	3229
Cube 3 (psi)	3546	2485	1661	1836	3165
average (psi)	**3504**	**2480**	**1694**	**1847**	**3249**
	2555				
COV	0.9%	1.1%	1.6%	0.6%	2.4%
	28.4%				

Table 3-2 Compressive strengths of masonry cement mortar cubes

mortar	masonry cement mortar			
corresponding wall specimens	UT CMU 1 and 2	UT CMU 3 and 4	UT CMU 1 and 2	UT CMU 3 and 4
type of wall	CMU	CMU	clay	clay
Cube 1 (psi)	2575	2067	1504	2675
Cube 2 (psi)	2494	2168	1478	2898
Cube 3 (psi)	2499	not well constructed	1462	2476
average (psi)	**2523**	**2118**	**1481**	**2683**
	2209			
COV	1.5%	2.4%	1.2%	6.4%
	22.3%			

Figure 3-4 Compressive testing of a typical mortar cube

3.4 COMPRESSIVE STRENGTH OF GROUT

Grout specimens were constructed and tested to determine compressive strength in accordance with ASTM C1019-07. Six grout specimens were constructed: three for Specimens UT CMU 1, 2 and 2 MC; and three for Specimens UT CMU 3, 4 and 4 MC. One grout specimen in the latter group was severely damaged while during de-molding. As a result, five specimens were tested: three for Specimens UT CMU 1, 2 and 2 MC; and two for Specimens UT CMU 3, 4 and 4 MC. Figure 3-5 shows a photo of compressive testing of a typical grout specimen. Results are listed in Table 3-3.

The average net compressive strengths of grout were 7499 psi for Specimens UT CMU 1, 2 and 2 MC, and 4302 psi for Specimens UT CMU 3, 4 and 4 MC.

Figure 3-5 Compressive testing of a typical grout specimen

Table 3-3 Compressive strengths of grout specimens

corresponding wall specimens	UT CMU 1, 2, 2 MC	UT CMU 3, 4, 4 MC
Grout Specimen 1 (psi)	8234	4554
Grout Specimen 2 (psi)	6788	4049
Grout Specimen 3 (psi)	7475	damaged before testing
average (psi)	**7499**	**4302**
COV	7.9 %	5.9 %

3.5 PROPERTIES OF CLAY MASONRY UNITS

The properties of five representative clay masonry units were measured and tested by the National Brick Research Center in accordance with ASTM C67-05. The average compressive strength was 10957 psi; the average void area was 29.1 %; the average initial rate of absorption (IRA) was 16.5 g/30 in.^{2}-min; and the average length, width and

height were 7.65 in., 3.61 in. and 2.28 in., respectively. The clay masonry units met the physical and visual requirements for ASTM C652-05, Grade SW, Type HBS, and Class H40V.

3.6 PROPERTIES OF CONCRETE MASONRY UNITS (CMU)

The properties of three samples of nominal 8- x 8- x 16-in. concrete masonry units (CMU) and three samples of nominal 8- x 8- x 8-in. CMU were evaluated by the National Concrete Masonry Association Research and Development Laboratory in accordance with ASTM C140-07.

The average net compressive strength of the 8- x 8- x 16-units was 4030 psi; the average percent solid was 56.8 %; and the average width, height and length were 7.66 in., 7.63 in. and 15.60 in., respectively. The 8- x 8- x 16-in. units met the compressive strength and dimensional requirements of ASTM C90-06.

The average net compressive strength of the 8- x 8- x 8-in. units was 2900 psi; the average percent solid was 65.9 %; and the average width, height and length were 7.66 in., 7.61 in. and 7.61 in., respectively. The 8- x 8- x 8-in. units met the compressive strength and dimensional requirements of ASTM C90-06, except for the minimum face shell thickness, for which the average was 1.22 in., slightly less than the required minimum of 1.25 in.

3.7 COMPRESSIVE STRENGTH OF CLAY MASONRY PRISMS

Compressive strengths of clay masonry prisms were determined according to ASTM C1314-07, and results are summarized in Table 3-4. Three replicates were constructed and tested for each corresponding wall specimen in Table 3-4. Figure 3-6 shows a photo of compressive testing of a typical clay masonry prism.

The prisms were capped with high-strength gypsum cement (Figure 3-7). The capping plates used did not satisfy the thickness of 1 in. required by ASTM C140-07,

which refers to ASTM C1552 for capping. Instead, the capped surfaces of prisms were checked using a feeler gage (Figure 3-10), and were found to be less than 0.002 in. in 10.5 in. This satisfies the requirements of ASTM C1552-03a, which requires that the surface of the capping plate be planar within 0.003 in. in 16 in.

The total average compressive strength of clay masonry prisms laid with masonry cement mortar was 8112 psi, about 1.7 times the corresponding value of 5155 psi for clay masonry prisms laid with cement-lime mortar.

Table 3-4 Compressive strengths of clay masonry prisms

mortar	**cement-lime mortar**		**masonry cement mortar**	
corresponding wall specimens	**UT CMU 1, 2**	**UT CMU 3, 4**	**UT CMU 2 MC**	**UT CMU 4 MC**
Prism 1 (psi)	5610	4961	8319	8629
Prism 1 (psi)	6229	5121	8345	9064
Prism 3 (psi)	6472	4587	8426	9128
average (psi)	**6104**	**4890**	**8364**	**8940**
	5497		**8652**	
COV	5.9%	4.6%	0.5%	2.5%
	12.3%		3.8%	

Figure 3-6 Compressive testing of a typical clay masonry prism

Figure 3-7 Capping of a typical clay masonry prism

3.8 COMPRESSIVE STRENGTH OF CMU PRISMS

Compressive strengths of CMU prisms were determined according to ASTM C1314-07. As shown in Table 3-5, three replicates were constructed and tested for each wall specimen. Results are summarized in the same table. Figure 3-8 shows a photo of compressive testing of a typical CMU prism.

The prisms were capped with high-strength gypsum cement (Figure 3-9). The capping plates used did not satisfy the thickness of 1 in. required by ASTM C140-07, which refers to ASTM C1552 for capping. Instead, the capped surfaces of prisms were checked using a feeler gage (Figure 3-10), and were found to be less than 0.002 in. in 10.5 in. This satisfies the requirements of ASTM C1552-03a, which requires that the surface of the capping plate be planar within 0.003 in. in 16 in.

The total average net compressive strength of 4191 psi for the prisms laid with masonry cement mortar was similar to that for cement-lime mortar, 4027 psi.

Table 3-5 Compressive strengths of CMU prisms

mortar	**cement-lime mortar**		**masonry cement mortar**	
corresponding wall specimens	**UT CMU 1, 2**	**UT CMU 3, 4**	**UT CMU 2 MC**	**UT CMU 4 MC**
Prism 1 (psi)	4845	3571	4246	4616
Prism 1 (psi)	4451	3406	4291	3639
Prism 3 (psi)	4165	3727	4470	3885
average (psi)	**4487**	**3568**	**4336**	**4047**
	4027		**4191**	
COV	6.2%	3.7%	2.2%	10.3%
	12.6%		8.0%	

Figure 3-8 Compressive testing of a typical CMU prism

Figure 3-9 Capping of a typical CMU prism

Figure 3-10 Checking the planarity of capped surfaces with a feeler gage

3.9 BOND WRENCH TESTING OF CLAY MASONRY PRISMS

Bond strengths of clay masonry prisms were determined according to the provisions for field-prepared specimens of ASTM C1357-05, which refers in turn to ASTM C1072-06. Fifteen joints were tested from field-prepared prisms comprising five joints each. Results are summarized in Table 3-6. Figure 3-11 shows a photo of bond-wrench testing of a typical clay masonry prism.

The total average bond strength for masonry cement mortar, 175 psi, was about 2.3 times that for cement-lime mortar, 75 psi. The moment of inertia (27.81 $in.^4$) used for the bond strength calculation was computed based on the average measured shell thickness and web thickness. The coefficient of variation of bond strength for masonry cement mortar (23.0 %) was less than that for cement-lime mortar (34.4 %).

During the testing, the mortar in the core-holes of the clay masonry prisms laid with cement-lime mortar was observed to be somewhat looser than in the clay masonry prisms laid with masonry cement mortar. The bed joints with cement-lime mortar were generally removed more easily and cleanly after bond wrench testing than the bed joints with masonry cement mortar. Figure 3-12 shows an example of loose mortar filling in the core-holes of clay masonry prisms laid with cement-lime mortar.

Figure 3-11 Bond-wrench testing of a typical clay masonry prism

Figure 3-12 Example of loose mortar in the core-holes of clay masonry prisms laid with cement-lime mortar

Table 3-6 Bond strengths of clay masonry prisms

mortar	cement-lime mortar		masonry cement mortar	
corresponding wall specimens	UT CMU 1, 2	UT CMU 3, 4	UT CMU 2 MC	UT CMU 4 MC
Prism 1 (psi)	111	124	86	153
Prism 2 (psi)	85	26	175	236
Prism 3 (psi)	51	failed before testing	186	216
Prism 4 (psi)	96	83	197	213
Prism 5 (psi)	96	88	158	236
Prism 6 (psi)	66	52	155	203
Prism 7 (psi)	69	85	107	124
Prism 8 (psi)	58	83	163	178
Prism 9 (psi)	77	41	160	174
Prism 10 (psi)	93	58	183	197
Prism 11 (psi)	104	49	185	125
Prism 12 (psi)	111	41	174	111
Prism 13 (psi)	100	18	153	220
Prism 14 (psi)	65	97	167	264
Prism 15 (psi)	83	66	139	206
average (psi)	**84**	**65**	**159**	**190**
	75		**175**	
COV	22.1%	43.8%	18.1%	23.0%
	34.4%		23.0%	

3.10 TENSILE TESTING OF REINFORCEMENT

Tensile properties of reinforcement (No. 4) used in the UT CMU wall specimens were determined according to ASTM A370-05. Strains were measured using an 8-in. extensometer. Vertical reinforcement for UT CMU wall specimens was from one heat, and horizontal reinforcement was from another heat; three replicates of each were tested For the vertical reinforcement, yield strength and tensile strength were 64.2 ksi and 92.1 ksi respectively; for the horizontal reinforcement, those values were 61.8 ksi and 94.6 ksi, respectively. Results are listed in Table 3-7. In Figure 3-13 is shown a typical stress-

strain curve (Bar 1 for horizontal reinforcement). Once strain hardening had started, the extensometer was removed from reinforcing bars to avoid being damaged. Therefore, the stress-strain curve shows only up to the initial portion of strain hardening. In Figure 3-14 is shown a photo of tensile testing of a typical reinforcing bar.

Table 3-7 Tensile properties of reinforcement (No. 4)

vertical reinforcement				**horizontal reinforcement**			
specimen	**yield strength**	**tensile strength**	**elongation at fracture**	**specimen**	**yield strength**	**tensile strength**	**elongation at fracture**
	ksi	ksi	%		ksi	ksi	%
Bar 1	64.2	92.7	14	**Bar 1**	61.6	93.9	14
Bar 2	65.4	92.3	14	**Bar 2**	61.0	94.3	13
Bar 3	62.9	91.5	14	**Bar 3**	62.6	95.5	15
average	**64.2**	**92.1**	**14**	**average**	**61.8**	**94.6**	**14**
COV	1.6%	0.5%		**COV**	1.1%	0.7%	

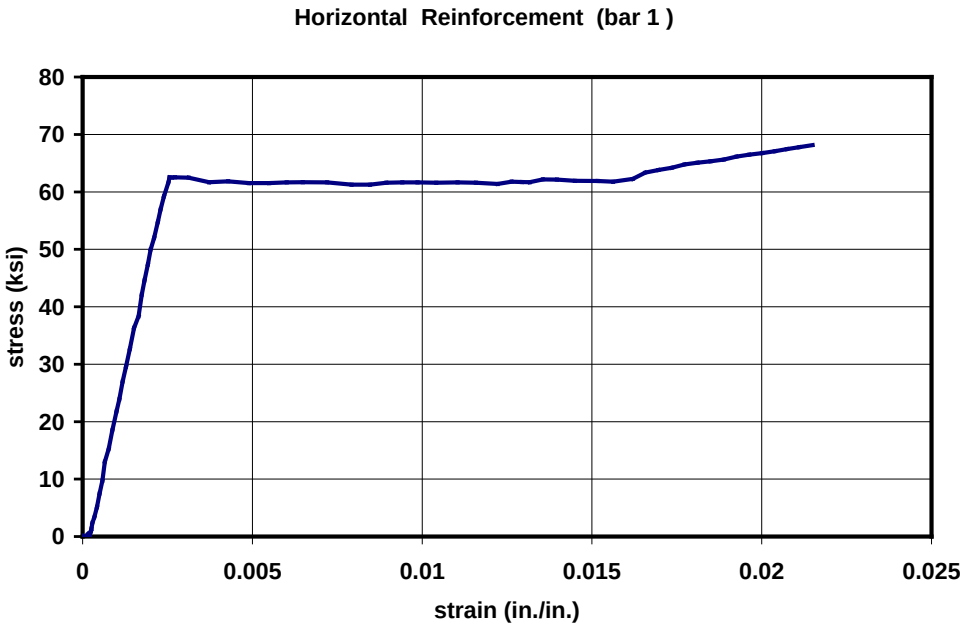

Figure 3-13 Typical stress-strain curve of reinforcement

Figure 3-14 Tensile testing of a typical reinforcing bar

CHAPTER 4
Quasi-static Tests of CMU Wall Specimens, Out-of-plane

As part of the NSF NEES masonry project, six reinforced concrete masonry wall specimens with clay masonry veneer (CMU wall specimens) were tested quasi-statically at The University of Texas at Austin (UT Austin). Three of those six quasi-static CMU wall specimens were tested under out-of-plane loading, and the other three under in-plane loading. The main purpose of the quasi-static testing of CMU wall specimens out of plane is to study the out-of-plane response of CMU walls with clay masonry veneer, and to provide experimental data to develop analytical models for out-of-plane (axial) response of connectors. In this chapter, the out-of-plane CMU wall specimens are addressed: test setup; instrumentation; loading protocol; results for each specimen; and overall observations.

4.1 OVERVIEW OF QUASI-STATIC, OUT-OF-PLANE CMU WALL SPECIMENS (UT CMU 1, 2, 2 MC)

Three out-of-plane reinforced concrete masonry wall specimens with clay masonry veneer (CMU wall specimens) were tested quasi-statically at The University of Texas at Austin. The overview of those wall specimens is provided in Table 4-1 and the design drawings are shown in Appendix A. The difference between UT CMU 1 and UT CMU 2 is the type of connectors, and the difference between UT CMU 2 and UT CMU 2 MC is the cementitious system used in the mortar (in the context of ASTM C270).

Table 4-1 Overview of quasi-static, out-of-plane CMU wall specimens

specimens	loading	dimensions	reinforcement	connectors	mortar
UT CMU 1	out-of-plane, quasi-static	8-ft wide by 8-ft high	five No. 4 bars vertically and three No. 4 bars horizontally	double eye-and-pintle	cement-lime
UT CMU 2				tri-wire	cement-lime
UT CMU 2 MC				tri-wire	masonry cement

A typical CMU wall specimen with its associated test setup for quasi-static, out-of-plane testing is shown in Figure 4-1. The CMU wall specimens consisted of CMU wall (also referred to as CMU backing) and clay masonry veneer. The CMU wall measured 8 ft in plan and 8 ft-8 in. in elevation, with the top 8-in. course being an additional bond beam for top support. The clay masonry veneer measured 8 ft in plan and 8 ft in elevation. The distance from the top surface of a base beam to the centerline of out-of-plane support was 8 ft-11 in. The vertical reinforcement ratio was 0.0014 with five No. 4 reinforcing bars, and the horizontal reinforcement ratio was 0.0011 with three No. 4 reinforcing bars and twelve W1.7 wires (joint reinforcement).

Two configurations of connectors and CMU joint reinforcement were used to connect the clay masonry veneer to the CMU backing. One configuration (used in UT CMU 1) consisted of W1.7 two-wire joint reinforcement at 16 in. vertically in the CMU wall with W2.8 wire double eye-and-pintle connectors at 16 in. horizontally, which satisfies 2008 MSJC requirements for Seismic Design Category (SDC) D. The other configuration (used in UT CMU 2 and UT CMU 2 MC) consisted of W1.7 tri-wire joint reinforcement (two wires in CMU walls and one wire in clay masonry veneer) at 16 in. vertically with W1.7 cross wires at 16 in. horizontally, which satisfies 2008 MSJC requirements for Seismic Design Category (SDC) E.

Quasi-static, out-of-plane CMU wall specimens used a 2-in. specified air space; nominal 8- x 8- x 16-in. lightweight concrete masonry units (ASTM C90); nominal 4-in.

standard modular clay masonry units (ASTM C652); coarse grout by proportion (ASTM C476); and 30-mil EPDM flashing (not self-adhering). Concrete masonry units (CMU) were knock-out units with every web knocked out except at wall ends. EPDM flashing was placed between a shelf angle and the clay masonry veneer; the clay masonry veneer was placed on top of the shelf angle that was fixed, using adhesive anchors, to the bottom course of the concrete masonry wall (CMU wall). Specimens UT CMU 1 and UT CMU 2 used ASTM C270 Type S cement-lime mortar by proportion in CMU walls and clay masonry veneer, while Specimen UT CMU 2 MC used Type S masonry cement mortar by proportion in CMU walls and clay masonry veneer.

The base beam was 13.5 feet long, with a square cross-section measuring 20 inches on each side. Four No. 7 longitudinal reinforcing bars were provided at the top and the bottom respectively, and No. 4 ties were used at a spacing of 6 inches. The sectional design flexural capacity and shear capacity of the base beam were about 160 kip-ft and 80 kips, respectively.

The out-of-plane CMU wall specimens were loaded by a 100-kip hydraulic ram with $\pm$ 9-in. stroke, connected to a compressed air-driven hydraulic pump. Area loading was simulated by a "whiffle-tree." Loading was based on target load levels until the maximum load capacity is reached, after which the loading was based on target displacement levels.

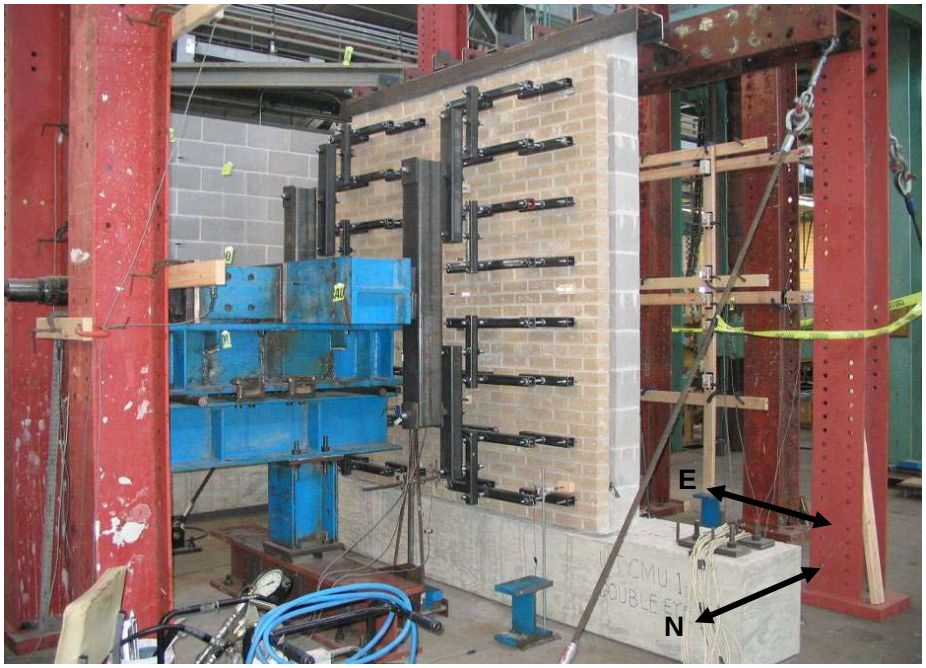

Figure 4-1 Typical quasi-static, out-of-plane CMU wall specimen (8- by 8-ft) with test setup

4.2 LIMIT STATES AND CORRESPONDING EXPECTED LOAD CAPACITIES OF QUASI-STATIC, OUT-OF-PLANE CMU WALL SPECIMENS

The limit states and corresponding load capacities of CMU wall specimens for quasi-static, out-of-plane loading were evaluated before testing and are summarized in Table 4-2, where the capacities for flexural cracking and flexural failure were calculated at the mid-height of the CMU walls.

The top support condition is a horizontal spring, and the bottom support condition is fixed. The bottom support cracks at a very small load, however, and might even crack before testing starts, as occurred in Specimen UT CMU 2 MC. Once the bottom support cracks, the bottom of the CMU wall can be assumed to rotate freely until the crack completely closes, probably until reaching the flexural cracking capacity at mid-height (assuming a horizontal spring at the top and a simple support at the bottom). Applied axial load consists of self-weight only, and it is not significant. The self-weight from the

CMU wall is about 3.3 kips at mid-height (based on 150 pcf), and the self-weight from clay masonry veneer is about 1.2 kips at mid-height (based on 120 psf). In addition, since the main concern in the quasi-static, out-of-plane testing of CMU wall specimens is connectors, the self-weight can be assumed to be zero for simplicity. Based on their relative uncracked flexural stiffnesses (EI), the CMU wall initially resists about 90% of the applied out-of-plane load, and clay masonry veneer about 10%.

Table 4-2 Limit states and corresponding load capacities of quasi-static, out-of-plane CMU wall specimens

limit state	nominal capacity	expected capacity	basis for capacities
flexural cracking	172 psf (PCL mortar) 104 psf (MC mortar)		2008 MSJC Code Table 3.1.8.2 and Section 3.2
flexural failure	418 psf	523 psf	2008 MSJC Code Section 3.3 and plastic design assumptions
connector yielding	574 psf (tri-wire) 1890 psf (double eye-and-pintle)		$A_s \ f_y$, no eccentricity
connector buckling	3703 psf (tri-wire) 1256 psf (double eye-and-pintle)		$\frac{\pi^2 EI}{(kL)^2}$, no eccentricity

For the Type S cement-lime (PCL) mortar used in UT CMU 1 and UT CMU 2, the nominal cracking moment for CMU wall (fully grouted) at zero axial load is 152 kip-in., and for clay masonry veneer (hollow, ungrouted), 13 kip-in. Because the ratio of the nominal flexural cracking capacity (CMU wall to clay masonry veneer) is larger than the ratio of the uncracked flexural stiffness (CMU wall to clay masonry veneer), the clay masonry veneer governs the flexural cracking capacity, at a total applied load intensity on the specimen of 172 psf.

For the Type S masonry cement (MC) mortar used in UT CMU 2 MC, the nominal cracking moment at zero axial load for the fully grouted CMU wall is 142 kip-in., and for the clay masonry veneer, 8 kip-in. Because the ratio of the nominal flexural cracking capacity (CMU wall to clay masonry veneer) exceeds the ratio of the uncracked

flexural stiffness (CMU wall to clay masonry veneer), the clay masonry veneer governs the flexural cracking capacity, at a total applied load intensity on the specimen of 104 psf.

A moment-axial force interaction diagram for the CMU wall section, calculated by spreadsheet, is shown in Figure 4-2. The interaction diagram includes strength-reduction factors (ϕ-factors), and gives design strengths. In developing the interaction diagram, 60 ksi was used for the yield strength of reinforcing bars (f_y) and 1500 psi for the compressive strength of masonry (f_m'). At zero axial load, design flexural strength is 193 kip-in. Nominal flexural strength is this design strength, divided by the ϕ-factor (0.9), and the expected strength is the nominal strength multiplied by 1.25 to address probable steel over-strength and strain-hardening of the reinforcement. The resulting nominal flexural capacity and expected flexural capacity of the CMU walls are 214 kip-in. and 268 kip-in., respectively. The corresponding nominal and expected out-of-plane capacities based on plastic design assumptions are 418 psf and 523 psf, respectively. For simplicity in this calculation, rotational hinges were assumed at the base and at mid-height.

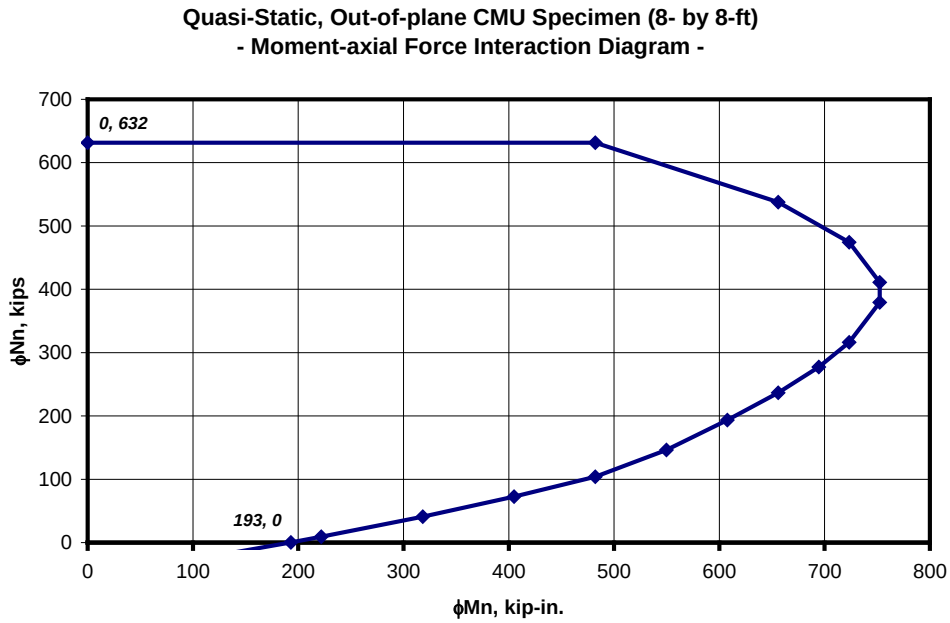

Figure 4-2 Moment-axial force interaction diagram for quasi-static, out-of-plane CMU wall specimens (8- by 8-ft)

For one W1.7 wire, the nominal yield strength is 1.02 kips based on a specified yield stress of 60 ksi, and the nominal buckling strength is 6.58 kips using an effective length of 1 inch and ignoring eccentricity. For specimens with tri-wire joint reinforcement, the corresponding nominal capacities are 574 psf due to connector yielding and 3703 psf due to connector buckling. Because of the very small radius of the wires (about 0.075 in.) and the inevitable eccentricities from fabrication and construction, however, the probable buckling strength is probably significantly less than these ideal values.

For two W2.8 wires, the nominal yield strength is 3.36 kips based on a specified yield stress of 60 ksi, and the nominal buckling strength is 2.23 kips, using an effective length of 4 inches and ignoring eccentricity. For specimens with double eye-and-pintle connectors, the corresponding nominal capacities are 1890 psf from connector yielding and 1256 psf from connector buckling. The probable yield strength and buckling strength

are probably significantly less than these ideal values, however, due to tensile eccentricity in the connectors, and due to fabrication and construction eccentricities in compression.

4.3 TEST SETUP FOR QUASI-STATIC, OUT-OF-PLANE TESTS OF CMU WALL SPECIMENS

A typical test setup for quasi-static, out-of-plane loading of CMU wall specimens is shown in Figure 4-1. CMU wall specimens were loaded by a 100-kip hydraulic ram with ± 9-in. stroke, connected to a compressed air-driven hydraulic pump. The distance from the top surface of the base beam to the centerline of out-of-plane support was 8 ft-11 in. Out-of-plane loading system consisted of three parts: a braced loading frame; a "whiffle-tree" to simulate distributed loading, and a braced reaction frame.

The braced loading frame (Figure 4-3) consisted of two steel columns (W12x58), one steel beam (W12x120), and two steel braces (W12x26).

Figure 4-3 Braced loading frame of out-of-plane test setup

The "whiffle-tree" distributed the load from hydraulic-ram into sixty-four point loads (eight rows and eight columns of loaded points), each covering 1 ft^2. The “whiffle-

tree" consisted of one steel beam (W12x65), sixty-two steel tubes (two HSS 6x6x3/8, four HSS 4x3x1/4, eight plus sixteen HSS2x2x1/4, and thirty-two HSS2x2x1/8), and one hundred twenty-four threaded rods (four 1-in. rods, eight plus sixteen 0.75-in. rods, thirty-two 0.5-in. rods, and sixty-four 0.25-in. rods). The "whiffle-tree" was designed for three limit states: flexural yielding of the steel tubes; tensile or compressive yielding of the threaded rods; and buckling of the entire "whiffle-tree." Based on a specified steel yield stress of 36 ksi, the lateral pressure corresponding to the nominal flexural yield capacity of the steel tubes was 1121 psf; and to the nominal yield capacity of the threaded rods, 1326 psf. Nominal buckling capacity was calculated using SAP2000. Half the "whiffle-tree" part was modeled (Figure 4-4), idealizing the CMU wall with a uniform thickness of 7.625 in. and ignoring the clay masonry veneer. The nominal buckling capacity was 1269 psf. All three capacities were far above the expected flexural capacity of the specimens (349 psf). The vertical load distribution from the "SAP2000" calculation, shown in Table 4-3, indicates an essentially uniform load distribution. In Figure 4-5 is shown a typical photo of the threaded rods anchored into the clay masonry veneer using the Hilti HIT HY-20 adhesive anchoring system. A typical connection between steel tubes of the "whiffle-tree" is shown in Figure 4-6, and the installed "whiffle-tree" attached to the CMU wall specimen is shown in Figure 4-7.

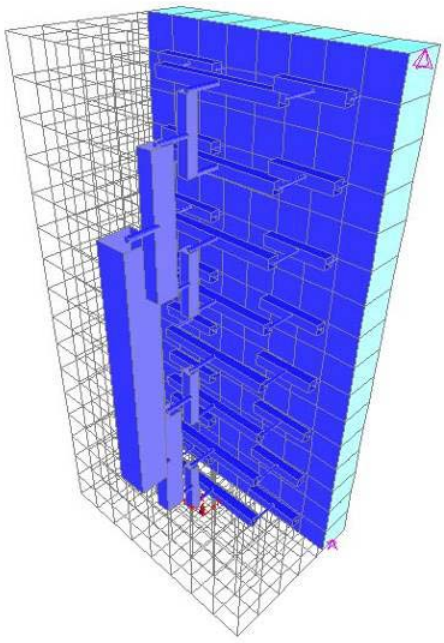

Figure 4-4 SAP2000 model to calculate buckling capacity and vertical load distribution for half the "whiffle-tree"

Table 4-3 Vertical load distribution in "Whiffle-tree"

row from the top	1st	2nd	3rd	4th	5th	6th	7th	8th
relative load	0.128	0.122	0.126	0.123	0.123	0.126	0.123	0.128

Figure 4-5 Typical steel rods anchored into clay masonry veneer using structural adhesive

Figure 4-6 Typical connection between steel tubes of "whiffle-tree"

Figure 4-7 Installed "whiffle-tree" attached to CMU wall specimen

The braced reaction frame (Figure 4-8) to support the tops of the CMU walls consisted of two steel columns (W12x65), one steel beam (W12x120), four 1-in. diameter steel cables, and four steel angles (L5x3x3/8). The top of the CMU wall was capped by steel angles and was simply connected to the four steel angles of the braced reaction frame (Figure 4-9).

Figure 4-8 Braced reaction frame of out-of-plane test setup

Figure 4-9 Simple connection between top of CMU wall and braced reaction frame

4.4 INSTRUMENTATION FOR QUASI-STATIC, OUT-OF-PLANE TESTS OF CMU WALL SPECIMENS

Out-of-plane load was measured using 100-kip load cell placed between the hydraulic ram and the clevis. Out-of-plane displacement was measured at thirty-two locations (Figure 4-10 and Figure 4-11), thirteen of which were on the CMU walls (Channels 1 through 13), six of which were on the base beams (Channels 14 through 19), and thirteen of which were on the clay masonry veneer (Channels 20 through 32). String potentiometers were generally used for displacement measurements of CMU walls and clay masonry veneer (except for Channels 11 through 13, which were linear potentiometers), and linear potentiometers were used for measurements of base beams and ch. 11 through 13. Data were recorded at one-second intervals.

All displacement measurements for CMU walls (except Channels 6 through 8) and all displacement measurements for clay masonry veneer (except Channels 25 through 27) were placed coincident with connectors, so that difference between the measured out-of-plane displacement measurements could be used to compute the deformation of the connectors. Channels 6 through 8 and Channels 25 through 27 were placed at the mid-height of the CMU walls and the clay masonry veneer (4 ft from the top of the base beams) to evaluate planar deflection of the CMU and the clay masonry veneer. The out-of-displacements of base beams was measured to check support movements.

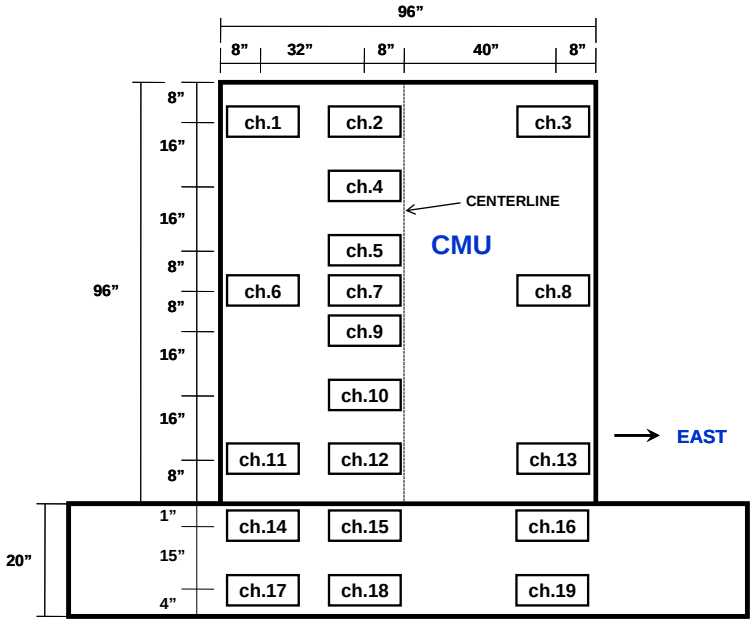

Figure 4-10 Instrumentation of quasi-static, out-of-plane CMU wall specimens (CMU side)

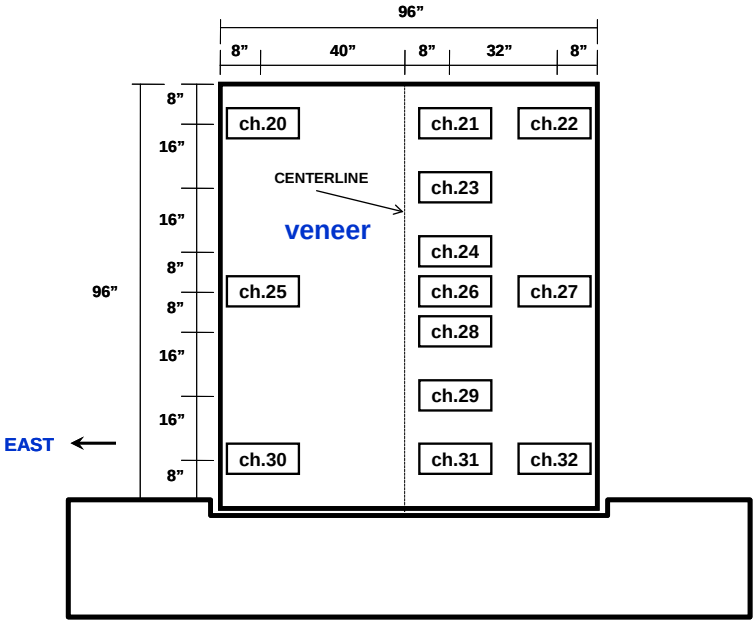

Figure 4-11 Instrumentation of quasi-static, out-of-plane CMU wall specimens (veneer side)

4.5 LOADING PROTOCOL FOR QUASI-STATIC, OUT-OF-PLANE TESTS OF CMU WALL SPECIMENS

Quasi-static, out-of-plane loading was based on target load levels until the maximum load capacity was reached, after which it was based on target displacement levels. As shown in Figure 4-12, the loading protocol consisted of series of three reversed cycles to a maximum load capacity that was increased monotonically in increments of 4.0 kips, corresponding to increments of 62.5 psf. After the specimen reached its maximum load capacity, series of three reversed cycles were continued to monotonically increasing maximum displacement levels at the mid-height of the clay masonry veneer equal to 1.5, 2.0, 3.0, and 5.0 times the displacement at maximum load capacity.

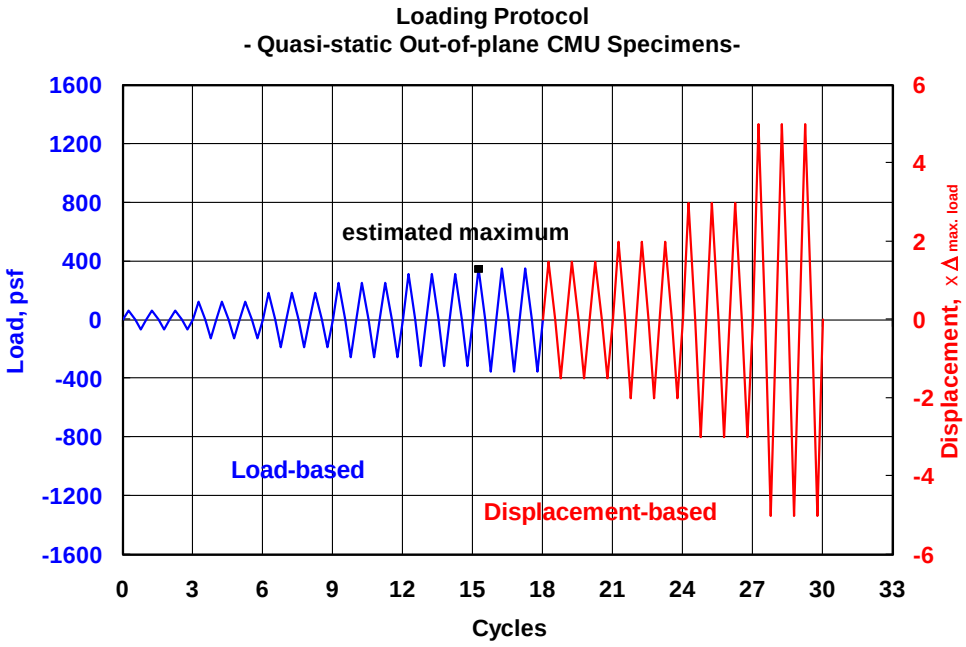

Figure 4-12 Loading protocol for quasi-static, out-of-plane CMU wall specimens

4.6 QUASI-STATIC, OUT-OF-PLANE TEST AND TEST RESULTS OF CMU WALL SPECIMEN UT CMU 1

Specimen UT CMU 1 was subjected to repeated series of reversed cyclic loading to monotonically increasing load or monotonically increasing displacement at the mid-height of the clay masonry veneer. Each cycle started with tension to the north (refer to Figure 4-1 for loading direction). Before reaching the maximum load capacity, the load level was increased in increments of 4.0 kips (corresponding to increments of 62.5 psf on the frontal area of the specimen). After reaching the maximum load (23.2 kips) in tension, it was judged that additional imposed displacement would cause failure due to the top row of double pintles pulling out of double eyes. Therefore, during the next cycle, the specimen was loaded in tension until the top row of double pintles was about to pull out of the double eyes (corresponding to 0.6 in. of displacement at the mid-height of the clay masonry veneer), and the same displacement was applied in compression. The specimen was then loaded in tension until the top row of double pintles pulled completely out of the double eyes (6.2 kips and 1.0 in.), as shown in Figure 4-16. The curve of load versus displacement at the mid-height of the clay masonry veneer is shown in Figure 4-13. Key observations in the response history are described in Table 4-4. All observations were made during the first cycle under target load or displacement unless specified otherwise.

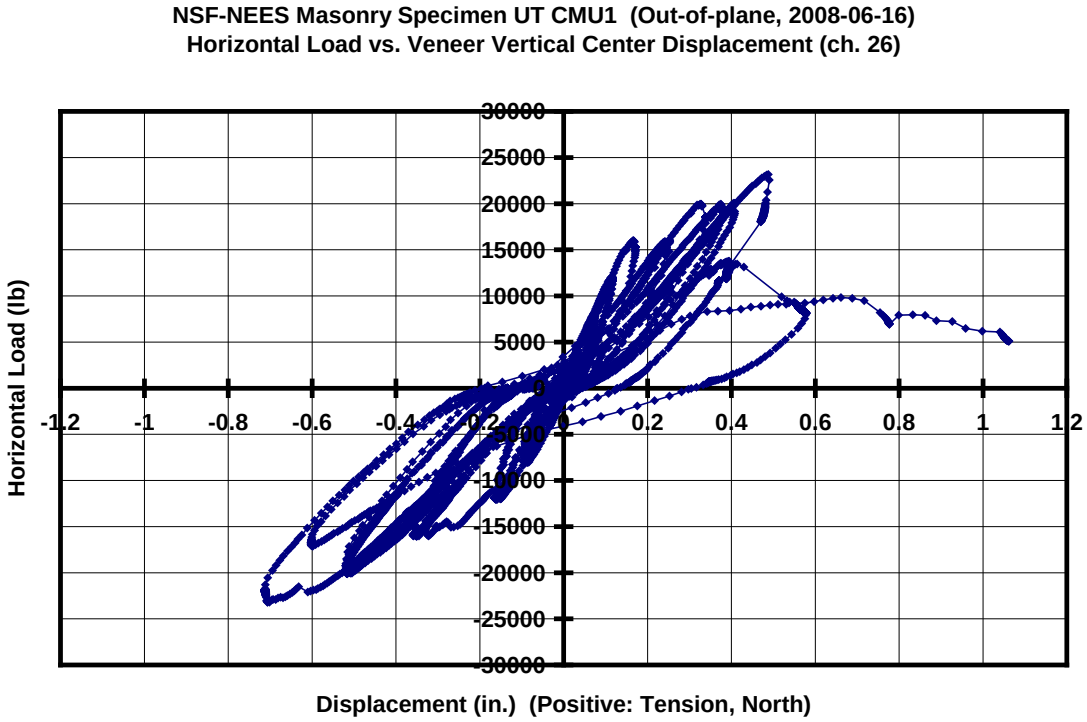

Figure 4-13 Load versus displacement at the mid-height of veneer (Specimen UT CMU 1)

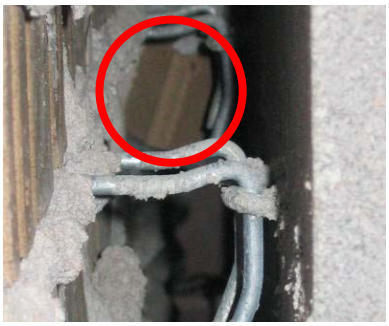

Figure 4-14 Pull-out failure of connectors in Specimen UT CMU 1

Table 4-4 Key observations in the response history of Specimen UT CMU 1

target load or displacement *	key observations
16 kips (250 psf)	- First cracking occurred near the mid-height of the CMU wall and the clay masonry veneer.
20 kips (313 psf)	- Pull-out failure (Figure 4-14) occurred at one connector at the third row from the top, which was checked later by comparing pictures; this pull-out failure did not govern the maximum load in this specimen. - Cracking was observed at the south bottom of the CMU wall, but it is not clear at what load the cracking occurred. However, it is supposed that this cracking occurred at a very low load, because the same type of crack was observed at 4 kips of loading in Specimen UT CMU 2 and even before loading in Specimen UT CMU 2 MC.
23.2 kips (363 psf)	- Maximum load was reached in tension (23.2 kips); the specimen seemed to have additonal load capacity in compression.
0.6 in.	- The clay veneer cracked and began to rotate at the top of the 15th course from the bottom (Figure 4-15). - The crack in the veneer opened up at the top of the 20th course at the west side (nearest to the viewer in Figure 4-15) and at the top of the 21st course at the east side, with those two cracks joining in the middle of the specimen.
1.0 in.	- The top row of double pintles pulled out of the corresponding double eyes. (Figure 4-16). - The clay veneer rotated at the top of 20th course at the west side (Figure 4-15) and at the top of the 21st course at the east side.

** at the mid-height of the clay masonry veneer*

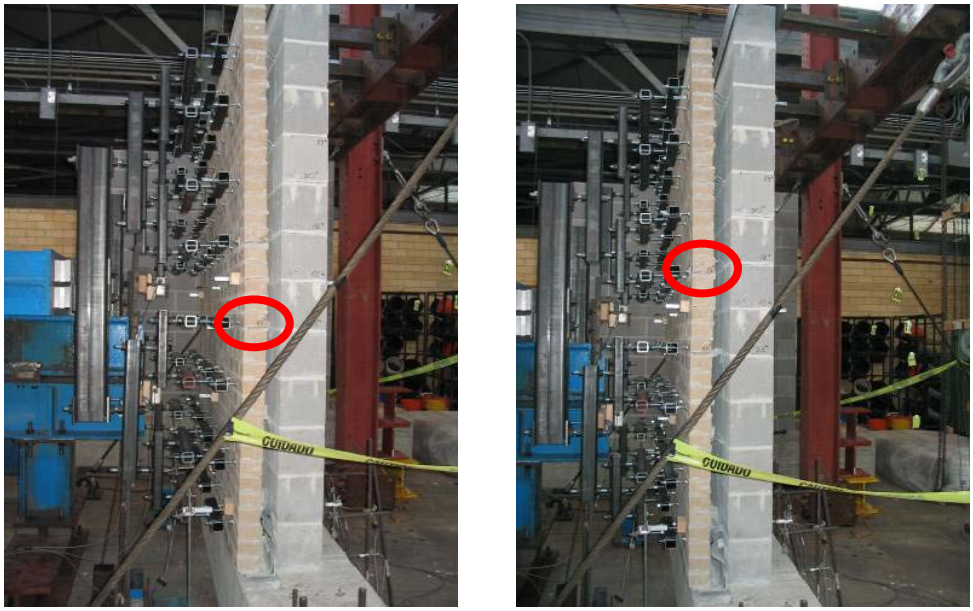

Figure 4-15 Rotation of the veneer at top of 15th (left) and 20th (right) courses from the bottom at west side (nearest to the viewer)

Figure 4-16 Connectors at 1-in. tensile displacement (top to bottom at west side, nearest to the viewer)

4.7 QUASI-STATIC, OUT-OF-PLANE TEST AND TEST RESULTS OF CMU WALL SPECIMEN UT CMU 2

Specimen UT CMU 2 was subjected to repeated series of reversed cyclic loading to monotonically increasing load or monotonically increasing displacement at the mid-height of the clay masonry veneer. Each cycle started with tension to the north (refer to Figure 4-1 for loading direction). Before reaching the maximum load capacity, the load

level was increased in increments of 4.0 kips (corresponding to increments of 62.5 psf on the frontal area of the specimen). After reaching a maximum load of 20 kips in tension and 18.7 kips in compression under the target load of 20 kips, another cycle was attempted to the same target load. A maximum load of 20 kips was again reached in tension, followed by only 16.0 kips of maximum load in compression. During the second cycle under the target load of 20 kips, one connector (second from the top, first from the west side) was found to have cracked at the bottom of the middle (Figure 4-18). At the next cycle, the specimen was loaded to its maximum capacity in tension (25.6 kips, developed at 0.50 in.) to find its load capacity in tension independent of low-cycle fatigue. Subsequently, the target displacement of 0.5 in. was again applied, during which the connectors fractured at 14.5 kips and 0.31 in., ending the test. The curve of load versus displacement at the center of the veneer is shown in Figure 4-17. Key observations in the response history are described in Table 4-5. All observations were made during the first cycle under target load or displacement unless specified otherwise.

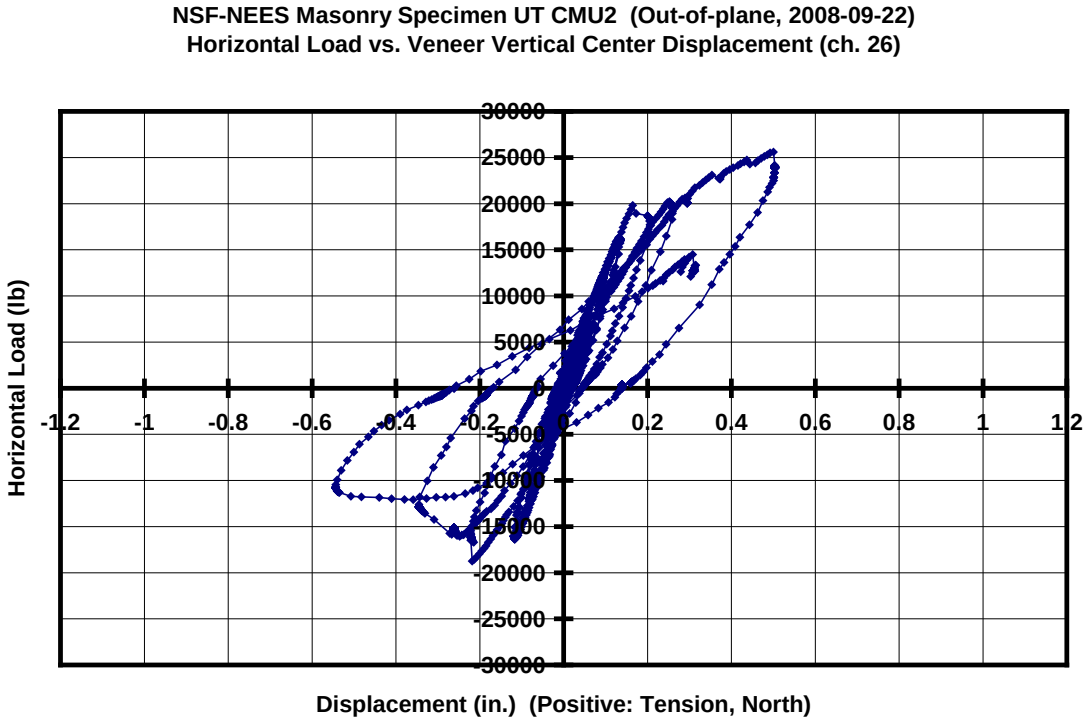

Figure 4-17 Load versus displacement at the mid-height of veneer (Specimen UT CMU 2)

Table 4-5 Key observations in the response history of Specimen UT CMU 2

target load or displacement*	key observations
4 kips (63 psf)	- The bottom of CMU wall cracked at the south side (refer to Figure 4-1) in tension.
18.7 kips (292 psf)	- Maximum load was reached in compression (18.7 kips). - First cracking occurred near the mid-height of the CMU wall and the clay masonry veneer. - Connectors at the top two rows began to buckle. - One connector, located second from the top, first from the west (refer to Figure 4-1), was observed to have cracked at the bottom of the middle (Figure 4-18).
0.5 in.	- Pull-out failure (Figure 4-19) occurred at the top-west corner connector at 0.5 in. (25.6 kips) in the first cycle of tension; 25.6 kips was the maximum load reached in tension. - The connector, where the pull-out failure had occurred, finally fractured at the veneer side (Figure 4-19) during the next (second) loading cycle. - During the second cycle in tension, the clay masonry veneer began to rotate at the top of the 24th course from the bottom at the west side and at the top of the 23rd course at the east side, with those cracks joining in the middle of the specimen (Figure 4-20). - Connectors fractured at the first and second rows from the top (Figure 4-21). The fractured location (veneer side, middle or CMU side) and the shape of fractured connectors (bent or straight) in the top two rows are as follows *the top row (west to east):* *veneer (bent) – veneer (bent) – veneer (bent) – CMU (bent) – middle (straight) – middle (straight)* *the second row from the top (west to east):* *middle (straight) – no fracture – no fracture – veneer (bent) – no fracture – middle (straight)*

** at the mid-height of the clay masonry veneer*

Figure 4-18 Cracked connector, second from the top, first from the west

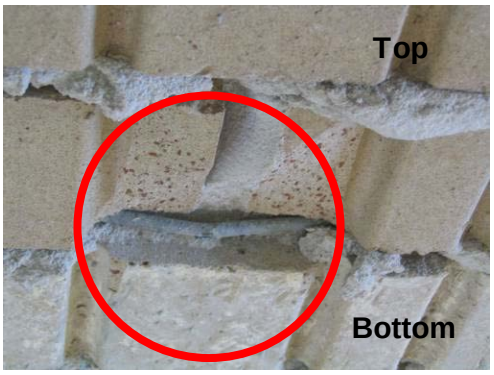

Figure 4-19 Pull-out of longitudinal wire followed by fracture of cross-wire at weld

Figure 4-20 Joining of cracks in the clay masonry veneer

Figure 4-21 Connectors at 0.5-in. tensile displacement (top to bottom at west side)

4.8 QUASI-STATIC, OUT-OF-PLANE TEST AND TEST RESULTS OF CMU WALL SPECIMEN UT CMU 2 MC

Specimen UT CMU 2 was subjected to repeated series of reversed cyclic loading to monotonically increasing load or monotonically increasing displacement at the mid-height of the clay masonry veneer. Each cycle started with tension to the north (refer to Figure 4-1 for loading direction). First, the load level was increased in increments of 4.0 kips (corresponding to 62.5 psf on the frontal area of the specimen). After reaching 13.0 kips in compression with a target load of 16 kips, it was judged that the specimen had reached its maximum load capacity in compression, because the load began to drop after the load versus displacement curve became almost flat from 12 kips to 13 kips; 16 kips of target load was reached in tension at this cycle. Therefore, the target loading was changed from load to displacement. During the next cycle (with a target displacement of 0.4 in.), the resistance of the specimen in compression kept increasing almost linearly, reaching 17.5 kips at a displacement of 0.4 in.

At the first cycle to a target displacement of 0.80 in., the bed joint of the clay veneer (around the mid-height) totally cracked and opened under compressive loading of the specimen (Figure 4-23), accompanied by a loud noise and a sudden drop in load from 22.8 kips to 12.5 kips. At the second cycle to a target displacement of 0.80 in., the maximum load was 12.8 kips, as governed by buckling of connectors. The high capacity of 22.8 kips in compression at the previous cycle is believed to have been developed by mortar droppings surrounding connectors (Figure 4-24) and thereby increasing their buckling capacity. The sudden drop in load from 22.8 kips to 12.5 kips was probably caused by the detachment of these mortar droppings from connectors. During the third cycle to a target displacement of 0.80 in., the connectors began to fracture in tension due to low-cycle fatigue, starting at the third row from the top. The test was ended after the load abruptly dropped at 22.0 kips. The maximum load that the specimen reached was 22.8 kips in compression and 27.6 kips in tension, both of which occurred at the first cycle to a target displacement of 0.8 in. In Specimen UT CMU 2 MC, all the connectors

in the third row from the top fractured, along with some connectors in the second and fourth rows from the top. The curve of load versus displacement at the center of the veneer is shown in Figure 4-22. Key observations in the response history are described in Table 4-6. Observations were made during the first cycle to each target load or displacement unless specified otherwise.

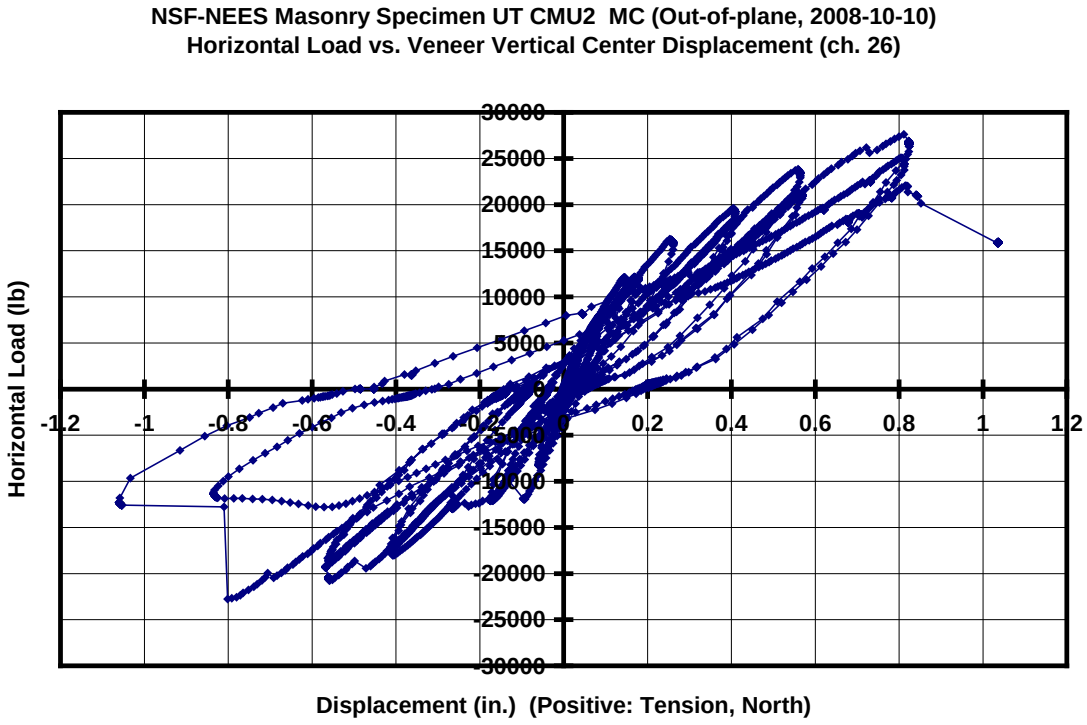

Figure 4-22 Load versus displacement at the mid-height of veneer (Specimen UT CMU 2 MC)

Figure 4-23 Bed joint of clay veneer at a target displacement of 0.80 in. under compressive loading of Specimen UT CMU 2 MC

Table 4-6 Key observations in the response history of Specimen UT CMU 2 MC

target load or displacement *	key observations
before loading	- The bottom of CMU wall cracked at the south side (refer to Figure 4-1) while attaching the specimen to the test set-up.
12 kips (188 psf)	- First cracking occurred near the mid-height of the CMU wall and the clay masonry veneer.
13 kips (203 psf)	- The load-displacement curve became almost flat after 12 kips in compression and the load began to drop at 13 kips.
0.4 in.	- The resistance in compression kept increasing almost linearly up to about 17.5 kips developed at 0.4 in. of displacement.
0.8 in.	- The bed joint the clay masonry veneer (around the mid-height) totally cracked and opened under compressive loading of the specimen at the first cycle (Figure 4-23), accompanied by a sudden load drop from 22.8 kips to 12.5 kips and a loud noise. The large load resistance of 22.8 kips in compression is supposed to have been developed by mortar droppings surrounding connectors and increasing their buckling capacity (compare Figure 4-24 and Figure 4-25). - At the second cycle, the maximum compressive resistance was 12.8 kips, as governed by buckling of connectors (Figure 4-25). - At the third cycle of tensile displacement, the connectors began to fracture starting at the third row from the top, and the load abruptly dropped at 22.0 kips. - Fractured connectors are all the connectors at the third row; the second and the sixth from the west at the fourth row; and the fifth from the west at the second row. All the fracture occurred at around the middle of the connectors after they straightened out.

** at the mid-height of the clay masonry veneer*

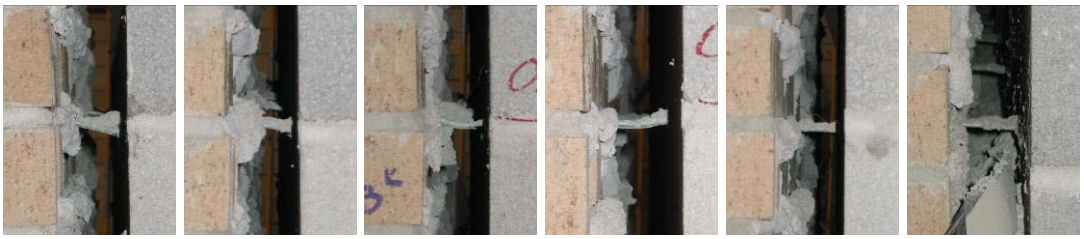

Figure 4-24 Connectors of UT CMU 2 MC at 0.55-in. compressive displacement (top to bottom at west side, nearest to viewer)

Figure 4-25 Connectors of UT CMU 2 MC at the 2nd cycle of 0.8-in. compressive displacement (top to bottom, west side)

Figure 4-26 Connectors of UT CMU 2 MC at 0.8-in. tensile displacement (top to bottom, west side)

4.9 Summary of and Observations on Quasi-static, Out-of-plane Tests of CMU Wall Specimens

The maximum capacity of the quasi-static, out-of-plane CMU wall specimens was always governed by the connectors. Tri-wire connectors failed by low-cycle fatigue in

tension, and double eye-and-pintle connectors failed by the pintles pulling out of the eyes in tension. In these tests, the load was applied to the clay masonry veneer only. Under real earthquake, however, because of the additional inertia forces induced in the CMU wall, capacity could be governed either by the connectors or by the CMU wall itself. In these quasi-static tests, the actual capacity load governed by connectors did not reach even the nominal capacity of the CMU wall (418 psf for flexural failure in Table 4-2) based on plastic analysis and nominal flexural capacity of the section. The main objective of this research is to study the in-elastic behavior of the CMU wall with clay masonry veneer rather than elastic behavior. Accordingly, the quasi-static, out-of-plane tests of the CMU wall specimens primarily provide information on the connectors (tri-wire and double eye-and-pintle). One observation on the behavior of the CMU wall and the clay masonry veneer is that the first flexural cracking (except for the base of the CMU wall) occurred around the mid-height in both the CMU wall and the clay masonry veneer in all the three specimens. The top and the bottom of the CMU wall had different boundary conditions, with a horizontal spring at the top and fixed support (before flexural yielding) at the bottom.

The double eye-and-pintle connectors (Specimen UT CMU 1) failed in tension by the double pintles pulling out of the double eyes after reaching 363 psf, and buckling of the connectors was not observed. The maximum load recorded in compression of the double eye-and-pintle connectors was 363 psf but the maximum compressive load capacity was not determined because the connectors failed in tension.

In the tri-wire connectors, the maximum load in tension was 400 psf (UT CMU 2) and 344 psf (UT CMU 2 MC) by low-cycle fatigue failure of the connectors. The maximum load of the tri-wire connectors in compression was 292 psf (UT CMU 2) and 356 psf (UT CMU 2 MC) by buckling of the connectors. In both specimens (UT CMU 2 and UT CMU 2 MC), the residual load after buckling was about 190 psf, corresponding to 12 kips. The difference between UT CMU 2 and UT CMU 2 MC is was the cementitious system used in the mortar: cement-lime mortar in UT CMU 2, and masonry

cement mortar in UT CMU 2 MC. UT CMU 2 and UT CMU 2 would be expected to behave identically with respect to buckling and low-cycle fatigue of connectors.

In Section 9.1, this information about the connectors is reevaluated from the viewpoint of analytical study, and is used for OpenSees analysis of the CMU wall specimens and the CMU building specimen.

CHAPTER 5
Quasi-static Tests of CMU Wall Specimens, In-plane

As part of the NSF NEES masonry project, six reinforced concrete masonry wall specimens with clay masonry veneer (CMU wall specimens) were tested quasi-statically at The University of Texas at Austin (UT Austin). Three were tested under out-of-plane loading, and the other three under in-plane loading. The main purpose of quasi-static, in-plane testing of the CMU wall specimens was to study the in-plane response of the CMU walls, and to provide experimental data to develop an analytical model for in-plane flexural response of the CMU walls. This chapter addresses the test setup; the instrumentation and loading protocol; the results of each test; and the significance of those results.

5.1 OVERVIEW OF QUASI-STATIC, IN-PLANE CMU WALL SPECIMENS (UT CMU 3, 4, 4 MC)

Three reinforced concrete masonry wall specimens with clay masonry veneer (CMU wall specimens) were tested quasi-statically under in-plane loading at The University of Texas at Austin. The overview of those wall specimens is provided in Table 4-1 and the design drawings are shown in Appendix A. The difference between Specimen UT CMU 3 and Specimen UT CMU 4 is the type of connectors, and the difference between Specimen UT CMU 4 and Specimen UT CMU 4 MC is the cementitious system used in the mortar (in the context of ASTM C270).

Table 5-1 Overview of quasi-static, in-plane CMU wall specimens

specimens	loading	dimensions	reinforcement	connectors	mortar
UT CMU 3	in-plane, quasi-static	4-ft wide by 8-ft high	two No. 4 bars vertically and three No. 4 bars horizontally	double eye-and-pintle	cement-lime
UT CMU 4				tri-wire	cement-lime
UT CMU 4 MC				tri-wire	masonry cement

A typical concrete masonry wall specimen (CMU wall specimen) with test setup for quasi-static, in-plane testing is shown in Figure 5-1. Design drawings are shown in Appendix A. The CMU wall specimen consisted of CMU walls (also referred to as CMU backing) and clay masonry veneer. The CMU wall measured 4 ft in plan and 8 ft-8 in. in elevation, with the top 8-in. course being an additional bond beam for loading. The clay masonry veneer measured 4 ft in plan and 8 ft in elevation. The height from the top surface of the base beam to the line of action of the in-plane loading was 8 ft-4 in. The vertical reinforcement ratio was 0.0011 with two No. 4 reinforcing bars (one bar at each wall end), and horizontal reinforcement ratio was 0.0022 with three No. 4 reinforcing bars and twelve W1.7 wires (joint reinforcement).

Two configurations of connectors and CMU reinforcement were used to connect the clay masonry veneer to the CMU backing. One configuration (used in UT CMU 3) consisted of W1.7 two-wire joint reinforcement at 16 inches vertically in the CMU wall with W2.8 wire double eye-and-pintle connectors at 16 inches horizontally, which satisfies 2008 MSJC requirements for Seismic Design Category (SDC) D. The other configuration (used in UT CMU 4 and UT CMU 4 MC) consisted of W1.7 tri-wire joint reinforcement (two wires in CMU walls and one wire in clay masonry veneer) at 16 inches vertically with W1.7 cross wires at 16 inches horizontally, satisfying 2008 MSJC requirements for SDC E. Additional requirements of 2008 MSJC Code for SDC E (above those for SDC D) include the use of joint reinforcement in veneer.

The quasi-static, in-plane CMU wall specimens used a 2-in. specified air space; nominal 8- x 8- x 16-in. lightweight concrete masonry units (ASTM C90); nominal 4-in. standard modular clay masonry units (ASTM C652); coarse grout by proportion (ASTM C476); and 30-mil EPDM flashing (not self-adhering). Concrete masonry units (CMU) were knock-out units with every web knocked out except at wall ends. EPDM flashing was placed between a shelf angle and the clay masonry veneer; the clay masonry veneer was placed on top of the shelf angle that was fixed, using adhesive anchors, to the bottom course of the concrete masonry wall (CMU wall). Specimens UT CMU 3 and UT CMU 4 used ASTM C270 Type S cement-lime mortar by proportion in the CMU wall and the clay masonry veneer, while UT CMU 4 MC used Type S masonry cement mortar by proportion in the CMU wall and the clay masonry veneer.

Each specimen was supported on a base beam 9.5-feet long, with a square cross-section measuring 20 inches on each side. Each base beam was reinforced with two No. 7 longitudinal reinforcing bars at the top and the bottom, and with No. 4 ties at a spacing of 8 in. The design flexural capacity and shear capacity of the base beam were about 80 kip-ft and 65 kips, respectively.

The in-plane CMU wall specimens were loaded by a 100-kip hydraulic ram with $\pm$ 9-in. stroke, connected to a compressed air-driven hydraulic pump. Loading was based on target load levels until flexural cracking occurred, after which the loading was based on target displacement levels.

5.2 LIMIT STATES AND CORRESPONDING EXPECTED LOAD CAPACITIES OF QUASI-STATIC, IN-PLANE CMU WALL SPECIMENS

The limit states and corresponding load capacities of quasi-static, in-plane CMU wall specimens were evaluated before testing, and are summarized in Table 5-2. Applied axial load consisted of self-weight only, and was 4.5 kips (3.3 kips from the CMU wall based on 150 pcf, and 1.2 kips from the clay masonry veneer based on 120 pcf).

Figure 5-1 Typical quasi-static, in-plane CMU wall specimen (4- by 8-ft) with test setup

Table 5-2 Limit states and corresponding load capacities of quasi-static, in-plane CMU wall specimens

limit state	nominal capacity	expected capacity	basis for capacities
flexural cracking	5.1 kips (PCL mortar) 4.8 kips (MC mortar)		2008 MSJC Code Table 3.1.8.2 and Section 3.2
flexural failure	6.4 kips	8.0 kips	2008 MSJC Code Section 3.3
shear failure	33.0 kips (V_{nm}) 47.4 kips (V_{nm} + V_{ns})		2008 MSJC Code Section 3.3.4
sliding shear failure	28.5 kips		ACI 318-08 Equation (11-25), μ=1.0

At 4.5 kips of axial load, the nominal flexural cracking strength of the CMU wall is 43 kip-ft for Type S cement-lime (PCL) mortar and 40 kip-ft for Type S masonry

cement (MC) mortar. Dividing those values by the distance from the top surface of a base beam to the line of action of the in-plane loading (8 ft-4 in.) gives a nominal in-plane cracking capacity of about 5.1 kips for the specimen with Type S cement-lime mortar, and 4.8 kips for the specimen with Type S masonry cement mortar.

A moment-axial force interaction diagram for the CMU wall, calculated by spreadsheet, is shown Figure 5-2. The interaction diagram includes strength-reduction factors (ϕ-factors), and gives design strengths. In developing the interaction diagram, 60 ksi was used for the yield strength of reinforcing bars (f_y), and 1500 psi for the specified compressive strength of masonry (f_m'). At 4.5 kips of axial load, the design flexural strength is 48 kip-ft. The nominal flexural strength is this design strength, divided by the ϕ-factor (0.9), and the expected strength is this nominal strength multiplied by 1.25 to address probable steel overstrength and strain-hardening of reinforcement. The resulting nominal strength and expected flexural capacity of the CMU wall are 53 kip-ft and 66 kip-ft, respectively. Those nominal and expected flexural strengths, divided by 8.33 ft (the distance from the top of the base beam to the line of action of the loading), give corresponding nominal and expected in-plane load capacities of about 6.4 kips and 8.0 kips, respectively.

At 4.5 kips of axial load, the nominal shear capacity is 33.0 kips from masonry alone (V_{nm}) and 47.4 kips from masonry and horizontal reinforcement ($V_{nm} + V_{ns}$), based on Section 3.3.4 of the 2008 MSJC Code. The straight lines in Figure 5-2 show flexural capacities corresponding to the design shear strengths, ϕV_{nm} and $\phi(V_{nm} + V_{ns})$, based on the required ϕ of 0.8.

The expected sliding shear strength, calculated using ACI 318-08 Equation 11-25 and a coefficient of friction of 1.0, is about 28.5 kips, and the corresponding design strength with a ϕ-factor of 0.8 is 22.8 kips.

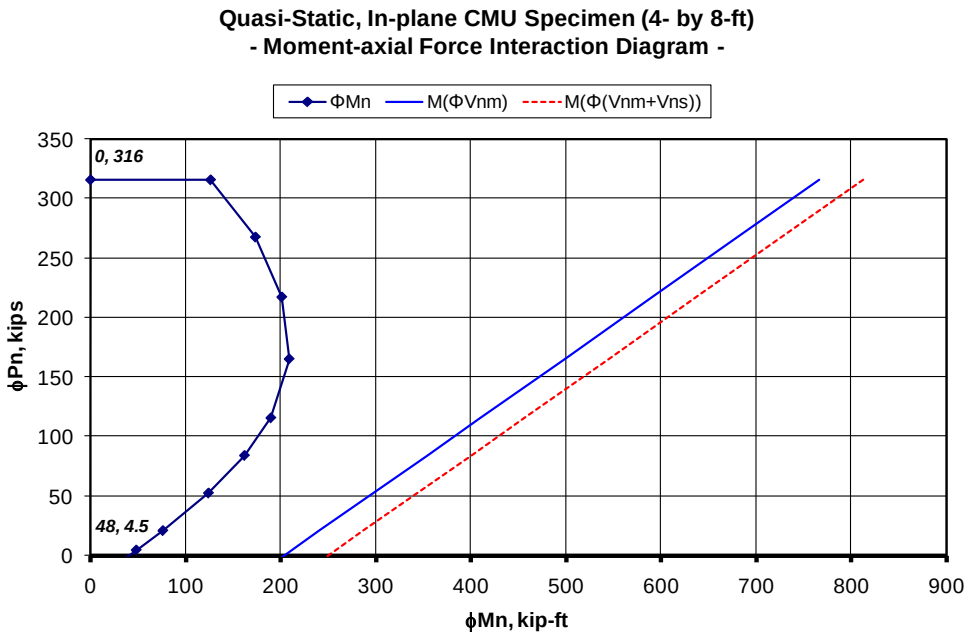

Figure 5-2 Moment-axial force interaction diagrams (governed by flexure and governed by shear) for quasi-static, in-plane CMU wall specimens (4- by 8-ft)

5.3 TEST SETUP FOR QUASI-STATIC, IN -PLANE TESTS OF CMU WALL SPECIMENS

A typical test setup for quasi-static, in-plane loading of CMU wall specimens is shown in Figure 5-1. The CMU wall specimens were loaded by a 100-kip hydraulic ram with ± 9-in. stroke, connected to a compressed air-driven hydraulic pump. The distance from the top surface of the base beam to the line of action of the in-plane loading was 8 ft-4 in. The in-plane loading system consisted of a braced reaction frame, a loading beam, and an out-of-plane support for stability.

The braced reaction frame was the same as that used in the out-of-plane loading system (Figure 4-8), without the four steel angles. The braced reaction frame consisted of two steel columns (W12x65), one steel beam (W12x120), and four 1-in. diameter steel cables. The loading beam consisted of two steel beams (W12x65), two steel pipes (3½-inch diameter with ¼-inch thickness), and four 1-inch pre-tensioned coil rods (Figure

5-3). Out-of-plane support components consisted of one column (W12x65), two rectangular steel tubes (HSS4x3) with ¼-inch thickness, and four steel angles (L5x3x3/8), illustrated in Figure 5-3. Teflon® sheets were placed between CMU wall and steel angles to minimize in-plane frictional resistance from the out-of-plane support.

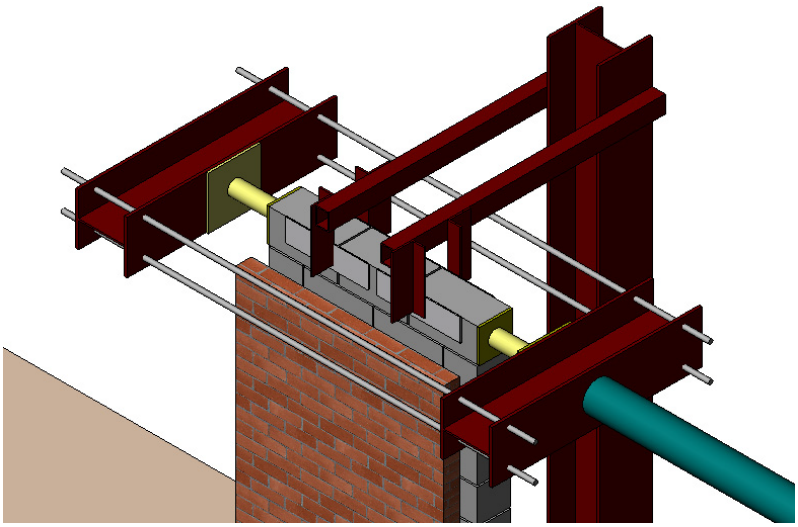

Figure 5-3 Illustration of loading beam and out-of-plane support components of in-plane loading system

5.4 INSTRUMENTATION FOR QUASI-STATIC, IN-PLANE TESTS OF CMU WALL SPECIMENS

In-plane load was measured using 100-kip load cell placed between the hydraulic ram and the clevis. In-plane displacements and deformations were measured using nineteen string potentiometers (Figure 5-4 and Figure 5-5); fourteen for the CMU walls (Channels 1 through 14), one for the base beam (Channel 15), and four for the clay masonry veneer (Channels. 16 through 19). Data were recorded at one reading per second.

In-plane displacements of the CMU walls were measured using Channels 1 through 3; in-plane flexural deformations of the CMU walls were measured using

Channels 4 through 11; in-plane shear deformations of the CMU walls were measured using Channels 12 and 13; and sliding between the CMU walls and the base beam was measured using Channel 14. Sliding between base beams and the foundation floor was checked using Channel 15. Rigid-body motion of the clay masonry veneer was measured using Channels 16 through 19.

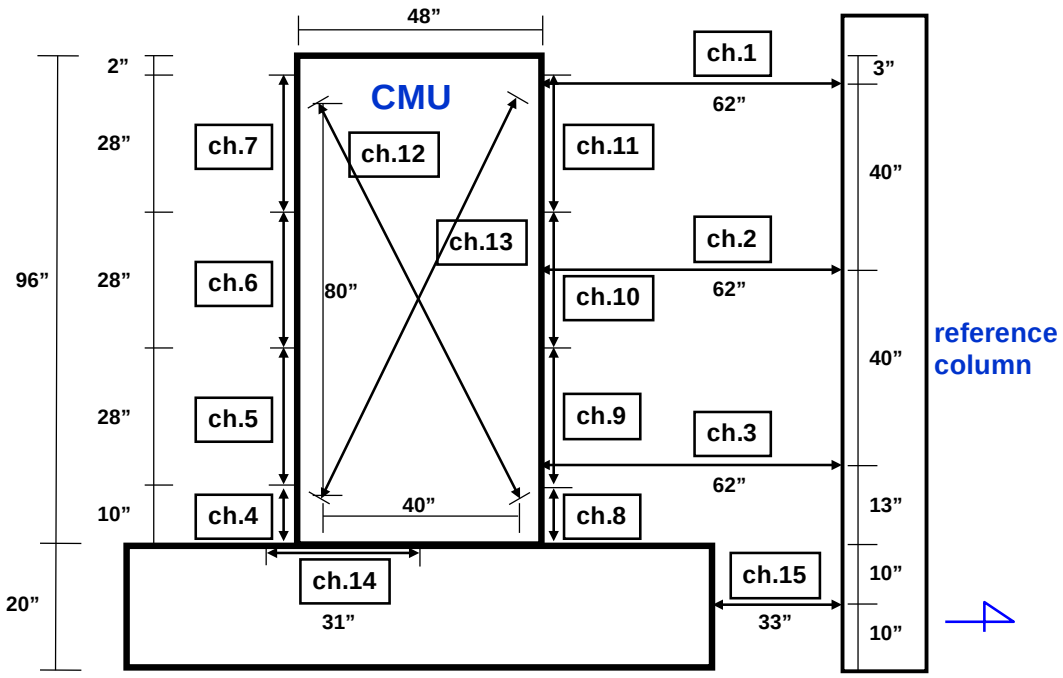

Figure 5-4 Instrumentation of quasi-static, in-plane CMU wall specimens (CMU side)

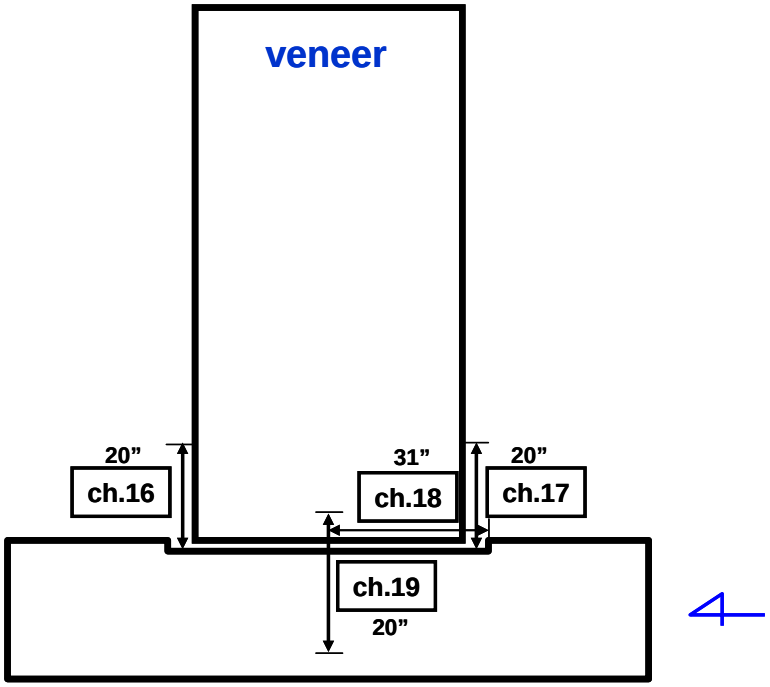

Figure 5-5 Instrumentation of quasi-static, in-plane CMU wall specimens (veneer side)

5.5 LOADING PROTOCOL FOR QUASI-STATIC, IN-PLANE TESTS OF CMU WALL SPECIMENS

Quasi-static, in-plane loading was based on target load levels until flexural cracking occurred, after which it was based on target displacement levels. As shown in Figure 5-6, the loading protocol consisted of three stages. The first stage was three reversed cycles of a load to flexural cracking. The second stage was series of three reversed cycles to target displacements, increased monotonically in increments of 0.25 inch until the specimen reached its maximum load capacity. The third stage was series of three reversed cycles to monotonically increasing maximum displacement levels equal to 1.5, 2.0, 3.0, and 5.0 times the displacement at maximum load capacity.

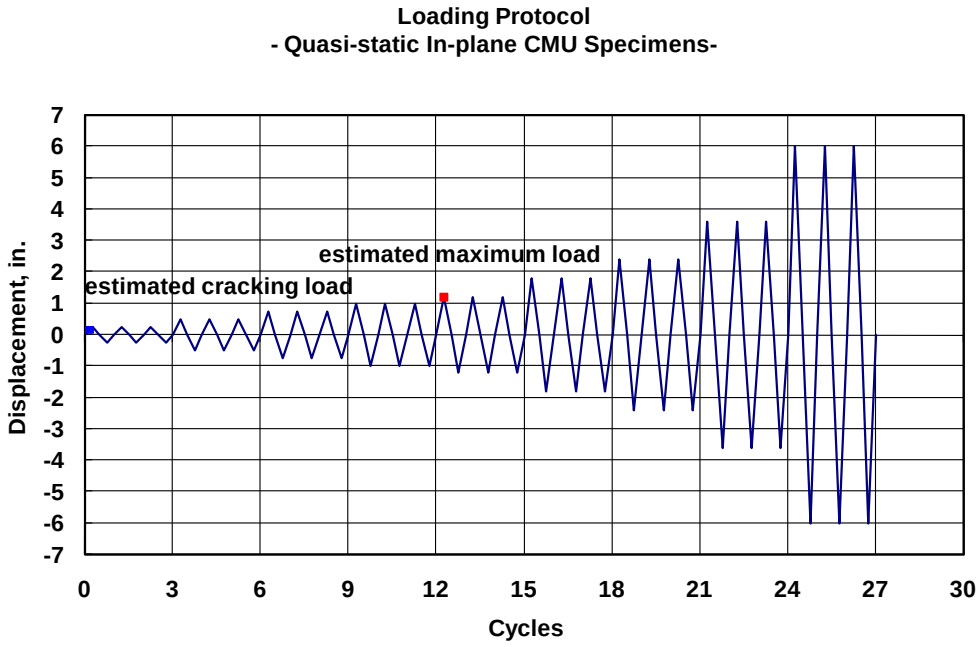

Figure 5-6 Loading protocol for quasi-static, in-plane CMU wall specimens

5.6 QUASI-STATIC, IN-PLANE TESTS AND TEST RESULTS OF CMU WALL SPECIMEN UT CMU 3

Specimen UT CMU 3 was subjected to three cycles of reversed loading at a load large enough to verify the cracking load, and then to repeated series of reversed cyclic loading to monotonically increasing tip displacement in increments of 0.25 in. (0.25 in., 0.50 in., 0.75 in. and 1.00 in.). Each cycle started with loading to the north (Figure 5-1). The curve of load versus displacement at the top of the CMU wall is shown in Figure 5-7. The overall hysteretic curve generally shows a shape similar to that of a reinforcing bar tested alone under reversed cyclic axial loading, because the behavior of Specimen UT CMU 3 is primarily governed by the longitudinal reinforcement. The initial portion of the data is re-plotted in Figure 5-8 to check the cracking load. The cracking load is about 2.1 kips to the north (first loading direction) and 3.5 kips to the south. The yielding load is about 5.6 kips to the north and 6.3 kips to the south. The test was ended by fracture of

the north longitudinal reinforcing bar at a CMU top displacement of 1.0 in. to the south under the third cycle to a displacement of 1.0 in., corresponding to a drift ratio of about 1%. Fracture occurred during the twelfth repeated reversed inelastic deformation cycle. The maximum load was about 7.7 kips to the north and 8.4 kips to the south.

Both the CMU wall and clay masonry veneer essentially showed only rigid-body rocking and sliding, with no noticeable flexural or shear deformations. The clay masonry veneer was irrelevant to the in-plane response of Specimen UT CMU 3 since the clay masonry veneer was placed on top of the shelf angle, and underwent only rigid-body motions.

Figure 5-9 shows the curve of load versus sliding of the CMU wall. Comparison of Figure 5-7 and Figure 5-9 shows that as the inelastic deformation of the longitudinal reinforcing bars increases, base sliding becomes an increasingly important contribution to the total top displacement. Before fracture of the north longitudinal reinforcing bar, base sliding is about 50 % of the northward displacement (to the left in Figure 5-7 and Figure 5-9) and about 30 % to the south direction. Maximum sliding is about 0.5 in. to the north and about 0.3 in. to the south in Figure 5-9, both of which correspond to a CMU top displacement of 1.0 in. in Figure 5-7.

The curve for the width of the crack at the base of the north end of the CMU wall is shown in Figure 5-10. After target displacements of 0.5 in., the crack does not completely close. This implies that in-plane flexural capacity is developed completely by the steel-steel couple of the longitudinal reinforcing bars. The crack at the base of the CMU wall prior to the first 1.0 in. of tip displacement is shown in Figure 5-11 (south end) and Figure 5-12 (north end). The curve for the width of the crack at the base of the CMU wall at the south end was similar to that at the north end. In contrast to Specimen UT CMU 4 and Specimen UT CMU 4 MC, Specimen UT CMU 3 did not exhibit local failure at the toe.

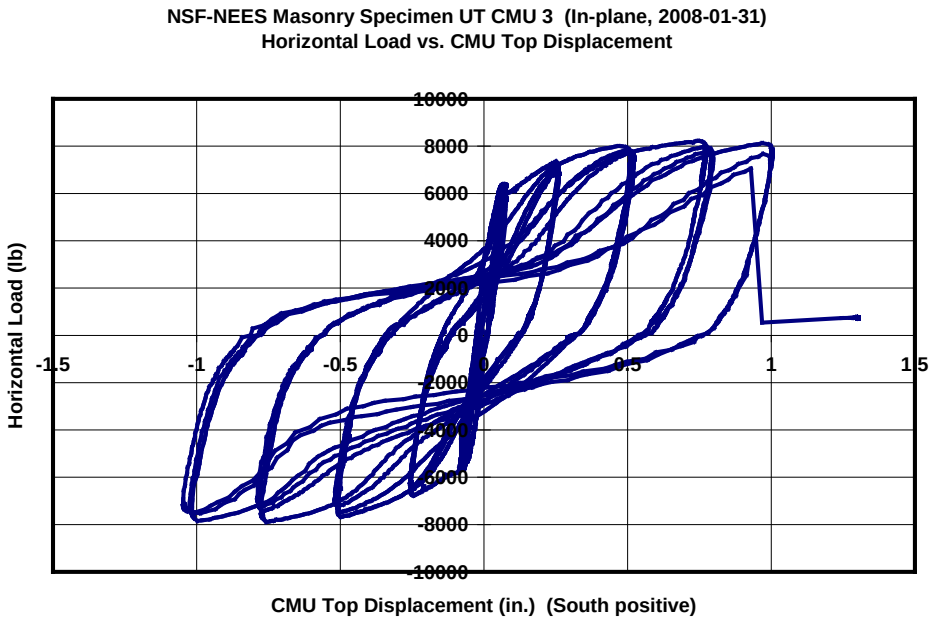

Figure 5-7 Load versus displacement at the top of CMU wall (Specimen UT CMU 3)

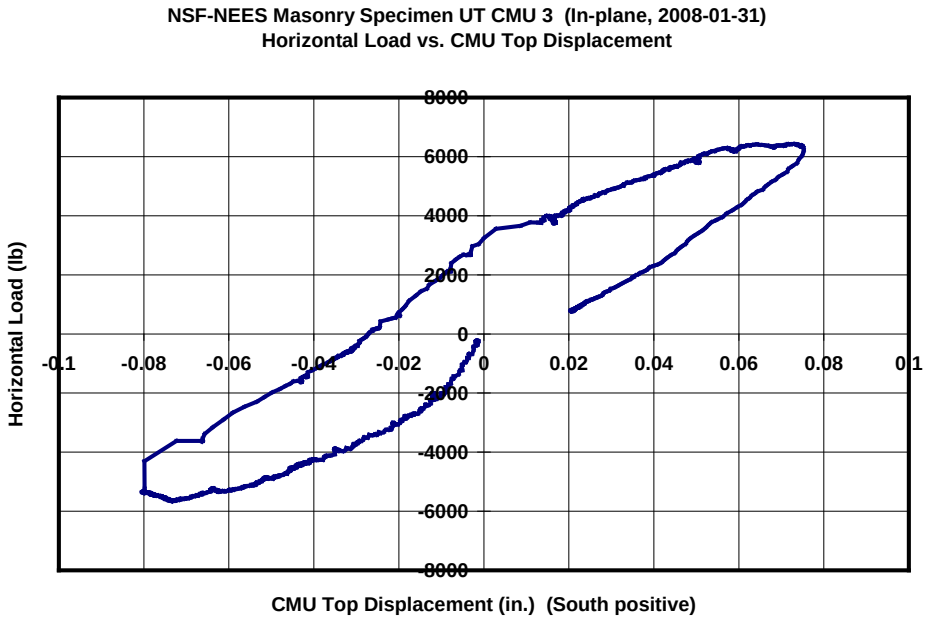

Figure 5-8 Part of load versus displacement at the top of CMU wall to check cracking load (Specimen UT CMU 3)

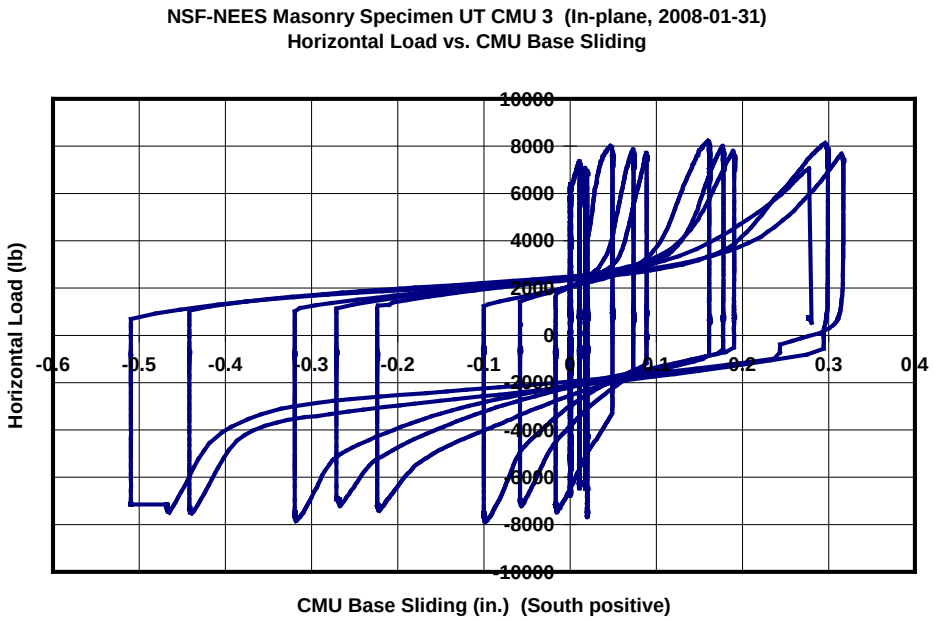

Figure 5-9 Base sliding of CMU wall (Specimen UT CMU 3)

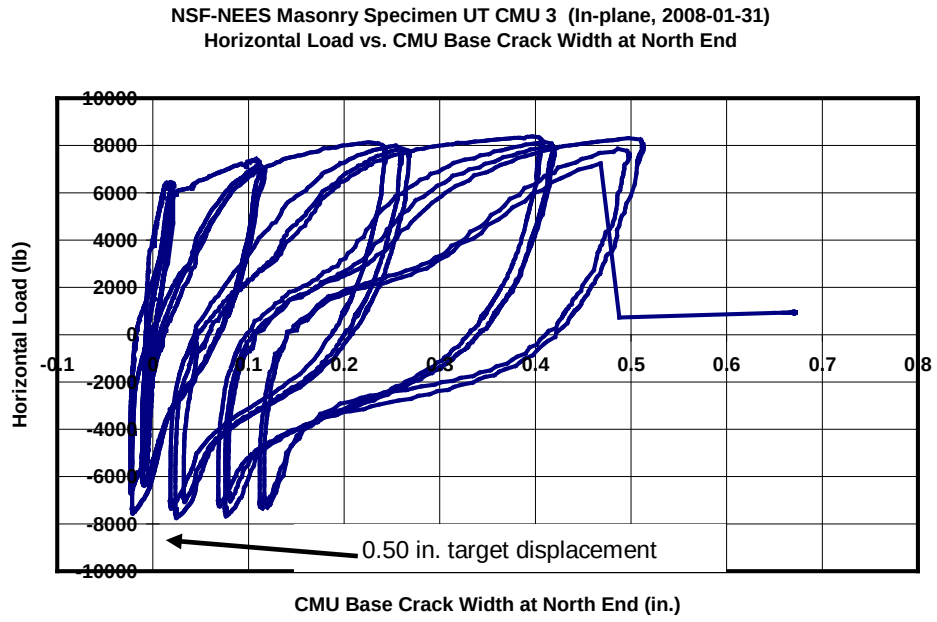

Figure 5-10 Width of crack at base of CMU wall at north end (Specimen UT CMU 3)

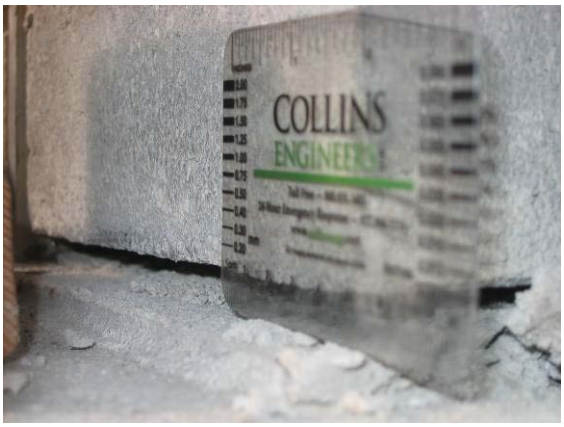

Figure 5-11 South end of CMU wall at the base under the first 1.0 in. loading to the north (Specimen UT CMU 3)

Figure 5-12 North end of CMU wall at the base under the first 1.0 in. loading to the north (Specimen UT CMU 3)

5.7 QUASI-STATIC, IN-PLANE TEST AND TEST RESULTS OF CMU WALL SPECIMEN UT CMU 4

Specimen UT CMU 4 was subjected to three cycles of reversed loading at a load large enough to verify the cracking load, and then to repeated series of reversed cyclic loading to monotonically increasing tip displacement in increments of 0.25 in. (0.25 in., 0.50 in., 0.75 in. and 1.00 in.). Finally, the specimen was subjected to reversed cyclic loading of 1.50 in. displacement at the top of the CMU wall. Each cycle started with loading to the south (refer to Figure 5-1). The curve of load versus displacement at the top of the CMU wall is shown in Figure 5-13. The overall hysteretic curve generally shows a shape similar to that of a reinforcing bar tested alone under reversed cyclic axial loading, because the behavior of Specimen UT CMU 4 is primarily governed by the longitudinal reinforcement. The initial portion of the data is re-plotted in Figure 5-14 to check the cracking load. The cracking load is about 1.8 kips to the south (first loading direction) and 3.0 kips to the north. The yield load is about 6.0 kips to the north and 5.9 kips to the south. The test was ended by fracture of the south longitudinal reinforcing bar

at a tip displacement of 1.2 in. to the north after going through a displacement of 1.5 in. to the south. Those displacements correspond to drift ratios of about 1.2 % and 1.5 %, respectively. Fracture occurred during the thirteenth inelastic deformation cycle. The maximum load was about 8.7 kips to the north and 8.1 kips to the south.

Both the CMU wall and the clay masonry veneer essentially showed only rigid-body rocking and sliding, without noticeable flexural or shear deformations. The clay masonry veneer was irrelevant to the in-plane response of Specimen UT CMU 4, because the clay masonry veneer was placed on top of the shelf angle, and thereby underwent only rigid-body motions.

Figure 5-15 shows the curve of load versus sliding of the CMU wall. Comparison of Figure 5-13 and Figure 5-15 shows that as the inelastic deformation of the longitudinal reinforcing bars increases, base sliding becomes an increasingly important contribution to the total top displacement. Before fracture of the south longitudinal reinforcement, base sliding is about 80 % of 1.0 in. of the southward tip displacement (to the right in Figure 5-13 and Figure 5-15) and about 30 % of 1.0 in. of the northward displacement.

The curve for the width of the crack width at the base of the north end of the CMU wall is shown in Figure 5-16. After target displacement of 0.75 in., the crack does not completely close. This implies that in-plane flexural capacity is developed completely by the steel-steel couple of the longitudinal reinforcing bars. The curve for the width of the crack at the base of the CMU wall at the south end was similar to that at the north end. Toes of the CMU wall under the first 1.0 in. loading is shown in Figure 5-17 (south end) and Figure 5-18 (north end). The toes began to crack, and these cracks propagated while those toes were under flexural tension. The toe at the north end completely split during the first cycle of 0.75 in. of tip displacement, while the toe at the south end cracked but did not completely split until the testing ended.

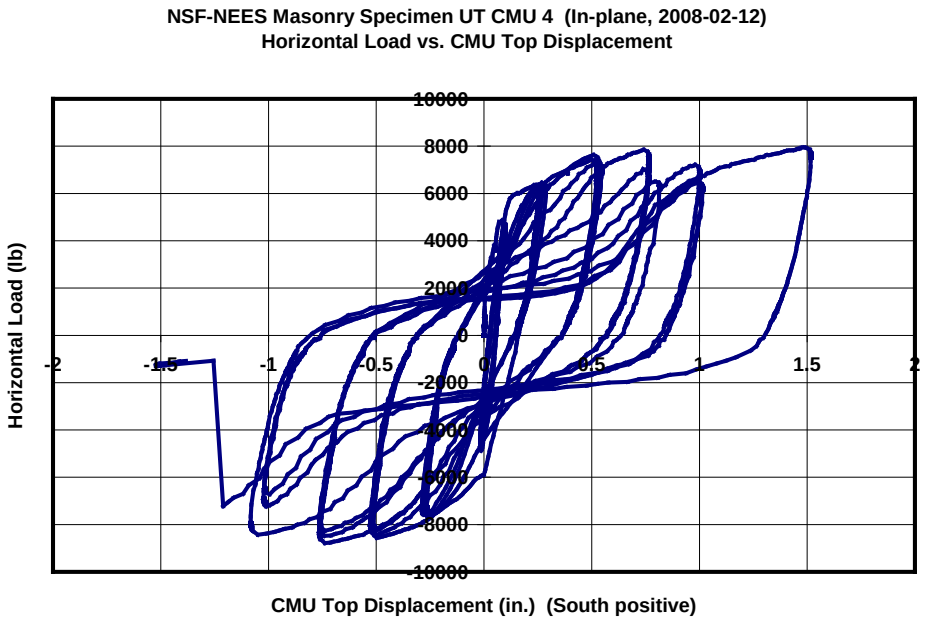

Figure 5-13 Load versus displacement at the top of CMU wall (Specimen UT CMU 4)

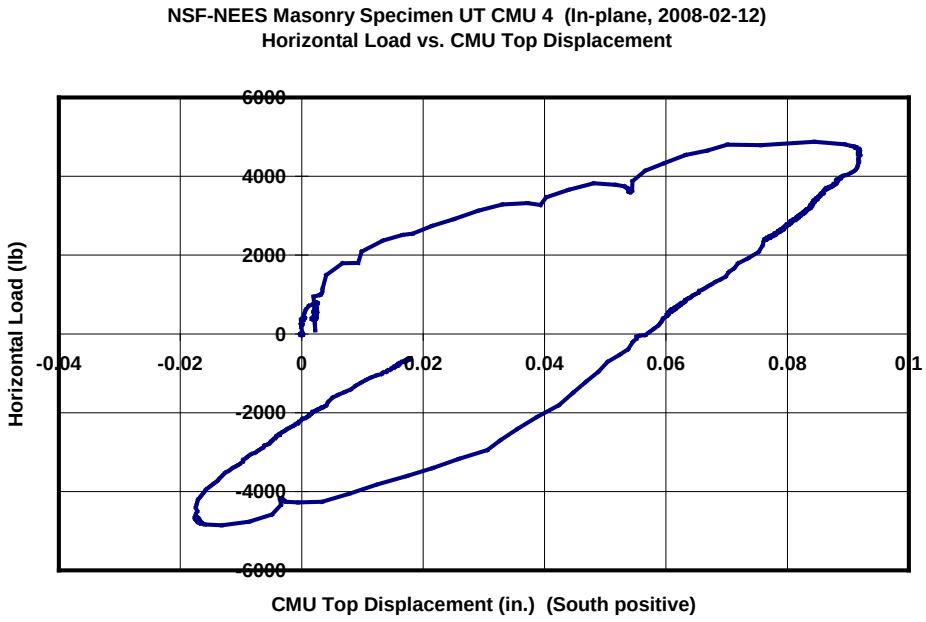

Figure 5-14 Part of load versus displacement at the top of CMU wall to check cracking load (Specimen UT CMU 4)

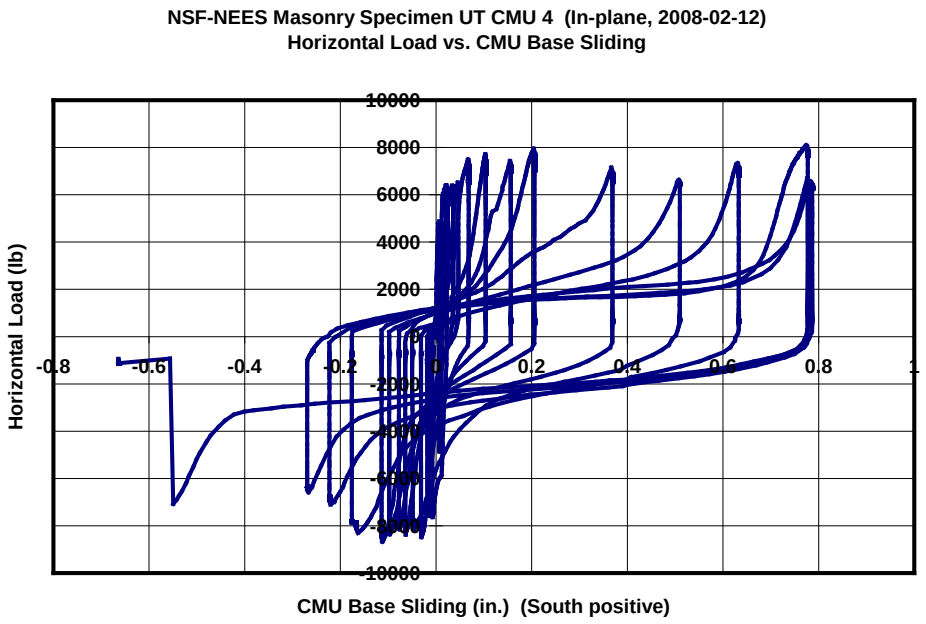

Figure 5-15 Base Sliding of CMU wall (Specimen UT CMU 4)

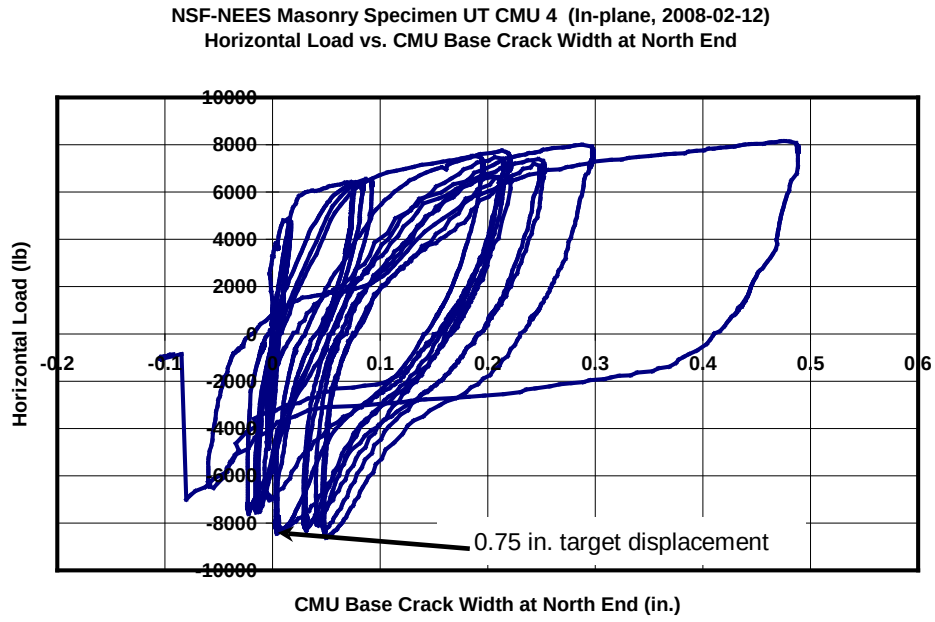

Figure 5-16 Width of crack at base of CMU wall at north end (Specimen UT CMU 4)

Figure 5-17 South end of CMU wall at the base under the first 1.0 in. loading to the north (Specimen UT CMU 4)

Figure 5-18 North end of CMU wall at the base under the first 1.0 in. loading to the north (Specimen UT CMU 4)

5.8 QUASI-STATIC, IN-PLANE TEST AND TEST RESULTS OF CMU WALL SPECIMEN UT CMU 4 MC

Specimen UT CMU 4 MC was subjected to three cycles of reversed loading at a load large enough to verify the cracking load, and then to repeated series of reversed cyclic loading to monotonically increasing displacement in increments of 0.25 in. (0.25 in., 0.50 in., 0.75 in. and 1.00 in.). Finally, the specimen was subjected to reversed cyclic loading of 1.50 in. displacement at the top of the CMU wall. Each cycle started with loading to the north (Figure 5-1). The curve of load versus displacement at the top of the CMU wall is shown in Figure 5-19. The overall hysteretic curve generally shows a shape similar to that of reinforcing bar under reversed cyclic axial loading, because the behavior of Specimen UT CMU 4 MC is primarily governed by the longitudinal reinforcement. The initial portion of the data is re-plotted in Figure 5-20 to check the cracking load. The cracking load is about 2.5 kips to the north (first loading direction) and 2.0 kips to the south. The yielding load is about 6.2 kips to the north and 5.6 kips to the south. The test was ended by fracture of the south longitudinal reinforcing bar at a tip displacement of 1.2 in. to the north after undergoing 1.0 in. to the south, corresponding to a drift ratio of

about 1.2 % and 1.0 % respectively. Fracture occurred during the thirteenth repeated reversed inelastic deformation cycle. The maximum load was about 8.2 kips to the north and 7.9 kips to the south.

Both the CMU wall and clay masonry veneer essentially showed only rigid-body rocking and sliding, with no noticeable flexural or shear deformations. The clay masonry veneer was irrelevant to the in-plane response of Specimen UT CMU 4 MC since the clay masonry veneer was placed on top of the shelf angle, and underwent only rigid-body motions.

Figure 5-21 shows the curve of load versus sliding of the CMU wall. Comparison of Figure 5-19 and Figure 5-21 shows that as the inelastic deformation of the longitudinal reinforcing bars increases, base sliding becomes an increasingly important contribution to the total top displacement. Before fracture of the south longitudinal reinforcing bar, base sliding is about 60 % of 1.0 in. of the southward tip displacement (to the right in Figure 5-19 and Figure 5-21) and about 30 % of 1.0 in. of the northward tip displacement.

The curve for the width of the crack at the base of the CMU wall at the north end is shown in Figure 5-22. After target displacements of 0.50 in., the crack does not completely close. This implies that in-plane flexural capacity is developed completely by the steel-steel couple of the longitudinal reinforcing bars. The curve for the width of the crack at the base of the CMU wall at the south end was similar to that at the north end. Toes of the CMU wall under the first 1.0 in. loading are shown in Figure 5-23 (south end) and Figure 5-24 (north end). The toe at the north end began to crack and propagated as it was under tensile force for flexural resistance. The toe at the north end completely split during the third cycle of 0.75 in. of tip displacement, while the toe at the south end did not crack until the testing ended.

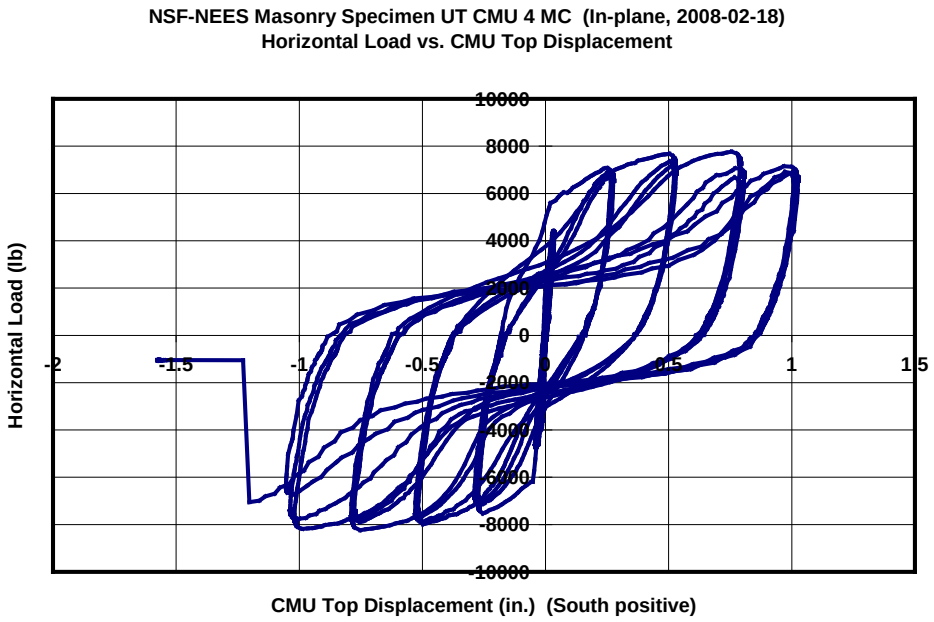

Figure 5-19 Load versus displacement at the top of CMU wall (Specimen UT CMU 4 MC)

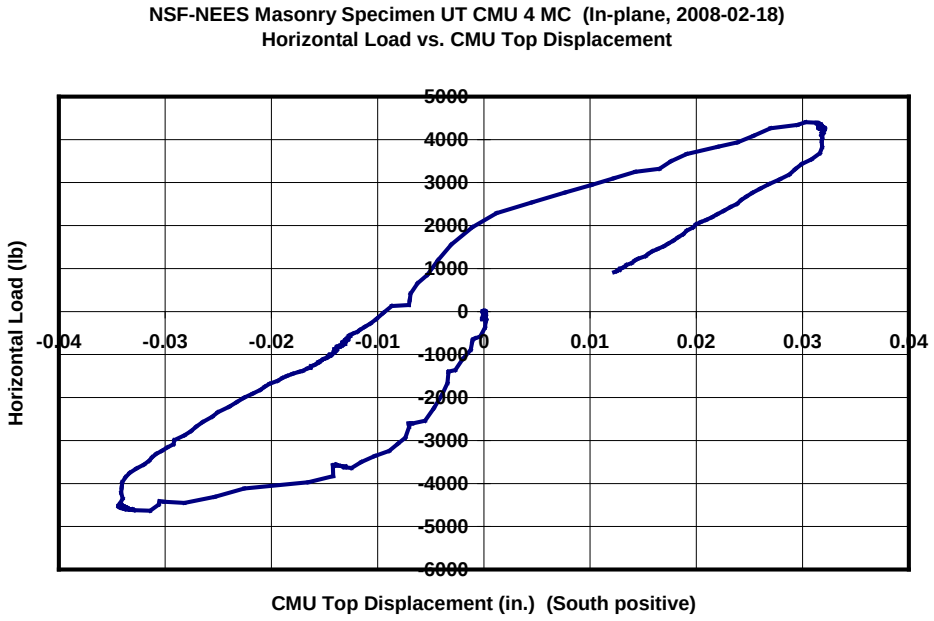

Figure 5-20 Part of load versus displacement at the top of CMU wall to check cracking load (Specimen UT CMU 4 MC)

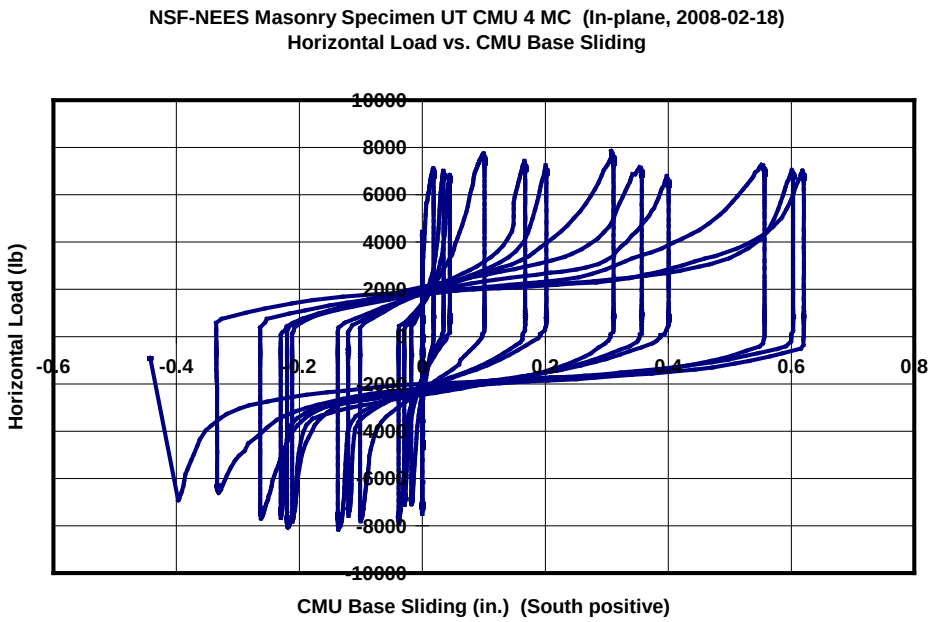

Figure 5-21 Base Sliding of CMU wall (Specimen UT CMU 4 MC)

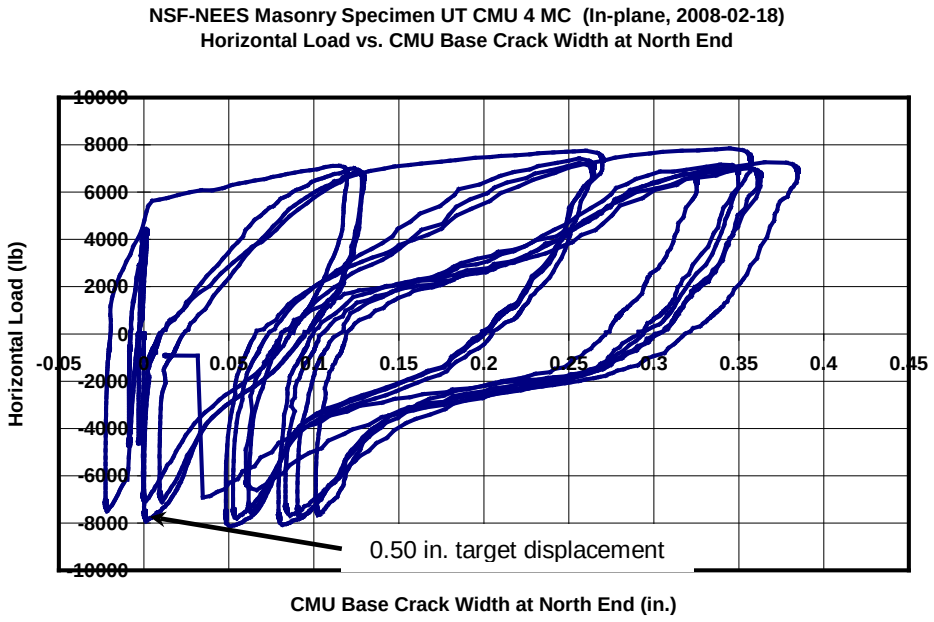

Figure 5-22 Width of crack at base of CMU wall at north end (Specimen UT CMU 4 MC)

Figure 5-23 South end of CMU wall at the base under the first 1.0 in. loading to the north (Specimen UT CMU 4 MC)

Figure 5-24 North end of CMU wall at the base under the first 1.0 in. loading to the north (Specimen UT CMU 4 MC)

5.9 SUMMARY OF AND OBSERVATIONS ON QUASI-STATIC, IN-PLANE TESTS OF CMU WALL SPECIMENS

All three quasi-static, in-plane CMU wall specimens responded essentially the same. Because the horizontal load was directly applied to the top of the CMU wall and the CMU wall was fully grouted, effects of differences in connectors and mortar are negligible. The vertical reinforcement governed the hysteretic behavior, yielding load and the maximum load of the CMU wall specimens for quasi-static, in-plane testing. In each such specimen, one No. 4 bar was placed at each wall end. Accordingly, the overall hysteretic curve (top displacement versus top horizontal load) of the CMU wall specimens generally showed a shape similar to that of simple reinforcing bars under reversed axial loading. The quasi-static, in-plane tests of the CMU wall specimens primarily provide information on the behavior of the vertical reinforcement within the CMU wall. The quasi-static, in-plane test results of the CMU wall specimens are summarized in Table 5-3.

Table 5-3 Summary of quasi-static, in-plane test results of CMU wall specimens

specimen		UT CMU 3	UT CMU 4	UT CMU 4 MC
nominal load		5.3 kips (based on nominal f_y = 60 ksi)		
yielding load	**measured**	5.6 kips (to the north) 6.3 kips (to the south)	6.0 kips (to the north) 5.9 kips (to the south)	6.2 kips (to the north) 5.6 kips (to the south)
	expected	5.7 kips (based on tested f_y = 64 ksi in Table 3-1)		
maximum load	**measured**	7.7 kips (to the north) 8.4 kips (to the south)	8.7 kips (to the north) 8.1 kips (to the south)	8.2 kips (to the north) 7.9 kips (to the south)
	expected	8.1 kips (based on tested f_u = 92 ksi in Table 3-1)		
maximum top displacement		1.0 in. (to the north) 1.0 in. (to the south)	1.2 in. (to the north) 1.5 in. (to the south)	1.2 in. (to the north) 1.0 in. (to the south)
base sliding at 1.0 in. of top displacement		0.5 in. (to the north) 0.3 in. (to the south)	0.3 in. (to the north) 0.8 in. (to the south)	0.3 in. (to the north) 0.6 in. (to the south)
maximum sliding before fracture of vertical reinforcement		0.5 in. (to the north) 0.3 in. (to the south)	0.6 in. (to the north) 0.8 in. (to the south)	0.4 in. (to the north) 0.6 in. (to the south)
sliding at fracture of vertical reinforcement		0.3 in. (to the south)	0.6 in.(to the north)	0.4 in. (to the north)
first loading direction		north	south	north
location of fractured vertical reinforcement		north end	south end	south end
top displacement at fracture of vertical reinforcement		1.0 in. (to the south)	1.2 in. (to the north)	1.2 in. (to the north)
toe cracking		none	at the north at the south	at the north

5.9.1 Toe Cracking of CMU Walls

In specimen UT CMU 2 and UT CMU 2 MC, the toes of the CMU wall cracked and sometimes completely split as shown in Figure 5-17, Figure 5-18 and Figure 5-24. The start, propagation and opening-up of this toe cracking always happened when the toe was in tension, not in compression. Therefore, toe cracking and splitting are believed to have been caused by the vertical reinforcement prying off the masonry at the toe, in dowel action.

5.9.2 Coupled Flexural and Sliding Behaviors in CMU Walls

Contrary to the expectation that the top displacement of the CMU wall would be governed by flexure only (rocking at the base), base sliding also contributed to the top displacement after some inelastic cyclic loading. Before about 0.5 in. of top displacement, the top displacement essentially came from rocking of the CMU wall at the base. The base sliding based on friction sliding resistance (even the base sliding based on the shear resistance of the vertical bars) was not expected due to the CMU wall's relatively low flexural capacity. After about 0.5 in. of top displacement, however, base sliding began to be significant as shown in Figure 5-25 through Figure 5-27. The 0.5 in. of top displacement corresponds to the about 0.25 in. of crack width at the base. This implies that rocking and base sliding began to be coupled after about 0.25 in. of crack width at the base. At about 1.0 in. of top displacement, the contribution of the base sliding to the top displacement ranged between 30 % and 80 %, which correspond to 0.3 in. and 0.8 in. of base sliding respectively (refer to Table 5-3). Vertical reinforcement fractured soon after the specimen reached about 1.0 in. of top displacement.

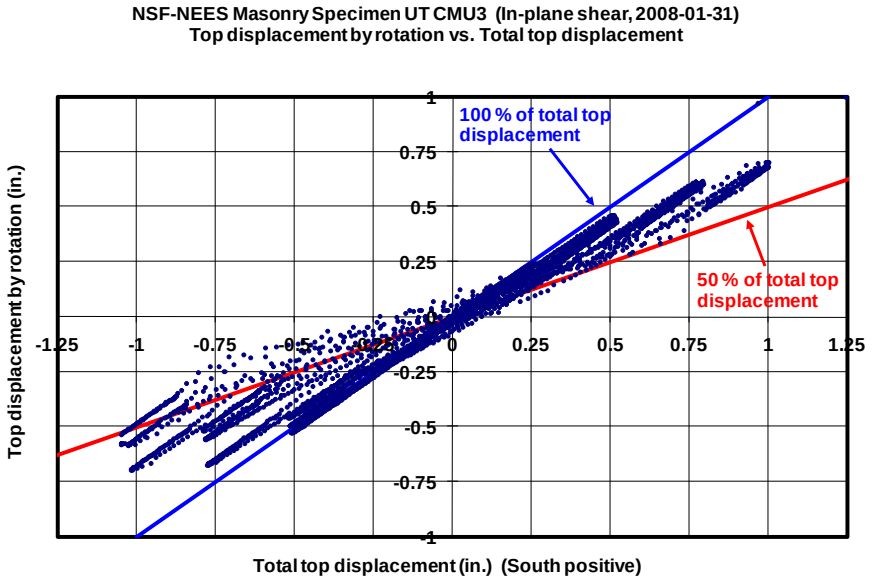

Figure 5-25 Top displacement from rotation versus total top displacement (UT CMU 3)

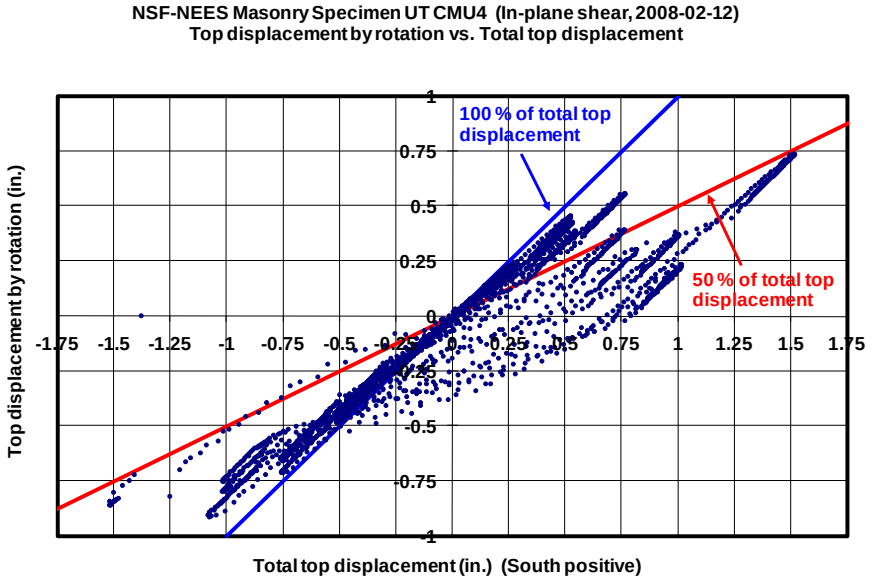

Figure 5-26 Top displacement from rotation versus total top displacement (UT CMU 4)

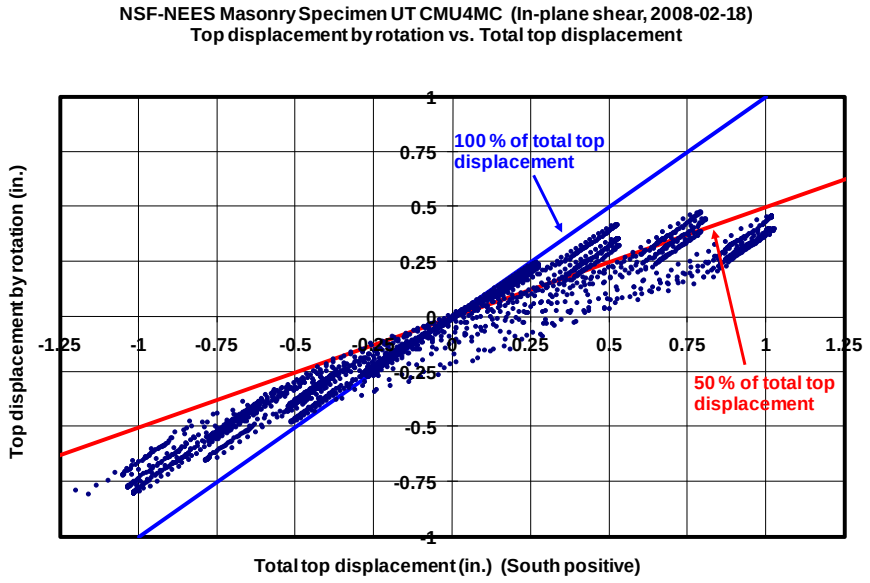

Figure 5-27 Top displacement from rotation versus total top displacement (UT CMU 4 MC)

5.9.3 Rigid-body Rotation (Rocking) of CMU Walls

To verify the assumption that the flexural deformation of the CMU wall can be idealized as a rigid body rotating at the base, the base rotation (θ_{base}) was calculated using two methods. For the first method, the top displacement (Channel 1) and the base sliding (Channel 14) were used as below:

$$\theta_{base} = \frac{\Delta_{Channel\ 1} - \Delta_{Channel\ 14}}{94\ in.},$$

where 94 in. is the vertical distance from the bottom of the CMU wall to the measuring location of the top displacement (Channel 1). For the second method, the vertical displacements (Channel 8 and Channel 4) at the base of each wall end were used as below:

$$\theta_{base} = \frac{\Delta_{Channel\ 8} - \Delta_{Channel\ 4}}{48\ in.},$$

where 48 in. is the plan length of the CMU wall. Channel locations are shown in Figure 5-4. The curve of base moment versus base rotation is shown in Figure 5-28 (for UT CMU 3), Figure 5-29 (for UT CMU 4) and Figure 5-30 (for UT CMU 4 MC). All the figures display good matches between the rotations calculated by two methods, implying that the flexural behavior of the CMU wall can be represented by a rigid body that rotates at the base. In addition, the measurements at Channels 5 through 11 for flexural deformation were negligible compared to those at Channels 4 and 8 for the width of the crack at the base of the CMU wall.

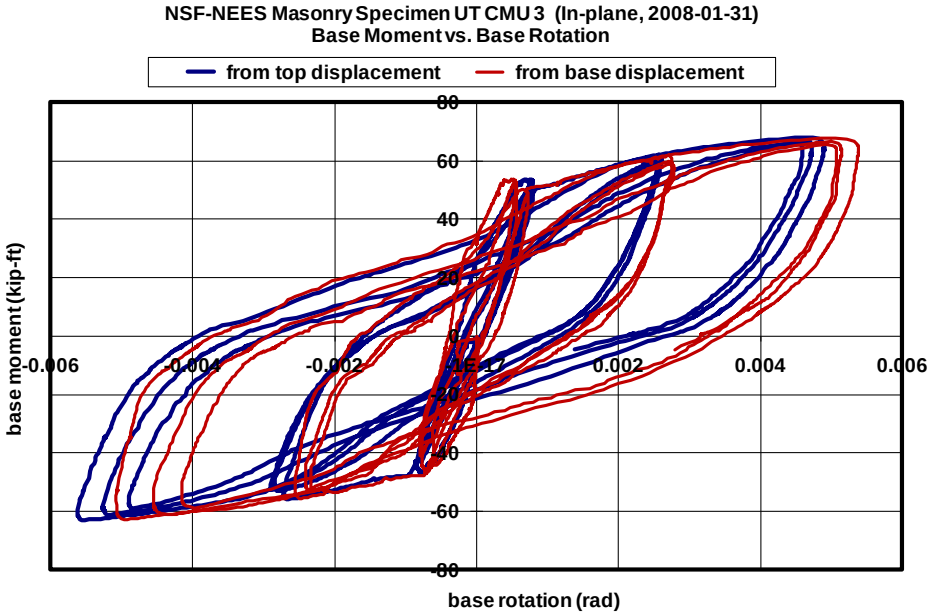

Figure 5-28 Base moment versus base rotation (UT CMU 3)

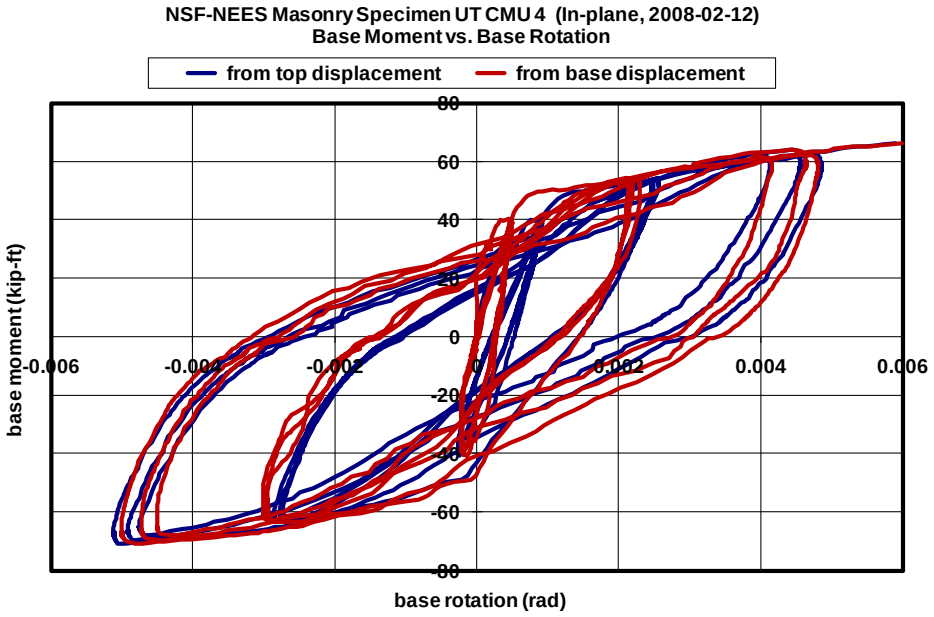

Figure 5-29 Base moment versus base rotation (UT CMU 4)

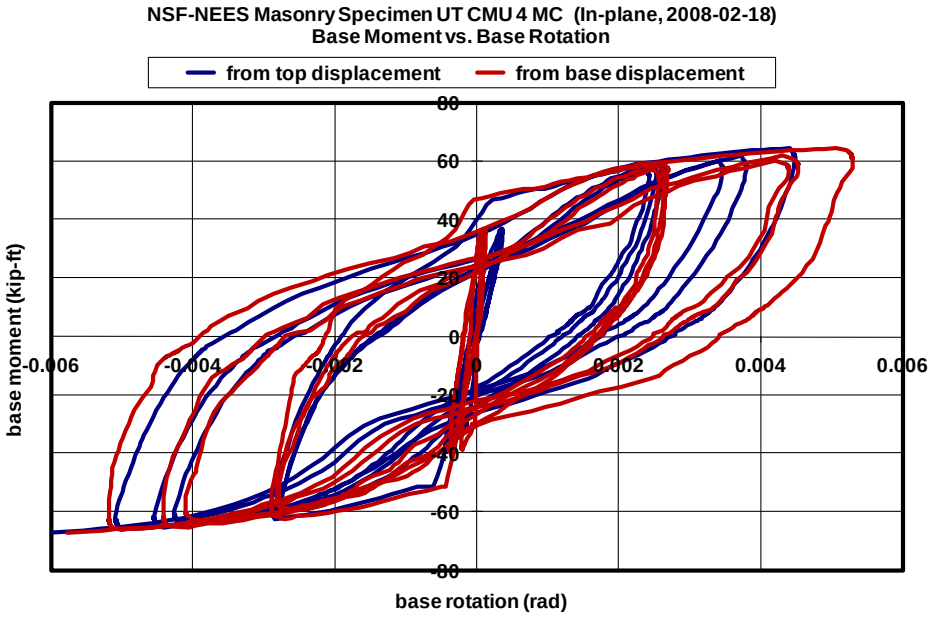

Figure 5-30 Base moment versus base rotation (UT CMU 4 MC)

5.9.4 Yielding of Vertical Reinforcement and Corresponding Width of Crack at Base of CMU Walls

Based on the test results (Figure 5-7, Figure 5-13 and Figure 5-19) of the CMU wall specimen for quasi-static, in-plane loading, the width of the crack at the base of the CMU walls corresponding to yielding of the vertical reinforcement was about 0.025 in.

5.9.5 Rotational (rocking) Limit of CMU Walls at the Base

Fracture of vertical reinforcement under in-plane flexure depends on the width of the crack at the vertical reinforcement, rather than on the rotation of the CMU wall itself. Consequently, to determine the base rotation limited by fracture of the vertical reinforcement, we first need to know the width of the crack at the base (vertical gap) that vertical reinforcement can develop without fracture. Based on Figure 5-31 through Figure 5-33, a conservative limit can be set as 0.4 in. Note that the vertical reinforcement was under significant shear as well as significant tension. Assuming that the acceptable crack width is proportional to the elongation, the allowable crack width for general application is about

$$0.4\ in. \times \frac{9\ \%}{14\ \%} = 0.25\ in.\ ,$$

where 14 % is the average elongation of the reinforcement used in the quasi-static testing (Table 3-7), and 9 % is the minimum elongation of ASTM A615 (Grade 60, No.4). Then, for the CMU wall specimens tested in this research, the nominal base rotation limited by fracture of the vertical reinforcement would be about

$$\frac{0.25\ in.}{44\ in.} = 0.00575\ rad\ ,$$

where 44 in. comes from 4 ft (length of the CMU walls) minus the in-plane concrete masonry cover to the vertical reinforcement.

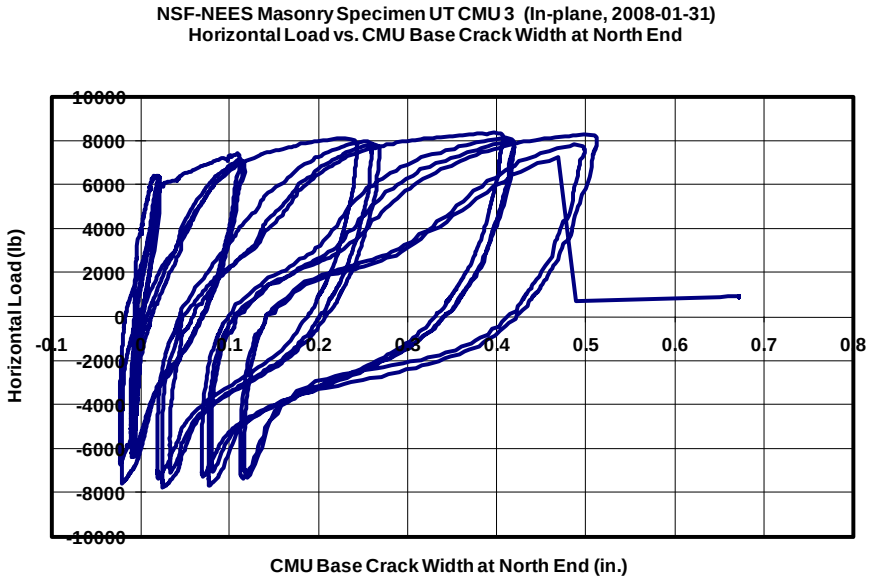

Figure 5-31 Width of crack at base of CMU wall at north end (Specimen UT CMU 3)

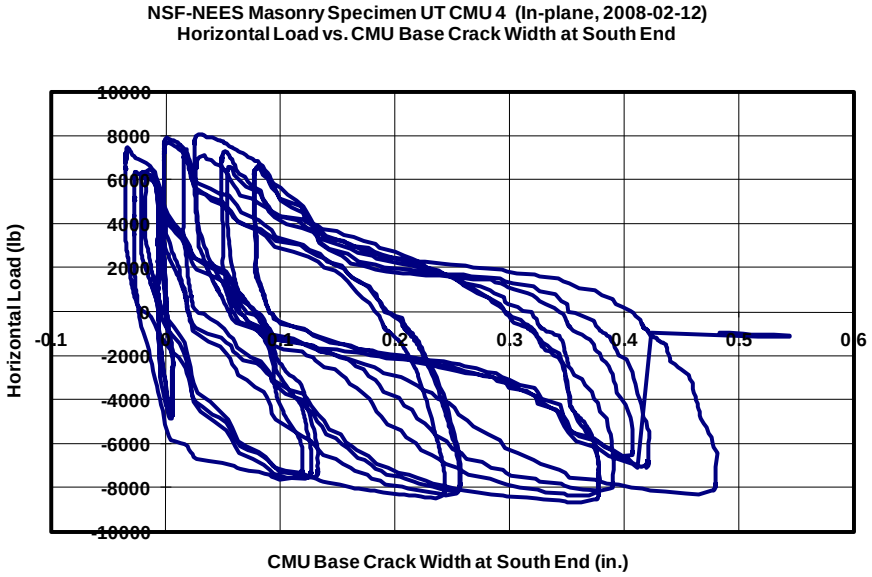

Figure 5-32 Width of crack at base of CMU wall at south end (Specimen UT CMU 4)

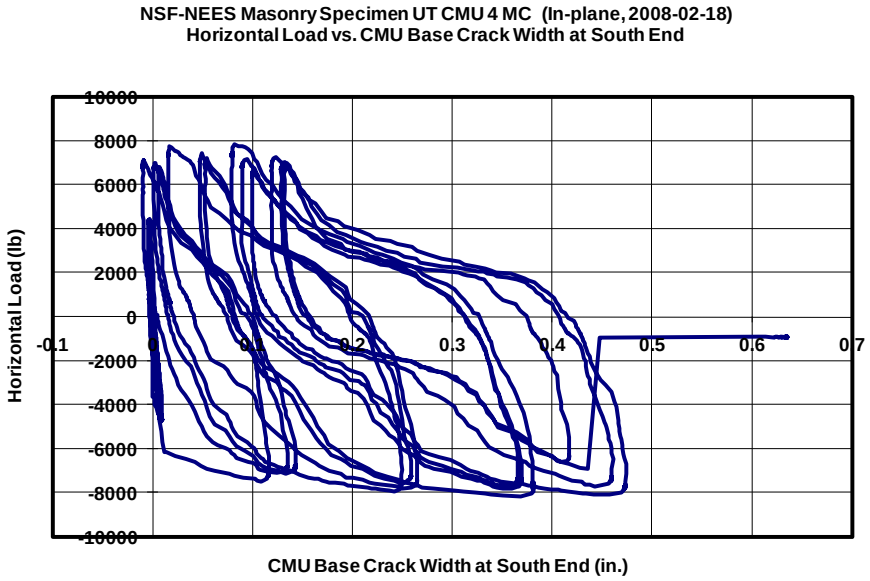

Figure 5-33 Width of crack at base of CMU wall at south end (Specimen UT CMU 4 MC)

CHAPTER 6
Shake-table Tests of CMU Wall Specimens, Out-of-plane and In-plane

As part of the NSF NEES masonry project, shake-table testing of six reinforced concrete masonry wall specimens with clay masonry veneer (CMU wall specimens) was conducted at the University of California at San Diego (UCSD). Three of those six specimens were tested under out-of-plane loading, and the other three under in-plane loading. In this chapter, the shake-table tests of those six CMU wall specimens are briefly described. Details will be provided in the PhD dissertation now being prepared by Hussein Okail at UCSD. The CMU wall specimens used for shake-table testing were constructed using the same design (Appendix A) as for quasi-static testing, except for the type of clay masonry units (refer to Section 6.1).

In the following sections, the six CMU wall specimens for shake-table testing are overviewed first. Then, the two ground motions used for shake-table testing are described. Finally, the shake-table test results of the six CMU wall specimens (three for out-of-plane testing and three for in-plane testing) are summarized.

The main purpose of out-of-plane, shake-table testing of the CMU wall specimens is to study out-of-plane response of the CMU walls with clay masonry veneer, and to provide experimental data to develop analytical models for out-of-plane responses of CMU walls and connectors. For out-of-plane responses, those models will focus on the flexural deformation of the CMU walls at mid-height, the yielding of the vertical bars in the CMU walls at mid-height, and the collapse of the clay masonry veneer by axial failure of the connectors. The clay masonry veneer will be considered as mass only for out-of-plane response. Since the out-of-plane flexural stiffness of the clay masonry veneer before cracking is small compared to the out-of-plane flexural stiffness of the

CMU walls, the out-of-plane veneer essentially acts as attached mass only, provided that the out-of-plane connectors continue to securely connect the veneer to the CMU walls.

The main purpose of in-plane, shake-table testing of the CMU wall specimens is to study in-plane response of the CMU walls with clay masonry veneer, and to provide experimental data to develop analytical models for in-plane responses of clay masonry veneer and connectors. For in-plane responses, those models will focus on rocking and sliding of the clay masonry veneer, and collapse of the clay masonry veneer by in-plane failure of the connectors. The in-plane response of the CMU walls is not of concern in shake-table testing of the CMU walls specimens because the mass of the specimens was so small that the in-plane response of the CMU wall was essentially rigid.

6.1 OVERVIEW OF SHAKE-TABLE CMU WALL SPECIMENS, OUT-OF-PLANE (UCSD CMU 1, 2, 2 MC) AND IN-PLANE (UCSD CMU 3, 4, 4 MC)

Shake-table testing of six reinforced concrete masonry wall specimens with clay masonry veneer (CMU wall specimens) was conducted at University of California at San Diego. The overview of those shake-table wall specimens is provided in Table 6-1, and the design drawings are shown in Appendix A. Shake-table specimens were constructed with the same design as quasi-static specimens, except for the type of clay masonry units: ASTM C652 for quasi-static testing and ASTM C216 for shake-table testing. The structural difference between each type of clay masonry unit is a difference of about 10 % in the out-of-plane moment of inertia, due to differences in permitted void area. These differences in moment of inertia change the predicted cracking strength by about the same 10%. In low-rise concrete masonry buildings with clay masonry, however, the flexural cracking of clay masonry veneer is not of importance, due to the building's structural characteristics. The out-of-plane response of CMU walls with clay masonry veneer is generally governed either by the connectors or the CMU walls, and the in-plane response is generally governed by rocking or sliding of the CMU walls and the veneer.

Like the quasi-static test specimens, the differences between UCSD CMU 1 and UCSD CMU 2 (or UCSD CMU 3 and UCSD CMU 4) is the type of connectors, and the difference between UCSD CMU 2 and UCSD CMU 2 MC (or UCSD CMU 4 and UCSD CMU 4 MC) is the cementitious system used in the mortar.

Table 6-1 Overview of shake-table CMU wall specimens

specimens	loading	dimensions	reinforcement	connectors	mortar
UCSD CMU 1	out-of-plane, table-shaking	8-ft wide 8-ft high	five No. 4 bars vertically and three No. 4 bars horizontally	double eye-and-pintle	cement-lime
UCSD CMU 2				tri-wire	cement-lime
UCSD CMU 2 MC				tri-wire	masonry cement
UCSD CMU 3	in-plane, table-shaking	4-ft wide 8-ft high	two No. 4 bars vertically and three No. 4 bars horizontally	double eye-and-pintle	cement-lime
UCSD CMU 4				tri-wire	cement-lime
UCSD CMU 4 MC				tri-wire	masonry cement

6.2 GROUND MOTIONS USED FOR SHAKE-TABLE TESTING

Shake-table testing was conducted using the Sylmar ground motion (Figure 6-1) and the Tarzana ground motion (Figure 6-2), both of which were recorded during the 1994 Northridge earthquake. Those records have total durations of 40 seconds for Sylmar and 60 seconds for Tarzana, and those total durations were used for each shake-table test. Because the ground accelerations from those records are negligible after the first 15 seconds for Sylmar and after the first 25 seconds for Tarzana, only those initial portions are shown in Figure 6-1 and Figure 6-2. In the analytical study of CMU wall specimens (Chapter 9) and in the analytical study of the CMU building specimen (Chapter 10), only the initial 15 seconds of the Sylmar record and the initial 25 seconds of the Tarzana record were used, because the responses thereafter were negligible.

The Sylmar record has a peak ground acceleration of 0.84 g in one direction and 0.59 g in the other. The Tarzana record has a peak ground acceleration of 1.79 g in one direction and 1.59 g in the other. The Tarzana record is atypically rich in high-frequency content, and has a higher ratio than Sylmar of peak ground acceleration to peak ground velocity or peak ground displacement. The Tarzana record was used precisely to permit the shaking table to apply higher peak ground accelerations without exceeding its velocity or displacement limits.

In Figure 6-3 are shown the response spectra for ASCE 7-05 SDC D, ASCE 7-05 SDC E, original 80 % Sylmar, and a table feedback for 80 % Sylmar. The response spectra will be described in detail in the PhD dissertation now being prepared by Hussein Okail at UCSD. It is briefly summarized in this section. The damping ratio of 5 % was used for the calculation of the spectral values. The most important aspect in the experimental work of this research was the behavior of the CMU building specimen (representing low-rise CMU buildings). The fundamental period for the CMU building specimen was estimated as about 0.03 sec based on

$$T = 2\pi \sqrt{\frac{k}{m}} \ ,$$

where k was calculated using the uncracked elastic properties of the CMU walls considering flexural deformation and shear deformation, and m was calculated as the sum of the mass of the roof diaphragm (including the additional weight of 19.5 kips), half the CMU walls, and half the clay masonry veneer. The spectral values for SDC D were picked based on a location in the East Coast, while those for SDC E were for a location in California using Figures 22-1 and 22-2 in ASCE 7-05. It was decided that the values of S_s would be the same for SDC D and SDC E, while those of S_1 would differ. The value of Ss selected is on the high side for either region but not the maximum expected for the West Coast to have a broader representation. For the period range of interest (around 0.03 sec), SDC D has a higher demand than SDC E due to the procedure used to obtain the response spectrum given in ASCE 7-05. Since the ground motion for SDC E has to

cover both SDC D and SDC E, the Sylmar record was scaled for ASCE 7-05 SDC D. For better estimation, the feedback of the shake table was evaluated, and it was determined the design basis earthquake (DBE) for SDC E (ASCE7-05) corresponded to 80 % of the Sylmar record Figure 6-3), or to 36 % of the Tarzana record. The maximum considered earthquake (MCE), approximately 1.5 times DBE, corresponded to 120 % of the Sylmar record and 54 % of the Tarzana record. These scaling factors were consistently applied in the CMU wall specimens because those specimens are the fundamental structural components of low-rise CMU buildings.

Shake-table testing of each specimen started with different scaled multiples of the acceleration history of the Sylmar record. After reaching the displacement and velocity capacity of the shaking table (before the specimen was severely damaged), testing switched to the scaled Tarzana record.

The ground motions applied to each CMU wall specimen are listed in Table 6-2, where white noise had peak ground acceleration (PGA) of 0.03g and swept a frequency range of 1 – 33 Hz. White noise was used to assess the dynamic properties of each specimen and to track the progression of damage. For shake-table testing of the CMU wall specimens, two specimens were mounted on the table (one out-of-plane specimen and one in-plane specimen). Consequently, the same shaking was applied to Specimen UCSD CMU 1 and Specimen UCSD CMU 3; to UCSD CMU 2 and UCSD CMU 4; and to UCSD CMU 2 MC and UCSD CMU 4 MC.

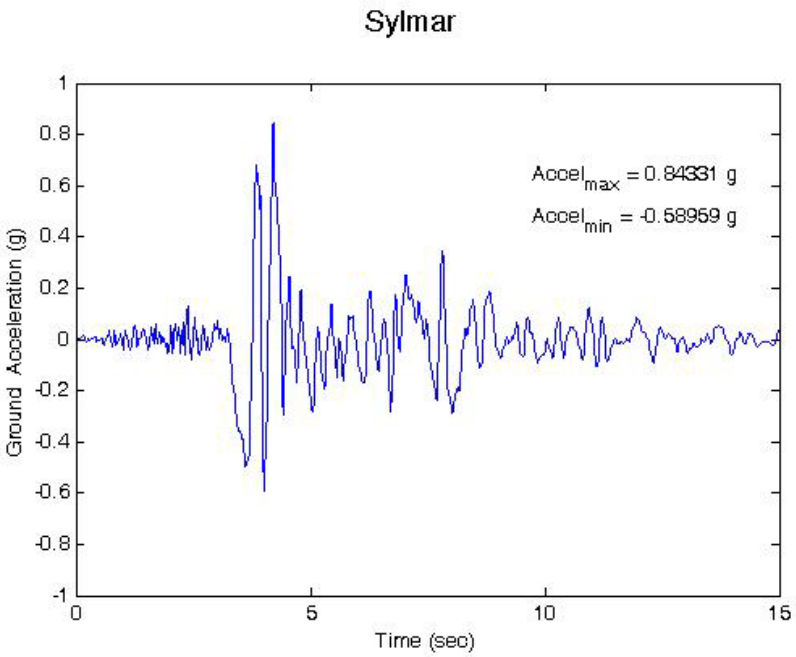

Figure 6-1 Sylmar record used for shake-table testing

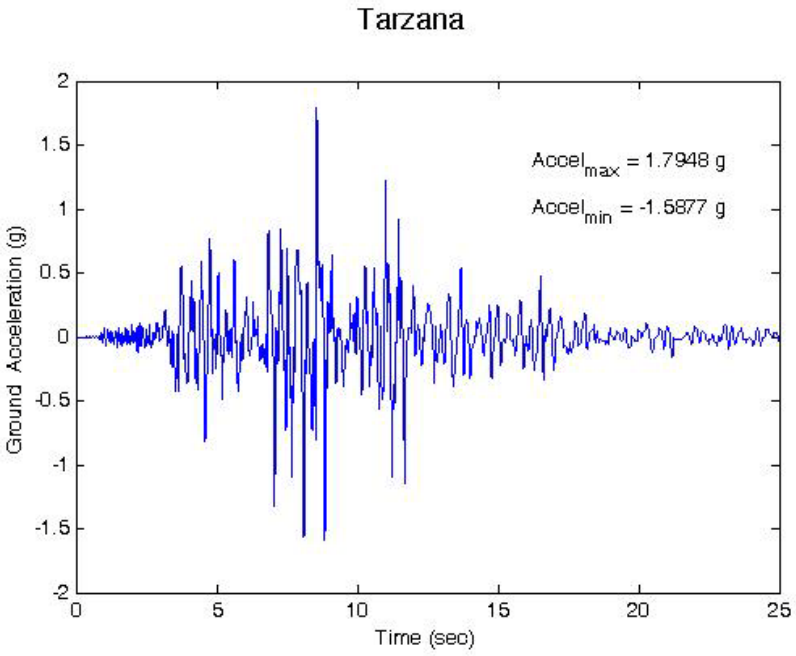

Figure 6-2 Tarzana record used for shake-table testing

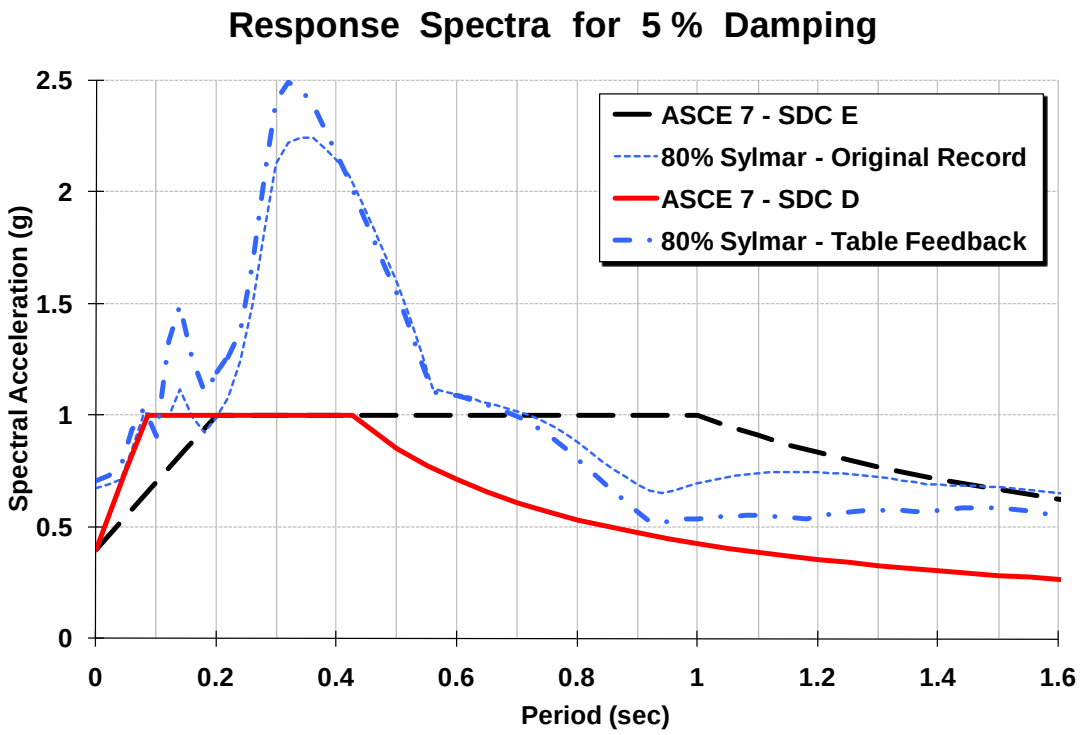

Figure 6-3 Response spectra for 5 % damping

Table 6-2 Target ground motions applied to each CMU wall specimen for shake-table testing

specimen / ground motion	UCSD CMU 1 UCSD CMU 3	UCSD CMU 2 UCSD CMU 4	UCSD CMU 2 MC UCSD CMU 4 MC
white noise	o	o	o
Sylmar 20 %	o	o	o
Sylmar 40 %	o	o	o
white noise		o	
Sylmar 80 % (DBE for SDC E)	o	o	o
white noise	o	o	o
Sylmar 100 %	o	o	o
white noise	o	o	o
Sylmar 125 % (MCE for SDC E)	o	o	o
white noise	o	o	o
Sylmar 150 %	o	o	o
white noise	o	o	o
Tarzana 70 %	o		o
white noise	o		o
Tarzana 100 %	o	o	o
white noise	o	o	o
Tarzana 125 %	o		o
white noise	o		o
Tarzana 150 %	o	o	o

6.3 SUMMARY OF SHAKE-TABLE, OUT-OF-PLANE TESTS OF CMU WALL SPECIMENS (UCSD CMU 1, 2, 2 MC)

A typical concrete masonry wall specimen (CMU wall specimen) with the associated test setup for shake-table, out-of-plane testing is shown in Figure 6-4. Key aspects and behaviors of CMU wall specimens for shake-table, out-of-plane loading are listed in Table 6-3. For Tarzana 125 % and Tarzana 150 %, where key behaviors were

observed, the measured PGA is listed in Table 6-4. The table output motions were about 10 to 20 % higher than the target ground motions at Tarzana 125 % and Tarzana 150 %.

The maximum responses in each direction (displacement and acceleration) of CMU walls and clay masonry veneer are listed in Table 6-5, Table 6-6 and Table 6-7. The positive direction is to the east (Figure 6-4). The responses at the top and at mid-height in Table 6-5, Table 6-6 and Table 6-7 were measured at the top row of connectors (88 in. from the base) and at the third row of connectors from the base (40 in. from the base), respectively. Typical response history near the mid-height (40 in. from the base) for the Sylmar record is shown in Figure 6-5 through Figure 6-8, using the data of UCSD CMU 1 at Sylmar 125 %. A typical response history near the mid-height (40 in. from the base) for the Tarzana record is shown in Figure 6-9 through Figure 6-12, using the data of UCSD CMU 1 at Tarzana 100 %.

In low-rise concrete masonry buildings with clay masonry veneer, the important behaviors of the out-of-plane CMU walls with clay masonry veneer (walls oriented perpendicular to the ground shaking) are the response of the CMU walls and the connectors. Because the clay masonry veneer, before and after cracking, is very flexible out-of-plane compared to the CMU walls, the out-of-plane veneer essentially acts as attached mass only, provided that the out-of-plane connectors continue to securely connect it to the CMU walls. When the out-of-plane connectors fail, the veneer generally collapses out of plane.

For the response of the CMU walls, yielding of the vertical reinforcement can be used to qualitatively assess the flexural behavior of the CMU walls. For the response of the connectors, failure (fracture) of the connectors can be used to qualitatively assess the axial behavior of the connectors.

Yielding of the reinforcement at the mid-height was observed in two of the three specimens (UCSD CMU 1 and UCSD CMU 2 MC). In Specimen UCSD CMU 2, the top support failed. The target ground motions at which the vertical reinforcement at mid-height first yielded are included in Table 6-3. Due to the absence of strain gages at the base of the CMU walls, the yielding of the vertical reinforcement at the base could not be

checked directly. Yielding of the vertical reinforcement at the base was, however, believed to have occurred at a low level of shaking, considering the relatively flexible support condition at the top of the CMU walls (based on test data).

Failure of connectors was observed in two of the three specimens (UCSD CMU 1 and UCSD CMU 2 MC). In UCSD CMU 2, the top support failed. The target ground motions at which the failure of the connectors first occurred are included in Table 6-3. Double eye-and-pintle connectors (UCSD CMU 1) failed by the top row of pintles pulling out of the eyes. This is consistent with the observed behavior of the corresponding quasi-static specimens, even though the two types of specimens were not loaded identically. Tri-wire connectors (UCSD CMU 2 MC) failed by fracture of cross-wires at weld points. It is believed that the connector fracture was caused by low-cycle fatigue, as in quasi-static, out-of-plane testing.

Table 6-3 Key aspects and behaviors of CMU wall specimens for shake-table, out-of-plane loading

specimen	UCSD CMU 1	UCSD CMU 2	UCSD CMU 2 MC
type of connectors	double eye-and-pintles	tri-wire	tri-wire
type of mortar	cement-lime	cement-lime	masonry cement
ground motion at yielding of CMU walls at the mid-height	Tarzana 125 %	top support failure at Tarzana 150 %	Tarzana 150 %
ground motion at connector failure	Tarzana 150 % (pintles pulling out of eyes at the top row)		Tarzana 150 % (fracture of crossing wires at welding)

Figure 6-4 Typical shake-table, out-of-plane CMU wall specimen with test setup

Table 6-4 Measured PGA for target ground motion Tarzana 125% and Tarzana 150 %

target ground motion	measured PGA (g)					
	UCSD CMU 1 UCSD CMU 3		UCSD CMU 2 UCSD CMU 4		UCSD CMU 2 MC UCSD CMU 4 MC	
	max	min	max	min	max	min
Tarzana 125 % (max: 1.99 g, min: - 2.24 g)	2.33	- 2.51	no testing		2.29	- 2.48
Tarzana 150 % (max: 2.39 g, min: - 2.69 g)	2.76	- 3.02	2.77	- 2.93	2.79	- 2.94

positive direction: to the east

Table 6-5 Shake-table, out-of-plane test results of UCSD CMU 1

ground motion			PGA (g), measured	acceleration (g)				displacement (in.)			
				CMU		veneer		CMU		veneer	
				mid-height *	top **	mid-height *	top **	mid-height *	top **	mid-height *	top **
Sylmar	80%	max	0.78	0.89	1.26	0.98	1.57	0.10	0.21	0.10	0.24
		min	-0.54	-0.82	-1.20	-0.88	-1.95	-0.11	-0.25	-0.12	-0.28
	100%	max	1.03	1.32	1.66	1.36	2.20	0.16	0.37	0.17	0.41
		min	-0.66	-1.04	-1.67	-1.16	-2.27	-0.18	-0.41	-0.19	-0.43
	125%	max	1.35	1.77	2.31	1.85	3.13	0.23	0.53	0.26	0.59
		min	-0.84	-1.44	-2.19	-1.47	-3.17	-0.28	-0.62	-0.30	-0.67
	150%	max	1.66	2.29	3.01	2.47	3.94	0.31	0.72	0.35	0.80
		min	-0.99	-2.21	-2.84	-2.18	-3.74	-0.34	-0.75	-0.37	-0.80
Tarzana	70%	max	1.29	1.83	2.61	1.74	3.98	0.33	0.74	0.36	0.83
		min	-1.42	-2.00	-2.94	-2.30	-4.46	-0.29	-0.63	-0.31	-0.68
	100%	max	1.88	2.21	3.88	2.77	4.37	0.48	1.04	0.54	1.17
		min	-2.00	-3.03	-4.75	-3.58	-5.29	-0.43	-0.86	-0.46	-0.93
	125%	max	2.33	3.93	4.53	5.60	5.50	0.82	1.24	0.91	1.59
		min	-2.51	-4.86	-5.36	-6.14	-6.37	-0.67	-0.95	-0.73	-1.07
	150%	max	2.76	-	-	-	-	-	-	-	-
		min	-3.02	-	-	-	-	-	-	-	-

positive direction: to the east

** mid-height: at the third row of connectors from the base (40 in. from the base)*

*** top: at the top row of connectors (88 in. from the base)*

Table 6-6 Shake-table, out-of-plane test results of UCSD CMU 2

ground motion			PGA (g), measured	acceleration (g)				displacement (in.)			
				CMU		veneer		CMU		veneer	
				mid-height *	top **	mid-height *	top **	mid-height *	top **	mid-height *	top **
Sylmar	80%	max	0.95	0.97	1.17	0.97	1.21	0.13	0.31	0.14	0.30
		min	-0.55	-0.82	-1.30	-0.82	-1.43	-0.12	-0.28	-0.12	-0.27
	100%	max	1.07	1.38	1.95	1.57	2.98	0.18	0.41	0.19	0.40
		min	-0.68	-1.04	-2.04	-1.18	-3.25	-0.20	-0.46	-0.20	-0.45
	125%	max	1.33	1.68	2.24	2.44	3.23	0.28	0.64	0.28	0.63
		min	-0.88	-1.38	-2.49	-1.55	-3.70	-0.31	-0.68	-0.32	-0.69
	150%	max	1.63	2.16	3.23	2.29	3.97	0.37	0.82	0.38	0.82
		min	-1.00	-1.88	-2.99	-1.87	-4.25	-0.54	-1.20	-0.55	-1.20
Tarzana	70%	max	no test								
		min									
	100%	max	1.93	2.57	2.95	2.65	4.13	0.73	1.59	0.73	1.60
		min	-1.97	-2.40	-4.51	-2.80	-5.02	-0.68	-1.45	-0.68	-1.45
	125%	max	no test								
		min									
	150%	max	2.77	-	-	-	-	-	-	-	-
		min	-2.93	-	-	-	-	-	-	-	-

positive direction: to the east

** mid-height: at the third row of connectors from the base (40 in. from the base)*

*** top: at the top row of connectors (88 in. from the base)*

Table 6-7 Shake-table, out-of-plane test results of UCSD CMU 2 MC

ground motion			PGA (g), measured	acceleration (g)				displacement (in.)			
				CMU		veneer		CMU		veneer	
				mid-height *	top **	mid-height *	top **	mid-height *	top **	mid-height *	top **
Sylmar	80%	max	0.83	0.92	1.36	0.96	1.39	0.07	0.18	-	-
		min	-0.54	-0.89	-1.35	-0.94	-1.41	-0.07	-0.16	-	-
	100%	max	1.05	1.06	1.44	1.08	1.48	0.09	0.22	-	-
		min	-0.68	-1.09	-1.56	-1.11	-1.57	-0.08	-0.17	-	-
	125%	max	1.34	1.47	1.92	1.50	2.00	0.12	0.29	-	-
		min	-0.85	-1.42	-1.85	-1.47	-1.92	-0.12	-0.25	-	-
	150%	max	1.66	1.83	2.48	1.85	2.64	0.19	0.43	-	-
		min	-0.99	-1.79	-2.61	-1.90	-2.67	-0.16	-0.34	-	-
Tarzana	70%	max	1.30	2.15	3.60	2.62	4.10	0.22	0.49	-	-
		min	-1.36	-1.68	-2.98	-2.11	-3.27	-0.28	-0.59	-	-
	100%	max	1.91	2.37	3.27	2.58	3.47	0.27	0.58	-	-
		min	-2.02	-2.19	-3.08	-2.29	-3.25	-0.28	-0.63	-	-
	125%	max	2.29	5.13	4.63	-	-	-	-	-	-
		min	-2.47	-4.09	-6.13	-	-	-	-	-	-
	150%	max	2.79	-	-	-	-	-	-	-	-
		min	-2.94	-	-	-	-	-	-	-	-

positive direction: to the east

** mid-height: at the third row of connectors from the base (40 in. from the base)*

*** top: at the top row of connectors (88 in. from the base)*

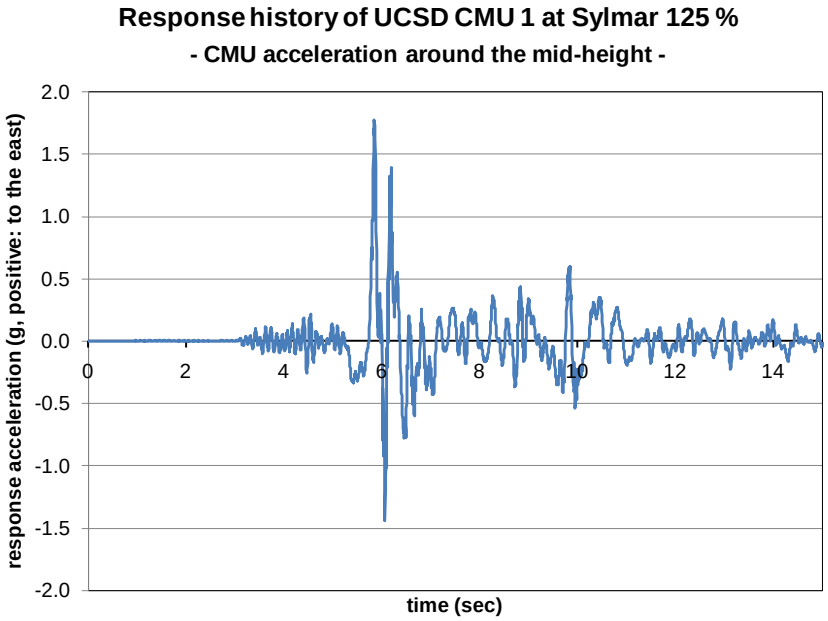

Figure 6-5 Response history of UCSD CMU 1 at Sylmar 125 %, CMU acceleration near mid-height (40 in. from the base)

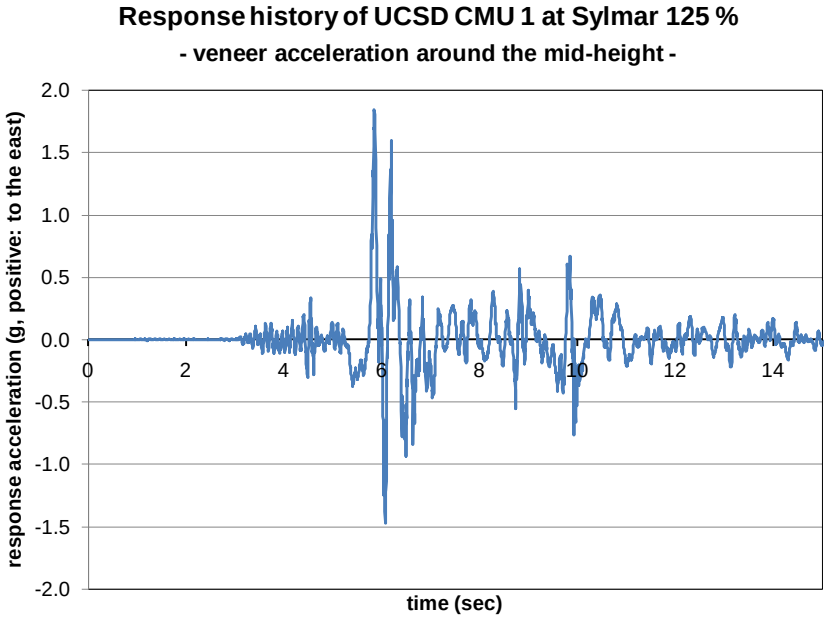

Figure 6-6 Response history of UCSD CMU 1 at Sylmar 125 %, veneer acceleration near mid-height (40 in. from the base)

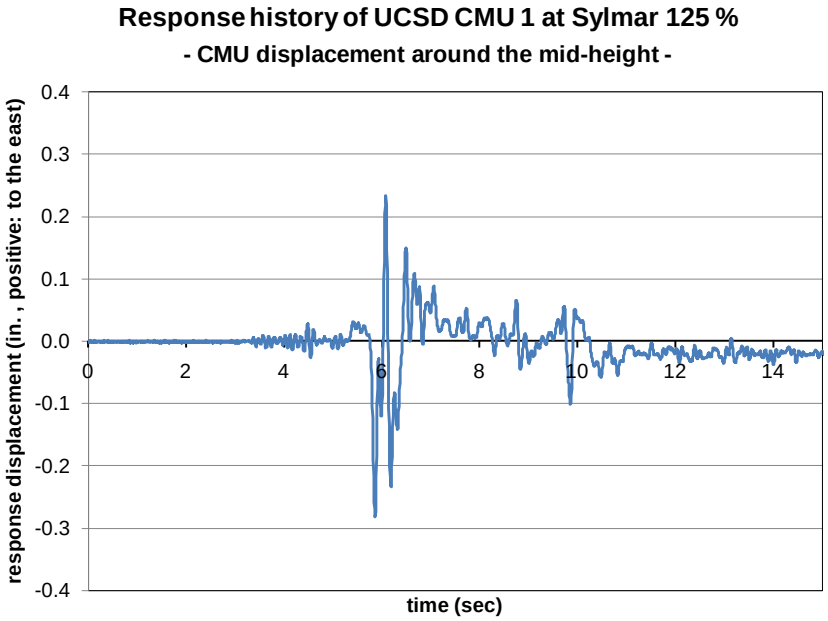

Figure 6-7 Response history of UCSD CMU 1 at Sylmar 125 %, CMU displacement near mid-height (40 in. from the base)

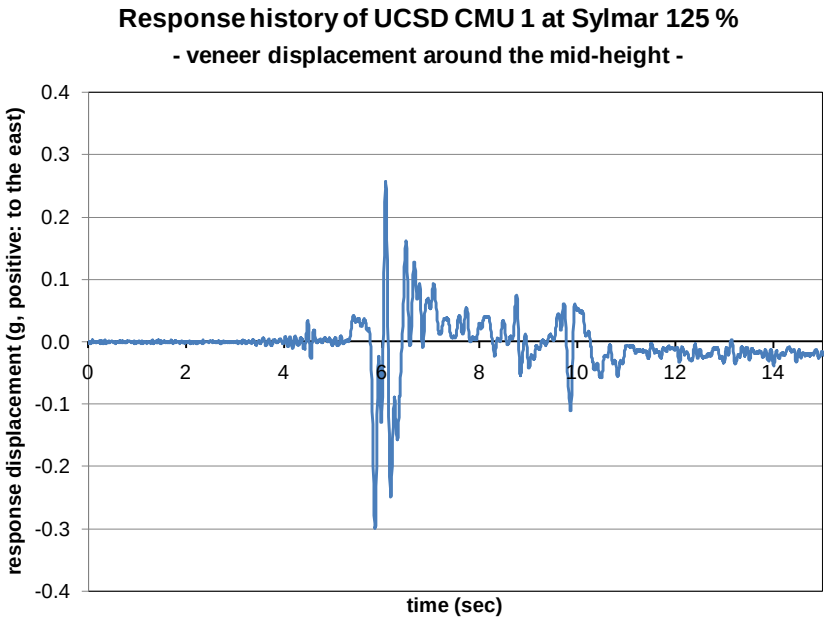

Figure 6-8 Response history of UCSD CMU 1 at Sylmar 125 %, veneer displacement near mid-height (40 in. from the base)

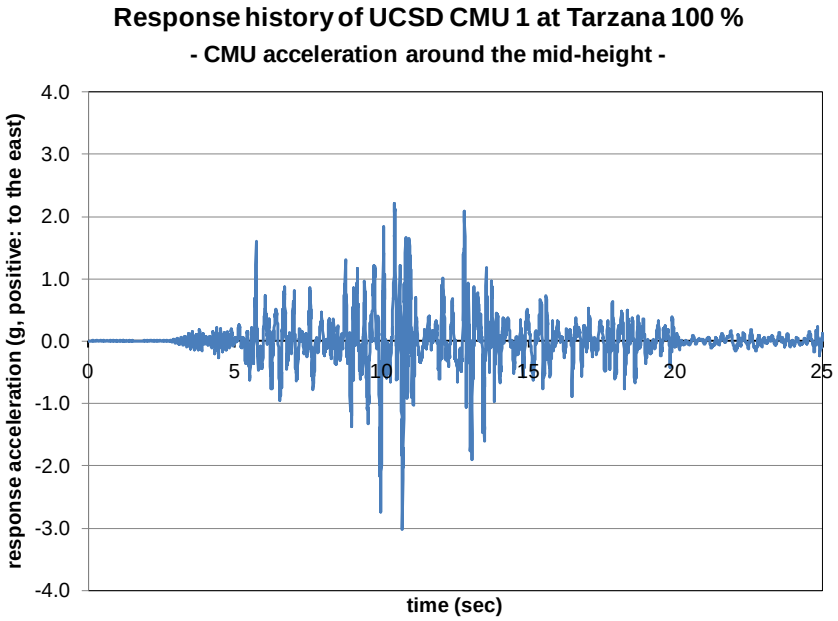

Figure 6-9 Response history of UCSD CMU 1 at Tarzana 100 %, CMU acceleration near mid-height (40 in. from the base)

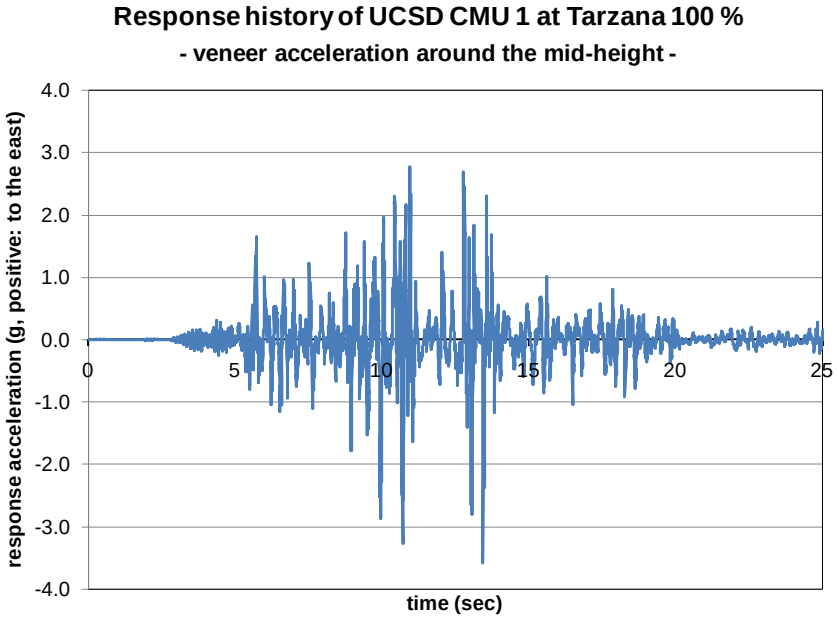

Figure 6-10 Response history of UCSD CMU 1 at Tarzana 100 %, veneer acceleration near mid-height (40 in. from the base)

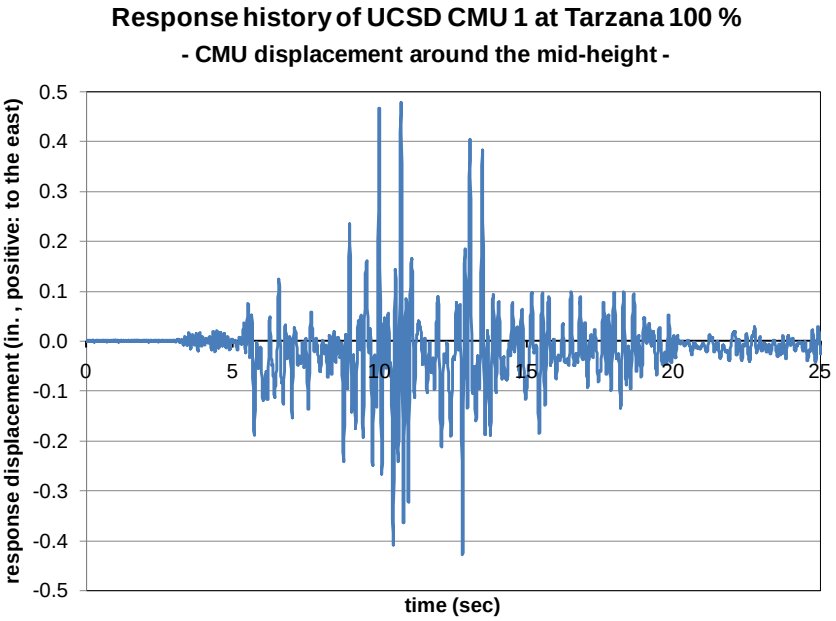

Figure 6-11 Response history of UCSD CMU 1 at Tarzana 100 %, CMU displacement near mid-height (40 in. from the base)

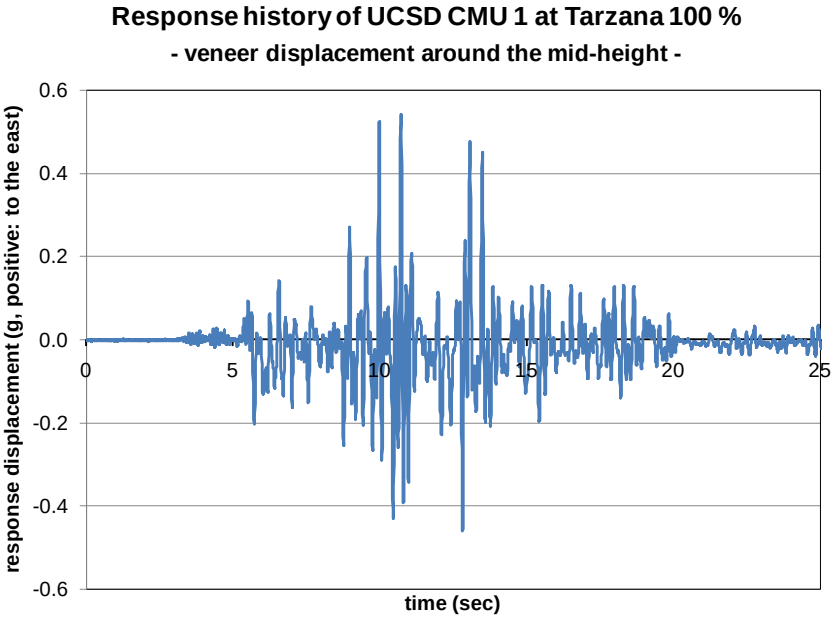

Figure 6-12 Response history of UCSD CMU 1 at Tarzana 100 %, veneer displacement near mid-height (40 in. from the base)

6.4 SUMMARY OF SHAKE-TABLE, IN-PLANE TESTS OF CMU WALL SPECIMENS (UCSD CMU 3, 4, 4 MC)

A typical concrete masonry wall specimen (CMU wall specimen) and the associated test setup for shake-table, in-plane testing is shown in Figure 6-13. Key aspects and behaviors of such specimens are listed in Table 6-8. For Tarzana 150 %, the level of shaking at which key behaviors were observed, the measured PGA is listed in Table 6-4. At this level of shaking, the table output motions were about 10 to 20 % higher than the target ground motions at Tarzana 150 %.

In each CMU wall specimen, the absolute displacements of the CMU wall at the top were less than 0.005 in. up to Sylmar 150 %, and less than 0.05 in. up to Tarzana 150 %. Due to its low mass, the CMU wall was elastic and essentially rigid. Therefore, the response of the clay masonry veneer is of primary importance for these tests. The maximum responses (displacement and acceleration) of the clay masonry veneer at the top row of connectors (88 in. from the base) and at the first row of connectors from the base (8 in. from the base) are listed in Table 6-9, Table 6-10 and Table 6-11. The positive direction is to the east (Figure 6-13). A typical response history near the top (88 in. from the base) and near the base (8 in. from the base) for the Sylmar record is shown in Figure 6-14 through Figure 6-16, using the data of Specimen UCSD CMU 3 at Sylmar 125 %. A typical response history near the top (88 in. from the base) and near the base (8 in. from the base) for the Tarzana record is shown in Figure 6-17 through Figure 6-19 using the data of Specimen UCSD CMU 3 at Tarzana 100 %.

In low-rise concrete masonry buildings with clay masonry veneer, the most important behavior of the in-plane CMU walls with clay masonry veneer (walls oriented parallel to the ground shaking) is rocking and base sliding of the CMU walls (with respect to the foundation). Of less importance is the rocking and base sliding of the clay masonry veneer (with respect to the CMU walls). In the shake-table testing of the in-plane CMU wall specimens, however, the response of the clay masonry veneer is of

primary concern, since the CMU wall themselves was essentially rigid due to the specimens' low mass until the in-plane veneer or the connectors failed. Rocking and sliding of the clay masonry veneer is mainly governed by the in-plane strength of the connectors (generally determined by fracture of crossing wires at welding) and by the frictional resistance and the rocking resistance (due to self-weight) of the veneer. Because connectors are far weaker in-plane than out-of-plane, they are likely to yield in-plane at low levels of shaking. Inelastic deformation of connectors and sliding friction at the base of the veneer dissipate energy.

The clay masonry veneer in all three specimens was governed essentially by rocking followed in some cases by sliding. Because rocking of the veneer was accompanied by impact against the shelf angle, it is believed to help the veneer in dissipating energy. On the other hand, if there is vertical movement of the gravity center of the clay masonry veneer, the energy dissipated by the friction at the base is likely to decrease. Therefore, in the clay masonry veneer, the sliding accompanying rocking will be somewhat different from the sliding without rocking in the viewpoint of energy dissipation.

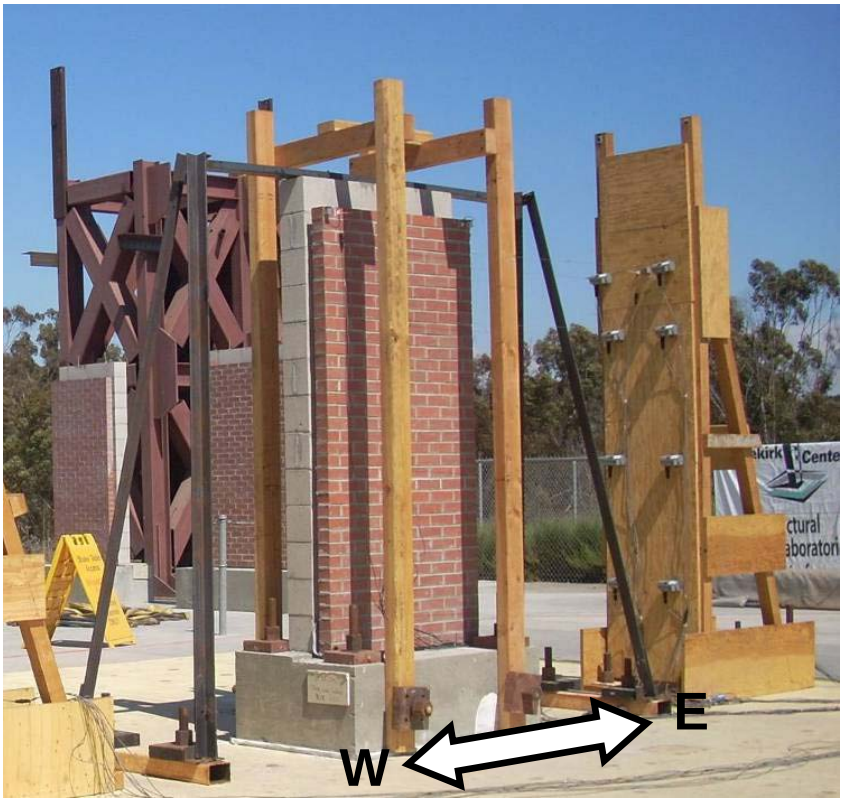

Figure 6-13 Typical shake-table, in-plane CMU wall specimen with test setup

Table 6-8 Key aspects and behaviors of CMU wall specimens for shake-table, in-plane loading

specimen	UCSD CMU 3	UCSD CMU 4	UCSD CMU 4 MC
type of connectors	double eye-and-pintles	tri-wire	tri-wire
type of mortar	cement-lime	cement-lime	masonry cement
ground motion at connector failure	no failure	Tarzana 150 % (low-cycle fatigue failure of crossing wires)	Tarzana 150 % (low-cycle fatigue failure of crossing wires)
comment		at Tarzana 150 %, cracking at a bed joint (above mid-height) with joint reinforcement, accompanying sliding at the bed joint	

Table 6-9 Shake-table, in-plane test results of UCSD CMU 3

ground motion			PGA (g), measured	responses of veneer		
				acceleration (g)	displacement	
				top *	bottom **	top *
Sylmar	80%	max	0.78	0.88	0.00	0.02
		min	-0.54	-0.68	0.00	-0.03
	100%	max	1.03	1.09	0.00	0.03
		min	-0.66	-0.83	0.00	-0.05
	125%	max	1.35	1.46	0.00	0.06
		min	-0.84	-1.05	0.00	-0.09
	150%	max	1.66	1.74	0.00	0.06
		min	-0.99	-1.17	-0.01	-0.13
Tarzana	70%	max	1.29	1.80	0.10	0.21
		min	-1.42	-2.11	0.00	-0.13
	100%	max	1.88	2.46	0.14	0.43
		min	-2.00	-3.07	-0.11	-0.17
	125%	max	2.33	3.04	0.20	0.64
		min	-2.51	-3.18	-0.20	-0.40
	150%	max	2.76	3.07	0.28	0.95
		min	-3.02	-3.98	-0.34	-0.76

positive direction: to the east

** top: at the top row of connectors (88 in. from the base)*

*** bottom: at the first row of connectors from the base (8 in. from the base)*

Table 6-10 Shake-table, in-plane test results of UCSD CMU 4

ground motion			PGA (g), measured	responses of veneer		
				acceleration (g)	displacement	
				top *	bottom **	top *
Sylmar	80%	max	0.95	1.13	0.00	0.09
		min	-0.55	-1.21	-0.01	-0.09
	100%	max	1.07	1.48	0.00	0.12
		min	-0.68	-1.31	-0.01	-0.14
	125%	max	1.33	1.81	0.00	0.17
		min	-0.88	-1.36	0.00	-0.22
	150%	max	1.63	1.95	0.02	0.32
		min	-1.00	-1.75	-0.03	-0.34
Tarzana	70%	max	no test			
		min				
	100%	max	1.93	2.34	0.12	0.91
		min	-1.97	-2.45	-0.14	-0.68
	125%	max	no test			
		min				
	150%	max	2.77	-	-	-
		min	-2.93	-	-	-

positive direction: to the east

** top: at the top row of connectors (88 in. from the base)*

*** bottom: at the first row of connectors from the base (8 in. from the base)*

Table 6-11 Shake-table, in-plane test results of UCSD CMU 4 MC

ground motion			PGA (g), measured	responses of veneer		
				acceleration (g)	displacement	
				top *	bottom **	top *
Sylmar	80%	max	0.83	0.98	0.00	0.09
		min	-0.54	-0.96	0.00	-0.09
	100%	max	1.05	1.21	0.01	0.15
		min	-0.68	-1.26	0.00	-0.14
	125%	max	1.34	1.61	0.04	0.21
		min	-0.85	-1.43	-0.03	-0.35
	150%	max	1.66	1.94	0.05	0.20
		min	-0.99	-1.71	-0.24	-0.76
Tarzana	70%	max	1.30	1.71	0.15	0.52
		min	-1.36	-2.00	-0.21	-0.54
	100%	max	1.91	2.08	0.26	1.20
		min	-2.02	-2.71	-0.31	-0.98
	125%	max	2.29	1.96	-	1.55
		min	-2.47	-2.98	-	-1.80
	150%	max	2.79	-	-	-
		min	-2.94	-	-	-

positive direction: to the east

** top: at the top row of connectors (88 in. from the base)*

*** bottom: at the first row of connectors above the base (8 in. from the base)*

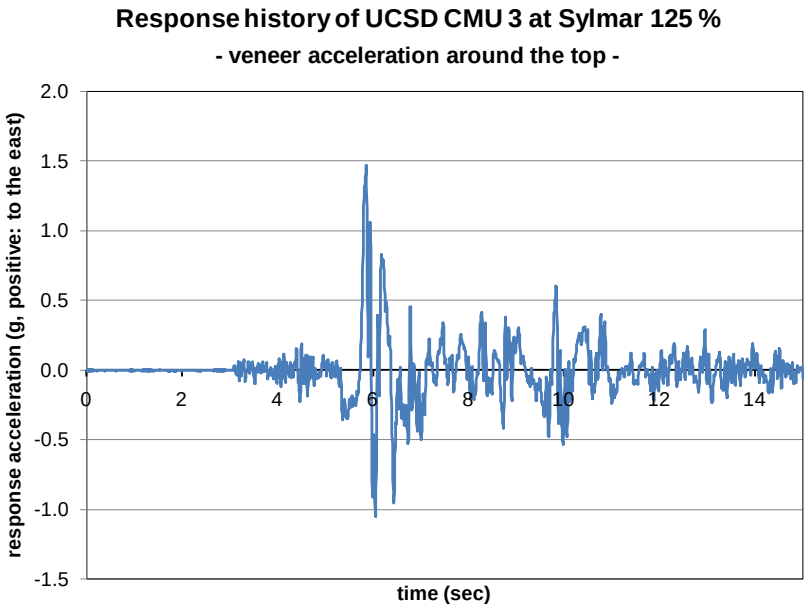

Figure 6-14 Response history of UCSD CMU 3 at Sylmar 125 %, veneer acceleration near the top (88 in. from the base)

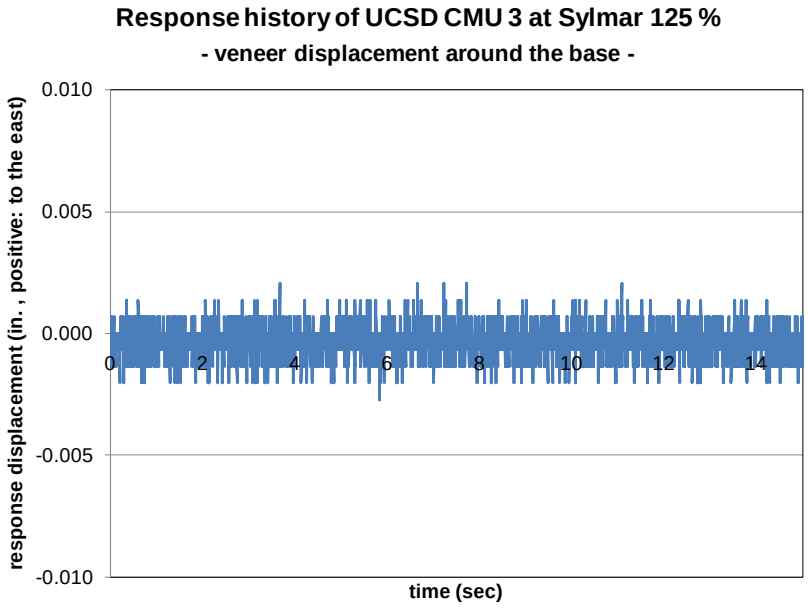

Figure 6-15 Response history of UCSD CMU 3 at Sylmar 125 %, veneer displacement near the base (8 in. from the base)

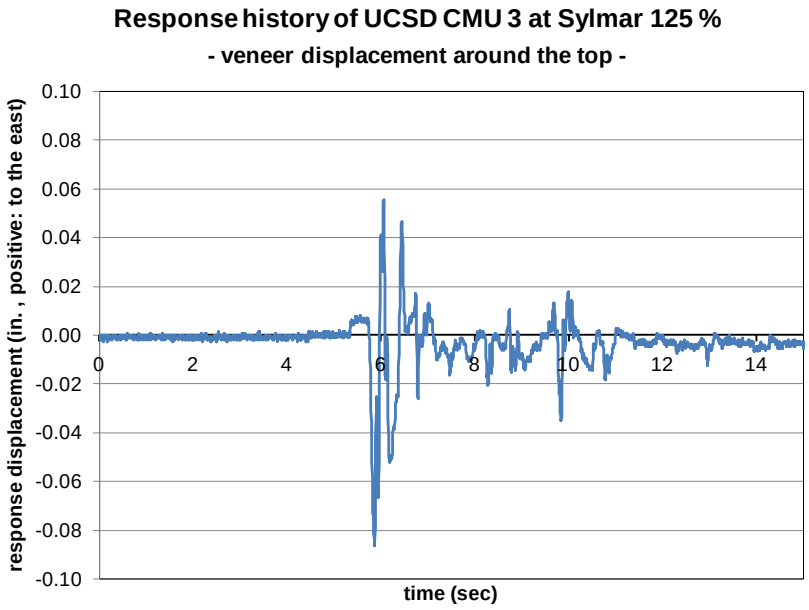

Figure 6-16 Response history of UCSD CMU 3 at Sylmar 125 %, veneer displacement near the top (88 in. from the base)

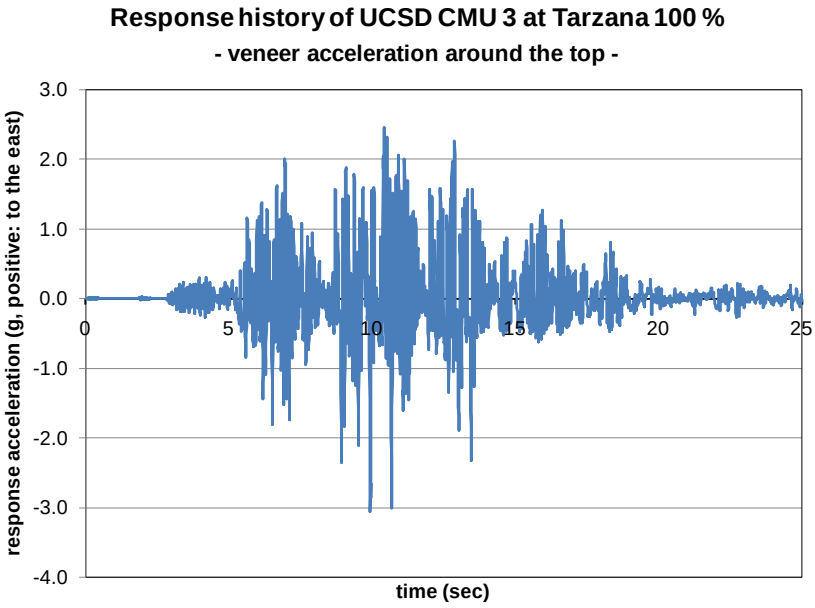

Figure 6-17 Response history of UCSD CMU 3 at Tarzana 100 %, veneer acceleration near the top (88 in from the base)

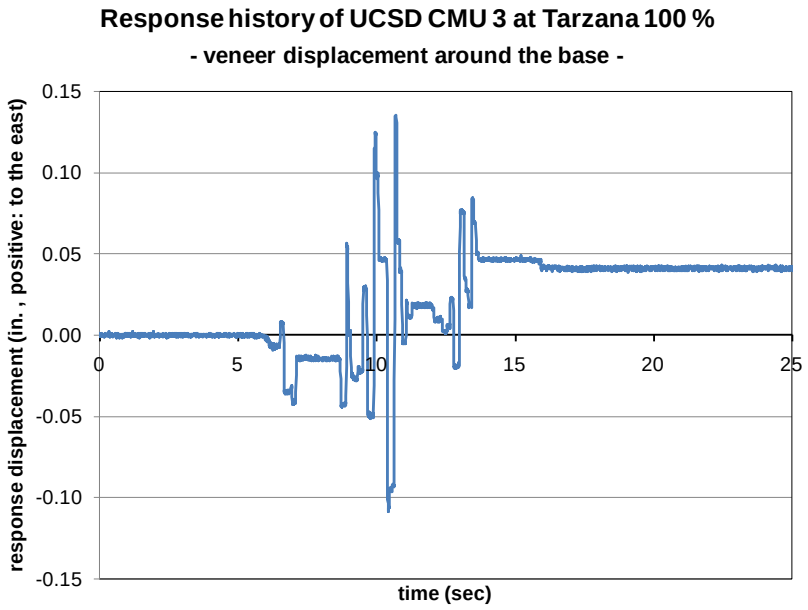

Figure 6-18 Response history of UCSD CMU 3 at Tarzana 100 %, veneer displacement near the base (8 in. from the base)

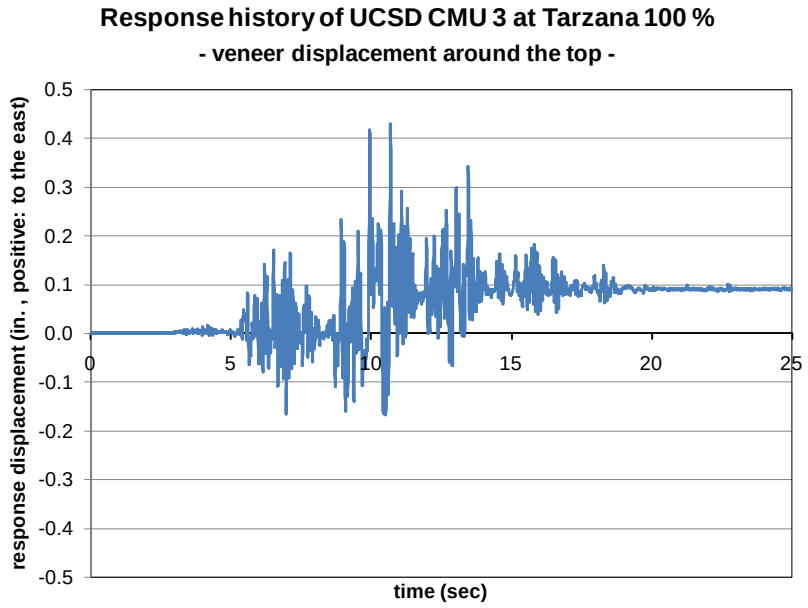

Figure 6-19 Response history of UCSD CMU 3 at Tarzana 100 %, veneer displacement near the top (88 in. from the base)

CHAPTER 7
Design and Shake-table Test Summary of CMU Building Specimen

As part of the NSF NEES masonry project, shake-table testing of a full-scale, one-story reinforced concrete masonry building specimen with clay masonry veneer (CMU building specimen) was conducted at the University of California at San Diego (UCSD). In this chapter, the overall description of the CMU building specimen is provided; the design of that specimen is described; the shake-table tests and test results of that specimen are summarized; and the observations from the shake-table tests are presented. Detailed shake-table tests and test results will be provided in the PhD dissertation now being prepared by Hussein Okail at UCSD.

The main purpose of shake-table testing of the CMU building specimens is to examine overall and local behaviors (in-plane and out-of-plane) of the low-rise concrete masonry building with clay masonry veneer, and to provide experimental data to extend the analytical models developed for the concrete masonry walls with clay masonry veneer (Section 9) to the low-rise concrete masonry building with clay masonry veneer.

7.1 Overall Description of CMU Building Specimen

The CMU building specimen was square in plan, with out-to-out dimensions of 240 in. for the concrete masonry on each side. It was designed and constructed in accordance with 2008 MSJC requirements for SDC D/E, including prescriptive reinforcement requirements for special reinforced masonry shear walls. 2008 MSJC requirements for SDC E includes the use of the joint reinforcement in the clay masonry veneer, and this was not satisfied on the south and west side of the CMU building specimen. Therefore, the clay masonry veneer on the south and west sides satisfied 2008

MSJC requirements for SDC D and, other than that, the CMU building specimen satisfied all the requirements of 2008 MSJC for SDC E.

The CMU building specimen for shake-table testing (Figure 7-1 and Figure 7-2) was symmetric in the direction of shaking (EW), with a 12-ft wall segment and a 4-ft wall segment on the north and south sides, and with two 8-ft wall segments on the east and west sides. During testing, 12-ft and 4-ft wall segments were loaded in-plane (shaking in the EW direction), and 8-ft wall segments were loaded out-of-plane.

The CMU building specimen used nominal 8- x 8- x 16-in. lightweight concrete masonry units (ASTM C90); ASTM C270 Type S cement-lime mortar by proportion for the CMU walls and the clay masonry veneer; and ASTM C476 coarse grout by proportion. Concrete masonry units (CMU) were A-units throughout, with knock-out units at wall ends. The CMU walls was fully grouted. A 2-in. air space was specified, because that is typical practice. Vertical control joints were located at the ends of reinforced lintels.

The CMU building specimen had shelf angles bolted to the CMU walls and covered with 30 mil EPDM flashing (not self-adhering), on which the veneer was placed. The veneer was constructed using nominal 4-inch clay masonry units (specified as ASTM C216, greater than 75% solid), and ASTM C270 Type S cement-lime mortar, specified by proportion. Vertical expansion joints were located at the ends of the loose lintel angles over the doors, and at northwest and southwest corners to separate the west veneer from the north and south veneer.

The roof diaphragm was composed of prestressed 6-in. concrete planks, spanning NS (oriented perpendicular to the direction of shaking) and covered by 3.5 in. of topping. An additional 19.5 kips of weight was placed on the roof to ensure that sufficient acceleration could be applied to produce flexural yielding of the concrete masonry walls without exceeding the limitations of the shaking table. The topping was reinforced with deformed reinforcement consisting of #4 bars at 16 in. in both directions. Two #4 perimeter bars were placed at the level of the planks to act as a bond beam. This is not

required by the 2008 MSJC Code, but is considered good practice in many west-coast design offices.

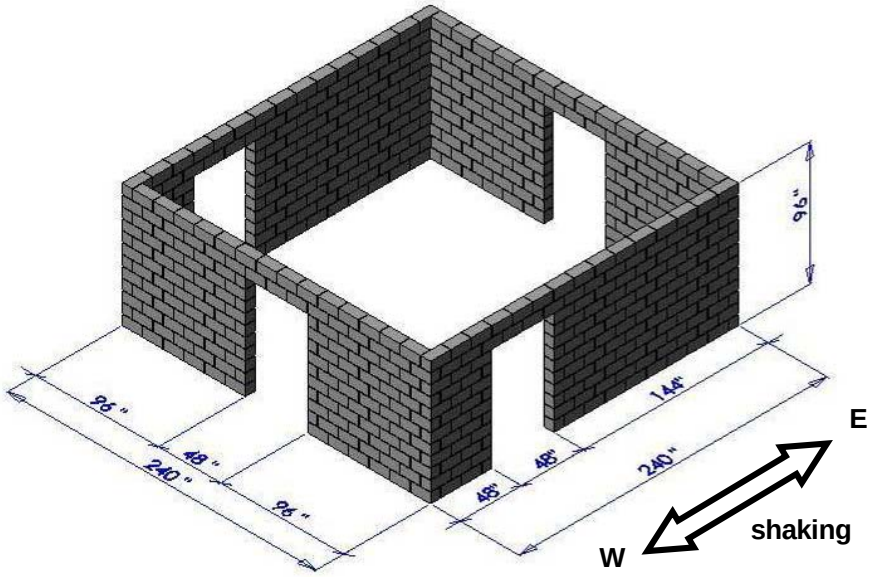

Figure 7-1 Overall view of CMU building specimen (CMU walls only)

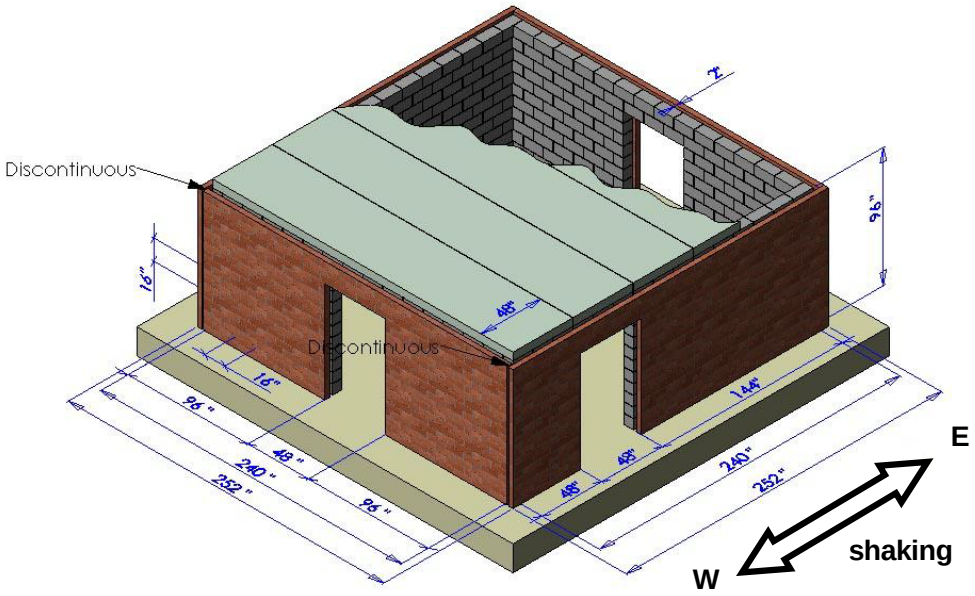

Figure 7-2 Overall view of CMU building specimen

The north side of the CMU building specimen had the first intermediate bond beam at the bottom course, while the other sides (south, east and west) had the first intermediate bond beam at the required spacing above the top of the foundation. Joint reinforcement in the CMU walls was used to satisfy prescriptive requirements of Section 1.17 of the 2008 MSJC Code, but not to satisfy the shear requirements of Chapter 3 of that document. This is implicit, because no f_y is specified in design for joint reinforcement.

On the east and north sides of the CMU building specimen, the veneer was connected with W1.7 tri-wire, ladder-type joint reinforcement at 16 in. vertically with W1.7 cross wires at 16 in. horizontally (meeting requirements for SDC E) as shown in Figure 2-11. On the west and south sides of the CMU building specimen, the masonry wythes were connected using W1.7 joint reinforcement at 16 in. vertically in the CMU walls, with W2.8 wire double eye and pintle, spaced at 16 in. horizontally in the veneer (meeting requirements for SDC D) as shown in Figure 2-12.

7.2 DESIGN OF CMU BUILDING SPECIMEN

7.2.1 Summary of Design Process

Principal design parameters for the CMU building specimen are presented in Table 7-1. The design process using the principal design parameters in Table 7-1 is summarized as follows, and is carried out in subsequent sections.

1. Select vertical reinforcement for CMU wall segments based on prescriptive requirements for special reinforced masonry shear walls (2008 MSJC Code Section 1.17.3.2.6). Make a preliminary selection of horizontal reinforcement based on prescriptive reinforcement requirements. This is preliminary because it is not known in the beginning whether or not horizontal reinforcement will be required for shear.

Table 7-1 Principal design parameters for CMU building specimen

Wall Segment	**12-ft**	**4-ft**	**8-ft**
	In-plane		Out-of-plane
Required Spacing of Reinforcement (2008 MSJC Section 1.17.3.2.6)			
Vertical: #4 bar ≤ $l/3$, $h/3$, 48 in.	$h/3$ = 32 in.	$l/3$ = 16 in.	$l/3$ = 32 in.
Horizontal: #4 bar when required to resist shear ≤ $l/3$, $h/3$, 48 in.	$h/3$ = 32 in.	$l/3$ = 16 in.	$l/3 = h/3$ = 32 in.
other cases ≤ 48 in.	48 in.	48 in.	48 in.
Check of Capacity Design Requirement (2008 MSJC Section 1.17.3.2.6.1.1) * when flange is in tension, no additional roof weight			
selected vertical reinforcement based on required spacing above	six #4 bars	4 #4 bars	4 #4 bars
selected horizontal reinforcement to satisfy capacity design requirement	#4 bars @ 16 in.	#4 bars @ 16 in.	#4 bars @ 16 in.
$\frac{\phi V_n}{V(M_n)} \geq 1.25$	$\frac{130.0^{kips}}{100.6^{kips}}$ = 1.29	$\frac{42.3^{kips}}{22.5^{kips}}$ = 1.88	$\frac{81.3^{kips}}{58.4^{kips}}$ = 1.39
Check of Required Ratio of Reinforcement (2008 MSJC Section 1.17.3.2.6) * joint wire reinforcement is included; horizontal bars at the top bond beam are ignored			
Vertical (ρ_v) ≥ 0.0007, $\rho_h/3$	0.0011 * six #4 bars	0.0022 * four #4 bars	0.0011 * four #4 bars
Horizontal (ρ_h) ≥ 0.0007	0.0019 * twelve W1.7 * six #4 bars	0.0019 * twelve W1.7 * six #4 bars	0.0019 * twelve W1.7 * six #4 bars
Sum ($\rho_v + \rho_h$) ≥ 0.002	0.0030	0.0041	0.0030
Comments			
Sliding at base is likely at 12-ft walls (ϕ=0.8, μ=1.0) * when flange is in tension with no additional roof weight	$\frac{\phi V_{sliding}}{V(M_n)} = 0.95$	$\frac{\phi V_{sliding}}{V(M_n)} = 2.98$	
Code Equation 3-23 might not quite right $V_{ns} = 0.5\left(\frac{A_v}{s}\right) f_y \, d_v$	- d_v cannot exceed height - $\frac{d_v}{s}$ must be "n"		

2. Using moment-axial force interaction diagrams computed by spreadsheet, 2008 MSJC equations for shear, and specified material strengths (1500 psi for masonry, 60 ksi for reinforcement), select horizontal reinforcement in all wall segments to satisfy the capacity design requirement for special reinforced masonry shear walls (2008 MSJC Code Section 1.17.3.2.6.1.1). In these calculations, the wall segments are assumed free to rotate at the top (flexural coupling from the roof diaphragm and the top bond beam is ignored). For each wall segment, the critical case is achieved when the effective flange is in tension (2008 MSJC Code Section 1.9.4.2.3). Symbolically, this check is expressed as

$$\frac{\phi V_n\left(P_{estimated}\right)}{V\left(M_n\left(P_{estimated}\right)\right)} \geq 1.25$$

In this calculation, the axial load $P_{estimated}$ is not known initially, because it depends on the additional roof weight, which has yet to be determined. Initially, an additional weight of zero was assumed. Axial load from the roof diaphragm was assumed to be distributed to in-plane walls according to tributary area, so that the 12-ft wall segment would support a tributary length of 14 ft. Axial load due to the effective flange was also included. However, the effect of axial load from the roof diaphragm and the effective flange on external moment was ignored because it was negligible, compared to the flexural strength of each wall segment. The roof diaphragm and the effective flange develop external moment in opposite directions. As shown in Table 7-1, the required spacing of horizontal reinforcement needed to meet capacity design requirements governs over the prescriptive spacing requirements for each wall segment.

3. Check reinforcement ratio requirements (2008 MSJC Code Section 1.17.3.2.6).

4. Using an effective weight equal to the weight of the roof diaphragm plus the upper half of the CMU walls (120 lb/ft^3), plus the upper half of the veneer (if

applicable), select the additional roof weight necessary to produce hinging in the in-plane shear-wall segments by iteration, within the probable maximum shaking-table accelerations for the frequency range of interest. Under the additional roof weight, the capacity design requirement must still be satisfied.

7.2.2 Select Vertical Reinforcement and Estimate Horizontal Reinforcement for Each Wall Segment based on Prescriptive Requirements

7.2.2.1 Prescriptive Reinforcement for 12-ft Segment

For the 12-ft segment, vertical reinforcement must be spaced at the least of $l/3$, $h/3$, and 48 in. The governing (least) dimension is $h/3$ = 32 in. At this point, since it is not known whether or not horizontal reinforcement is required for shear, horizontal reinforcement must be spaced at not more than 48 in. The horizontal reinforcement to resist shear, if required, must be deformed reinforcement surrounded by grout, because joint reinforcement is not included in the ASTM material standards referenced by Chapter 3 of the 2008 MSJC Code. However, horizontal reinforcement required to meet the prescriptive requirements of Section 1.17 of the 2008 MSJC Code is by default permitted to be joint reinforcement. Since joint reinforcement is used to attach the veneer connectors, it is spaced at 16 in. vertically.

7.2.2.2 Prescriptive Reinforcement for 4-ft Segment

For the 4-ft segment, vertical reinforcement must be spaced at the least of $l/3$, $h/3$, and 48 in. The governing (least) dimension is $l/3$ = 16 in. At this point, since it is not known whether or not horizontal reinforcement is required for shear, horizontal reinforcement must be spaced at not more than 48 in. Since joint reinforcement is used to attach connectors, it is spaced at 16 in. vertically.

7.2.2.3 Prescriptive Reinforcement for 8-ft Segments

For the 8-ft segments, vertical reinforcement must be spaced at the least of $l/3$, $h/3$, and 48 in. The governing (least) dimension is $l/3 = h/3 = 32$ in. At this point, since it is not known whether or not horizontal reinforcement is required for shear, horizontal reinforcement must be spaced at not more than 48 in. Since joint reinforcement is used to attach connectors, it is spaced at 16 in. vertically.

7.2.3 Select Horizontal Reinforcement to Meet MSJC Capacity Design Requirement

Using moment-axial force interaction diagrams computed by spreadsheet, 2008 MSJC equations for shear, and specified material strengths (1500 psi for masonry, 60 ksi for reinforcement), select horizontal reinforcement in all wall segments to satisfy the capacity design requirement for special reinforced masonry shear walls (2008 MSJC Code Section 1.17.3.2.6.1.1). In the following subsections, essential values are given for each wall segment. Detailed calculations for each value are provided in Appendix C.

The strength values associated with MSJC capacity design requirement for the 12-ft segment are summarized in Table 7-1 ($\frac{\phi V_n}{V(M_n)} \geq 1.25$, or $\frac{130.0^{kips}}{100.6^{kips}} = 1.29$). Each of those values is taken from Table 7-2. For example, the 130.0 kips is from the ϕV_n row for the 12-ft segment, and the 100.6 kips is from the $V(M_n)$ row for the 12-ft segment. Corresponding values for the 4-ft segment and 8-ft segment are given in the same way.

The strength values given in Table 7-1 and Table 7-2 correspond to the final selected bar size and spacing of horizontal reinforcement for each wall segment. Table 7-1 and Table 7-2 do not show the process by which those values were determined. That process is given in detail in Appendix C.1. For example, for the 12-ft segment, the same

values of 130.0 kips and 100.6 kips are given in Table C.1, where each number in parentheses is the calculation step by which the number was produced.

Table 7-2 In-plane design strengths of wall segments (no additional roof weight)

wall segment		**12-ft long wall**		**4-ft long wall**		**8-ft long wall**
load direction (to)		**east**	**west**	**east**	**west**	**when flange is in tension**
roof weight		87.75 psf (6-in. planks with 3.5-in. concrete topping, no additional weight)				
P	kips	22.3	23.8	11.9	10.4	7.4
ϕM_n	kips-ft	518.5	724.3	162.0	107.9	420.4
$V(\phi M_n)$	kips	64.8	90.5	20.3	13.5	52.5
$V(M_n)$	kips	72.0	100.6	22.5	15.0	58.4
ϕV_{nm}	kips	100.9	101.2	27.9	27.6	52.5
ϕV_n	kips	129.7	130.0	42.3	42.0	81.3
$\phi V_{n\_sliding}$	kips	85.0	95.9	67.1	56.3	73.1
$\frac{\phi V_{nm}}{V(M_n)}$		1.40	1.01	1.24	1.84	0.90
$\frac{\phi V_n}{V(M_n)}$		1.80	1.29	1.88	2.80	1.39

7.2.4 Check Required Table Acceleration with No Additional Roof Weight

From expected in-plane strengths of the CMU building specimen (Table 7-3), the lowest base shear capacity (271.0 kips) corresponds to the base shear associated with flexural hinging of the 12-ft and 4-ft flanged wall segments under loading to the east. For calculation of expected strengths, specified material strengths for masonry (1500 psi) and expected material strengths for vertical and horizontal reinforcement (86 ksi) were used. The effective weight equals the weight of the roof diaphragm (35.1 kips), the upper half of the CMU walls (19.5 kips) and the upper half of the veneer (9.3 kips), if applicable. Without veneer, the total is 52.1 kips; with veneer, 63.9 kips. The response acceleration

of the CMU building specimen is assumed to be the input acceleration of the table, multiplied by a dynamic response amplification factor of 1.5. The required table acceleration is then 3.31 g without veneer, and 2.83 g with veneer.

The expected load-displacement curve under loading to the east is shown in Figure 7-3. The calculation for the relative stiffness between 12-ft long wall segments and 4-ft long wall segments, on which the plot in Figure 7-3 is based, is described in Appendix C.3. Because the ratio of the stiffness of a 12-ft long wall to that of a 4-ft long wall is 3.7, while the ratio of $V(M_{n\_\exp})$ of the12-ft long wall to that of the 4-ft long wall is 3.2, the 12-ft long wall will yield a little bit earlier than the 4-ft long wall.

Table 7-3 Expected* in-plane strengths of CMU building specimen (no additional roof weight)

wall segment		**12-ft long wall**		**4-ft long wall**		**sum (two 12-ft and two 4-ft)**	
load direction (to)		**east**	**west**	**east**	**west**	**east**	**west**
roof weight		87.75 psf (6-in. planks with 3.5-in. concrete topping, no additional weight)					
$V(M_{n\_\exp})$	kips	103.2	144.2	32.3	21.5	271.0	331.3
$V_{n\_\exp}$	kips	177.7	178.1	60.7	60.3	476.9	476.9
$V_{n\_sliding\_\exp}$	kips	142.7	161.4	115.1	96.4	515.5	515.5
required table (base) acceleration $\ddot{u}_{g\_required} = \frac{V(M_{n\_\exp})}{1.5 \times W_{eff}}$		without veneer $W_{eff} = 54.6\,kips$				3.31 g	4.04 g
		with veneer $W_{eff} = 63.9\,kips$				2.83 g	3.46 g

** specified material strengths for masonry (1500 psi) and expected material strengths for vertical and horizontal reinforcement (86 ksi) were used.*

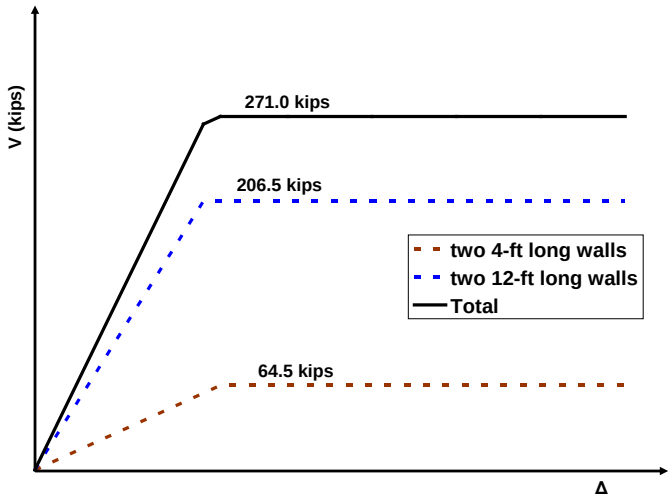

Figure 7-3 Expected behavior of CMU building specimen, loaded to east, no additional roof weight

The nominal acceleration, velocity, and displacement limits of the UCSD LHPOST facility are shown in Figure 7-4. The weight of the bare table is about 250 MTons; the weight of our specimen will range between 50 and 100 MTons; and the maximum available acceleration with a 100-MTon specimen is probably about 3 g. Based on September 2007 testing at UCSD, we can conservatively expect a maximum table shaking of about 2.5 g.

The required table accelerations, 3.31 g and 2.83 g, probably exceed the table capacity. To produce the same base shear with lower table acceleration, it is necessary to add weight to the roof diaphragm.

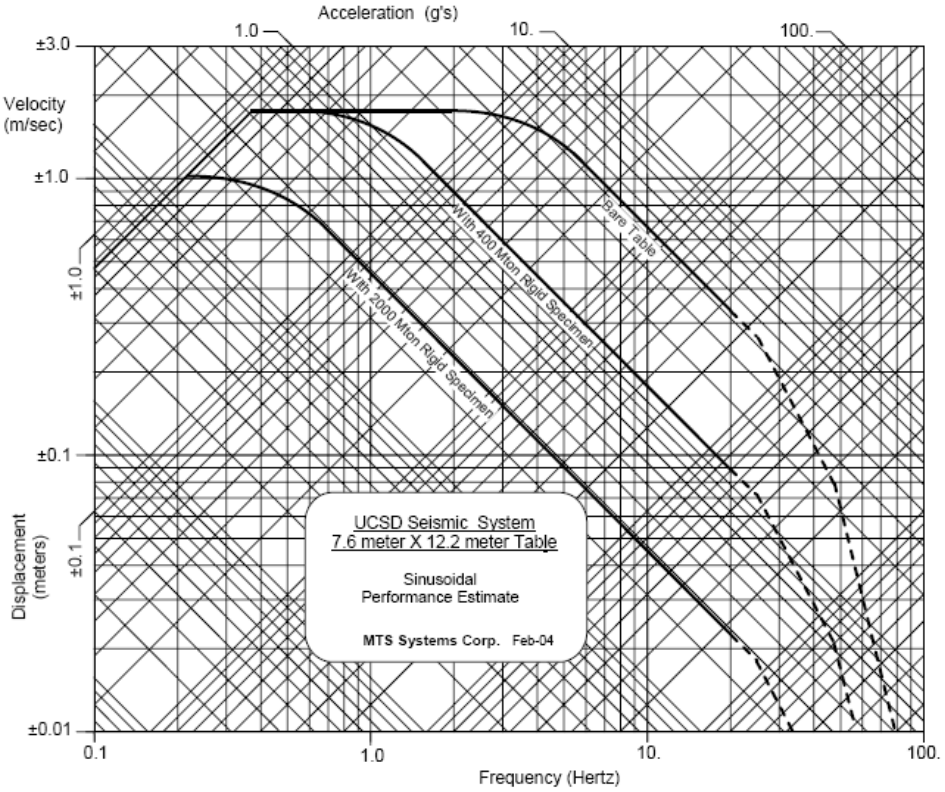

Figure 7-4 Nominal acceleration, velocity, and displacement limits of UCSD LHPOST facility

7.2.5 Check Required Table Acceleration with Additional Roof Weight of 19.5 kips

Using the same computational steps discussed above for the case of zero additional roof weight, a trial case was run with 19.5 kips of additional roof weight. Based on detailed calculations given in Appendix C.2, the maximum additional roof weight at the roof diaphragm that can still satisfy the 2008 MSJC capacity design requirement, $\frac{\phi V_n}{V(M_n)} \geq 1.25$, is 19.5 kips.

The values from Appendix C.2 are given in Table 7-4 and Table 7-5. The total effective weight is 74.1 kips without veneer, and 83.4 kips with veneer. The governing

expected base shear capacity becomes 288.5 kips (Table 7-5), corresponding to a required table acceleration of about 2.59 g without veneer, and 2.31 g with veneer. These requiring maximum table accelerations will probably be equal to or within the table limits since the conservatively expected maximum table shaking is 2.5 g.

In Figure 7-5 is shown the expected in-plane load-displacement curve under loading to the east. The calculation of the relative stiffnesses of the 12-ft and the 4-ft long wall segments, on which the plot of Figure 7-3 is based, is described in Appendix C.3.

Table 7-4 In-plane design strengths of wall segments (19.5-kip additional roof weight)

wall segment		**12-ft long wall**		**4-ft long wall**		**8-ft long wall**
load direction (to)		**east**	**west**	**east**	**west**	**when flange is in tension**
roof weight		136.5 psf (6-in. planks with 3.5-in. concrete topping, 19.5-kip additional weight)				
P	kips	29.1	30.6	14.8	13.3	7.4
ϕM_n	kips-ft	558.9	757.0	165.7	113.5	420.4
$V(\phi M_n)$	kips	69.9	94.6	20.7	14.2	52.5
$V(M_n)$	kips	77.6	105.1	23.0	15.8	58.4
ϕV_{nm}	kips	102.3	102.6	28.5	28.2	52.5
ϕV_n	kips	131.1	131.4	42.9	42.6	81.3
$\phi V_{n\_sliding}$	kips	90.5	101.3	69.5	58.6	73.1
$\frac{\phi V_{nm}}{V(M_n)}$		1.32	0.98	1.24	1.79	0.90
$\frac{\phi V_n}{V(M_n)}$		1.69	1.25	1.86	2.70	1.39

Table 7-5 Expected* in-plane strengths of CMU building specimen (19.5-kip additional roof weight)

wall segment		12-ft long wall		4-ft long wall		Sum (two 12-ft and two 4-ft)	
load direction (to)		east	west	east	west	east	west
roof weight		136.5 psf (6-in. planks with 3.5-in. concrete topping, 19.5-kip additional weight)					
$V(M_{n\_\exp})$	kips	111.3	150.7	33.0	22.6	288.5	346.6
$V_{n\_\exp}$	kips	179.4	179.8	61.4	61.0	481.7	481.7
$V_{n\_sliding\_\exp}$	kips	149.5	168.2	118.0	99.3	535.0	535.0
required table (base) acceleration $\ddot{u}_{g\_required} = \frac{V(M_{n\_\exp})}{1.5 \times W_{eff}}$				without veneer $W_{eff} = 74.1 kips$		2.59 g	3.12 g
				with veneer $W_{eff} = 83.4 kips$		2.31 g	2.77 g

* *specified material strengths for masonry (1500 psi) and expected material strengths for vertical and horizontal reinforcement (86 ksi) were used.*

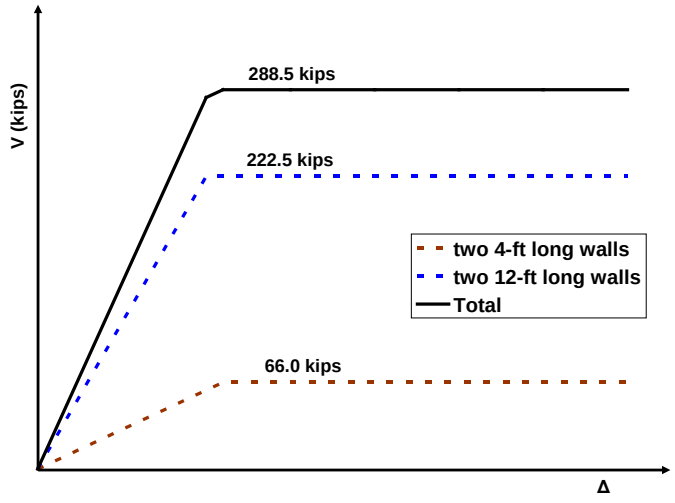

Figure 7-5 Expected behavior of CMU building specimen, loaded to east, 19.5-kip additional roof weight

7.2.6 Preliminary Remarks on Effects of Veneer on above Requirements

At the moment, the effects of the veneer on the behavior and the strength of back-up walls, CMU walls in this study, are not known clearly. As a preliminary assessment, treating the veneer as an addition to the effective weight of the CMU building specimen is straightforward.

The veneer on the upper half of the CMU building specimen is assumed to contribute to the effective weight of the specimen. That weight is about 9.3 kips. While it is not connected rigidly to the roof diaphragm, it is similar in effect to additional roof weight. To note is that the veneer increases the axial load on the walls at the base only, because the veneer is supported vertically on the shelf angle that is bolted to the CMU walls just above the foundation.

7.2.7 Check of Out-of-Plane Capacity of 8-ft CMU Wall Segments

Finally, it is necessary to check out-of-plane capacity of 8-ft CMU wall segments on the east and west sides of the CMU building specimen, with and without veneer. Here, the out-of-plane capacity means the flexural strength of CMU walls excluding the failure of veneer or connectors.

Using a moment-axial force interaction diagram computed by spreadsheet (Figure C.5) based on specified material strengths for masonry (1500 psi) and expected material strengths for reinforcement (70 ksi), the expected flexural strength of an 8-ft wall segment is 208 kips-in., as shown below, under the 2.4-kip axial load from self-weight only (the CMU walls on the east and west sides are non-load-bearing walls).

$$M_{n\_\exp} = 200\,kips\cdot in. + \frac{2.4kips}{22kips}\times(272-200)kips\cdot in. = 208\,kips\cdot in.$$

Because veneer does not contribute to axial load, the presence of veneer does not change this capacity. While expected material strength for reinforcement (86 ksi) was

used for expected in-plane strengths of wall segments, 70 ksi is used for expected out-of-plane strength; 86 ksi will probably be too high for the out-of-plane strengths because the reinforcement is close to the neutral axis and therefore strains will not be high.

Before calculating the required table acceleration, support condition of 8-ft CMU walls needs to be determined. An individual specimen tested at UT Austin was of the same size but had five #4 vertical bars; the CMU wall segments in the CMU building specimen will have four #4 vertical bars. The expected flexural strength of the individual specimen is about 260 kips-in. that is 208 kips-in. multiplied by $5/4$. The CMU wall in the individual specimen did not fail until 375 psf of simulated pressure load, where connectors failed. If hinge-hinge support condition is applied, the expected pressure load capacity is

$$p_{n\_\exp} = w \times \frac{1}{8\,ft} = \frac{8 \times M_{n\_\exp}}{l^2} \times \frac{1}{8\,ft} = \frac{8 \times 260\,kips \cdot in.}{(8\,ft)^2} \times \frac{1}{8\,ft} = 339\ psf\ ,$$

which is less than 375 psf. In addition, at 375 psf of load, the CMU wall did not show significant yielding or significant crack opening. Therefore, fixed-hinge support condition is applied under the assumption that moment distribution can occur. Then, the expected pressure load capacity becomes

$$p_{n\_\exp} = w \times \frac{1}{8\,ft} \approx \frac{12 \times M_{n\_\exp}}{l^2} \times \frac{1}{8\,ft} = \frac{12 \times 260\,kips \cdot in.}{(8\,ft)^2} \times \frac{1}{8\,ft} = 508\ psf\ ,$$

which is consistent with the observed behavior of the individual specimen at 375 psf of load (not showing significant yielding or significant crack opening). Consequently, if fixed-hinge support condition is applied to the 8-ft wall segment, the load capacity becomes

$$p_{n\_\exp} = w \times \frac{1}{8\,ft} \approx \frac{12 \times M_{n\_\exp}}{l^2} \times \frac{1}{8\,ft} = \frac{12 \times 208\,kips \cdot in.}{(8\,ft)^2} \times \frac{1}{8\,ft} = 406\ psf\ .$$

Assume that the weight of the CMU wall and the attached veneer act as an inertia force that is distributed uniformly in the horizontal direction and sinusoidally in the vertical direction over the surface of out-of-plane wall segments. Applying the same response amplification factor of 1.5 used earlier, the table acceleration required to fail the 8-ft wall segment with veneer is

$$\ddot{u}_{g\_required} = \frac{p_{n\_\exp} \times \frac{\pi^2}{8}}{1.5 \times {W_{eff}}/{ft^2}} = \frac{406\,psf \times \frac{\pi^2}{8}}{1.5 \times 120\,pcf \times (7.63in. + 3.63in.) \times {ft}/{12in.}} = 2.97\,g\,,$$

where the factor ${\pi^2}/{8}$ is to account for the sinusoidal, vertical load distribution. The required table acceleration of 2.97 g slightly exceeds the level of shaking of 2.83 g required to yield the in-plane CMU walls of the CMU building specimen, with veneer and without additional roof weight. If we add about 19.5 kips of weight to the roof diaphragm, the level of shaking of 2.83 g required to yield the in-plane CMU walls reduces to 2.31 g, which is somewhat less than 2.97 g required to fail the 8-ft CMU wall segments out-of-plane. The additional weight at the roof diaphragm does not affect the table acceleration required to fail the CMU wall segments out-of-plane.

Without veneer, the table acceleration required to fail the 8-ft long wall segment becomes

$$\ddot{u}_{g\_required} = \frac{p_{n\_\exp} \times \frac{\pi^2}{8}}{1.5 \times {W_{eff}}/{ft^2}} = \frac{406\,psf \times \frac{\pi^2}{8}}{1.5 \times 120\,pcf \times 7.63in. \times {ft}/{12in.}} = 4.38\,g\,,$$

where the factor ${\pi^2}/{8}$ is to account for the sinusoidal, vertical load distribution. The required table acceleration of 4.38 g exceeds the level of shaking required to yield the in-plane CMU walls of the CMU building specimen (3.31 g without additional roof weight and 2.59 g with 19.5 kips of additional roof weight).

7.2.8 Concluding Remarks

To reduce the required table accelerations, the additional roof weight should be as large as possible without violating the 2008 MSJC capacity design requirement. Based on Section 7.2.5, that additional weight should be 19.5 kips, resulting in required table accelerations of 2.59 g without veneer, and 2.31 g with veneer. These are less than the acceleration corresponding to out-of-plane failure of the 8-ft walls (4.38 g without veneer, and 2.97 g with veneer), and will also permit us to fail the 4-ft and 12-ft walls in-plane without exceeding the probable limits (conservatively estimated as about 2.5 g) of the UCSD LHPOST facility.

7.3 ADDITIONAL DESIGNS FOR CMU BUILDING SPECIMEN

The roof diaphragm of the CMU building specimen consists of 6-in. prestressed concrete planks, spanning north-south (oriented perpendicular to the direction of shaking) and covered by 3.5 in. of concrete topping. Additional weight of 19.5 kips is also placed on the roof diaphragm. The size of prestressed concrete planks was selected so that the capacity for gravity load is enough. In this section is provided the design of horizontal reinforcement in the roof diaphragm to transfer horizontal forces developed in the roof diaphragm and the out-of-plane walls to the in-plane CMU walls. The design of roof-wall connections and lintels are also provided.

7.3.1 Design of Horizontal Reinforcement in the Roof Diaphragm

Gravity loads are calculated using 44 lb/ft^2 for 6-in. prestressed concrete planks (from manufacturer's catalog), 150 lb/ft^3 for 3.5-in. concrete topping, and 19.5 kips of added roof weight. This gives a uniformly distributed roof weight of 136.5 lb/ft2, calculated as shown below:

$$D_{roof} = 44\ lb/\ ft^2 + 150\ lb/\ ft^3\left(\frac{3.5\ in.}{12\ in./\ ft}\right) + \frac{19{,}500\ lb}{20^2\ ft^2} = 136.5\ lb/\ ft^2.$$

Lateral loads are calculated assuming a maximum table acceleration of 2.31 g, the value required to produce flexural yielding at the bases of the in-plane walls of the big CMU specimen (veneer attached), and using a dynamic response amplification factor of 1.5.

For flexure and shear under a vertical dead load of 136.5 psf (54.6 kips), 6-in. prestressed concrete planks with 3.5-in. concrete topping were selected based on manufacturer's catalog. Two #4 bars are placed, by engineering judgment, along the perimeter of the roof diaphragm for integrity to act as a bond beam. In this section, the 3.5-in. concrete topping is checked for shear and flexure under horizontal load, using a specified concrete compressive strength of 5000 psi.

The thickness of 3.5 in. (as shown in the equation below) for concrete topping is the minimum value satisfying the spacing and cover requirement for #4 reinforcement placed in both principal plan directions of the roof diaphragm.

$$1\ in. + 2 \times 0.5\ in. + 1.5\ in. = 3.5\ in.$$

The clear cover above the top bars was selected as 1.5 in. Because clear guidance is not provided in ACI 318-08 for the minimum distance between the top surface of the concrete planks and the bottom bar of the concrete topping, 1 in. was selected, which is the minimum vertical clear spacing when reinforcement is placed in two or more layers.

The horizontal inertial force developed in the upper half of out-of-plane CMU walls with veneer is assumed to be transferred to the roof diaphragm and then to the in-plane CMU walls. Based on 54.6 kips of roof weight, 14.4 kips due to the upper half of the out-of-plane CMU walls with veneer, the table acceleration of 2.31 g, and the dynamic amplification factor of 1.5, the maximum horizontal load at the roof diaphragm is 239 kips as calculated below. Then, 120 kips must be resisted at the north side and at the south side, respectively.

$$W_{roof\ diaphragm} = 136.5\ {}^{lb}\!/_{ft^2} \times (20\ ft)^2 = 54.6\ kips$$

$$W_{upper\ half\ of\ out-of-plane\ CMU} = 120\ {}^{lb}\!/_{ft^2} \times \left\{ 8\ ft \times 8\ ft \times \left(\frac{7.63+3.63}{12}\ ft \right) \times 4 \right\} \times \frac{1}{2} = 14.4\ kips$$

$$V_{roof} = (54.6\,kips + 14.4\,kips) \times 2.31\,g \times 1.5 = 239\,kips$$

Try #4 bars @ 16 in. in each principal plan direction. Because the module of masonry is 8 in., a 16-in. spacing will make the construction easy. If the roof diaphragm satisfies elastic beam theory, factored design shear and axial stresses are as follow:

$$\tau_u = \frac{VQ}{Ib} = \frac{3V}{2A} = \frac{3 \times 120\,kips}{2 \times (240\ in. \times 3.5\ in.)} = 214\ psi$$

$$\sigma_u = \frac{My}{I} = \frac{\left(120\,kips \times \frac{240\ in.}{4} \right) \times 120\ in.}{\left[\frac{3.5\ \ in. \times (240\ in.)^3}{12} \right]} = 214\ psi\ ,$$

and the corresponding design capacities are

$$\phi \tau_{n\_friction} = 0.75 \times \mu \times \frac{N}{A} = 0.75 \times 1.4 \times \frac{60\,ksi \times 0.2\ in.^2}{16\ in. \times 3.5\ in.} = 225\ psi \quad \geq 214\,psi$$

$$\phi \sigma_n = 0.9 \times \frac{60\,ksi \times 0.2\ in.^2}{16\ in. \times 3.5\ in.} = 193\ psi \quad \leq 214\,psi$$

The coefficient of friction (μ) of 1.4 was adopted from ACI 318-08, corresponding to concrete placed monolithically. Even though the design shear capacity appears sufficient, check the design shear capacity considering principal stresses:

$$\sigma_{\tau\_u\_principal} = \tau_u \times \frac{\sqrt{2}}{\sqrt{2}} = 214\ psi$$

$$\phi \sigma_{\tau\_n} = 0.75 \times 2 \times \left\{ \left(\frac{1}{\sqrt{2}} \times \frac{60\ ksi \times 0.2\ in.^2}{16\ in. \times 3.5\ in.} \right) \times \frac{1}{\sqrt{2}} \right\} = 161\ psi \quad \leq 214\,psi$$

Consequently, when applying elastic beam theory, #4 bars @ 16 in. in each principal plan direction do not satisfy both flexural strength requirements and shear strength requirements (for principal stresses). Due to the aspect ratio of the roof diaphragm (20-ft by 20-ft), however, elastic beam theory is not appropriate in this case. Therefore, recalculate the factored design stresses (or forces) and design capacities based on strength design, assuming that the reinforcement of #4 bars @ 16in. provides enough ductility to apply strength design.

For shear strength, assume that the shear load is uniformly distributed along the roof-wall interface. Then the factored shear stress and corresponding principal stress are as follow:

$$\tau_u = \frac{V}{A} = \frac{120\,kips}{240\,in. \times 3.5\,in.} = 143\,psi$$

$$\sigma_{\tau\_u\_principal} = \tau_u \times \frac{\sqrt{2}}{\sqrt{2}} = 143\,psi\,.$$

Because the design shear capacities do not change, they are as before:

$$\phi\,\tau_{n\_friction} = 0.75 \times \mu \times \frac{N}{A} = 0.75 \times 1.4 \times \frac{60\,ksi \times 0.2\,in.^2}{16\,in. \times 3.5\,in.} = 225\,psi \quad \geq 143\,psi$$

$$\phi\sigma_{\tau\_n} = 0.75 \times 2 \times \left\{ \left(\frac{1}{\sqrt{2}} \times \frac{60\,ksi \times 0.2\,in.^2}{16\,in. \times 3.5\,in.} \right) \times \frac{1}{\sqrt{2}} \right\} = 161\,psi \quad \geq 143\,psi$$

For flexural strength, the compressive area of concrete is assumed to be in elastic range and the strain in longitudinal reinforcement is limited to 0.005 to prevent significant deformation of the roof diaphragm. To calculate the flexural strength, try 27.7 in. as the distance from the neutral axis to the extreme compressive fiber.

$$E_{concrete} = 57000\sqrt{5000}\;psi = 4031ksi$$

$$\varepsilon_c = \frac{27.7\ in.}{240\ in. - 27.7\ in.} \times 0.005 = 0.00065$$

** concrete is practically in elastic range*

$$C = \frac{1}{2} \times E_c \times \varepsilon_c \times A_c = \frac{1}{2} \times 4031 ksi \times 0.00065 \times 27.7\ in. \times 3.5\ in. = 127\ kips$$

$$T = 60\ ksi \times 0.2\ in.^2 \times \left\{ \frac{(240 - 27.7)\ in.}{16} \times \frac{0.005 - 0.002}{0.005} + \frac{(240 - 27.7)\ in.}{16} \times \frac{0.002}{0.005} \times \frac{1}{2} \right\}$$

$$= 95\ kips + 32\ kips = 127\ kips$$

$$\phi M_n = 0.9 \times \left[95\ kips \times \left\{ \frac{2}{3} \times 27.7\ in. + \left(1 - \frac{1}{2} \times 0.6 \right) \times 212.3\ in. \right\} \right]$$

$$+ 0.9 \times \left[32\ kips \times \left(\frac{2}{3} \times 27.7\ in. + \frac{2}{3} \times 0.4 \times 212.3\ in. \right) \right] = 1380\ kips \cdot\ ft$$

$$M_u = 120\ kips \times \frac{20\ ft}{4} = 600\ kips \cdot\ ft \quad \le \phi M_n = 1380\ kips \cdot\ ft$$

From above based on strength design, the horizontal shear and flexural strength of the roof diaphragm is enough with 3.5-in. concrete topping and #4 bars @ 16 in. in each principal plan direction. In addition, the assumption that shear stress is uniformly distributed along the roof-wall interface is consistent with the in-plane roof-wall connection design (Section 7.3.2), in which horizontal force is assumed to be transferred uniformly along the in-plane roof-wall connections on the north and south sides.

7.3.2 Design of Roof-wall Connections

From Section 7.3.1, the maximum horizontal load transferred from the roof diaphragm to the in-plane CMU walls is 239 kips. This is assumed to be uniformly

transferred along in-plane roof-wall connections, resulting in 120 kips at the north and south sides respectively.

For in-plane roof-wall connections, use #4 L-shaped bars (at east and west sides respectively) whose horizontal legs are placed into 3.5-in. concrete topping and whose vertical legs are placed into CMU walls. Twenty-eight bars were selected so that one L-shaped bar is placed at every CMU cell except for corners. For #4 bars, the required development lengths are:

$$l_{d\_concrete} = \left(\frac{f_y \cdot \psi_t \cdot \psi_e \cdot \lambda}{25\sqrt{f'_c}} \right) d_b = \left(\frac{60{,}000\,psi \times 1 \times 1 \times 1}{25 \times \sqrt{5{,}000}\,psi} \right) \times 0.5 = 17.0\,in.$$

from ACI 318-08 with f'_c = 5,000 psi

$$l_{d\_masonry} = \frac{0.13 \cdot {d_b}^2 \cdot f_y \lambda}{K \cdot \sqrt{f'_m}} = \frac{0.13 \times (0.5in.)^2 \times 60{,}000\,psi \times 1}{(5 \times 0.5in.) \times \sqrt{1500}\,psi} = 20.1\,in.$$

from 2008 MSJC Code with f'_m = 1,500 psi

In determining the dimension of L-shaped bars, at least 18 in. of development length was provided for horizontal legs and at least 22 in. for vertical legs. Only 14.13 in. of development length is available for the vertical legs in the lintels due to depth limitations, however. Assuming the capacity of those bars to be reduced linearly in proportion to their embedment, the effective number of L-shaped bars is slightly fewer than 28:

$$28 - 6 + 6 \times \frac{14.13\,in.}{20.1\,in.} = 26.2$$

The shear transfer capacity of each L-shaped bar is governed either by shear friction between the concrete topping and the CMU walls, or by the shear strength of the #4 bars:

$$\phi V_{shear\_friction} = \phi \times \mu \times N_{bar} = 0.8 \times 0.6 \times 60ksi \times 0.2in.^2 = 5.76\,kips$$

$$\phi V_{shear\_strnegth} = \phi \times V_{bar} = 0.9 \times (0.6 \times 60ksi) \times 0.2in.^2 = 6.48\,kips$$

For shear friction, a coefficient of friction of 0.6 was used based on the assumption that the top surface of CMU walls is not intentionally roughened. Then, the required number of L-shaped bars at the east and west sides respectively becomes:

$$\frac{125\,kips}{5.76\,kips} = 21.7\,.$$

Therefore, the provided twenty-eight #4 L-shaped bars will be enough to transfer the maximum horizontal load from the roof diaphragm to the in-plane CMU walls.

Even though this test specimen will be shaken in the east-west direction only, it should be designed as though it were a real building, capable of being shaken in either principal plan direction. For this reason, the roof-wall connections for the east and west CMU walls should be designed for sufficient in-plane capacity in the east-west direction.

The moment strength of the big CMU specimen for east-west shaking is about 15% smaller than that for the east-west shaking. The required number of L-shaped bars is therefore 17.9 (21.7 multiplied by 0.85). Use twenty-eight #4 L-shaped bars on the east side and on the west side for easy construction.

7.3.3 Design of Lintels

The lintels over the door openings have a clear span of 4 ft and a total depth of 16 in. (two courses of CMU). Since the center of vertical supports is 4 in. from side edges of an opening, an effective span of 4 ft - 8 in. is used to calculate flexure and shear. Based on 136.5 psf of roof load and 120 pcf of CMU wall weight, the load on the lintel is:

$$w_{dead} = w_{roof} + w_{CMU} = (136.5\ psf \times 10\,ft) + \left(120\ pcf \times 1.33\,ft \times \frac{7.63}{12}\ ft\right) = 1467\ lbs/ft\,.$$

In the calculation, the veneer over the opening is not included because it is supported by the loose lintel. Then the factored design moment and shear are respectively

$$M_u = \frac{w_u \times l^2}{8} = \frac{(1.2 \times 1467\ plf) \times (4.67\ ft)^2}{8} \times \frac{12\ in.}{ft} = 57.5\ kips \cdot in.$$

$$V_u = \frac{w_u \times l}{2} = \frac{(1.2 \times 1467\ plf) \times 4.67\ ft}{2} = 4.11\ kips$$

Using an approximate internal lever arm of 11 in., the required amount of flexural reinforcement is

$$A_{s\_required} = \frac{M_u}{\phi \cdot f_y \cdot d} = \frac{57.5\ kips \cdot in.}{0.9 \times 60\ ksi \times 11\ in.} = 0.10\ in.^2$$

In addition, the nominal flexural strength of the lintel must not be less than the nominal cracking moment multiplied by 1.3. The modulus of rupture (f_r) of PCL mortar is 163 psi for fully grouted hollow units. Then the nominal cracking moment and the corresponding amount of reinforcement are

$$M_{cr} = S \cdot f_r = \frac{b \cdot t^2}{6} \cdot f = \frac{7.63\ in. \times (16\ in.)^2}{6} \cdot 163\ psi = 53.1\ kips \cdot in.$$

$$A_{s\_1.3Mcr} = \frac{1.3\ M_{cr}}{f_y \cdot d} = \frac{1.3 \times 53.1 kips \cdot in.}{60\ ksi \times 11\ in.} = 0.10\ in.^2$$

Use one #4 bar (0.2 in.^{2}) for longitudinal reinforcement at the bottom course.

The design shear strength from masonry is

$$\phi V_{nm} = 0.8 \times 2.25 \times \sqrt{1500}\ psi \times (16\ in. \times 7.63\ in.) = 8.51 kips \quad \geq V_u = 4.11 kips,$$

indicating that shear reinforcement is not needed.

7.4 SUMMARY OF SHAKE-TABLE TESTS AND TEST RESULTS OF CMU BUILDING SPECIMEN

In this section, the shake-table tests and test results of the CMU building specimen are briefly summarized. Detailed description of the tests and the test results will be provided in the PhD dissertation now being prepared by Hussein Okail at UCSD. The same ground motions (Sylmar record and Tarzana record) used for the shake-table testing of the CMU wall specimens were used. Those ground motions are described in Section 6.2.

The main purpose of shake-table testing of the CMU building specimens is to examine overall and local behaviors (in-plane and out-of-plane) of the low-rise concrete masonry building with clay masonry veneer, and to provide experimental data to extend the analytical models developed for the concrete masonry walls with clay masonry veneer (Section 9) to the low-rise concrete masonry building with clay masonry veneer.

The overall behavior of the CMU building specimen can be represented by the in -plane acceleration and displacement at the planar center of the roof diaphragm, which is governed primarily by the in-plane response of the CMU shear walls and partially by in-plane deformation of the roof diaphragm. To examine the local behaviors of the specimen, the following key responses will be looked into:

- flexural yielding and base sliding of the CMU walls, in-plane;
- rocking, sliding and collapse of the clay masonry veneer, in-plane;
- flexural yielding of the CMU walls, out-of-plane; and
- collapse of the clay masonry veneer, out-of-plane.

7.4.1 Instrumentation for and Credibility of Recorded Data from Shake-table Tests of CMU Building Specimen

The instrumentation scheme for the CMU building specimen is shown in Appendix D (Figures D-1 through D-13). For the first letter of each channel name in

those figures, ‘A’ stands for Accelerometer; ‘D’ stands for Displacement transducer; ‘L’ stands for LVDT; and ‘E’ stands for strain gage.

In shake-table tests of the CMU building specimen, more than usual displacement data were questioned about their credibility. Most of the doubtful data showed exaggerated values. Primary cause seems to be the flexible reference frame system (Figure 7-6 through Figure 7-9). The wood studs crossing the steel frames or other wood studs were not stiff enough in some cases: probably due to flexural stiffness of the wood studs, or the stiffness of the connection to the steel frames or to other wood studs. Accordingly, before analyzing the response of the CMU building specimen, reliable displacement data should have been determined. The recorded displacement data, which are believed to be reliable, are listed in Table 7-6 by their channel names. Those data are checked as described below. It would also have been possible to obtain displacement data by double integration and judicious filtering of recorded acceleration data. In this dissertation, however, recorded displacement data are used directly, to avoid the need for any numerical processing.

To determine whether the displacement data is reliable, consistency with other displacement data was checked using structural symmetry or the location of the measuring device on the reference frame system. For example, in Figure 7-10 is plotted displacement data recorded at the following three locations (Tarzana 100 %):

- near the base of the 12-ft long in-plane CMU wall on the north side (LVDT);
- near the top of the 12-ft long in-plane CMU wall on the north side (LVDT); and
- near the top of the out-of-plane CMU at the north-west corner.

These transducers were attached to different reference frames (supports). They would be expected to be affected somewhat by the flexibility of those supports, and this was checked. The recorded displacement data (plotted in Figure 7-10) are consistent throughout the peak response of the building specimen under Tarzana 100 % (about 22 to 28 sec), indicating the recorded displacements are reliable. The similarity in measured

displacements near the base and near the top of the 12-ft long CMU wall is because the CMU wall responded by base sliding. In case of DEC 11 through 16 (Figure D-8) and DWC 11 through 16 (Figure D-11), near the top of the out-of-plane CMU walls, most of the recorded displacement data gave similar values throughout shake-table testing because the roof diaphragm was essentially rigid horizontally. In case of DEV 06 in Figure D-10 and DWV 06 in Figure D-13, the displacement data that were located around them were compared considering the arrangement of the crossing wood studs. If the connection to the steel frames or to other wood studs is stiff enough but the wood stud is flexible in bending, the measured displacement can be expected to decrease as the displacement transducers are located closer to the steel frames.

Table 7-6 Reliable recorded displacement data

location of measurement			reliable recorded displacement data
north side	CMU	at base	LNC 01, LNC 02
		near top	DNC 07, DNC 08
	veneer	at base	LNV 01, LNV 02
		near top	DNV 08 *
south side	CMU	at base	LSC 02
		near top	DSC 07, DSC 08
	veneer	at base	LSV 01
		near top	DSV 08 *
east side	CMU	at base	LEC 01, LEC 02
		near top	DEC 11, DEC 12, DEC 13, DEC 14, DEC 15, DEC 16
	veneer	at base	LEV 01, LEV 02
		near mid-height	DEV 06, DEV 10
west side	CMU	at base	LWC 01, LWC 02
		near top	DWC 11, DWC 13, DWC 14, DWC 15, DWC 16
	veneer	at base	LWV 01, LWV 02
		near mid-height	DWV 02, DWV 06

** DNV 08 and DSV 08 (displacement data for 4-ft long veneer) were somewhat questionable compared to others listed in this table. However, DNV 08 and DSV 08 were judged to be satisfactory for their use, because the movement of the 4-ft long veneer on the north and south side was large enough to make DNV 08 and DSV 08 useful.*

Figure 7-6 CMU wall on east side with reference frame system

Figure 7-7 Clay masonry veneer on east side with reference frame system

Figure 7-8 CMU wall on west side with reference frame system

Figure 7-9 Clay masonry veneer on west side with reference frame system

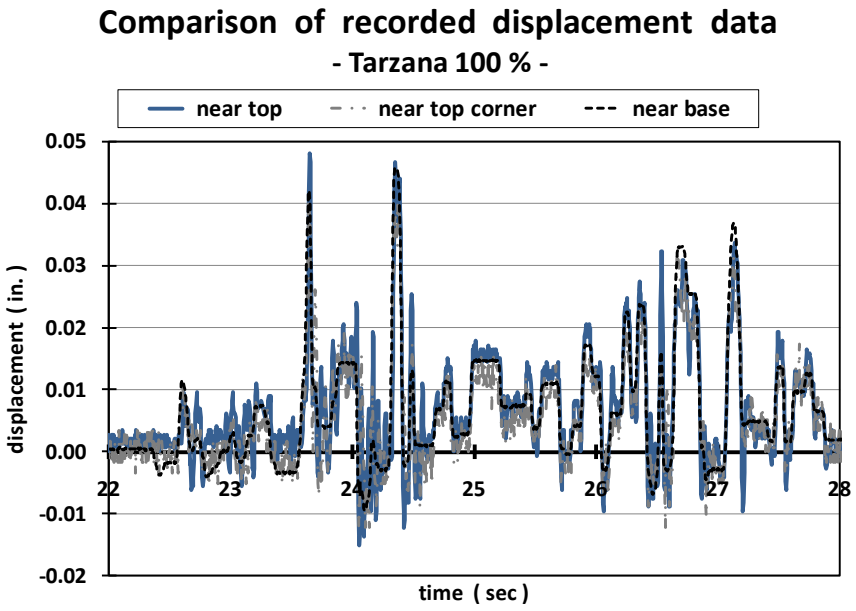

Figure 7-10 Comparison of displacement data recorded at three locations, Tarzana 100 %

7.4.2 Overall Summary of Shake-table Tests and Test Results of CMU Building Specimen

The overall view the CMU building specimen was shown in Figure 7-1 and in Figure 7-2. A photo of the specimen on the shake table, from the southwest corner, is shown Figure 7-11. The specimen was shaken in east-west direction. In general, the response of the CMU building specimen was as described in Section 2.3.

The CMU building specimen shown in Figure 7-11 was subjected to the sequence of ground motions listed in Table 6-2. That table lists peak ground accelerations (PGA): targeted ones and measured ones. Positive values are PGA to the east while negative values are PGA to the west. After Sylmar 200%, Tarzana record was used so as not to exceed the capacity of the table. White noise (0.03g of PGA with sweeping frequency range of 1 – 33 Hz) was used to assess the dynamic properties of each specimen, and to assist tracking the progression of damage. The table output motions were generally

higher than the target ground motions. Key behaviors of the CMU building specimen are listed in Table 7-8. Most visible damages began to take place during the first run to Tarzana 150 %, and the CMU building specimen was essentially failed by base sliding of the in-plane CMU walls during the first Tarzana 150 %. Representative photos of response after the first Tarzana 150 % are shown in Figure 7-12 through Figure 7-17. During the second run to Tarzana 150 %, severe damage occurred as shown Figure 7-18 through Figure 7-23.

The local failure of the CMU walls near the door openings (Figure 7-15) is not toe crushing. It is produced when the wall slides in-plane, and the vertical reinforcement at the jamb pries off the masonry between the bar and the jamb. Similar local cracking was seen in the quasi-static testing of the in-plane CMU wall specimens.

The flexural cracking in the out-of-plane CMU walls at the west and east sides (Figure 7-17) was caused by out-of-plane bending (combination of out-of-plane inertia forces and imposed deformation pattern produced by in-plane sliding of the in-plane CMU walls). The south and north walls slid east-west; the centers of the east and west walls did not slide; and the deformation between the center and the edges of the east and west walls caused the flexural cracking.

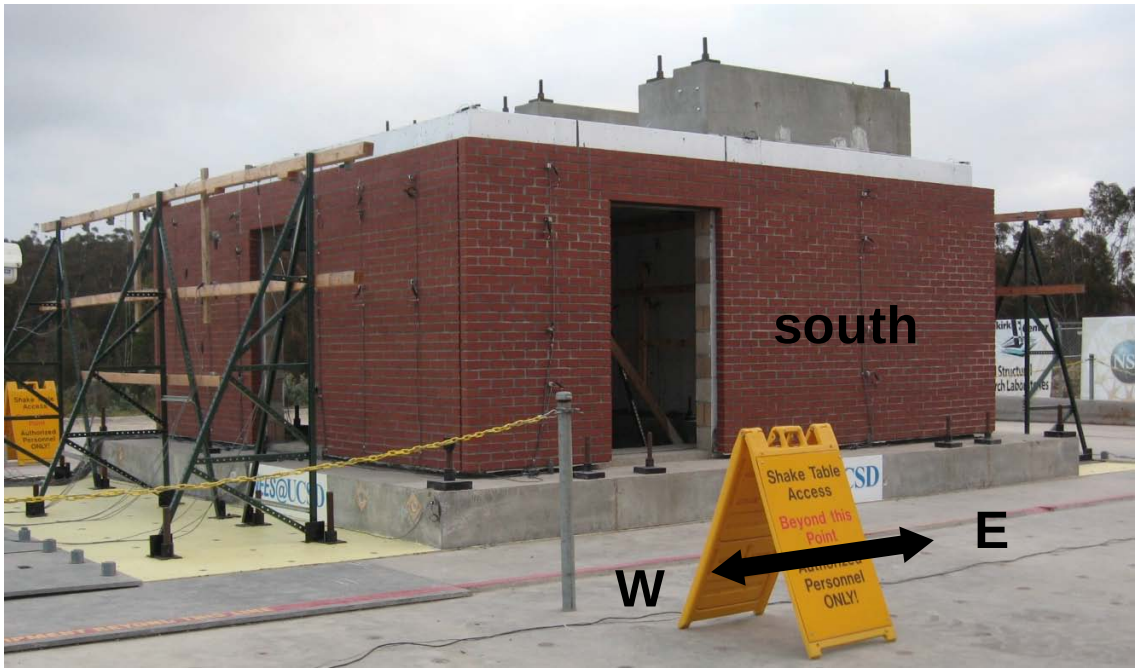

Figure 7-11 CMU building specimen on shake table

Table 7-7 Targeted and measured PGA of each ground motion for CMU building specimen

ground motion	PGA (g, positive to east)			
	targeted		measured **	
	max	min	max	min
white noise	0.03g with sweeping frequency range of 1 – 33 Hz			
Sylmar 20 %	0.17	- 0.12	0.19	- 0.22
Sylmar 40 %	0.34	- 0.24	0.31	- 0.35
Sylmar 80 % (DBE for SDC E)	0.67	- 0.47	0.79	- 0.71
white noise	0.03g with sweeping frequency range of 1 – 33 Hz			
Sylmar 120 % (MCE for SDC E)	1.01	- 0.71	1.18	- 1.11
white noise	0.03g with sweeping frequency range of 1 – 33 Hz			
Sylmar 200 %	1.69	- 1.18	2.03	- 1.62
white noise	0.03g with sweeping frequency range of 1 – 33 Hz			
Tarzana 100 % *	1.59	-1.79	1.55	- 2.40
white noise	0.03g with sweeping frequency range of 1 – 33 Hz			
Tarzana 150 % (1st) *	2.38	-2.69	2.27	- 3.48
white noise	0.03g with sweeping frequency range of 1 – 33 Hz			
Tarzana 150 % (2nd) *	2.38	-2.69	2.34	- 3.36

** the sign was flipped from the original record*

Table 7-8 Key behaviors of CMU building specimen

target ground motion	Comments
Sylmar 80 % (DBE)	No visible damage was observed. 4-ft in-plane veneer began to rock (up to about 0.04 in. at the top) with regard to the CMU wall.
Sylmar 120 % (MCE)	No visible damage was observed. 4-ft in-plane veneer moved up to about 0.08 in. at the top by sliding and rocking with regard to the CMU wall.
Sylmar 200 %	Hairline cracking was observed at the bases of the CMU walls in- and out-of-plane, indicating flexural cracking of the in-plane walls and the out-of-plane walls. Up to this level of shaking, the maximum displacement at the roof diaphragm was negligible (less than 0.02 in.). 12-ft in-plane veneer began to slide (up to about 0.03 in.) with regard to the CMU wall. 4-ft in-plane veneer moved about 0.16 in. at the top by sliding and rocking with regard to the CMU wall.
Tarzana 100 % *	The in-plane veneer rocked and slid visibly. The maximum displacement at the roof diaphragm was about 0.05 in., which was primarily by sliding in 12-ft CMU walls and by rocking in 4-ft CMU walls. Planar response of the roof diaphragm was essentially rigid. 12-ft in-plane veneer slid up to about 0.07 in. with regard to the CMU wall. 4-ft in-plane veneer moved about 0.46 in. at the top by sliding and rocking with regard to the CMU wall.
Tarzana 150 % (1st) *	The vertical bars in 12-ft CMU walls became loose at the base at about 0.2 in. of sliding and fractured soon after due to sliding. The maximum displacement at the roof diaphragm was about 1.5 in., which was primarily by sliding in 12-ft CMU walls and by combination of rocking and sliding in 4-ft CMU walls. Planar response of the roof diaphragm was essentially still rigid. 12-ft in-plane veneer slid more than 1.9 in. with regard to the foundation. 4-ft in-plane veneer moved up to about 2 in. at the top by sliding and rocking with regard to the CMU wall. The veneer at the northeast corner cracked due to a combination of out-of-plane bending on the east side, plus in-plane sliding of the veneer on the north side. These actions were accompanied by general back-and-forth sliding between the CMU and the foundation, and differential sliding between the veneer and the CMU on the north and south sides. They may also have been accompanied by hammering contact between the veneer on the east side and the adjacent CMU wall. The building specimen experienced fracture of the veneer at the northeast and southeast corners, and generalized out-of-plane cracking of the veneer on the east side.
Tarzana 150 % (2nd) *	The specimen was subjected for the second time to Tarzana 150 %. The maximum displacement at the roof diaphragm was about 9 in. Except for the east side, the toes of the CMU walls badly damaged. On the east side, the CMU walls themselves were badly damaged. The veneer was badly damaged at the northeast and southeast corners, and on the east side.

** the sign was flipped from the original record*

Figure 7-12 Cracking near lintel end on north side (1st Tarzana 150 %)

Figure 7-13 Cracking of veneer at northeast corner (1st Tarzana 150 %)

Figure 7-14 Cracking of veneer at southeast corner (1st Tarzana 150 %)

Figure 7-15 Local failure of CMU at edge of long segment on south side, due to in-plane sliding (1st Tarzana 150 %)

Figure 7-16 Relative displacement at expansion joint in clay veneer at door on South side (1st Tarzana 150 %)

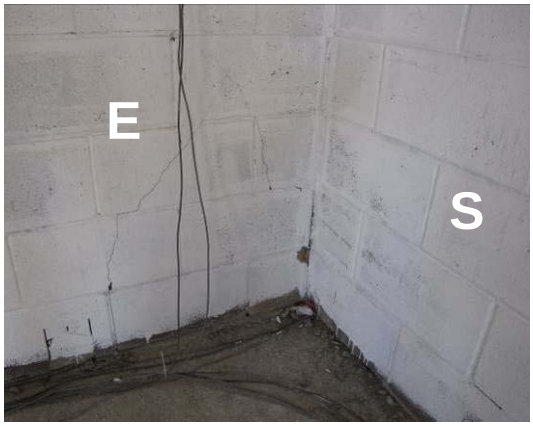

Figure 7-17 Flexural cracking of CMU wall at southeast corner due to out-of-plane flexure of horizontal wall strips as structure slid east-west (1st Tarzana 150 %)

Figure 7-18 Damage to veneer on northeast corner and east side (2nd Tarzana 150 %)

Figure 7-19 Damage to CMU at southeast corner (2nd Tarzana 150 %)

Figure 7-20 Damage to lintel over door on north side (2nd Tarzana 150 %)

Figure 7-21 Inelastic buckling of splice in longitudinal reinforcement at west side of door on south side (2nd Tarzana 150 %)

Figure 7-22 Detail of damage to northeast corner (2nd Tarzana 150 %)

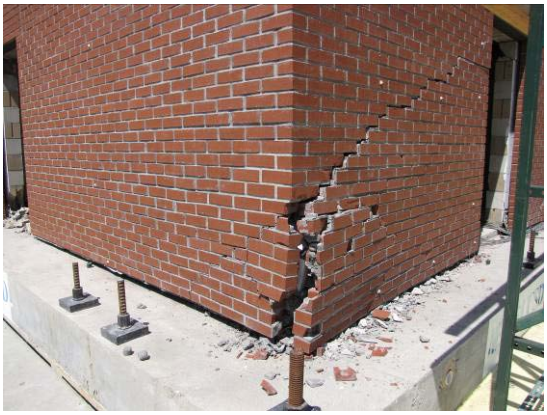

Figure 7-23 Damage to southeast corner (2nd Tarzana 150 %)

7.4.3 Overall Behavior of CMU Building Specimen

The peak in-plane accelerations and displacements at the planar center of the roof diaphragm are used to represent the overall behavior of the CMU building specimen. Those peak accelerations and displacements are governed primarily by the in-plane response of the CMU shear walls and partially by in-plane deformation of the roof diaphragm. Since the roof diaphragm was essentially rigid horizontally in the big CMU specimen, the overall behavior of that specimen was governed by the in-plane response of the in-plane CMU walls (due to flexural yielding and base sliding).

In Table 7-9 are listed the peak in-plane accelerations and displacements at the planar center of the roof diaphragm. Maximum and minimum values in that table are the peak responses to the positive direction (to the east in Figure 7-11) and to the negative direction (to the west in Figure 7-11), respectively. The acceleration at the roof diaphragm was measured at the planar center of the roof diaphragm, and was consistent with the accelerations measured at other locations of the roof diaphragm. The displacement measurement at the roof diaphragm showed defective values as described in Section 7.4.1. Therefore, the average of the displacements near the top of the 12-ft long in-plane CMU walls, one on the north side and one on the south, is used to represent the displacement at the roof diaphragm in this dissertation. Since the 12-ft in-plane CMU walls showed essentially only base sliding without in-plane flexural deformation (refer to Section 7.4.4), the displacements near the top of the 12-ft long in-plane CMU walls is equivalent to the displacement at the top of the 12-ft long in-plane CMU walls. The peak displacements near the top of the out-of-plane CMU walls (DEC 11 through 16 in Figure D-8 and DWC 11 through 16 in Figure D-11) showed consistent results throughout shake-table testing, indicating that there was essentially no horizontal out-of-plane deformation in the roof diaphragm.

The maximum and minimum responses up to Sylmar 120 % are not shown in Table 7-9 because the peak displacements were too small (less than 0.005 in.) to be used. The displacement of the roof diaphragm at Sylmar 120 % (equivalent to SDC E) indicates

that the overall response of the CMU building specimen is essentially rigid for ground motion corresponding to SDC E. The specimen was almost rigid up to Tarzana 100 %; the displacement was about 0.03 in. and the amplification factor for the absolute maximum acceleration was less than 10 %. The 12-ft long in-plane CMU walls that govern the overall response of the CMU building specimen failed during 1st Tarzana 150 % by fracture of vertical reinforcement due to base sliding. Accordingly, the displacement went up to about 1.5 in. at 1st Tarzana 150 % and up to about 9 in. at 2nd Tarzana 150 %. The absolute maximum acceleration at the roof diaphragm at 2nd Tarzana 150 % (1.95 g) is significantly less than the absolute peak ground acceleration (PGA, 3.36 g) due to the fracture of the vertical reinforcement in the 12-ft in-plane CMU walls during 1st Tarzana 150 %.

Table 7-9 Peak responses at roof diaphragm

ground motion			PGA (g), measured	peak responses at roof diaphragm	
				acceleration (g)	displacement (in.)
Sylmar	200 %	max	2.03	2.20	0.01
		min	-1.62	-1.76	-0.01
Tarzana	100 %	max	1.55	1.82	0.03
		min	-2.40	-2.50	-0.01
	150 % (1st)	max	2.27	3.39	1.47
		min	-3.48	-3.13	-0.61
	150 % (2nd)	max	2.34	1.47	3.83
		min	-3.36	-1.95	-9.07

Overall response (displacement and acceleration at the roof diaphragm) of the CMU building specimen at Tarzana 100 % and at 1st Tarzana 150 % are shown in Figure

7-24 and Figure 7-25, respectively. The figures plot the data only from 15 sec to 35 sec because the fluctuation of the response outside that range was negligible. Until the CMU building fails at (between 24 sec and 30 sec at 1st Tarzana 150 %), the displacements and the accelerations show similar pattern to the ground motion due to large stiffness. The natural period based on the data from white noise was about 30 Hz until after Tarzana 100 %, and decreased to about 15 Hz after 1st Tarzana 150 %.

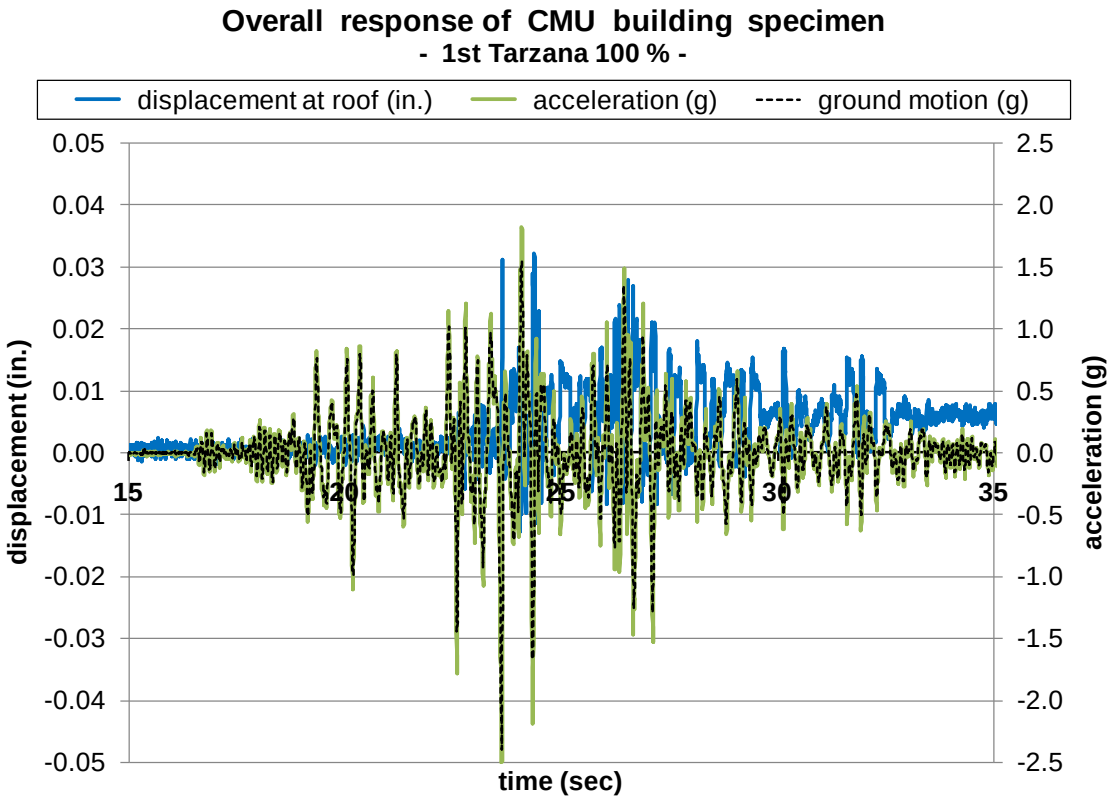

Figure 7-24 Overall response of CMU building specimen at Tarzana 100 % (displacement and acceleration along with ground motion)

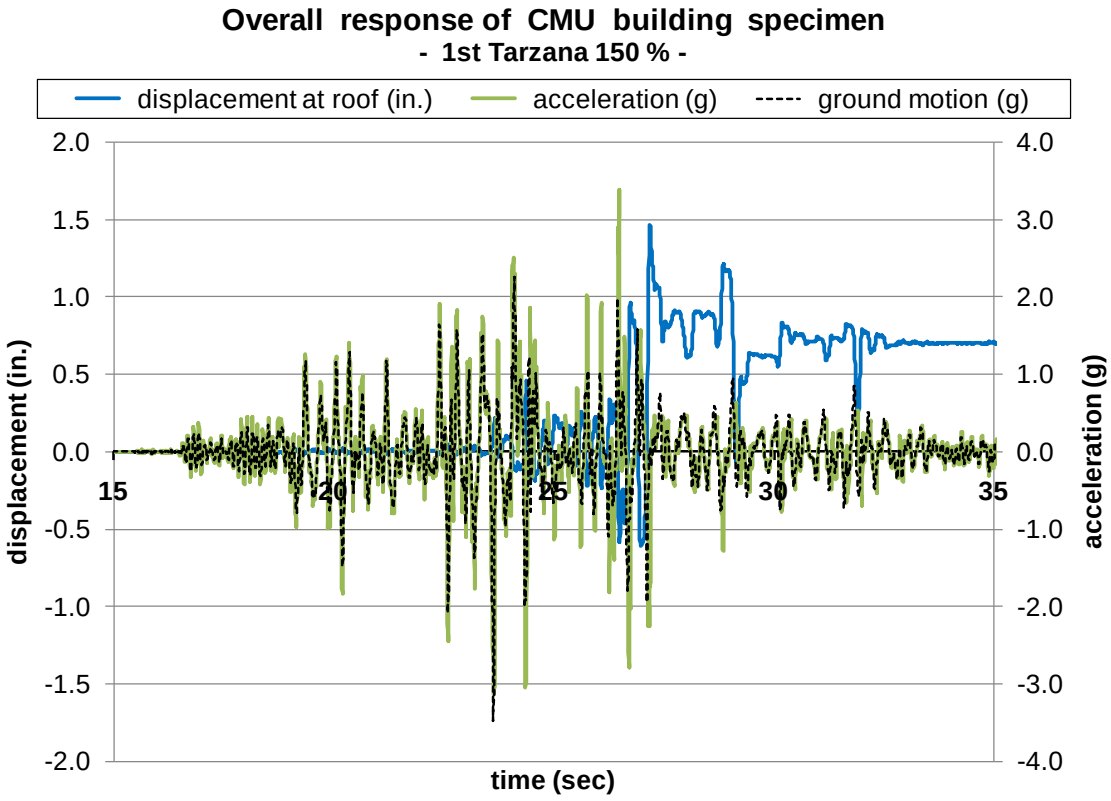

Figure 7-25 Overall response of CMU building specimen at 1st Tarzana 150 % (displacement and acceleration along with ground motion)

7.4.4 Flexural Yielding and Base Sliding of In-plane CMU Walls

The location of strain gages placed at the base of in-plane CMU walls is shown in Figure D-3 and Figure D-6, which are reproduced in Figure 7-26 and Figure 7-27, respectively. Six strain gages were used at the base of each in-plane CMU wall segment. At wall ends, two strain gages were attached to reduce the probability of losing data.

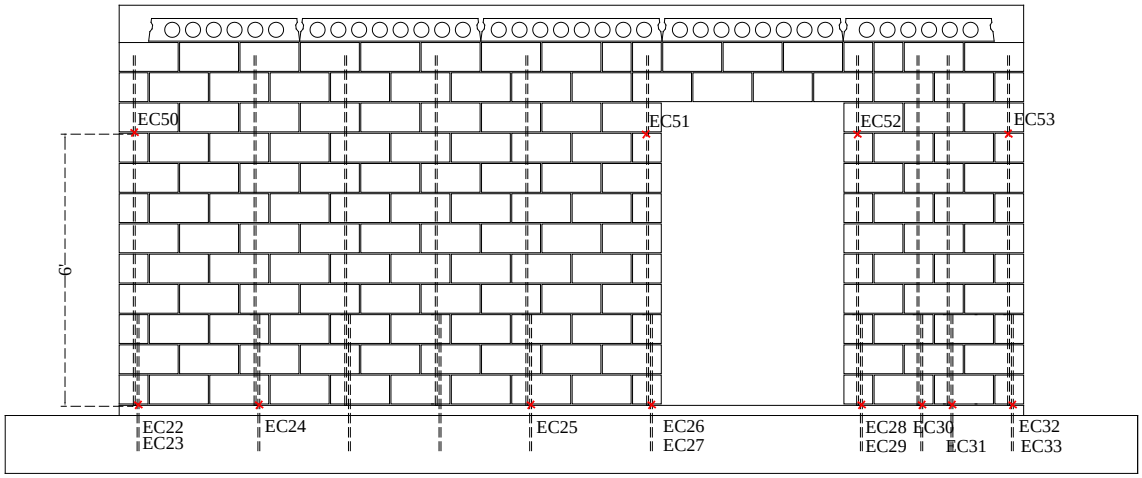

North Elevation - CMU

Figure 7-26 Location of strain gages at base of in-plane CMU walls, south side

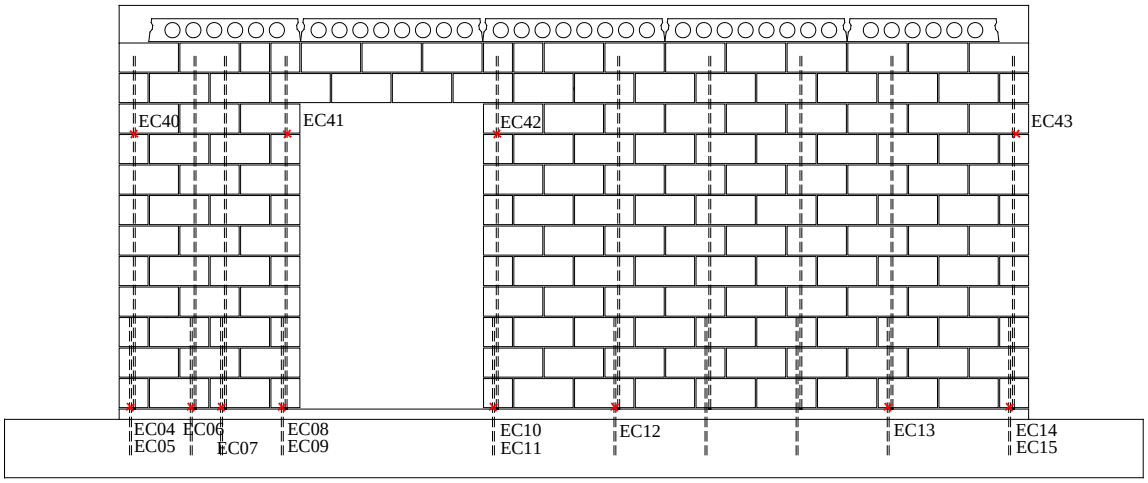

South Elevation - CMU

Figure 7-27 Location of strain gages at base of in-plane CMU walls, south side

Maximum strains are listed in Table 7-10 through Table 7-13. The vertical reinforcement began to yield at Sylmar 200 % in the 12-ft long in-plane CMU walls (Table 7-10 and Table 7-11), and at Tarzana 100 % in the 4-ft long in-plane CMU walls (Table 7-12 and Table 7-13). The strain gages were broken during 1st Tarzana 150 % in all the in-plane CMU walls.

From Table 7-10 and Table 7-11, it is not clear whether the 12-ft long CMU walls were governed by flexure or base sliding. Figure 7-28 plots the displacements near the base and near the top of the north 12-ft long CMU wall during 1st Tarzana 150 % from 20 sec to 26 sec. The two graphs in Figure 7-28 are essentially the same, which indicates that the 12-ft long in-plane CMU wall was governed by base sliding. If flexural behavior is significant, the two graphs in Figure 7-28 should be different. Since the overall response of the CMU building specimen was governed primarily by the 12-ft long in-plane CMU walls due to their large in-plane stiffness and strength, the 4-ft long in-plane CMU walls yielded by flexure immediately after the 12-ft long CMU walls began to slide.

Table 7-10 Maximum strains of vertical reinforcement at base of in-plane CMU wall (south, 12-ft long)

ground motion	EC10	EC11	EC12	EC13	EC14	EC15
Sylmar 2.0	0.0021	0.0025	0.0019	0.0018	-	0.0046
Tarzana 1.0	0.0097	0.0125	0.0095	0.0014	-	0.0045
Tarzana 1.5 (1st)	0.0253*	0.0253*	0.0253*	0.0253*	-	0.0251*

** strain gage was broken*

Table 7-11 Maximum strains of vertical reinforcement at base of the in-plane CMU wall (north, 12-ft long)

ground motion	EC22	EC23	EC24	EC25	EC26	EC27
Sylmar 2.0	0.0036	0.0022	0.0020	0.0015	0.0021	0.0030
Tarzana 1.0	0.0037	0.0023	0.0016	0.0060	0.0037	0.0137
Tarzana 1.5 (1st)	0.0251*	0.0252*	0.0253*	0.0254*	0.0251*	0.0251*

** strain gage was broken*

Table 7-12 Maximum strains of vertical reinforcement at base of in-plane CMU wall (south, 4-ft long)

ground motion	EC04	EC05	EC06	EC07	EC08	EC09
Sylmar 2.0	0.0006	-	0.0010	0.0015	-	-
Tarzana 1.0	0.0021	-	0.0013	0.0014	-	-
Tarzana 1.5 (1st)	0.0247*	-	0.0253*	0.0253*	-	-

** strain gage was broken*

Table 7-13 Maximum strains of vertical reinforcement at base of in-plane CMU wall (north, 4-ft long)

ground motion	EC28	EC29	EC30	EC31	EC32	EC33
Sylmar 2.0	0.0015	0.0019	0.0011	0.0013	0.0014	0.0014
Tarzana 1.0	0.0015	0.0017	0.0011	0.0015	0.0025	0.0024
Tarzana 1.5 (1st)	0.0248*	0.0248*	0.0246*	0.0247*	0.0247*	0.0248*

** strain gage was broken*

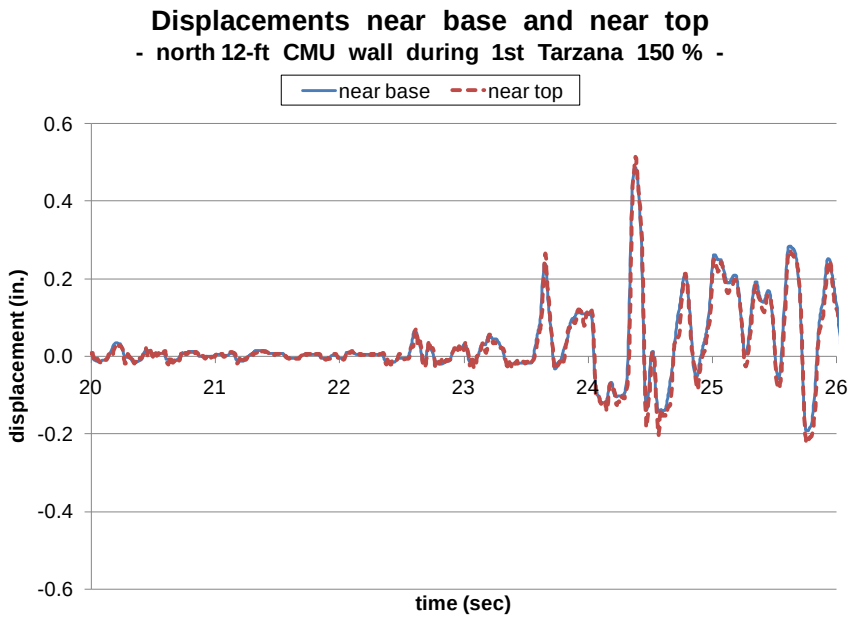

Figure 7-28 Displacements near base and near top of north 12-ft long CMU wall at 1st Tarzana 150 %

In Table 7-14 and Table 7-15 are listed the maximum displacements near the top of the 12-ft CMU walls and the maximum displacement near the top and near the base of the 4-ft CMU wall. The absolute maximum displacements up to Tarzan 100 % were less than 0.05 in., and increased up to about 1.5 in. at 1st Tarzana 150 %.

Figure 7-29 plots the average displacements near the top of the two 12-ft in-plane CMU walls along with ground motion during 1st Tarzana 150 %, from 22 sec to 28 sec. The peak ground acceleration (PGA) is about 3.5 g at about 24 sec, when the displacement of the CMU wall is about 0.20 in. After this point, the CMU wall effectively becomes uncoupled from the foundation. Note that the displacements become larger even though the ground motion is a lot smaller. From the plot (Figure 7-29), it is judged that the vertical reinforcement at the base of the 12-ft long in-plane CMU wall fractured between 24 sec and 28 sec. This fracture of the vertical reinforcement explains the large displacement near the top at 1st and 2nd Tarzana 150 % in Table 7-14 and Table 7-15.

Table 7-14 Response of in-plane CMU walls (north)

ground motion			PGA (g), measured	12-ft long CMU (sliding only)	4-ft long CMU (rocking and sliding)	
				displacement near the top (in.)	displacement near the top (in.)	displacement near the base (in.)
Sylmar	200 %	max	2.03	0.01	0.00	0.00
		min	-1.62	-0.00	-0.01	-0.00
Tarzana	100 %	max	1.55	0.05	0.03	0.00
		min	-2.40	-0.02	-0.02	-0.00
	150 % (1st)	max	2.27	1.53	1.33	0.19
		min	-3.48	-0.58	-0.64	-0.40
	150 % (2nd)	max	2.34	4.18	3.75	-
		min	-3.36	-8.65	-9.78	-

Table 7-15 Response of in-plane CMU walls (south)

ground motion			PGA (g), measured	12-ft long CMU (sliding only)	4-ft long CMU (rocking and sliding)	
				displacement near the top (in.)	displacement near the top (in.)	displacement near the base (in.)
Sylmar	200 %	max	2.03	0.01	0.01	0.00
		min	-1.62	-0.01	-0.01	-0.01
Tarzana	100 %	max	1.55	0.03	0.03	0.01
		min	-2.40	-0.01	-0.02	-0.00
	150 % (1st)	max	2.27	1.40	1.63	0.17
		min	-3.48	-0.64	-0.61	-0.52
	150 % (2nd)	max	2.34	3.48	3.89	-
		min	-3.36	-9.49	-7.22	-

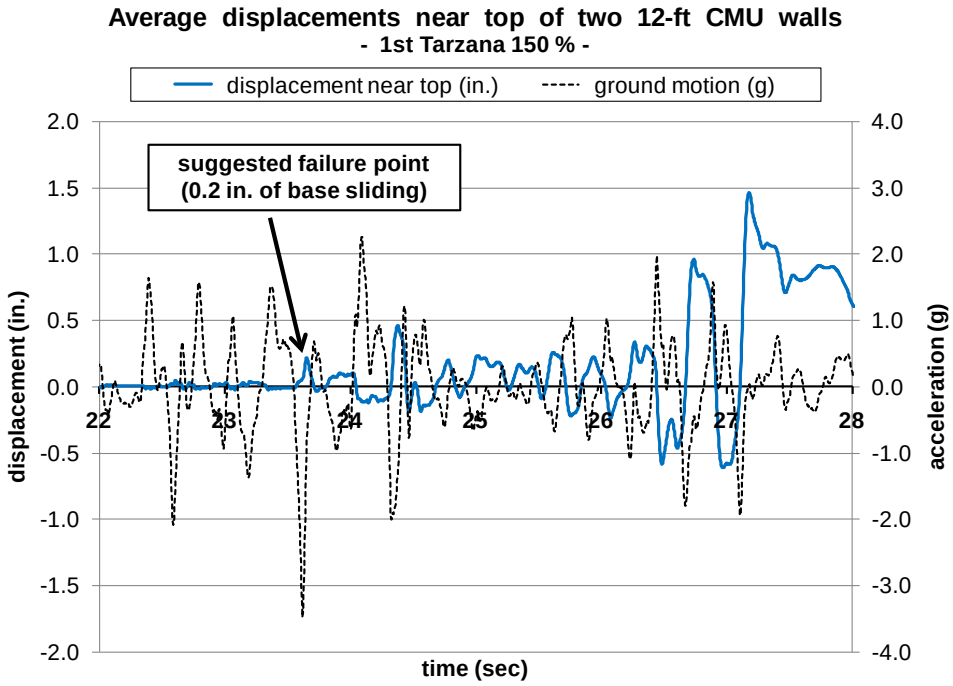

Figure 7-29 Average displacements near top of two 12-ft CMU walls along with ground motion at 1st Tarzana 150 %, 22 sec to 28 sec

7.4.5 Rocking, Sliding and Collapse of In-plane Veneer

The peak relative displacements of the in-plane veneer (with regard to the CMU walls) on the north side and on the south side are listed in Table 7-16 and Table 7-17, respectively: the peak relative displacements near the base of the 12-ft long veneer with regard to 12-ft long CMU walls, and the peak relative displacements near the top and near the base of the 4-ft long veneer with regard to 4-ft long CMU walls. The positive direction in Table 7-16 and Table 7-17 is to the east in Figure 7-11, and the minimum values indicate the peak response to the west direction.

The in-plane veneer on the north side was connected to the in-plane CMU walls using tri-wire connectors, while the in-plane veneer on the south side was connected to the in-plane CMU walls using double eye-and-pintle connectors. The 12-ft long in-plane veneer essentially slid only with regard to the CMU walls while the 4-ft long in-plane veneer is primarily governed by rocking with regard to the CMU walls, which was visually obvious during shake-table testing. At 2nd Tarzana 150 %, the displacements were not measured to prevent the loss of measuring devices since it was judged that the veneer might collapse during the shaking. After 2nd Tarzana 150 %, none of the in-plane veneer collapsed but some of the tri-wire connectors were observed to have fractured.

The 12-ft long veneer (Table 7-16 and Table 7-17) did not slide until Sylmar 120 %. The peak displacements of the 12-ft long veneer with tri-wire connectors (Table 7-16) are similar to those for double eye-and-pintle connectors (Table 7-17) at Sylmar 200 %, and become large at Tarzana 100 %. This seems to be because the in-plane strength of the double eye-and-connectors is larger than tri-wire connectors.

The peak displacements of the 4-ft long veneer with tri-wire connectors (Table 7-16) are smaller than those for double eye-and-pintle connectors (Table 7-17) up to Sylmar 200 %, and become larger since Tarzana 100 %. This seems to be because the double eye-and-pintle connectors have some tolerance between the diameter of the eyes and the diameter of the pintles, while the in-plane strength of the double eye-and-connectors is larger than tri-wire connectors.

Table 7-16 Relative response of in-plane veneer with regard to CMU walls (north, tri-wire connectors)

ground motion			PGA (g), measured	12-ft long veneer (sliding only)	4-ft long veneer (rocking and sliding)
				displacement near base (in.)	displacement near top (in.)
Sylmar	80 %	max	0.79	0.00	0.01
		min	-0.71	-0.00	-0.02
	120 %	max	1.18	0.00	0.04
		min	-1.11	-0.00	-0.04
	200 %	max	2.03	0.03	0.08
		min	-1.62	-0.02	-0.14
Tarzana	100 %	max	1.55	0.07	0.20
		min	-2.40	-0.03	-0.46
	150 % (1st)	max	2.27	-	1.95
		min	-3.48	-	-1.72

Table 7-17 Relative response of in-plane veneer with regard to CMU walls (south, double eye-and-pintle connectors)

ground motion			PGA (g), measured	12-ft long veneer (sliding only)	4-ft long veneer (rocking and sliding)
				displacement near base (in.)	displacement near top (in.)
Sylmar	80 %	max	0.79	0.00	0.04
		min	-0.71	0.00	-0.03
	120 %	max	1.18	0.00	0.07
		min	-1.11	0.00	-0.07
	200 %	max	2.03	0.02	0.12
		min	-1.62	-0.02	-0.16
Tarzana	100 %	max	1.55	0.03	0.16
		min	-2.40	-0.01	-0.17
	150 % (1st)	max	2.27	0.20	0.26
		min	-3.48	-1.06	-0.32

7.4.6 Flexural Yielding of Out-of-plane CMU Walls and Collapse of Out-of-plane Veneer

For the out-of-plane CMU walls on the east and west sides, the strain of the vertical reinforcement (except for the reinforcing bar at the corner) was measured at the base and at the mid-height (refer to Figure D-9 and Figure D-12). At the base, none of the vertical reinforcing bars in the out-of-plane CMU walls yielded up to Tarzana 100 %, and many vertical reinforcing bars yielded at 1st Tarzana 150 %. Note that the vertical reinforcement of the 12-ft long in-plane CMU walls fractured at the base during 1st Tarzana 150 %., resulting in loss of most of the in-plane resistance of the entire building. At the mid-height, there was negligible strain up to 1st Tarzana 150 % on both east and west sides.

Therefore, in the CMU building specimen tested in this research, the out-of-plane CMU walls had enough flexural yield strength even at the base until the in-plane CMU walls failed by base sliding. This is because the overall stiffness of the entire building and the small mass assigned to the out-of-plane CMU walls (self mass only by out-of-plane CMU walls and out-of-plane veneer). The in-plane CMU walls were stiff until they failed by base sliding and the roof diaphragm was stiff throughout shake-table testing, which imposed negligible horizontal displacement at the top of the out-of-plane CMU walls until the in-plane CMU walls slid. If large displacement is imposed to the top of the out-of-plane CMU walls, flexural yielding is likely to occur at the base of the out-of-plane CMU walls.

Peak response accelerations near the mid-height of out-of-plane CMU wall are listed in Table 7-18. The accelerations were measured 58 in. above the base. For each side (east and west), the acceleration was measured at two locations; the north and at the south of each door opening. The accelerations listed for each side are the average of the accelerations measured at two locations. As shown in Table 7-18, the absolute peak response accelerations near the mid-height of the out-of-plane CMU walls were not larger

than 1.1 times the absolute peak ground accelerations, indicating the out-of-plane CMU walls essentially responded stiff.

Table 7-18 Peak response acceleration near the mid-height of out-of-plane CMU wall (next to door openings)

ground motion			PGA (g), measured	peak response acceleration near * mid-height of out-of plane CMU walls (next to door openings)	
				on the east side (g)	on the west side (g)
Sylmar	200 %	max	2.03	2.10	2.14
		min	-1.62	-1.82	-1.81
Tarzana	100 %	max	1.55	2.00	1.79
		min	-2.40	-2.64	-2.43
	150 % (1st)	max	2.27	3.81	3.01
		min	-3.48	-3.49	-3.36
	150 % (2nd)	max	2.34	-	3.33
		min	-3.36	-	-3.42

** 56 in. above the base*

The out-of-plane veneer on the east and west sides did not collapse until 2nd Tarzana 150 %. The east side had tri-wire connectors and the west side had double eye-and-pintle connectors. The test results indicate that both types of connectors had enough out-of-plane (axial) strength to prevent out-of-plane collapse of the clay masonry veneer in the CMU building specimen. Until the in-plane CMU wall slid at the base (Tarzana 100 %), no significant cracking was observed on the out-of-plane veneer.

On the east side, local fracture occurred at the northeast (Figure 7-13) and southeast corners (Figure 7-14) at 1st Tarzana 150 %, and caused diagonal cracking on the veneer. As shown in Figure 7-30, Figure 7-31 and Figure 7-32, the local fracture at the corners and the diagonal cracking became worse after 2nd Tarzana 150 %. On the west side, the diagonal cracking similar to Figure 7-32 developed at 2nd Tarzana 150 %, but no local damage was observed at the corners throughout shake-table testing as shown

in Figure 7-33 and Figure 7-34. On the west side, the in-plane veneer was discontinuous (vertical gap between in-plane veneer and out-of-plane veneer in Figure 7-33 and Figure 7-34) to the veneer unlike on the east side. This discontinuity allowed the movement of in-plane veneer without local damage at the corners.

Figure 7-30 Northeast corner (2nd Tarzana 150 %)

Figure 7-31 Southeast corner (2nd Tarzana 150 %)

Figure 7-32 Veneer on east side (2nd Tarzana 150 %)

Figure 7-33 Northwest corner (2nd Tarzana 150 %)

Figure 7-34 Southwest corner (2nd Tarzana 150 %)

7.5 SIGNIFICANCE OF TEST RESULTS FOR CMU BUILDING SPECIMEN

The shake-table tests of the CMU building specimen have demonstrated that a low-rise concrete masonry building with clay masonry veneer, designed and constructed according to the requirements of the 2008 MSJC Code and Specification for SDC E, can resist earthquakes above MCE without collapse. The observed performance of the CMU building specimen may not apply to all such buildings. In the building specimen, the vertical and horizontal reinforcement in the CMU walls were governed by minimum prescriptive requirements, so that the ratio of flexural capacity to flexural demand was relatively high. Also, the test building was configured very favorably in plan. Those circumstances would not apply to all low-rise concrete masonry buildings.

The 2008 MSJC Code and Specification deals with only shear and flexure, and does not consider base sliding as a behavior of CMU walls which governed the CMU building specimen tested in this research. Therefore, the MSJC code needs to address this base sliding (or sliding between any floor and CMU walls).

The seismic response of the CMU building specimen was generally consistent with performance expectations listed below.

- Overall response of the building was controlled by the in-plane response of the CMU shear walls (possible flexural hinging at the base, and base sliding above MCE).
- Clay masonry veneer and veneer connectors (tri-wire and double eye-and-pintle), designed and constructed according to the requirements of the 2008 MSJC Code and Specification, generally behaved well, in-plane and out-of-plane. The clay masonry veneer experienced only minor cracking and, by help of the veneer connectors, stayed fully connected to the CMU walls above MCE.
- The presence or absence of joint reinforcement in veneer caused no observable differences in response of the veneer.

- Vertical control joints in the CMU at the ends of the lintels delayed the onset of damage to the CMU walls at the lintel ends until well past MCE. Vertical expansion joints in the veneer at the ends of the lintels permitted the masonry veneer supporting the lintels to rock without damage to the veneer around the lintel ends.
- Vertical expansion joints in the veneer at the corners prevented damage there due to differential movement of the in-plane veneer and the out-of-plane veneer.

Additional issues are discussed below based on the shake-table test results of the CMU building specimen.

- Base sliding of CMU walls and the associated energy dissipation can enhance the performance of masonry structures. Current design standards do not address this. Sliding is related to shear-friction and to the longitudinal bars crossing the interface. It may be useful for the MSJC to develop shear-friction provisions, and to limit the base sliding at DBE and at MCE. Criteria should be developed to limit sliding-induced story drift that might lead to the collapse of other elements in the structure, including gravity systems and walls deflecting out-of-plane.
- Base sliding of CMU walls is probably not acceptable at DBE, because of problems with utility connections. The base sliding is probably acceptable under MCE, provided that structural integrity is maintained to prevent collapse under gravity loads.
- Sliding of veneer and the associated energy dissipation can enhance the performance of masonry structures. Current design standards do not address this. This is investigated further through parameter studies later in Chapter 10.
- Both tri-wire and eye-and-pintle connectors performed well in resisting damage beyond MCE-level shaking. For in-plane loading, it is possible that damage of the connectors due to relative in-plane sliding between CMU and veneer began

earlier on the north side (tri-wire connectors) than on the south side (double eye-and-pintle connecotrs) due to the lower strength of the tri-wire connectors, compared to the eye-and-pintle connectors.

- CMU walls loaded seismically out of plane behave in a more complex manner than the design idealization of vertically spanning strips. They cracked (Figure 7-17) as a result of out-of-plane bending (combination of out-of-plane inertia forces and imposed deformation pattern produced by in-plane sliding of shear walls). The south and north walls slide east-west; the centers of the east and west walls do not slide; and the deformation between the center and the edges of the east and west walls causes flexural cracking.
- There appeared to be no need to put horizontal reinforcement in the bottom course. In this location, reinforcement is too high to be effective in restraining the compression toe of the CMU.
- The 90-degree hook at the intersection of the shear walls and the perpendicular walls was effective in tying the walls together even under shaking in excess of MCE.
- The local failure of the CMU near the door openings (Figure 7-15) is not toe crushing. The failure was produced when the wall slid, and the vertical reinforcement at the jamb pried off the masonry between the bar and the jamb. Similar local cracking was seen in the quasi-static tests of the in-plane CMU wall specimens.
- Cracking of the roof topping and planks in the NS direction (parallel to the planks) was caused by rocking of 4-ft long (plan) wall segments to the west of the door, contrasted with sliding of the 12-ft long wall segments.
- Roof diaphragm and wall-to-diaphragm connections behaved satisfactorily, with no sign of distress.

CHAPTER 8
Introduction to Analytical Study

In this research, the seismic response of low-rise concrete masonry structures with clay masonry veneer is studied experimentally and analytically. The vehicle for the analytical studies of this dissertation is the OpenSees platform developed by the PEER Center at the University of California at Berkeley. Key seismic behaviors of low-rise concrete masonry structures with clay masonry veneer are identified; general analytical models for those behaviors are developed; those general analytical models are calibrated (key parameters are set) using some experimental results; and those general analytical models are verified using other experimental results. In this chapter, the development of the analytical models and the analytical study, described in Chapter 9 (CMU wall specimens) and Chapter 10 (CMU building specimen), are introduced.

The main objectives of the analytical study in this research are as follows:

- to develop a nonlinear hysteretic "macro-model" capable of predicting essential aspects of the seismic behavior of low-rise concrete masonry structures with clay masonry veneer;
- to extend observed experimental test results to more general cases, and to refine design provisions for such structures;
- to supply general information about such structures through parameter studies; and
- to supply information about experimental test specimens not directly available from test results.

The nonlinear hysteretic macro-model developed here addresses basic elements of low-rise concrete masonry structures with clay masonry veneer in ways that are fundamentally sound and internally consistent. The macro-model and the analytical elements composing the macro-model satisfy equilibrium, kinematics, and constitutive relationships. Each analytical element can represent a wide range of properties, enabling different behaviors of the macro-model. The analytical elements and the macro model were generally consistent with experimental test results from quasi-static CMU wall specimens, shake-table CMU wall specimens, and the CMU building specimen. The developed nonlinear hysteretic macro-model will predict the following essential aspects of the seismic behavior of low-rise concrete masonry structures with clay masonry veneer:

- overall response of such structures, governed primarily by the response of in-plane CMU walls (flexural yielding and base sliding) and partially by in-plane deformation of the roof diaphragm;
- rocking, sliding and collapse of in-plane veneer;
- flexural response of out-of-plane CMU walls; and
- collapse of out-of-plane veneer

In the left-hand column of Table 8-1, each of those essential aspects is listed, from most important to least important. In the second column are listed the independent parameters that must be set in order to apply the model. In the third column are listed the test specimens or assumptions used to set those parameters. Finally, in the fourth column are listed the test specimens used to verify those parameters. Columns 3 and 4 also refer to the section numbers in this dissertation where the associated steps are carried out.

Table 8-1 Essential aspects of seismic response of low-rise concrete masonry along with associated measurements and test specimens

essential aspects of seismic response	independent parameters to be set	test specimens (or assumptions) used to set parameters	test specimens used to verify parameters
overall response of building (response of in-plane CMU walls and roof diaphragm)	in-plane yield moment and corresponding gap (width of flexural crack) at extreme tensile reinforcement; same for ultimate moment	strength design assumptions (Section 9.2.1) and CMU wall specimens (quasi-static, in-plane, Section 9.2.1)	CMU building specimen (Section 10.3.1)
	coefficient of sliding friction between CMU and foundation, dowel stiffness for frictional resistance, maximum shearing displacement	CMU building specimen (Section 10.1)	none (no additional test data because only one CMU building specimen was tested)
	in-plane stiffness of roof diaphragm		
rocking and sliding of in-plane veneer	coefficient of friction between veneer and shelf angle; in-plane stiffness and strength of connectors	CMU wall specimens (shake-table, in-plane, Section 9.2.5)	CMU building specimen (Section 10.3.2)
failure (collapse) of in-plane veneer	ultimate deformation capacity of connectors in-plane	CMU wall specimens (shake-table, in-plane, Section 9.2.7)	CMU building specimen (Section 10.3.2)
flexural response of out-of-plane CMU walls with clay masonry veneer	out-of-plane yield moment and corresponding gap at extreme tensile reinforcement	strength design assumptions (Sections 9.1.1) and CMU wall specimens (quasi-static, in-plane, Sections 9.1.1)	CMU wall specimens (shake-table, out-of-plane, Section 9.1.5) and CMU building specimen (Section 10.3.3)
failure (collapse) of out-of-plane veneer	ultimate deformation capacity of connectors out-of-plane	CMU wall specimens (quasi-static and shake-table, out of plane, Sections 9.1.2, 9.1.3 and 9.1.5)	CMU building specimen (Section 10.3.3)

The most important aspect of the seismic response of low-rise concrete masonry structures with clay masonry veneer is the overall response, which is governed primarily

by flexural yielding and base sliding of the in-plane CMU walls and partially by in-plane deformation of the roof diaphragm. The OpenSees analysis must consistently predict the displacements at the base and at the top of the in-plane CMU walls and at the roof diaphragm from experimental test results. Based on test results, including quasi-static, in-plane tests of the CMU wall specimens and shake-table tests of the CMU building specimen, deformation or displacement failure criteria of the CMU walls are suggested, and the OpenSees analysis is conducted.

Another important aspect of the seismic response of low-rise concrete masonry structures with clay masonry veneer is the rocking and sliding response and failure (collapse) of the in-plane veneer. The overall response of the veneer by rocking or sliding is represented by the top displacement of the veneer in-plane. If this displacement is well predicted by the OpenSees analysis, the effect of the in-plane veneer on the overall response of the structure can be examined through parameter studies. A good estimate of this displacement also implies a good estimate of the maximum in-plane deformation of the veneer connectors. The maximum connector deformation typically occurs at the top row, and can be used as a failure criterion for the connectors. Failure of the in-plane connectors is significant because it implies the collapse (out-of-plane) of the in-plane veneer. Therefore, the failure of the in-plane connectors is equivalent to the failure of the in-plane veneer. Based on shake-table test results of in-plane CMU wall specimens, the in-plane deformation capacity of the connectors is proposed, and the OpenSees analysis is checked with the test results, using shake-table tests of the in-plane CMU wall specimens and the CMU building specimen.

Another important aspect of the seismic response of low-rise concrete masonry structures with clay masonry veneer is the flexural response of the out-of-plane CMU walls with clay masonry veneer, which can be represented by the mid-height displacement (out-of-plane) of the CMU walls. A good estimate of this mid-height displacement implies a good estimate of the interaction between the out-of-plane CMU walls and the in-plane CMU walls. A good prediction of that mid-height displacement is also significant because it implies that the effect of the out-of-plane veneer on the out-of-

plane CMU walls is well captured. To check the flexural response of the out-of-plane CMU walls, shake-table tests of the out-of-plane CMU wall specimens and the CMU building specimen were used. The same gap (width of flexural crack) at extreme tensile reinforcement, corresponding to yield moment, is used as in in-plane CMU walls. No criterion is proposed in this research for the flexural failure of the out-of-plane CMU walls, because other structural elements (in-plane CMU walls or out-of-plane veneer) always failed first.

The last important aspect of the seismic response of CMU structures with clay masonry veneer is the failure (collapse) of the out-of-plane veneer. Due to its low flexural stiffness and strength compared to the out-of-plane CMU walls, the out-of-plane veneer essentially acts as added mass to the out-of-plane CMU walls. Then, the failure of the out-of-plane veneer is governed by the out-of-plane (axial) failure of the connectors. Based on test results of quasi-static tests of out-of-plane CMU wall specimens, the axial deformation capacity of the connectors is suggested as a criterion to determine the failure of connectors. The OpenSees analysis is then verified using the results from shake-table tests of out-of-plane CMU wall specimens and the CMU building specimen.

CHAPTER 9
Analytical Study of CMU Wall Specimens

In this chapter, analytical models are developed and checked for CMU walls, clay masonry veneer, and connectors, based on the quasi-static and shake-table test results of the CMU wall specimens described in Chapters 4 through 6. The models are implemented using OpenSees, a structural analysis framework developed by the PEER Center of the University of California at Berkeley. Primary responses of concern in the analytical models for CMU wall specimens are out-of-plane flexural behavior of the CMU walls; out-of-plane collapse of the clay masonry veneer by out-of-plane (axial) failure of the connectors; in-plane flexural behavior of the CMU walls; in-plane rocking and sliding of the clay masonry veneer; and collapse of the in-plane clay masonry veneer by in-plane failure of the connectors. Those primary responses are evaluated as follows:

- Out-of-plane flexural behavior of the CMU walls is evaluated using the shake-table, out-of-plane test results of the CMU wall specimens, particularly yielding of the vertical bars at mid-height and maximum acceleration and displacement responses near mid-height.
- Out-of-plane collapse of the clay masonry veneer by out-of-plane (axial) failure of the connectors is evaluated using shake-table, out-of-plane test results of the CMU wall specimens. In the OpenSees analysis, failure criteria for the out-of-plane connectors are determined based on the quasi-static, out-of-plane test results of the CMU wall specimens. For out-of-plane response, the clay masonry veneer is considered as mass only, because the out-of-plane flexural stiffness of the clay masonry veneer (before and after cracking) is small compared to that of the CMU walls.

- The in-plane flexural behavior of the CMU walls is evaluated using the quasi-static, in-plane test results of the CMU walls specimens.
- In-plane rocking and sliding of the clay masonry veneer is evaluated using the shake-table, in-plane test results of the CMU wall specimens.
- Collapse of the in-plane clay masonry veneer by in-plane failure of the connectors is evaluated using shake-table, in-plane test results of the CMU wall specimens. In the OpenSees analysis, the failure criteria for the in-plane connectors are determined based on the shake-table, in-plane test results of the CMU wall specimens.

9.1 OUT-OF-PLANE BEHAVIOR OF CMU WALLS WITH CLAY MASONRY VENEER

The out-of-plane flexural behavior of CMU walls with clay masonry veneer is governed by the flexural behavior of the CMU walls and the axial behavior of the veneer connectors. The out-of-plane flexural properties of the CMU walls are determined based on the quasi-static, in-plane test results of CMU wall specimens, and on the assumed material properties of reinforcement and concrete masonry. The out-of-plane (axial) properties of connectors are determined based on the quasi-static, out-of-plane testing of CMU wall specimens.

9.1.1 Out-of-plane Flexural Behavior of CMU Walls

To represent the out-of-plane flexural behavior of the CMU walls, we need to determine the yield moment and its corresponding rotation. The rotation of the out-of-plane CMU walls at flexural yielding depends on the width of the flexural crack. The information on the crack width is obtained from quasi-static testing of the in-plane CMU wall specimens (Section 9.2.1), where the flexural reinforcement yielded at the base at a crack width of about 0.025 in. Based on this, and assuming the vertical reinforcement to

be located at the mid-thickness of the wall, the rotation at flexural yielding of out-of-plane CMU walls can be estimated as about 0.0065 rad:

$$Rotation = \frac{0.025 in.}{0.5 \times 7.63 in.} = 0.0065 rad ,$$

where 7.63 in. is the thickness of the CMU walls. The yield moment at the base of the CMU walls (19.4 kip-ft from Figure 9-1) was calculated using a spreadsheet program, assuming reinforcement with the expected yield strength of 65 ksi, 1 % strain hardening, and 9 % elongation at fracture; and assuming masonry with the specified compressive strength of 1500 psi. For reinforcement, the expected yield strength of 65 ksi was used instead of the specified strength of 60 ksi, because the out-of-plane yield moment of the CMU walls is essentially governed by the yield strength of reinforcement, and 65 ksi is, usually, close to the real yield strength of reinforcement. The strength reduction factor for flexural strength (0.9) was not applied. The expected yield moment at mid-height was 18.9 kip-ft (Figure 9-2). Self-weight of the CMU wall (about 4.8 kips at the base and about 2.4 kips at mid-height with 120 pcf) was considered.

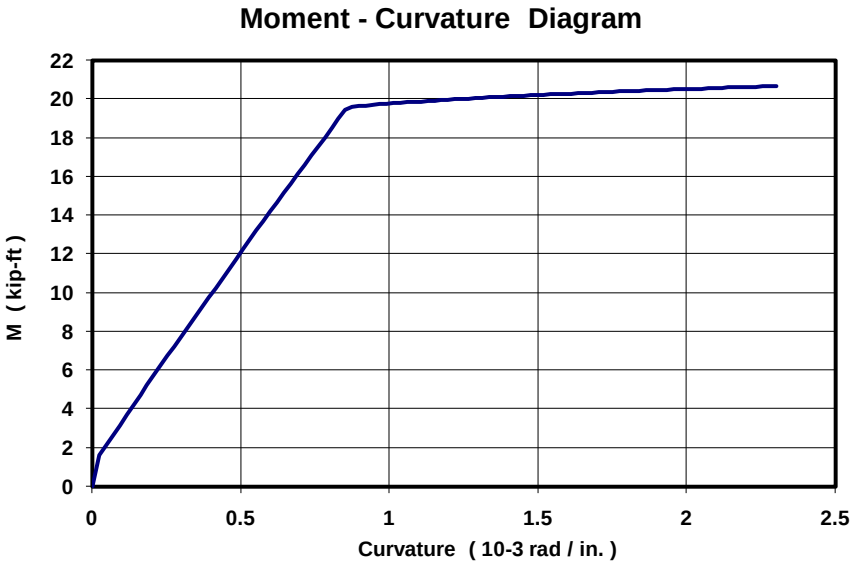

Figure 9-1 Moment-curvature diagram of out-of-plane CMU walls at base

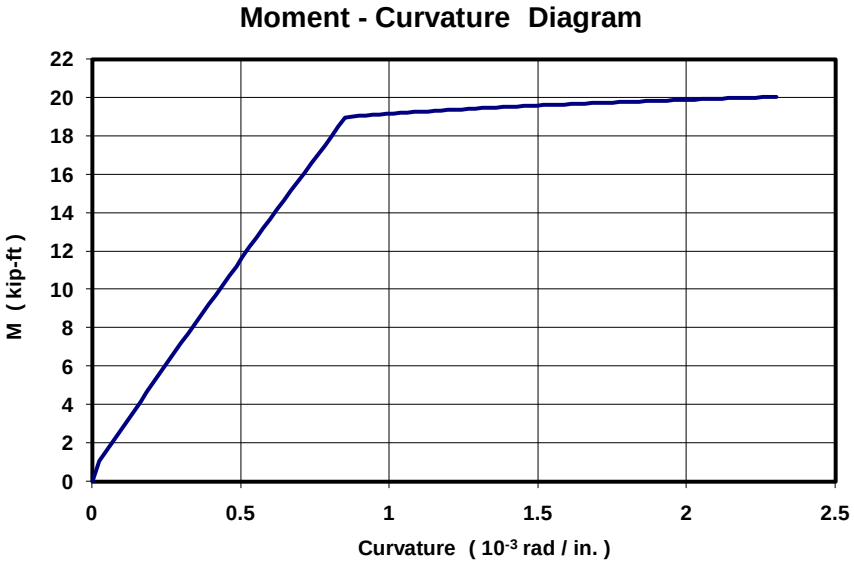

Figure 9-2 Moment-curvature diagram of out-of-plane CMU walls at mid-height

9.1.2 Out-of-plane (Axial) Behavior of Double Eye-and-pintle Connectors

To represent the out-of-plane (axial) behavior of the double eye-and-pintle connectors, we need to determine the envelope curve for the connectors. The information on the enveloped curve is obtained from the quasi-static test results of the out-of-plane CMU wall specimen (UT CMU 1). From the same test results, a deformation limit for the double eye-and-pintle connectors is also suggested as a failure criterion. After the OpenSees analysis, if the maximum deformation of the connectors exceeds this deformation limit, the out-of-plane veneer could be considered to have collapsed.

The axial stiffness of double eye-and-pintle connectors depends primarily on the amount of mortar droppings (Figure 9-3) between the veneer and the CMU walls; the vertical eccentricity between the eye and the pintle; and the difference between the diameters of the pintles and the eyes. The axial strength of double eye-and-pintle connectors in tension and in compression depends mainly on the vertical eccentricity, an

example of which is shown by the vertical distance between the two red arrows in Figure 9-3. In this research, given uncertainty associated with both of these, the axial properties of the double eye-and-pintle connectors used in OpenSees modeling are estimated with the quasi-static, out-of-plane test results of the CMU wall specimen (UT CMU 1).

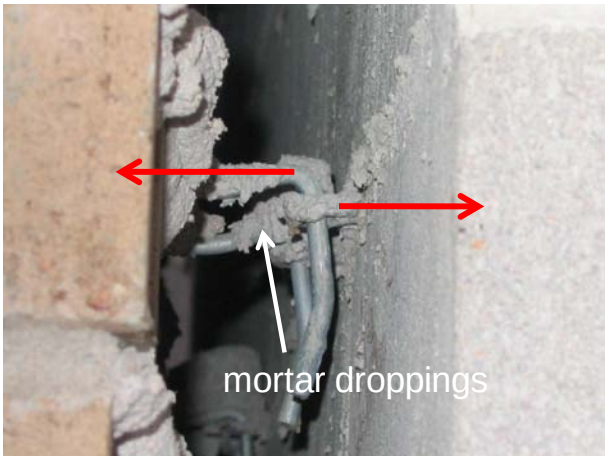

Figure 9-3 Example of vertical eccentricity and mortar droppings at double eye-and-pintle connectors

In Specimen UT CMU 1, the deformation of the double eye-and-pintle connector in the second row from the top was judged to be representative of the average deformation of Specimen UT CMU 1. Under a given total horizontal load, the top row always showed the most deformation. The initial load versus deformation curve for the second row (up to about 15 kips of total horizontal load) is shown in Figure 9-4, and is compared with a simplified model (symmetric, with increasing stiffness). The initial stiffness is 1.7 kip/in. up to 0.03 in. of displacement in both directions. The test results are a bit asymmetric, due to the asymmetric initial gap between the eyes and the pintles. The load in Figure 9-4 is the total horizontal load divided by the total number of connectors (36). The second stiffness is 16.0 kip/in.

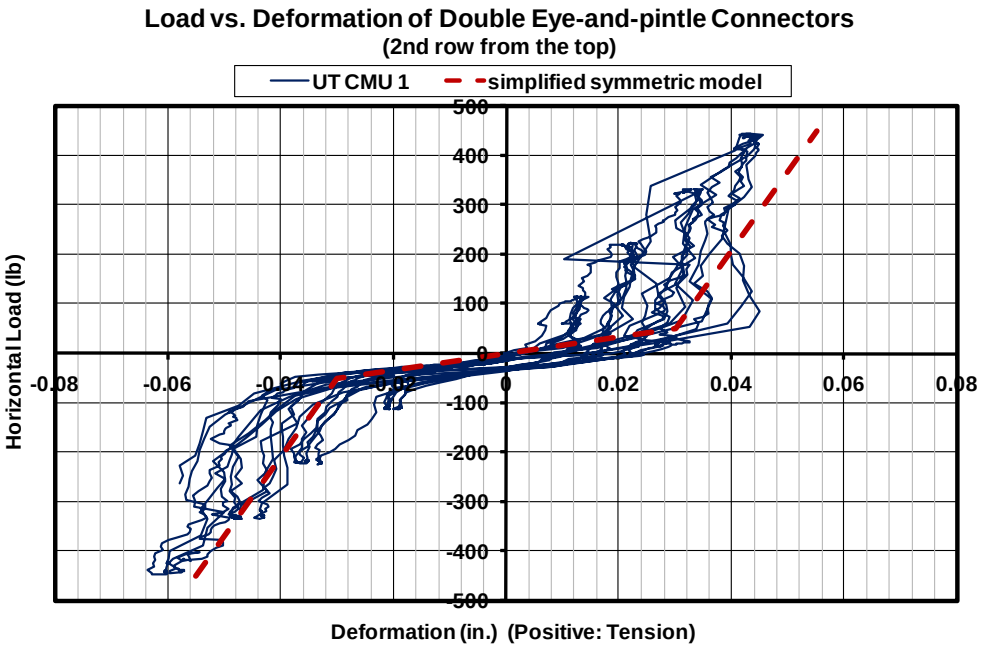

Figure 9-4 Initial load versus deformation curve of double eye-and-pintle connectors (2nd row from the top), compared with simplified model

Specimen UT CMU 1 (quasi-static, out-of-plane loading) was subjected to maximum loads of 23.2 kips in compression and in tension (Figure 4-13). The specimen probably had additional compression capacity. After the maximum load in tension, the specimen showed residual strengths of first about 13 kips and then about 9 kips. An analytical model for this connector is developed based on a maximum capacity of 20 kips, rather than the maximum observed capacity of 23.2 kips. This is because that maximum capacity was observed for only one cycle, while in contrast a capacity of 20 kips was maintained over three reversed cycles (Figure 3-27). The corresponding maximum capacity in tension and compression of each double eye-and-pintle connector is therefore the total capacity of 20 kips, divided by the number of connectors (36), or 0.56 kip. The simplified load-displacement curve (implemented using a combination of an elasto-plastic material with an initial gap and a bilinear elastic material) is shown in Figure 9-5.

Specimen UT CMU 1 lost significant strength immediately after the connectors experienced about 0.1 in. of tensile deformation, probably due to slip between the eyes and pintles. That value is suggested as the maximum tensile deformation capacity of double eye-and-pintle connectors. No maximum deformation capacity in compression is suggested in this research due to lack of information.

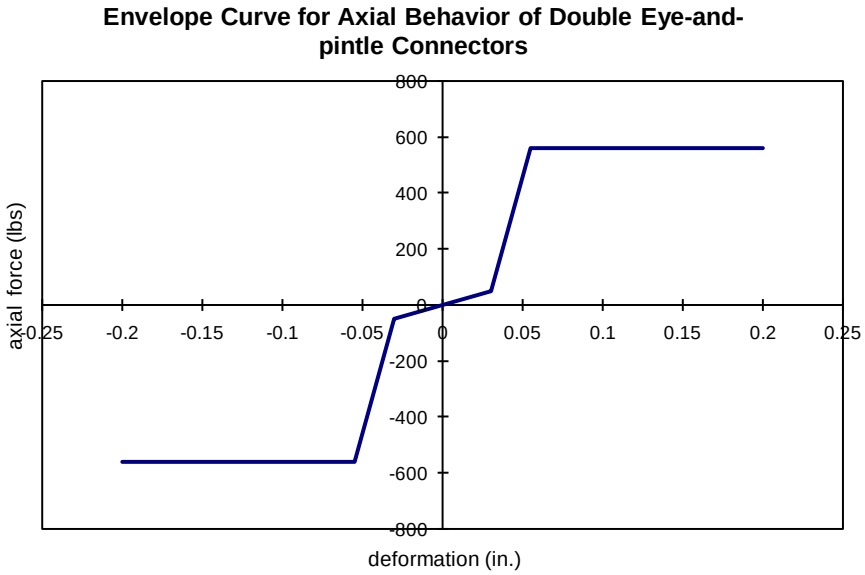

Figure 9-5 Simplified envelope curve for axial behavior of double eye-and-pintle connectors

9.1.3 Out-of-plane (axial) Behavior of Tri-wire Connectors

To represent the out-of-plane (axial) behavior of the tri-wire connectors, we need to determine the envelope curve for the connectors. That information is obtained from the quasi-static test results of the out-of-plane CMU wall specimens (UT CMU 2 and UT CMU 2 MC). From the same test results, a deformation limit for the tri-wire connectors is also suggested as a failure criterion. After the OpenSees analysis, if the maximum deformation of the connectors exceeds this deformation limit, the out-of-plane veneer

could be considered to have collapsed. Each aspect of the envelope curve is discussed below.

In axial tension, the initial axial stiffness is affected by mortar droppings (Figure 9-6); without mortar droppings, the axial stiffness in elastic range can be estimated using the simple axial stiffness, EA/L.

$$\frac{EA}{L} = \frac{29000\ ksi \times 0.017\ in.^2}{2\ in.} = 247\ kip/in.$$

The axial strength of tri-wire connectors in tension is essentially independent of mortar droppings and can be estimated using $A\ f_y$.

$$A\ f_y = 0.017\ in.^2 \times 80\ ksi = 1.36\ kip$$

The corresponding displacement at tensile yielding (yield strain in the steel multiplied by the 2-in. gage length) is 0.0055 in., which is smaller than that observed in the quasi-static testing. This underestimate is believed due to ignoring other sources of deformation, such as bond-slip of the embedded wires at each end of the connector.

In axial compression, the axial stiffness and the axial strength of tri-wire connectors depend on the mortar droppings and on the vertical and horizontal eccentricity, an example of which is shown in Figure 9-6. The stiffness in compression will be similar to that in tension until near compressive strength by yielding or buckling. Without mortar droppings and vertical and horizontal eccentricity, the compressive strength can be estimated using the classic formula for elastic buckling without initial imperfections:

$$P_{compression} = \frac{\pi^2 \cdot E \cdot I}{(0.5 \cdot L)^2} = \frac{\pi^2 \times 29000\ ksi \times 2.36\ in.^4}{1\ in.^2} = 6.74\ kips,$$

where the factor of 0.5 in the denominator is based on fixed-fixed support conditions. This buckling capacity given by this equation, 6.74 kips, far exceeds the yield strength of 1.36 kips (based on a probable steel yield strength of 80 ksi). In addition, that theoretical

buckling strength will, in practice, not be reachable due to inevitable vertical or horizontal eccentricities. Those eccentricities can dramatically decrease buckling capacity because of the small diameter of the wire (0.148 in.).

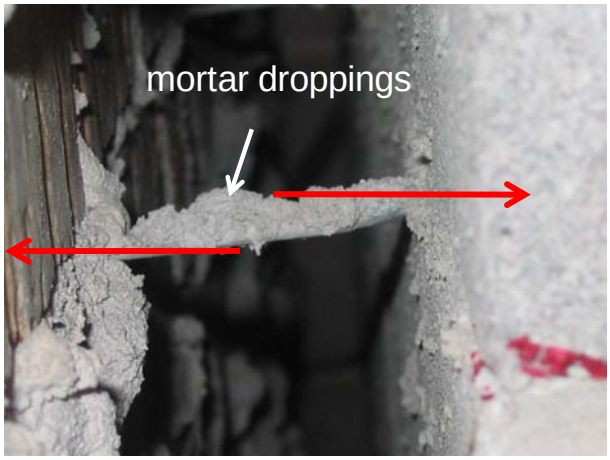

Figure 9-6 Example of vertical eccentricity and mortar droppings in tri-wire connectors

In this research, the axial properties of the tri-wire connectors for OpenSees modeling are estimated using the quasi-static test results of the out-of-plane CMU wall specimens (UT CMU 2 and UT CMU 2 MC), because the stiffnesses or strengths calculated above based on mechanics did not match the test results. Even though the test setup for quasi-static out-of-plane loading was intended to simulate pressure load, in reality, the connectors cannot share the load equally. For both specimens, the initial stiffness of the connector in the second row from the top was judged to be representative of the average deformation after checking the deformation of each row of connector. Under a given total horizontal load, the top row always showed the most deformation. The load versus deformation curve for the second row of connector, up to about 15 kips of total horizontal load, is shown in Figure 9-7, along with linear trend lines. The load in that figure is the total horizontal load on the specimen, divided by the total number of

connectors (36). Based on the trend lines for both specimens, the average out-of-plane stiffness of a single connector is about 36 kip/in.

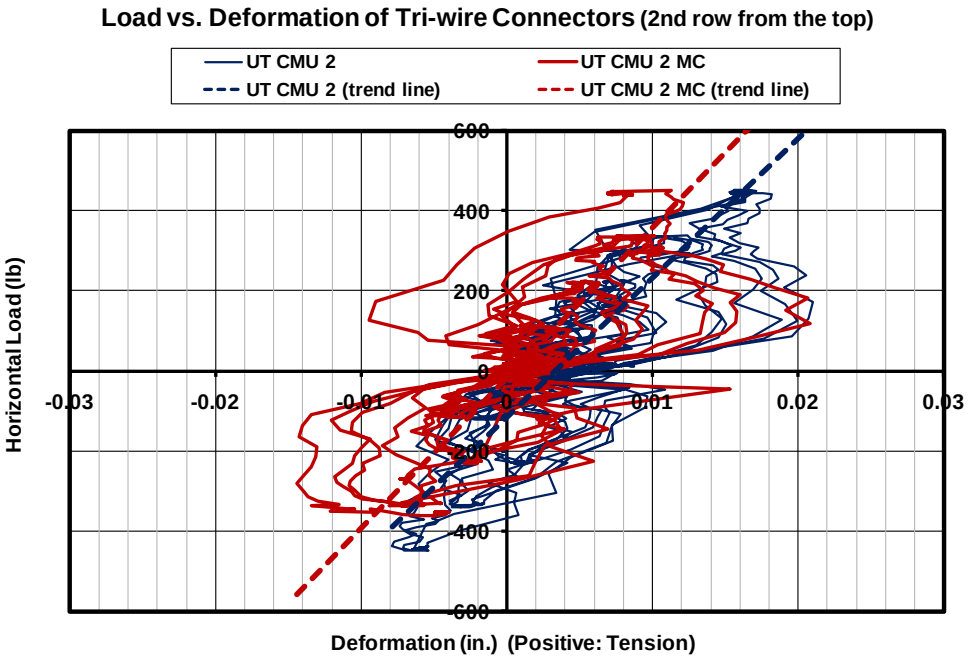

Figure 9-7 Load versus deformation curve of tri-wire connectors (2nd row from the top)

Specimen UT CMU 2 showed a maximum load of 18.7 kips in compression and 25.6 kips in tension (Figure 4-17). Specimen UT CMU 2 MC showed a maximum load of 22.8 kips in compression and 27.6 kips in tension (Figure 4-22). After reaching the maximum load in compression, both specimens showed a residual strength of about 12 kips. The lesser of the observed tensile capacities of 25.6 kips and 27.6 kips (25.6 kips), divided by the number of connectors (36), or 0.71 kips, is taken as the tensile strength of a single tri-wire connector for OpenSees modeling. In the same way, the lesser of the observed compressive capacities of 18.7 kips and 22.8 kips (18.7 kips), divided by the number of connectors (36), or 0.52 kips, is taken as the compressive strength (governed by buckling) of a single tri-wire connector for OpenSees modeling. The residual strength

after buckling in compression is taken as 0.33 kips (12 kips divided by 36). The displacements at yielding and buckling, determined using the initial stiffness (36 kip/in.) obtained above, are 0.020 in. in tension and 0.014 in. in compression. The top row of connectors fractured after reaching about 0.16 in. of tensile deformation in Specimen UCSD CMU 2 and after reaching about 0.09 in. of tensile deformation in Specimen UCSD CMU 2 MC. Therefore, for tri-wire connectors, 0.09 in. is suggested as the deformation capacity of the tri-wire connectors in tension. These deformation capacities can be used as failure criteria. The deformation capacity in compression is suggested in Section 9.1.5 using OpenSees analysis results.

The strengths and deformation capacities proposed above are generally conservative, because all connectors did not share horizontal load equally, and the strength in tension was limited by low-cycle fatigue failure after several cycles of reversed inelastic deformations. This low-cycle fatigue capacity is enough to withstand several repetitions of significant ground shaking, because the seismic response of structures generally has only a few critical large-deformation spikes. The deformation capacity of the connectors is not included in the OpenSees model. Instead, if the maximum deformation of the connectors from OpenSees analysis is within that deformation capacity in tension and in compression, the connectors can be estimated not to have fractured. The simplified envelope curve for the axial behavior of tri-wire connectors (implemented using the hysteretic model of OpenSees) is shown in Figure 9-8.

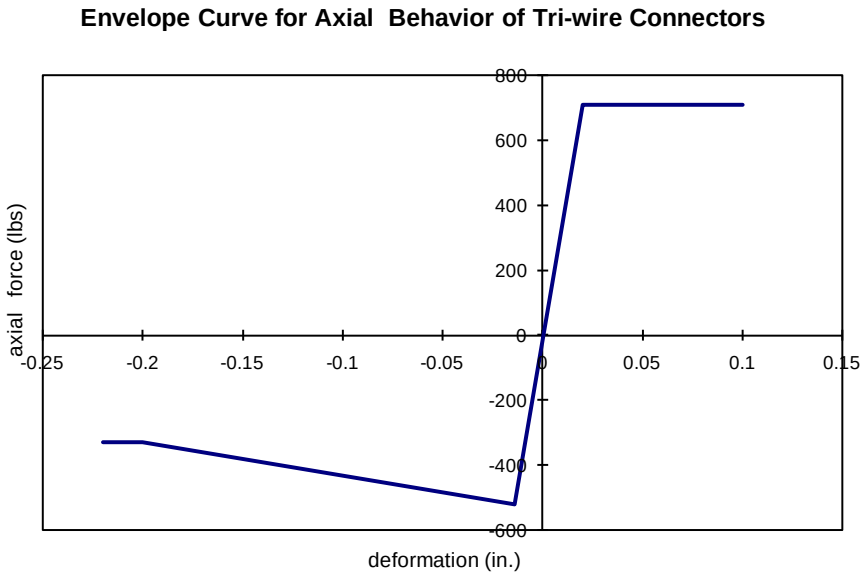

Figure 9-8 Simplified envelope curve for axial behavior of tri-wire connectors

9.1.4 OpenSees Modeling of Out-of-plane CMU Wall Specimens

The OpenSees model for the out-of-plane CMU wall specimens is schematically shown in Figure 9-9. In the OpenSees model, the CMU wall is idealized as an elastic beam with a flexural hinge (bilinear inelastic) at the base and at the mid-height, and the clay masonry veneer is idealized as an elastic beam with a simple flexural hinge at the base and at the mid-height. In this way, the deformation of the CMU wall and the veneer are essentially governed by the rotation at the hinges, and the veneer essentially responds dynamically as added mass only, imparting a force that is limited by the strength of the out-of-plane connectors. In the OpenSees model (Figure 9-9), the CMU wall and the veneer are assumed to have cracked at the hinge locations before loading for simplicity, since this research focuses on the inelastic behavior of the CMU wall. This simplification results in the underestimation of the out-of-plane flexural stiffnesses of the CMU wall and the veneer, but only until flexural cracking.

The out-of-plane connectors are idealized in the OpenSees model using a truss element with general hysteretic material. The elastic section property of the CMU wall is based on a specified masonry compressive strength (f_m') of 1500 psi and an elastic modulus E equal to 900 f_m' (as prescribed by the 2008 MSJC Code), and the section property of clay masonry veneer is based on a specified masonry compressive strength (f_m') of 1500 psi and an elastic modulus E equal to 700 f_m' (as prescribed by the 2008 MSJC Code). In the model, a bilinear inelastic flexural hinge is located at the base and at the mid-height of the CMU wall, and a simple hinge is located at the mid-height of the veneer. The inelastic flexural hinge is located at the mid-height of the CMU wall because, in the quasi-static and shake-table testing of the out-of-plane CMU wall specimens, once a flexural hinge developed at the base, the second flexural hinge was always observed to form at mid-height. The assumed moment-curvature diagrams used for the CMU wall are shown in Figure 9-1 (at the base) and in Figure 9-2 (at the mid-height). Since the effects of self-weight are negligible, a yield moment of 19 kip-ft is used both at the base and at the mid-height. For simplicity, the stiffness after yielding is set as 1 % of the elastic stiffness (a typical assumption for steel). The rotation at flexural yielding is set as 0.0065 rad, as explained in Section 9.1.1.

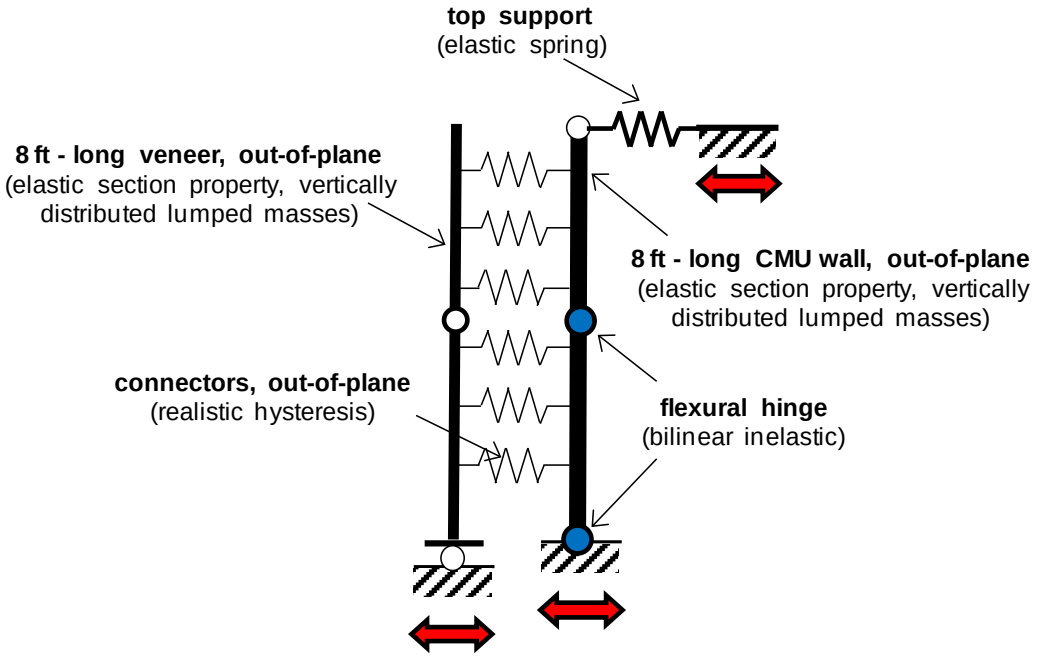

Figure 9-9 OpenSees model for out-of-plane CMU wall specimens

9.1.5 OpenSees Analysis of Out-of-plane CMU Wall Specimens, Shake-table Loading

OpenSees analysis of out-of-plane CMU wall specimens is conducted only for the shake-table testing, and not for the quasi-static testing. There are two reasons for this, considering that the out-of-plane response of the CMU wall specimens is governed by the axial behavior of the connectors and the out-of-plane flexural behavior of the CMU walls. First, the OpenSees model for the connectors out-of-plane was established based on the test results of the quasi-static testing and, therefore, OpenSees analysis of the quasi-static testing would not be meaningful. Second, in the quasi-static testing, the loading was applied through the clay masonry veneer only, and the magnitude of the load was limited by the capacity of the connectors. As a result, in the quasi-static testing, the CMU walls could not be loaded enough to produce inelastic response. Since the OpenSees model for

the CMU walls was focused on the inelastic response (Section 9.1.4), OpenSees analysis of the quasi-static testing would not be practical.

To evaluate the analytical results of the out-of-plane CMU wall specimens for shake-table loading, the analytical results are compared with the shake-table test results in this section in two ways: qualitatively and quantitatively. For qualitative evaluation, the most important information is flexural yielding of CMU walls (at the base and at mid-height) and axial yielding or buckling and fracture of connectors. Test results of the shake-table testing, however, permitted assessment only of flexural yielding of the CMU walls at mid-height and of fracture of the connectors. For quantitative evaluation, maximum response accelerations and displacements (near the top and near the mid-height) of the CMU walls and the veneer are used. The responses near the top are compared to check the properties of the top support, because the response of the CMU walls with clay masonry veneer depended greatly on the properties of the top support, which can only be obtained indirectly by comparing the OpenSees analysis with the test results. Then, the analytical and test results (accelerations and displacements) near the mid-height are compared.

For flexural yielding of the CMU walls at mid-height, OpenSees analysis underestimates the extent of yielding, as shown in Table 9-1. The horizontal stiffness of the top simple support used in this OpenSees analysis was 9 kip/in. for Specimen UCSD CMU 1, 6 kip/in. for Specimens UCSD CMU 2 and 15 kip/in. for Specimen UCSD CMU 2 MC. Those horizontal stiffnesses were selected so that the maximum responses (acceleration and displacement) of the CMU walls near the top from OpenSees analysis would be close to the corresponding values from test results. Because the purpose was to calibrate the OpenSees models against shake-table results, the input motions used in these OpenSees analyses were those measured on the table (rather than the slightly different values input to the table). At Tarzana 150% (maximum ground motion applied to the CMU wall specimens), the maximum moment of the CMU walls at mid-height from OpenSees analysis and the horizontal stiffness of the top simple support used in the OpenSees analysis are listed in Table 9-2. The difference between the maximum

moments of UCSD CMU 2 and UCSD CMU 2 MC shows that the response from OpenSees analysis of out-of-plane CMU wall specimens was not sensitive to the horizontal stiffness of the top support. The maximum moment of UCSD CMU 2 MC was just 1.2 times that of UCSD CMU 2, while the stiffness of the top support of UCSD CMU 2 MC was 2.5 times that of UCSD CMU 2. By comparison of UCSD CMU 1 with UCSD CMU 2 and UCSD CMU 2 MC in Table 9-2, it might be supposed that the lower moment at mid-height of UCSD CMU 1 comes from the lower tensile strength of connectors given in the OpenSees model. For double eye-and-pintle connectors in UCSD CMU 1, 0.56 kips was given for tensile strength (0.56 kips for compressive strength) while 0.71 kips was given for tensile strength (0.52 kips for compressive strength) of tri-wire connectors in UCSD CMU 2 and UCSD CMU 2 MC.

Table 9-1 Comparison of shake-table test results with OpenSees analysis for flexural yielding of CMU walls at the mid-height

Specimen	flexural yielding at mid-height		Comment
	test results	OpenSees analysis	
UCSD CMU 1	yielded at Tarzana 125 %	does not yield up to Tarzana 150% *	at Tarzana 125 %, moment at mid-height from OpenSees analysis was 13 kip-ft (M_y = 19 kip-ft)
UCSD CMU 2	did not yield up to Tarzana 150% *	does not yield up to Tarzana 150% *	top support failure at Tarzana 150 %
UCSD CMU 2 MC	yielded at Tarzana 150 %	does not yield up to Tarzana 150%*	at Tarzana 150 %, moment at the mid-height from OpenSees analysis was 18 kip-ft (M_y = 19 kip-ft)

Table 9-2 Maximum moment in CMU walls at mid-height and horizontal stiffness of top simple support for Tarzana 150 %, OpenSees analysis

specimen	horizontal stiffness of the top simple support (OpenSees analysis)	maximum moment in CMU walls at mid-height (OpenSees analysis)
UCSD CMU 1	9 kip/in.	13 kip-ft
UCSD CMU 2	6 kip/in.	15 kip-ft
UCSD CMU 2 MC	15 kip/in.	18 kip-ft

For connector failure, a deformation capacity was suggested in Sections 9.1.2 and 9.1.3 as 0.1 in. in tension for double eye-and-pintle connectors and 0.09 in. in tension for tri-wire connectors, respectively. Based on those deformation capacities, it is not clear whether OpenSees analysis provides a good estimate in Table 9-3. For Specimen UCSD CMU 1, it accurately predicted the level of shaking for connector failure based on that tensile deformation capacity. In UCSD CMU 2, the specimen had a problem at the top support at Tarzana 150 %. In UCSD CMU 2 MC, the tensile deformation capacity was enough at Tarzana 150 %, but the excessive deformation in compression (1.2 in.) suggests the possibility of low-cycle fatigue failure. In this research, however, an estimate for low-cycle fatigue failure is not proposed due to lack of information. Instead, 1.0 in. is suggested as a simple estimate for the maximum deformation capacity of tri-wire connectors in compression. From OpenSees analysis of UCSD CMU 2 MC, the maximum deformation of the tri-wire connectors in compression was about 0.6 in. at Tarzana 125 % and 1.2 in. at Tarzana 150 %, and, in shake-table testing, the connectors of Specimen UCSD CMU 2 MC failed at Tarzana 150 %. The hysteresis of connectors of each CMU wall specimen at Tarzana 150 % is shown in Figure 9-10 through Figure 9-12, where the positive direction is in tension.

Table 9-3 Comparison of shake-table test results with OpenSees analysis for connector failure of CMU walls

specimen	connectors	ground motion for failure at the top row of connectors		comment
		test results	OpenSees analysis	
UCSD CMU 1	double eye-and-pintle	Tarzana 150 % (pintles slipping out of eyes at the top row)	Tarzana 150 % (0.16 in. of tensile deformation)	based on 0.1 in. tensile deformation capacity in OpenSees analysis
UCSD CMU 2	tri-wire	none * (top support failure at Tarzana 150 %)	Tarzana 150 % (0.13 in. of tensile deformation)	based on 0.09 in. tensile deformation capacity in OpenSees analysis
UCSD CMU 2 MC	tri-wire	Tarzana 150 % (fracture of cross wires at welding)	none * (0.050 in. of tensile deformation at Tarzana 150 %)	based on 0.09 in. tensile deformation capacity in OpenSees analysis. At Tarzana 150 %, 1.2 in. of compressive deformation

** up to Tarzana 150 %*

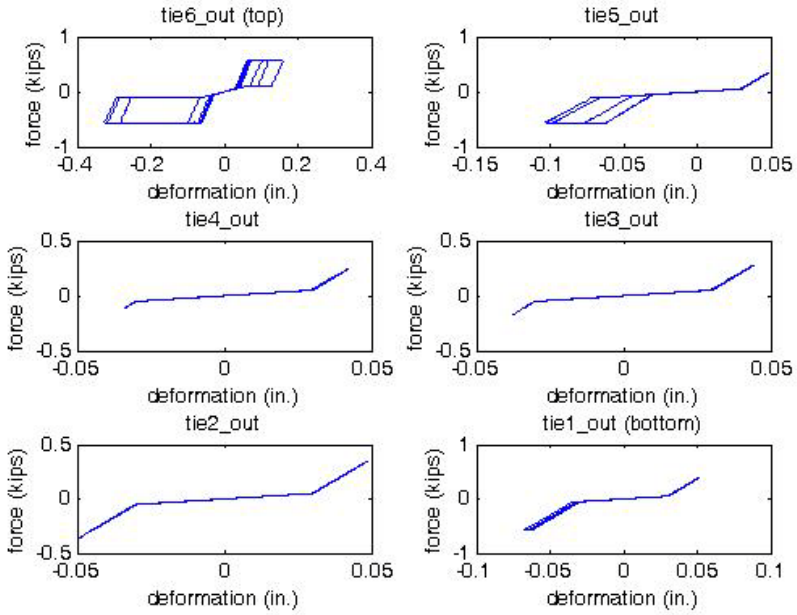

Figure 9-10 Connector hysteresis of UCSD CMU 1 at Tarzana 150 % (OpenSees)

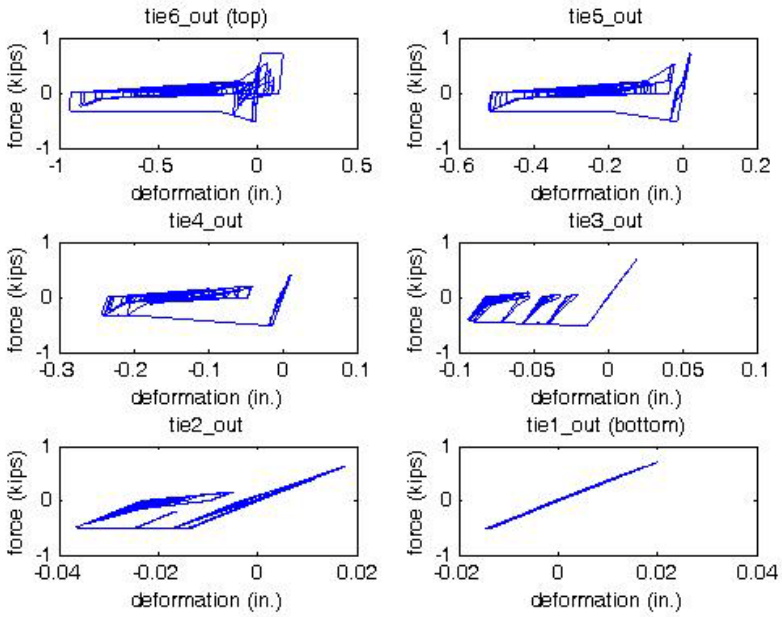

Figure 9-11 Connector hysteresis of UCSD CMU 2 at Tarzana 150 % (OpenSees)

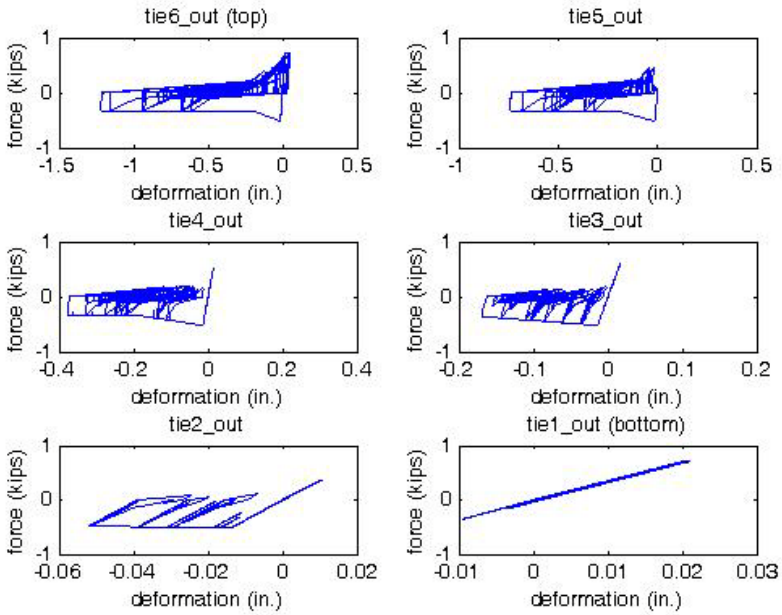

Figure 9-12 Connector hysteresis of UCSD CMU 2 MC at Tarzana 125 % (OpenSees)

The maximum and minimum responses (displacement and acceleration) of CMU walls and clay masonry veneer from OpenSees analyses are listed in Table 9-4, Table 9-5 and Table 9-6. The positive direction is to the east (Figure 6-5). The responses near the top and near the mid-height in Table 9-4 through Table 9-6 were measured at the top row of connectors (88 in. from the base) and at the third row of connectors from the base (40 in.from the base), respectively.

The responses (accelerations and displacements) from OpenSees analyses and test results are compared near the top and near the mid-height, and the ratios of test results to OpenSees analysis are plotted in Figure 9-13 through Figure 9-20. Test results are provided in Section 6.3. The ratios in Figure 9-13 through Figure 9-20 were obtained for positive values (to the east direction in Figure 6-5); the overall ratios for negative values were similar. The ratios for the responses (acceleration and displacement) of the CMU walls near the top (Figure 9-13 and Figure 9-15) demonstrates that the horizontal stiffness of the top support used in OpenSees analysis accurately represents the actual horizontal stiffness. For the veneer displacements of UCSD CMU 2 MC, the ratios are not shown because the displacement recording for the clay masonry veneer had some problem. As shown in Figure 9-13 through Figure 9-20, the test results generally range from 0.5 times to 1.5 times the OpenSees analysis, implying that the OpenSees model can reasonably predict the maximum responses of the out-of-plane CMU wall specimens. OpenSees analysis generally overestimated the responses at low ground motions, which is consistent with the assumption used in OpenSees modeling (described in Section 9.1.4), that the CMU wall and the veneer are assumed for simplicity to have cracked at the hinge locations before loading. This results in an underestimation of the out-of-plane flexural stiffnesses of the CMU wall and the veneer until flexural cracking.

Table 9-4 OpenSees analysis results of UCSD CMU 1 for shake-table, out-of-plane loading

ground motion			PGA (g), measured	acceleration (g)				displacement (in.)			
				CMU		veneer		CMU		veneer	
				mid-height *	top **	mid-height *	top **	mid-height *	top **	mid-height *	top **
Sylmar	80%	max	0.78	1.11	1.42	1.21	2.27	0.18	0.31	0.19	0.35
		min	-0.54	-1.01	-1.34	-0.92	-1.41	-0.20	-0.33	-0.21	-0.37
	100%	max	1.03	1.41	1.71	1.92	2.97	0.22	0.40	0.23	0.44
		min	-0.66	-1.22	-1.71	-1.34	-1.82	-0.25	-0.43	-0.26	-0.47
	125%	max	1.35	1.79	2.34	2.35	3.55	0.27	0.49	0.28	0.54
		min	-0.84	-1.40	-2.14	-1.51	-2.48	-0.32	-0.54	-0.32	-0.58
	150%	max	1.66	2.19	2.84	2.74	4.25	0.32	0.58	0.33	0.63
		min	-0.99	-1.65	-2.69	-2.15	-3.15	-0.39	-0.66	-0.39	-0.71
Tarzana	70%	max	1.29	1.85	2.82	2.71	4.63	0.38	0.71	0.39	0.76
		min	-1.42	-2.06	-3.31	-2.60	-4.10	-0.30	-0.56	-0.31	-0.60
	100%	max	1.88	2.57	4.07	3.75	6.58	0.59	1.04	0.59	1.14
		min	-2.00	-2.76	-4.67	-3.46	-5.48	-0.41	-0.79	-0.42	-0.84
	125%	max	2.33	3.16	5.24	4.49	7.11	0.76	1.24	0.74	1.44
		min	-2.51	-3.99	-6.21	-3.94	-7.52	-0.48	-0.92	-0.49	-0.98
	150%	max	2.76	3.71	5.91	3.90	11.07	0.94	1.41	0.90	1.71
		min	-3.02	-4.69	-7.23	-5.76	-7.64	-0.60	-1.11	-0.61	-1.23

positive direction: to the east (Figure 4-4)

** mid-height: at the third row of connectors from the base (40 in. from the base)*

*** top: at the top row of connectors (88 in. from the base)*

Table 9-5 OpenSees analysis results of UCSD CMU 2 for shake-table, out-of-plane loading

ground motion			PGA (g), measured	acceleration (g)				displacement (in.)			
				CMU		veneer		CMU		veneer	
				mid-height *	top **	mid-height *	top **	mid-height *	top **	mid-height *	top **
Sylmar	80%	max	0.95	1.27	1.59	1.27	1.60	0.21	0.43	0.21	0.44
		min	-0.55	-0.86	-1.31	-0.86	-1.33	-0.25	-0.51	-0.26	-0.52
	100%	max	1.07	1.48	1.87	1.48	1.88	0.27	0.55	0.27	0.56
		min	-0.68	-1.12	-1.66	-1.12	-1.67	-0.32	-0.65	-0.32	-0.66
	125%	max	1.33	1.81	2.36	1.81	2.38	0.32	0.68	0.32	0.69
		min	-0.88	-1.27	-2.10	-1.28	-2.13	-0.40	-0.81	-0.40	-0.82
	150%	max	1.63	2.25	2.90	2.25	2.92	0.40	0.83	0.40	0.85
		min	-1.00	-1.60	-2.56	-1.60	-2.59	-0.49	-0.98	-0.49	-1.00
Tarzana	70%	max									
		min									
	100%	max	1.93	2.79	4.37	2.79	6.14	0.90	1.60	0.89	1.80
		min	-1.97	-3.44	-5.62	-3.46	-6.77	-0.71	-1.40	-0.71	-1.44
	125%	max									
		min									
	150%	max	2.77	3.84	5.27	3.68	7.50	1.24	2.00	1.22	2.62
		min	-2.93	-4.58	-6.57	-4.47	-9.61	-1.07	-1.93	-1.07	-2.05

positive direction: to the east (Figure 4-4)

** mid-height: at the third row of connectors from the base (40 in. from the base)*

*** top: at the top row of connectors (88 in. from the base)*

Table 9-6 OpenSees analysis results of UCSD CMU 2 MC for shake-table, out-of-plane loading

ground motion			PGA (g), measured	acceleration (g)				displacement (in.)			
				CMU		veneer		CMU		veneer	
				mid-height *	top **	mid-height *	top **	mid-height *	top **	mid-height *	top **
Sylmar	80%	max	0.83	1.07	1.52	1.06	1.56	0.17	0.25	0.17	0.26
		min	-0.54	-1.16	-1.46	-1.15	-1.50	-0.16	-0.25	-0.16	-0.26
	100%	max	1.05	1.36	1.66	1.35	1.70	0.20	0.31	0.20	0.32
		min	-0.68	-1.44	-1.81	-1.43	-1.86	-0.18	-0.28	-0.18	-0.29
	125%	max	1.34	1.70	1.99	1.69	2.06	0.25	0.39	0.25	0.40
		min	-0.85	-1.78	-2.29	-1.77	-2.44	-0.23	-0.34	-0.23	-0.35
	150%	max	1.66	2.13	2.28	2.13	2.30	0.31	0.46	0.30	0.51
		min	-0.99	-2.11	-2.88	-2.12	-3.94	-0.28	-0.41	-0.28	-0.43
Tarzana	70%	max	1.30	2.43	2.67	2.40	2.76	0.24	0.38	0.24	0.39
		min	-1.36	-1.83	-2.45	-1.83	-2.52	-0.31	-0.46	-0.31	-0.48
	100%	max	1.91	3.42	3.88	3.39	4.49	0.37	0.55	0.36	0.65
		min	-2.02	-2.76	-4.07	-2.75	-6.45	-0.43	-0.63	-0.42	-0.67
	125%	max	2.29	3.65	4.69	3.55	7.62	0.57	0.73	0.57	1.20
		min	-2.47	-3.50	-4.97	-3.46	-8.65	-0.52	-0.76	-0.50	-0.80
	150%	max	2.79	4.00	5.30	4.01	10.07	0.88	0.97	0.89	1.86
		min	-2.94	-4.79	-6.28	-4.78	-9.59	-0.58	-0.79	-0.53	-0.84

positive direction: to the east (refer to Figure 4-4)

** mid-height: at the third row of connectors from the base (40 in. from the base)*

*** top: at the top row of connectors (88 in. from the base)*

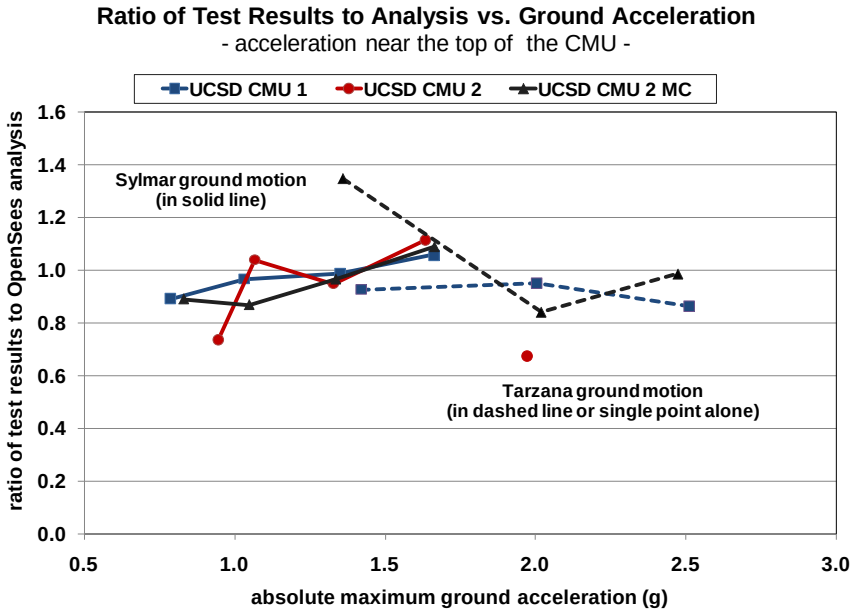

Figure 9-13 Ratios of test results to OpenSees analysis versus ground acceleration (CMU, maximum positive accelerations at the top row of connectors)

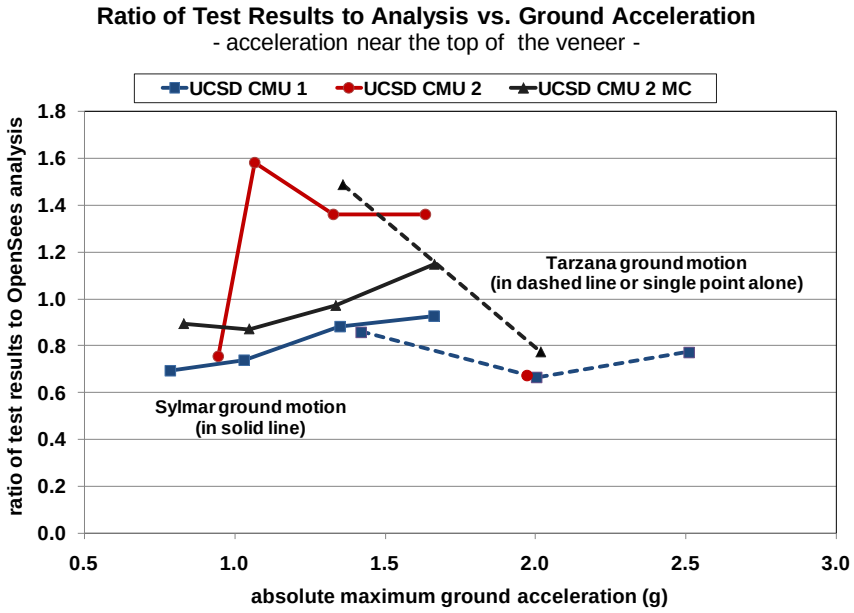

Figure 9-14 Ratios of test results to OpenSees analysis versus ground acceleration (veneer, maximum positive accelerations at the top row of connectors)

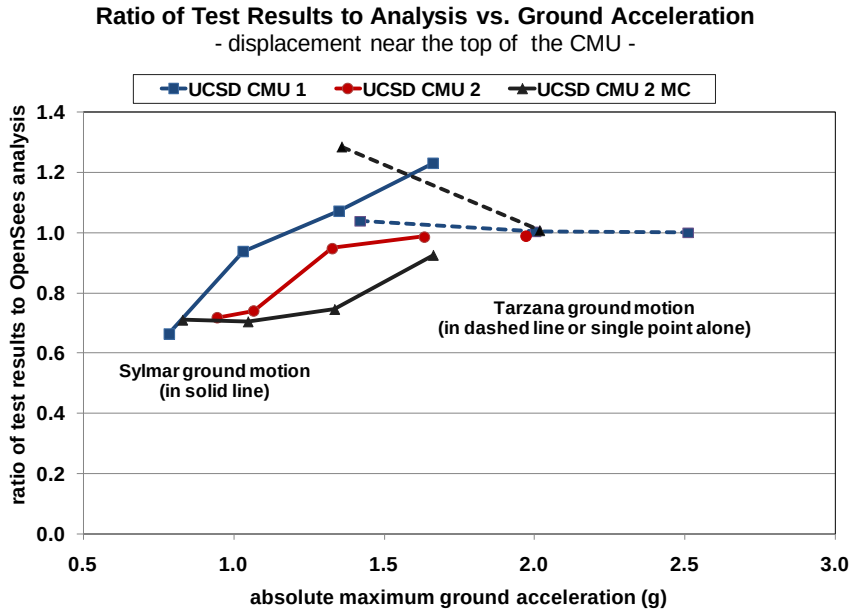

Figure 9-15 Ratios of test results to OpenSees analysis versus ground acceleration (CMU, maximum positive displacement at the top row of connectors)

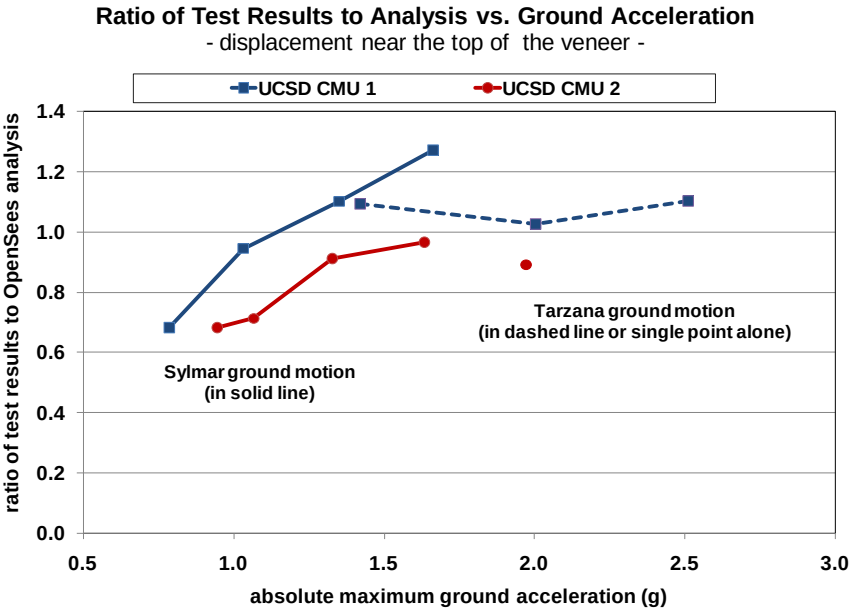

Figure 9-16 Ratios of test results to OpenSees analysis versus ground acceleration (veneer, maximum positive displacement at the top row of connectors)

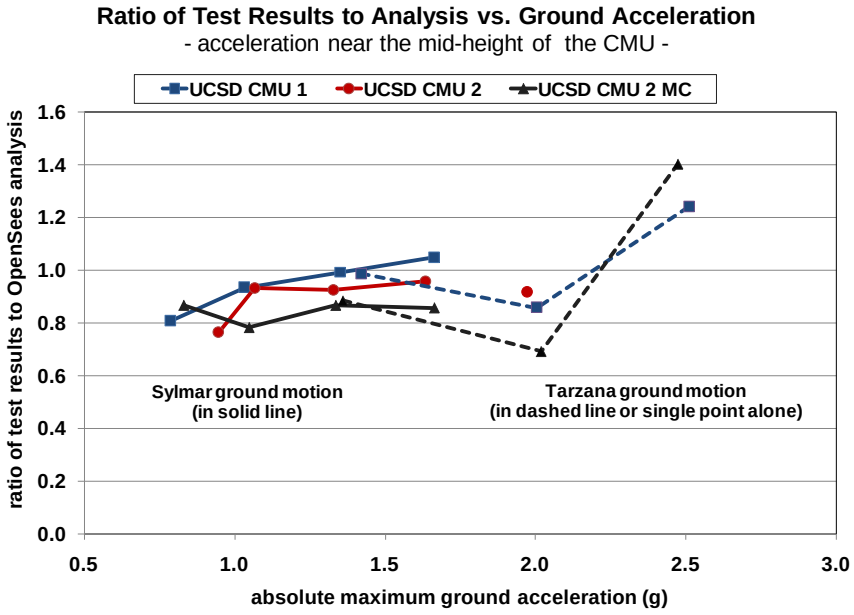

Figure 9-17 Ratios of test results to OpenSees analysis versus ground acceleration (CMU, maximum positive accelerations at the 3rd row of connectors from the base)

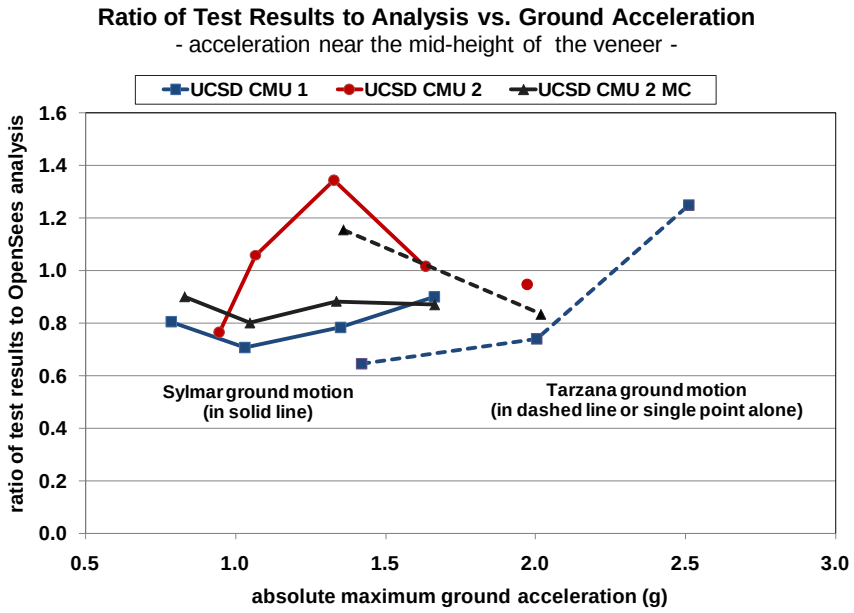

Figure 9-18 Ratios of test results to OpenSees analysis versus ground acceleration (veneer, maximum positive accelerations at the 3rd row of connectors from the base)

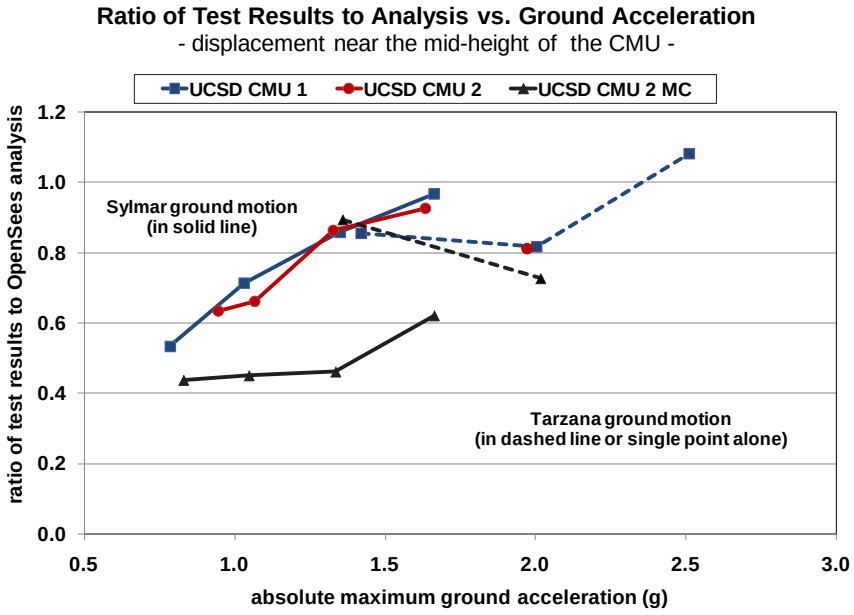

Figure 9-19 Ratios of test results to OpenSees analysis versus ground acceleration (CMU, maximum positive displacements at the 3rd row of connectors from the base)

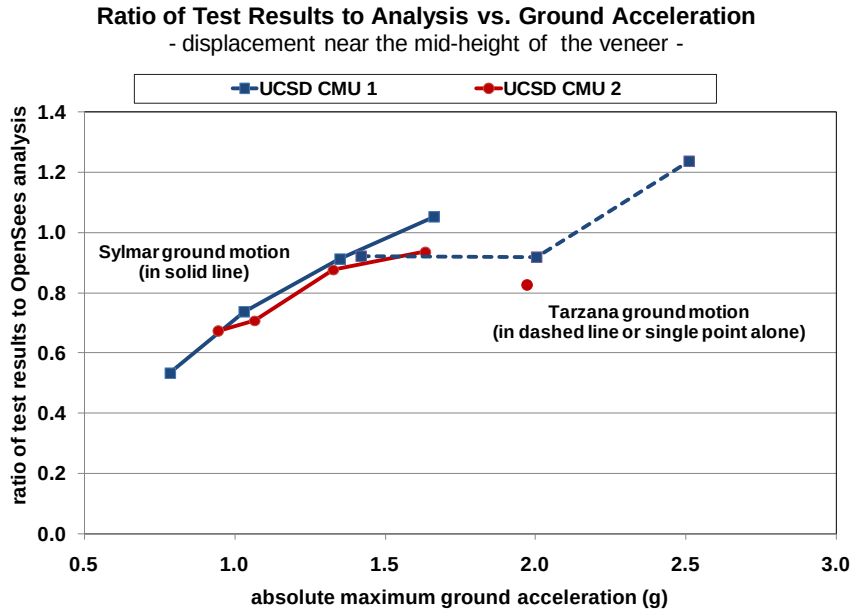

Figure 9-20 Ratios of test results to OpenSees analysis versus ground acceleration (veneer, maximum positive displacements at the 3rd row of connectors from the base)

9.2 IN-PLANE BEHAVIOR OF CMU WALLS WITH CLAY MASONRY VENEER

The CMU wall specimens for in-plane testing were lightly reinforced (one #4 reinforcing bar at both wall ends). In quasi-static testing of those in-plane specimens, horizontal load was applied to the top of CMU wall only, and the clay masonry veneer did not display any observable or measurable movement relative to the CMU wall. Before significant yielding, the flexural and shear behavior at the base of the in-plane walls can be considered uncoupled. Flexural behavior is dominated by the tensile stress-strain behavior and the tensile bond-slip behavior of the longitudinal reinforcement; shear behavior is dominated by shear friction, and differential sliding displacement across the base interface is small. As the horizontal load to the top of CMU walls increased, the gap (flexural crack) between the CMU wall and the base developed and widened. After significant yielding of the longitudinal reinforcement, the gap did not fully close, and sliding of the CMU wall was resisted less and less by shear friction, and more and more by dowel action. This phenomenon is referred to here as "coupled" flexure and shear behavior at the base of the in-plane walls. The behaviors are coupled because the base rotation (the width of the base crack) influences the shearing stiffness. Because not enough test data are available for that coupled case, the results of OpenSees analysis for the quasi-static, in-plane CMU wall specimens are compared using the test results in the uncoupled range only.

In shake-table testing of the in-plane CMU wall specimens, the CMU walls were elastic and essentially rigid compared to the movement of the clay masonry veneer due to lack of roof mass. Accordingly, the comparison between shake-table test results and OpenSees analysis for in-plane CMU wall specimens will focus on the in-plane response of the clay masonry veneer and connectors.

9.2.1 In-plane Flexural Behavior of CMU Walls

As observed in the quasi-static testing described in Section 5.9.3, the in-plane flexural behavior of a CMU wall can be represented by a rigid element rotating at the base. The moment-curvature diagram for the in-plane CMU wall specimens is shown in Figure 9-21. Yield moment (M_y, 52 kip-ft) and ultimate moment (M_u, 70 kip-ft) of the CMU walls were calculated using a spreadsheet program (Figure 9-21), assuming reinforcement with the expected yield strength of 65 ksi, 1 % strain hardening, and 9 % elongation at fracture; and assuming masonry with the specified compressive strength of 1500 psi. For reinforcement, the expected yield strength of 65 ksi was used instead of the specified strength of 60 ksi, because the in-plane yield moment of the CMU walls is essentially governed by the yield strength of reinforcement, and 65 ksi is usually close to the real yield strength of reinforcement. No strength-reduction factor for flexure was used. Self-weight of the CMU wall (about 2.4 kips based on 120 pcf) and the veneer (about 1.1 kips based on 114 pcf) was considered. Even though the weight of the veneer is transferred to the CMU wall just above the foundation, it increases the flexural capacity of the CMU wall at the base, because when the CMU wall rotates at the base, the veneer rotates along with the CMU wall. Based on the quasi-static test results of the in-plane CMU wall specimens, 0.025 in. of flexural crack width at the base (refer to Section 5.9.4) was selected to determine the rotation of the CMU walls at M_y in, and 0.25 in. of flexural crack width (refer to Section 5.9.5) was selected for M_u . These values (yield moment, ultimate moment and corresponding flexural crack widths) are used in Section 9.2.5 to establish the OpenSees model for the in-plane CMU wall specimens.

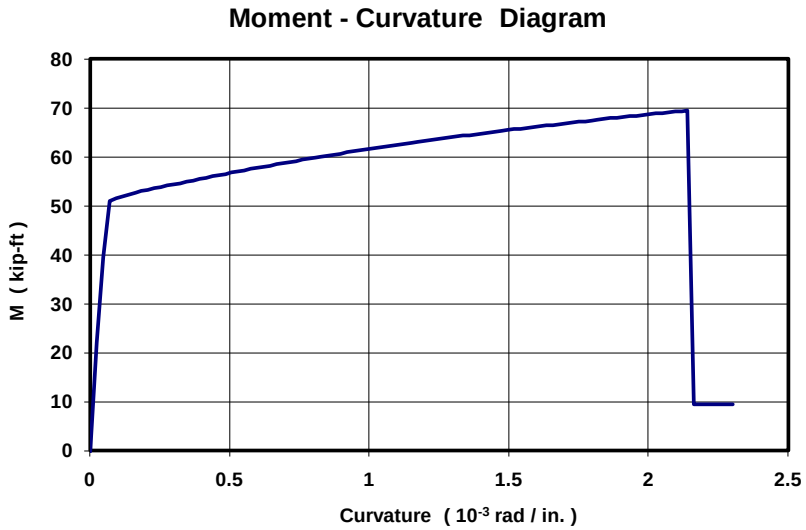

Figure 9-21 Moment-curvature diagram for in-plane CMU walls

9.2.2 In-plane Rocking and Sliding Behaviors of Veneer

The base of the in-plane veneer rests on top of the shelf angle, which is in turn fixed to the in-plane CMU wall just above the floor or foundation. The in-plane veneer can slide and rock on the shelf angle. In the real structure, resistance to sliding comes from friction between the veneer and the shelf angle, and from horizontal forces developed in the distributed connectors between the in-plane veneer and the in-plane CMU; resistance to rocking comes from the self-weight of the veneer, and from horizontal and vertical forces developed in the distributed connectors. Sliding resistance due to friction is determined by the sum of the self-weight of the veneer and the vertical force in the connectors. Because sliding resistance and rocking resistance both depend on the horizontal and vertical forces in the connectors, sliding and rocking of the in-plane veneer are coupled.

When μ is less than b/h, the in-plane veneer slides only, without rocking. When μ is greater than or equal to b/h, the in-plane veneer rocks, and may also slide. Both of these statements are discussed below.

The first statement is discussed as follows: When $\mu < b/h$ (μ is coefficient of friction, b is width of the veneer panel, and h is height of the veneer panel), the in-plane veneer will generally slide without rocking as will be demonstrated below. When $\mu < b/h$, we need to consider sliding behavior only of the in-plane veneer. Now, we will demonstrate that the in-plane veneer only slides without rocking when $\mu < b/h$ with the assumption that, in the beginning (at time t_0), the resultant force of the connectors is horizontal only, and acts through the mid-height of the in-plane veneer panel. First, it will be shown that the in-plane veneer starts sliding without rocking (at time t_0). Then, it will be shown that it cannot rock while it is sliding (at time t after t_0).

At time t_0, the forces applied to the in-plane veneer are shown in Figure 9-22. In the free-body diagram (Figure 9-22), μ is the coefficient of friction between the in-plane veneer and the shelf angle; F is the resultant horizontal force in the distributed connectors; and $\ddot{u}_{tot}$ is the total horizontal acceleration of the in-plane veneer.

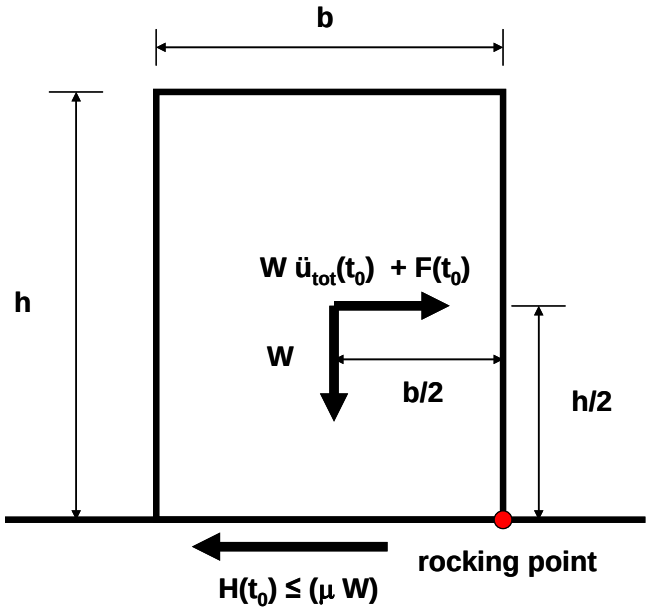

Figure 9-22 Forces applied to the in-plane veneer in the beginning (at time t0)

From horizontal equilibrium in Figure 9-22,

Equation 1

$$W\ddot{u}_{tot}(t_0) + F(t_0) = H(t_0) \leq W\mu$$

For sliding to start from Figure 9-22,

Equation 2

$$W\ddot{u}_{tot}(t_0) + F(t_0) = W\mu$$

For rocking to start at time t_0 from Figure 9-22,

Equation 3

$$\left[W\ddot{u}_{tot}(t_0) + F(t_0)\right]\frac{h}{2} \geq W\frac{b}{2} \quad \Rightarrow (\equiv) \quad W\ddot{u}_{tot}(t_0) + F(t_0) \geq W\frac{b}{h}$$

Note that the left-hand sides of Equation 2 and Equation 3 are identical. From those two equations, we can see that in-plane veneer starts sliding without rocking because μ is smaller than b/h. Note also that the direction of $F(t_0)$ does not matter.

At time t after t_0, while the in-plane veneer is sliding, let's check again the equilibrium of the veneer panel. Figure 9-22, Equation 2 and Equation 3 are still valid while the in-plane veneer is sliding, except that t_0 is replaced by t. Therefore, while sliding, the veneer cannot start rocking while sliding because μ is smaller than b/h. If the veneer panel stops sliding, the in-plane veneer will be in the same state as at time t_0.

The second statement is discussed as follows: When $\mu \geq$ b/h, the in-plane veneer will start rocking, with sliding if μ = b/h. Once the veneer panel rocks, the connectors will develop both horizontal force, whose resultant force is not around the mid-height, and vertical force. After the veneer panel starts rocking, due to lack of simplifying

assumptions, we need to consider both sliding and rocking behaviors of the in-plane veneer in the OpenSees modeling.

9.2.3 In-plane (Shear) Behavior of Double Eye-and-pintle Connectors

To represent the in-plane behavior of double eye-and-pintle connectors, we need to determine the envelope curve for the connectors, based on the theoretical calculation in this section. A deformation limit for the double eye-and-pintle connectors is suggested as a failure criterion in Section 9.2.7, by comparing the shake-table test results of the in-plane CMU wall specimens with OpenSees analysis. After OpenSees analysis, if the maximum deformation of the connectors exceeds the deformation limit, the in-plane veneer could be considered to have collapsed.

The vertical shear behavior of the double eye-and-pintle connectors depends on the direction of the applied load (horizontal or vertical), due the characteristic of eyes and pintles. When the pintles move upward, vertical shear force can be developed only by friction between the eyes and the pintles. Since the friction depends on the horizontal shear force (out-of-plane and in-plane), to predict the vertical shear force is difficult and accuracy is uncertain. For simplicity, this force will be ignored in OpenSees modeling. Considering the kinematics of the in-plane CMU wall and the in-plane veneer, the pintles cannot move vertically below the eyes. When the pintles go downward, without initial vertical eccentricity, the behavior is similar to the simplified horizontal shear behavior as described below.

The horizontal shear behavior can be estimated by considering the double pintles as cantilever beams, because the horizontal portions of the pintles (Figure 9-3) can be idealized as cantilever beams loaded upward by the eyes. The horizontal stiffness depends on the amount of mortar droppings, the difference between the diameters of pintles and eyes, the amount of vertical eccentricity, and the amount of protrusion of the eyes. The vertical eccentricity can be caused by construction tolerance, by differential thermal expansion of the CMU and the clay masonry, and by rocking of the in-plane

veneer. The maximum strength (shear strength) as governed by flexural yielding is affected by the amount of vertical eccentricity and the amount of protrusion of the eyes. For simplicity, all those factors are ignored: the amount of mortar droppings, the difference between the diameters of pintles and eyes, the amount of vertical eccentricity, and the amount of protrusion of the eyes. Since our main concern is the inelastic behavior of the in-plane veneer with the in-plane connectors, ignoring the mortar droppings and the gap will not be significant. Ignoring the vertical eccentricity will overestimate the horizontal shear stiffness and strength of the connectors, while ignoring the protrusion of the eyes underestimates the horizontal shear stiffness and strength. With all those factors ignored, the horizontal shear stiffness by the two cantilevered beams (double pintles) can be estimated as

$$K_{shear} = 2 \times \frac{3EI}{L^3} = \frac{6 \times 29000\ ksi \times 6.00 \times 10^{-5}\ in.^4}{(2\ in.)^3} = 1.31\ kip/in.,$$

and the shear strength (governed by flexural yielding at the ends) can be estimated as

$$V_y = 2 \times \frac{f_y \cdot S}{L} = \frac{2 \times 80\ ksi \times 6.42 \times 10^{-4}\ in.^3}{2\ in.} = 0.051\ kip,$$

where a probable yield stress of 80 ksi is used for f_y . The displacement at flexural yielding based on the theoretical equation ($\Delta_y = V_y / K$) is about 0.039 in. The simplified load-displacement curve (elasto-plastic) is shown in Figure 9-23, which is used for OpenSees modeling in Section 9.2.5 after some calibration of shear strength based on comparison of OpenSees analysis and test results.

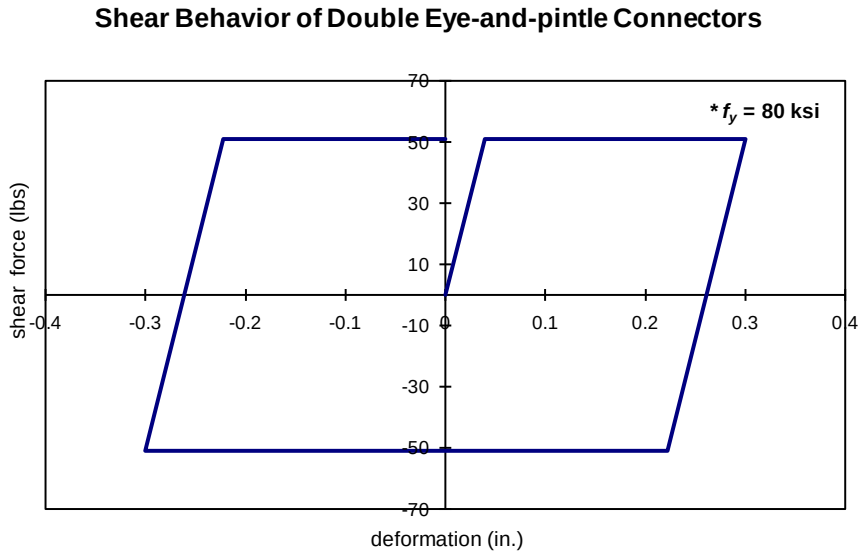

Figure 9-23 Simplified horizontal shear behavior of double eye-and-pintle connectors

9.2.4 In-plane (Shear) Behavior of Tri-wire Connectors

To represent the in-plane behavior of tri-wire connectors, we need to determine the envelope curve for the connectors, based on the theoretical calculation in this section. A deformation limit for the tri-wire connectors is suggested as a failure criterion in Section 9.2.7, by comparing the shake-table test results of the in-plane CMU wall specimens with OpenSees analysis. After OpenSees analysis, if the maximum deformation of the connectors exceeds the deformation limit, the in-plane veneer could be considered to have collapsed.

The shear behavior of the tri-wire connectors is essentially unaffected by the direction of shear (vertical or horizontal). The shear behavior can be estimated by considering a tri-wire connector as a fixed-fixed beam with a sidesway displacement of one end. The effective length of the beam, and hence its stiffness and strength, are influenced by mortar droppings. Ignoring mortar droppings, the elastic shear stiffness of the beam can be estimated as

$$K_{shear} = \frac{12\,E\,I}{L^3} = \frac{12 \times 29000\ ksi \times 2.35 \times 10^{-5}\ in.^4}{(2\ in.)^3} = 1.02\ kip/in.,$$

and the shear strength (governed by flexural yielding at the ends) can be estimated as

$$V_y = \frac{2\,f_y\,S}{L} = \frac{2 \times 80\ ksi \times 3.2 \times 10^{-4}\ in.^3}{2\ in.} = 0.025\ kip,$$

where a probable yield stress of 80 ksi is used for f_y . The displacement at flexural yielding based on the theoretical equation ($\Delta_y = V_y / K$) is about 0.025 in. Without significant mortar droppings, the load-displacement curve can be simplified as an elasto-plastic curve as shown in Figure 9-24, which is used for OpenSees modeling in Section 9.2.5 after some calibration of shear strength based on comparison of OpenSees analysis and test results. Since the mortar droppings affects the initial stiffness only and our main concern is the inelastic, in-plane behavior of the connectors, the effect of ignoring the mortar droppings is not significant.

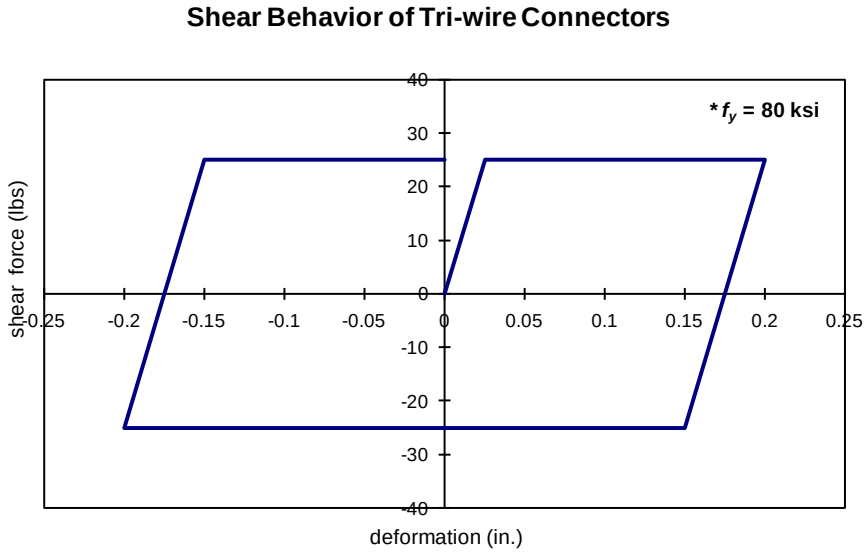

Figure 9-24 Simplified shear behavior of tri-wire connectors

9.2.5 OpenSees Modeling of In-plane CMU Wall Specimens

The OpenSees model for the in-plane CMU wall specimens is schematically shown in Figure 9-25. In that model, the in-plane CMU wall and the in-plane veneer are idealized as elastic beams. The section property of the CMU wall is based on a specified masonry compressive strength (f_m') of 1500 psi and an elastic modulus E equal to 900 f_m' (as prescribed by the 2008 MSJC Code), and the section property of clay masonry veneer is based on a specified masonry compressive strength (f_m') of 1500 psi and an elastic modulus E equal to 700 f_m' (as prescribed by the 2008 MSJC Code). Due to their sectional properties, the elastic beams behave essentially as rigid bodies in OpenSees analysis, rotating and sliding at their bases, as in a typical low-rise masonry structure. Although the flashing that is located between the shelf angle and the in-plane veneer is not explicitly included in the OpenSees model, its presence is accounted for by the coefficient of friction assumed between the in-plane veneer and the shelf angle.

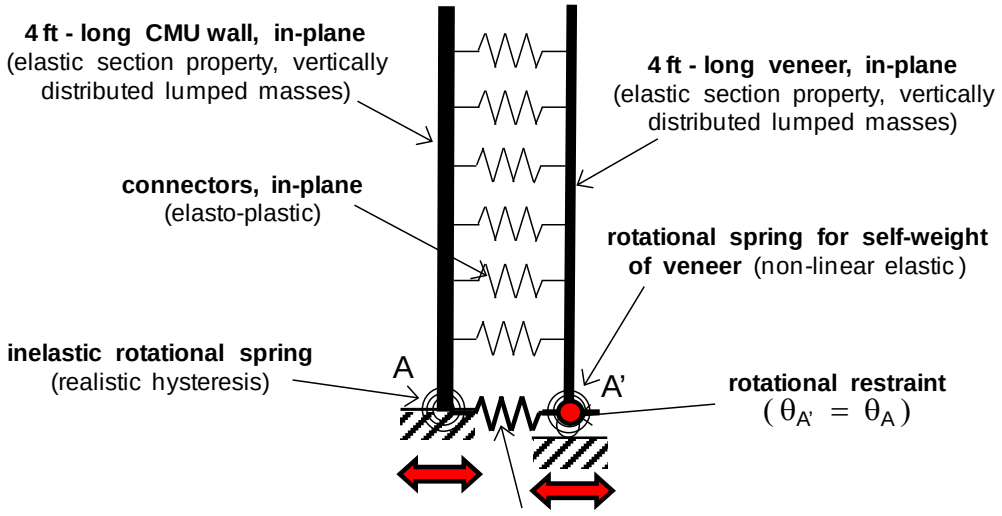

Figure 9-25 OpenSees model for in-plane CMU wall specimens

In the OpenSees model (Figure 9-25), the in-plane veneer can slide and rock at its base. When $\mu < b/h$, however, we need to consider only in-plane sliding of the veneer as demonstrated in Section 9.2.2. In that model, sliding resistance due to the self-weight of the veneer is idealized using an elasto-plastic horizontal spring at the base of the veneer, and rocking resistance due to the self-weight is idealized using a non-linear, elastic rotational spring at the base of the veneer (Figure 9-26). The coefficient of sliding friction between the veneer and the shelf angle was set as 0.6 based on shake-table results for the in-plane CMU wall specimens. Sliding and rocking resistances due to the connectors are represented by elasto-plastic springs distributed vertically with the same spacing as in the test specimen.

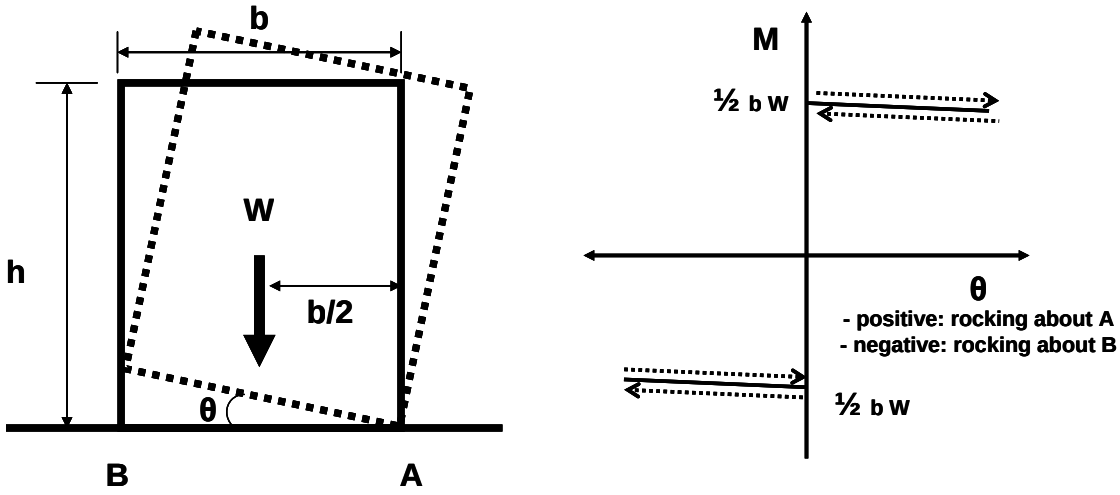

Figure 9-26 Nonlinear elastic rocking resistance of the in-plane veneer due to self-weight

For the connectors, we need to consider the difference between the plastic section modulus and the elastic section modulus for a circular cross section, because the connectors are expected to undergo substantial inelastic deformation. The simplified envelope curve for each type of connector (Figure 9-23 and Figure 9-24) used the elastic section modulus to calculate the shear strength. Because the ratio of the plastic section

modulus to the elastic section modulus is about 1.7, using the plastic section modulus result in significant increase in the calculated shear strength of the connectors. Applying the plastic section modulus, however, might overestimate the shear strength of the connectors. To address this issue, a multiplier to the shear strength of the connectors is used in this research. After trying several multipliers, a value of 1.4 was selected by comparing OpenSees analysis and test results.

Another issue for the connectors is that only horizontal deformations and horizontal forces are considered in Figure 9-26 due to simplicity of the model, and vertical components are disregarded. When the veneer panel rocks, this simplification might introduce errors, whose magnitude depends on several factors: the amount of rocking; the amount of sliding; the hysteretic characteristics of the connectors; the spatial distribution of the connectors; and the coefficient of friction between the veneer and the shelf angle. To include all those factors, however, is not practical for the simple modeling used in this research. More importantly, the purpose of modeling the connectors in-plane is to evaluate the in-plane behavior of the veneer (rocking and sliding). Rocking is affected by the self-weight of the veneer, and sliding is affected by the weight of the veneer and the coefficient of friction. Accordingly, it was judged that some error due to ignoring those factors would not be significant in evaluating the in-plane behavior of the veneer. Therefore, those factors are not considered in this dissertation.

9.2.6 OpenSees Analysis of In-plane CMU Wall Specimens, Quasi-static Loading

The OpenSees analysis of the in-plane CMU wall specimens for quasi-static loading is compared with the test results for in-plane flexural behavior of the CMU walls, using the OpenSees model described in Section 9.2.5. In this analysis, the elements for the clay masonry veneer and the connectors are not included for simplicity because they do not affect the response of the CMU walls under given loading conditions.

The OpenSees analysis, based on M_y and M_u at their corresponding base rotations (refer to Section 9.2.1), is compared with the quasi-static test results of the in-plane CMU wall specimens in Figure 9-27 through Figure 9-29. In those figures, the test results are marked in dark blue and the OpenSees analysis in dark red. All the three in-plane CMU specimens are represented by the same model in OpenSees, because the OpenSees model for the in-plane CMU walls is not affected by the type of connectors or the type of mortar. The OpenSees analysis matches the test results well until the vertical reinforcement fractures at 9 % elongation (refer to Section 5.9.5), as assumed in the OpenSees modeling.

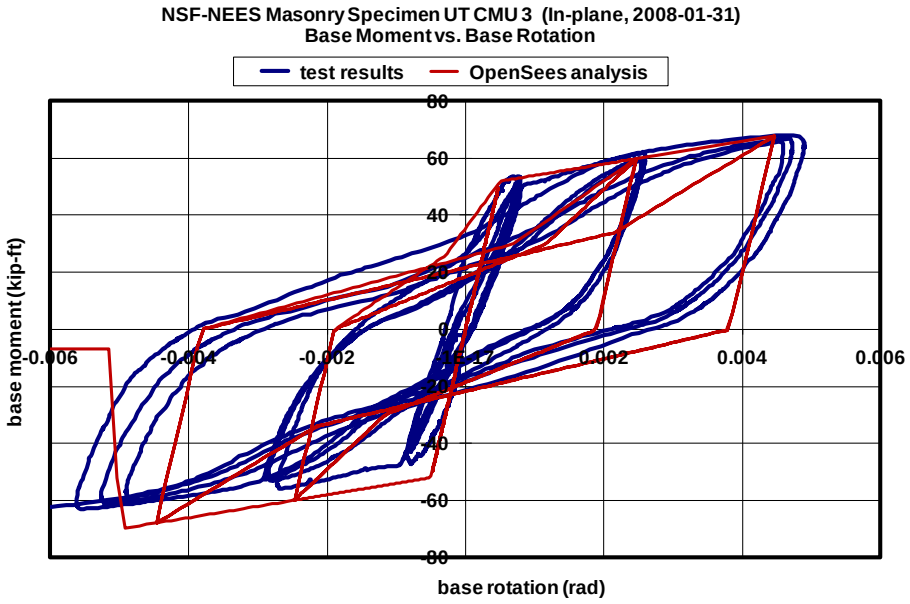

Figure 9-27 Comparison between test results and OpenSees analysis, base moment versus base rotation (UT CMU 3)

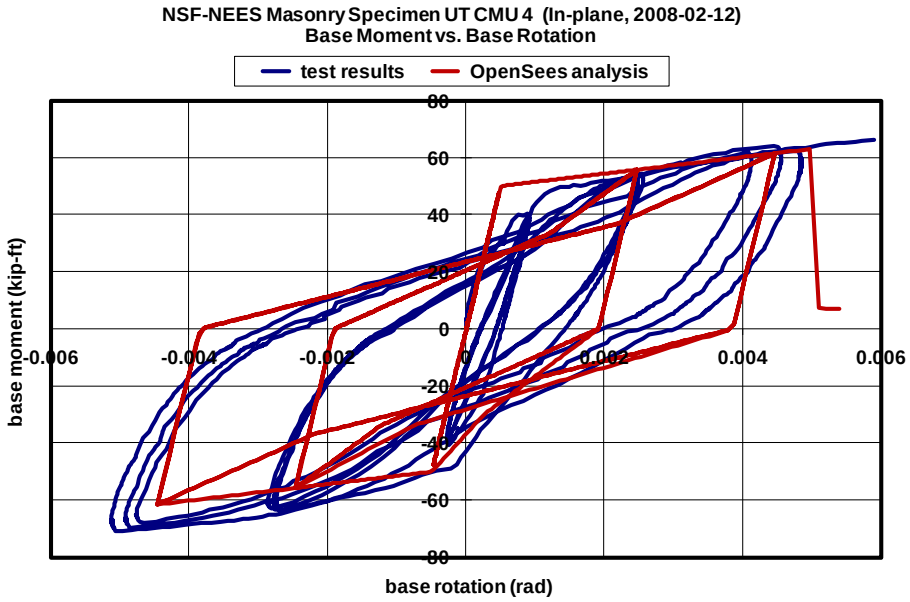

Figure 9-28 Comparison between test results and OpenSees analysis, base moment versus base rotation (UT CMU 4)

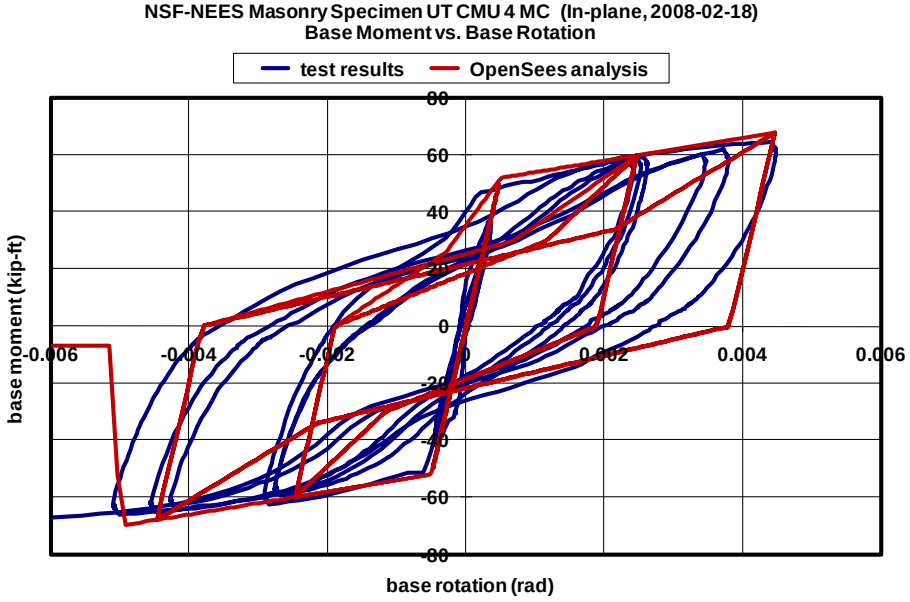

Figure 9-29 Comparison between test results and OpenSees analysis, base moment versus base rotation (UT CMU 4 MC)

9.2.7 OpenSees Analysis of In-plane CMU Wall Specimens, Shake-table Loading

The OpenSees analysis of the in-plane CMU wall specimens for shake-table loading is compared with the test results. In this analysis, we focus on in-plane rocking and sliding of the clay masonry veneer, and collapse of that veneer due to in-plane failure of the connectors. The in-plane response of the CMU walls is not considered in this section because the self-mass of the specimens was so small that the in-plane response of the CMU wall was negligible in the test results and the OpenSees analysis.

The in-plane responses (accelerations and displacements near the top and displacements near the bottom) of the clay masonry veneer from OpenSees analysis are listed in Table 6-9, Table 9-8 and Table 9-9 for each CMU wall specimen. The top accelerations and the top displacements were measured at the top row of connectors (88 in. from the base), and the bottom displacements were measured at the bottom row of connectors (8 in. from the base).

The absolute maximum top displacements of the veneer are listed in Table 9-10 from shake-table testing and OpenSees analysis. Ratios of those displacements (test results to OpenSees analysis) versus ground acceleration are plotted in Figure 9-30. The Sylmar motion generally developed maximum displacement responses in the west direction, while Tarzana motions generally developed maximum displacement responses in the east direction. Therefore, the ratios in Figure 9-30 were calculated using maximum values in the west direction (negative) for Sylmar motions and maximum values in the east direction (positive) for Tarzana motions. The ratios range between 0.4 and 1.8, with an average of 1.1.

As shown in Figure 9-30, the analytical results from the OpenSees analysis do not at first seem to provide a satisfactory estimate of the maximum displacement response near the top of the in-plane veneer. Considering the level of scatter inherent in real structures (as described below), however, the OpenSees analysis using the simple model

provides a reasonable estimate of the maximum displacement response of the in-plane veneer,

Specimens UCSD CMU 4 and UCSD CMU 4 MC are the same from the viewpoint of structural response. The only difference between those two specimens are the type of mortar (cement-lime mortar versus masonry cement mortar), and the in-plane behaviors of those specimens are essentially unaffected by the flexural cracking strength, which depends on the mortar. At 1.5 Sylmar (Table 9-10), however, the displacement of UCSD CMU 4 is 0.340 in. while the displacement of UCSD CMU 4 MC is 0.761 in., or about 2.2 times that of UCSD CMU 4. This indicates a significant level of scatter inherent in the response of the in-plane veneer in real structures. This implies that OpenSees analysis (compared in Figure 9-30) provides a reasonable estimate of the maximum displacement response of the in-plane veneer, which in turn can be used to estimate the in-plane deformation of the connectors.

From Specimens UCSD CMU 4 and UCSD CMU 4 MC in Table 9-10, 1.8 in. can be proposed as an estimate for the in-plane deformation capacity of tri-wire connectors. The entire length of the tri-wire connectors, as well as double eye-and-pintle connectors, was 2 in. For double eye-and-pintle connectors, the deformation limit cannot be determined from Specimen UCSD CMU 3 in Table 9-10 because the connectors did not fail. In Sections 9.2.4 and 9.2.5, however, the deformation of tri-wire connectors for in-plane flexural yielding was calculated as about 0.025 in. while that of double eye-and-pintle connectors was about 0.039 in. Assuming that double eye-and-pintle connectors are the same type of material as tri-wire connectors, the deformation capacity of double eye-and-pintle connectors might be estimated as about

$$1.8\ in. \times \frac{0.039\ in.}{0.025\ in.} = 2.8\ in.$$

Since the length of the connectors is only 2 in., however, an in-plane deformation of 2.8 in. is not possible. Therefore, 2 in. of in-plane deformation capacity could be used as a

rough estimate in the OpenSees analysis because that much deformation (about 2 in.) is likely to cause low-cycle fatigue failure under repeated cycling.

Table 9-7 OpenSees analysis results of UCSD CMU 3 for shake-table, in-plane loading

ground motion			PGA (g), measured	responses of veneer		
				acceleration (g)	displacement	
				top *	bottom **	top *
Sylmar	80%	max	0.78	0.98	0.00	0.01
		min	-0.54	-0.63	0.00	-0.04
	100%	max	1.03	1.25	0.00	0.03
		min	-0.66	-0.92	-0.01	-0.06
	125%	max	1.35	1.50	0.01	0.05
		min	-0.84	-1.08	-0.03	-0.08
	150%	max	1.66	1.95	0.01	0.02
		min	-0.99	-1.52	-0.04	-0.12
Tarzana	70%	max	1.29	2.09	0.04	0.12
		min	-1.42	-2.77	-0.03	-0.05
	100%	max	1.88	2.95	0.11	0.34
		min	-2.00	-2.65	-0.02	-0.07
	125%	max	2.33	4.83	0.24	0.61
		min	-2.51	-4.76	-0.04	-0.35
	150%	max	2.76	4.85	0.58	1.09
		min	-3.02	-5.16	-0.03	-0.57

positive direction: to the east

** top: at the top row of connectors (88 in. from the base)*

*** bottom: at the first row of connectors from the base (8 in. from the base)*

Table 9-8 OpenSees analysis results of UCSD CMU 4 for shake-table, in-plane loading

ground motion			PGA (g), measured	responses of veneer		
				acceleration (g)	displacement	
				top *	bottom **	top *
Sylmar	**80%**	max	0.95	1.23	0.00	**0.02**
		min	-0.55	-1.55	-0.01	**-0.07**
	100%	max	1.07	1.33	0.00	**0.04**
		min	-0.68	-2.57	-0.01	**-0.13**
	125%	max	1.33	1.70	0.01	**0.28**
		min	-0.88	-4.39	-0.05	**-0.38**
	150%	max	1.63	4.25	0.00	**0.39**
		min	-1.00	-4.57	-0.17	**-0.84**
Tarzana	**70%**	max	**no test**			
		min				
	100%	max	1.93	4.11	0.25	**0.90**
		min	-1.97	-4.15	-0.01	**-0.27**
	125%	max	**no test**			
		min				
	150%	max	2.77	4.99	0.85	**2.26**
		min	-2.93	-5.63	-0.08	**-1.68**

positive direction: to the east

** top: at the top row of connectors (88 in. from the base)*

*** bottom: at the first row of connectors from the base (8 in. from the base)*

Table 9-9 OpenSees analysis results of UCSD CMU 4 MC for shake-table, in-plane loading

ground motion			PGA (g), measured	responses of veneer		
				acceleration (g)	displacement	
				top *	bottom **	top *
Sylmar	**80%**	max	0.83	1.06	0.00	**0.01**
		min	-0.54	-0.78	-0.01	**-0.05**
	100%	max	1.05	1.35	0.00	**0.04**
		min	-0.68	-2.08	-0.01	**-0.11**
	125%	max	1.34	2.18	0.01	**0.25**
		min	-0.85	-4.27	-0.05	**-0.37**
	150%	max	1.66	4.30	0.00	**0.39**
		min	-0.99	-4.76	-0.18	**-0.86**
Tarzana	**70%**	max	1.30	2.15	0.05	**0.29**
		min	-1.36	-2.62	-0.01	**-0.09**
	100%	max	1.91	3.93	0.30	**0.93**
		min	-2.02	-4.14	-0.01	**-0.19**
	125%	max	2.29	4.96	0.64	**1.51**
		min	-2.47	-4.88	-0.03	**-0.46**
	150%	max	2.79	4.95	0.82	**2.56**
		min	-2.94	-5.78	-0.06	**-2.00**

positive direction: to the east

** top: at the top row of connectors (88 in. from the base)*

*** bottom: at the first row of connectors from the base (8 in. from the base)*

Table 9-10 Absolute maximum displacement of the veneer near the top (88 in. from the base)

ground motion		UCSD CMU 3		UCSD CMU 4		UCSD CMU 4 MC	
		test results (in.)	OpenSees (in.)	test results (in.)	OpenSees (in.)	test results (in.)	OpenSees (in.)
Sylmar	0.8	0.03	0.04	0.09	0.07	0.09	0.05
	1.0	0.05	0.06	0.14	0.13	0.15	0.11
	1.25	0.09	0.08	0.22	0.38	0.35	0.37
	1.5	0.13	0.12	0.34	0.84	0.76	0.86
Tarzana	0.7	0.21	0.12	no test	no test	0.54	0.29
	1.0	0.43	0.34	0.91	0.90	1.20	0.93
	1.25	0.64	0.61	no test	no test	1.80	1.51
	1.5	0.95	1.09	failure	2.26	failure	2.56

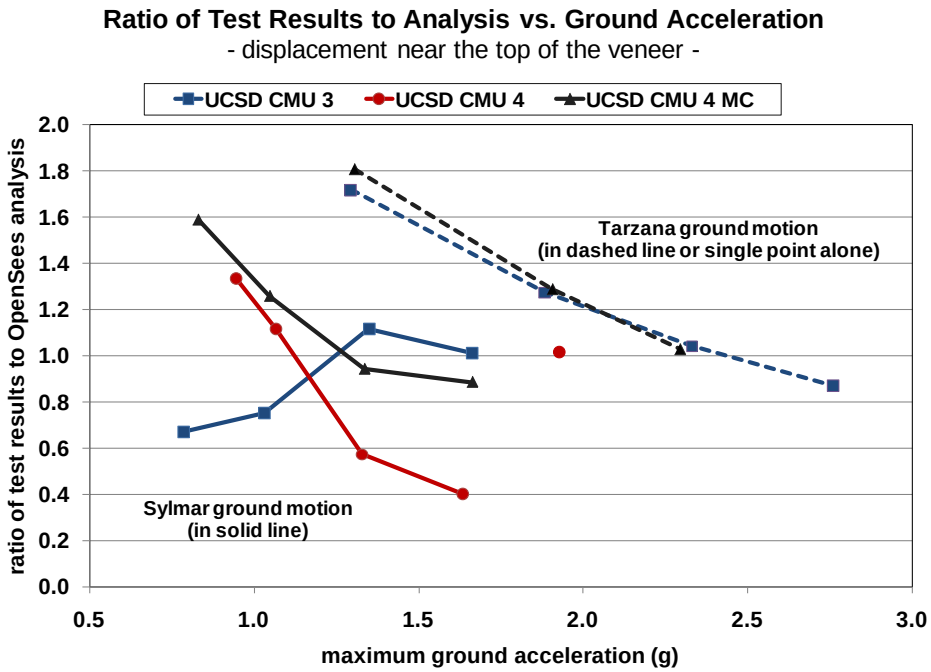

Figure 9-30 Ratio of test results to OpenSees analysis versus ground acceleration (veneer, maximum displacements at the top row or connectors)

CHAPTER 10
Analytical Study of CMU Building Specimen

10.1 Introduction to Analytical Study of CMU Building Specimen

In this chapter, the analytical model developed in Chapter 9 for concrete masonry walls with clay masonry veneer is extended to the low-rise concrete masonry building with clay masonry veneer. The extended model is calibrated and established using the shake-table test results of the CMU building specimen. Observations made during the calibration provide information about experimental test specimens not directly available from test results. The established model is then used for parameter studies, whose primary purpose is to supply general information about the seismic response of low-rise concrete masonry buildings with clay masonry veneer. This analytical study is conducted using the structural analysis framework OpenSees, developed by the PEER Center of the University of California at Berkeley.

Key seismic responses in the low-rise concrete masonry building with clay masonry veneer are overall response of the entire building; flexural behavior and base sliding of the in-plane CMU walls; rocking, base sliding and collapse of the in-plane clay masonry veneer; flexural behavior of the out-of-plane CMU walls; and collapse of the out-of-plane clay masonry veneer. The analytical model for the CMU building specimen also focuses on these key responses. To calibrate and establish the analytical model for the CMU building specimen, the recorded ground motion for each shake-table testing is used to compare the analytical results from OpenSees and the shake-table test results. For parameter study, the scaled, original ground motions (Sylmar and Tarzana) are used.

10.2 OVERVIEW OF OPENSEES MODELING OF CMU BUILDING SPECIMEN

The CMU building specimen, shown in Figure 7-2 (reproduced as Figure 10-1), was modeled in OpenSees using "macro" elements whose geometric and material properties were developed to represent the essential aspects of the real structure.

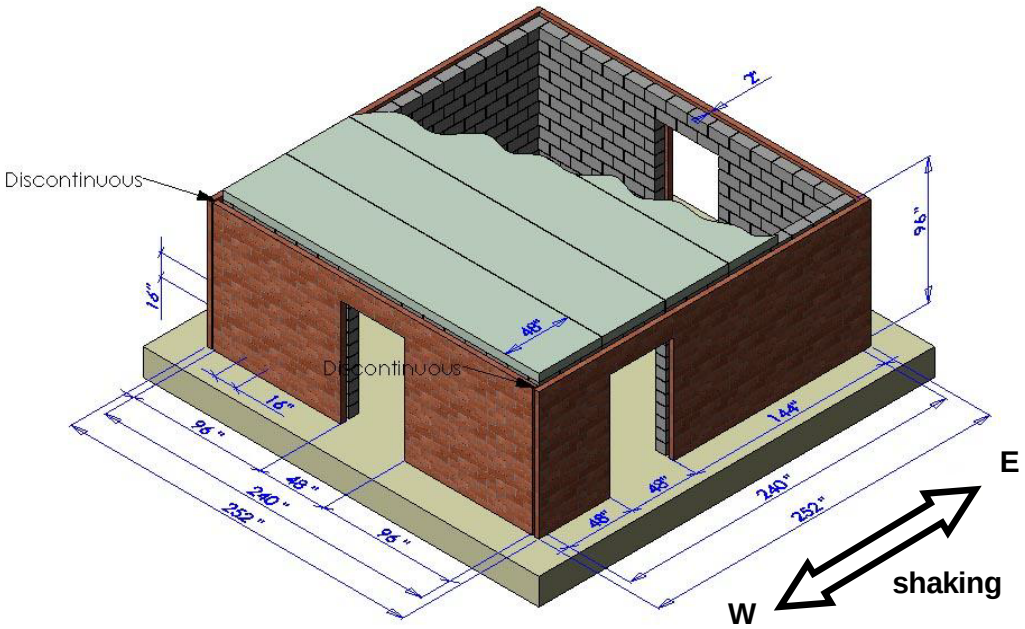

Figure 10-1 Overall view of CMU building specimen

The decision to use macro elements rather than a detailed finite-element model was based on several considerations: first, as described in Chapter 9, such macro elements had been used successfully to model the in- and out-of-plane behavior of the individual wall segments tested quasi-statically at UT Austin and on the shaking table at UC San Diego. Second, the OpenSees framework, while very powerful, cannot be described as user-friendly, and it is exceedingly difficult to debug. Parallel analytical efforts at UC San Diego had indicated that the development of a micro-level finite element mesh would probably take at least a month, and researchers decided that it would

be better to use that time at UT Austin to calibrate a macro-model and use it to conduct parametric studies.

With that decision made, the researchers proceeded to develop the macro-model, using the steps summarized below and addressed in more detail in the rest of this section.

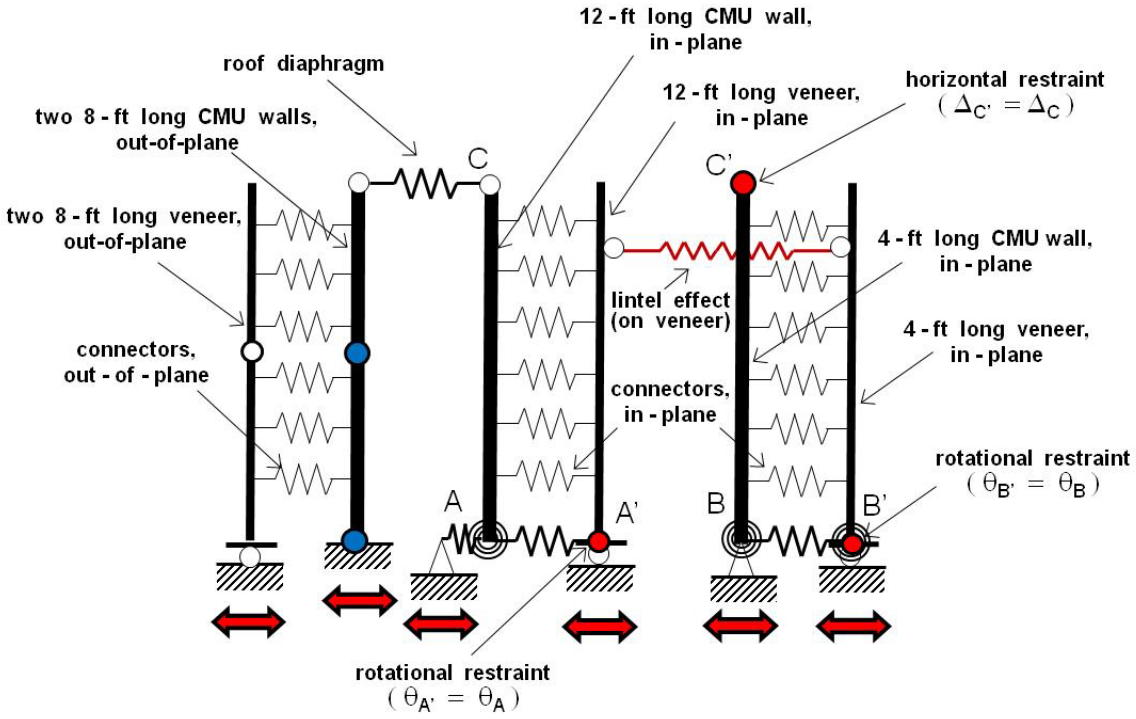

Figure 10-2 OpenSees model for CMU building specimen

1) As shown in Figure 10-1, the building is geometrically symmetric about the direction of shaking, and it is therefore necessary only to model one-half of it. Slight asymmetries (for example, connector details) are ignored in this macro-model.

2) As shown in Figure 10-2, the macro-model consists of three sets of walls. Each set is represented by a pair of vertical line elements, connected over their heights

by springs. In each case, one line of the pair represents the inner wythe of CMU, and the other line, the outer wythe of veneer.

a) The foundation is considered rigid, and the bases of each wythe of all three pairs are considered to be shaken identically by the input motion. That shaking is indicated by the back-and forth arrows at the base of each wythe.

b) The left-most set of walls in the figure represents the two 8-ft wall segments (one on the west side and the other on the east side of the half-structure), which are shaken out-of-plane at their bases by the foundation, and at the top by the roof diaphragm. The diaphragm is idealized as an axial element, whose equivalent axial flexibility represents the combined flexural and shearing flexibility of a simply supported beam spanning between the two sets of in-plane walls. That flexibility is expressed in terms of the relative displacement in the direction of shaking between the mid-span of the diaphragm (at the plane of symmetry of the structure) and the diaphragm supports. To capture the effects of diaphragm flexibility on the response of the out-of-plane walls, the tops of those walls are idealized as being connected to the mid-span of the diaphragm (the left end of the axial element in the figure). The diaphragm supports (Point C of the figure) coincide with the tops of the in-plane walls.

c) The remaining two pairs of walls in the figure represent the in-plane walls. The center pair represents the 12-ft segment, and the right-hand pair, the 4-ft segment. Again, all pairs of line elements are considered to be shaken identically at their bases. Because the diaphragm is considered to have no membrane flexibility in the direction of shaking, the horizontal displacements of Points C and C′ in the figure are constrained to be equal.

3) Now consider each pair of wythes in more detail.

a) The left-hand pair (out-of-plane wythes) is inter-connected by nonlinear springs, whose hysteretic force-deformation behavior represents the axial response of out-of-plane connectors. The line element representing the reinforced CMU wythe must have moment-rotation behavior representing that of the out-of-plane CMU walls, and the line element representing the veneer wythe must do the same for the veneer.

b) The center pair (in-plane wythes) represents the 12-ft long wall segment. The base of the CMU wythe (Point A) is connected to the foundation by a rotational spring whose stiffness represents the combined in-plane moment-rotation behavior of the reinforced CMU wythe, plus the geometric stiffness associated with that wythe's rigid-body rotation. The base of the veneer wythe (Point A′) requires no rotational spring representing the geometric stiffness associated with that wythe's right-body rotation, because this veneer segment does not rock with respect to the CMU wythe. The base of the veneer wythe (Point A′) is constrained to have the same in-plane rotation as the base of the CMU wythe, because in the real structure the veneer rests on a shelf angle attached to the base of the CMU wythe. The linear spring connecting Points A and A′ represents the hysteretic relationship between frictional resistance and relative displacement of the base of the veneer wythe with respect to the flashing-covered shelf angle. The center pair is inter-connected by nonlinear springs, whose hysteretic force-deformation behavior represents the horizontal and vertical shearing responses of the in-plane connectors. The line element representing the reinforced CMU wythe must have moment-rotation behavior representing that of the in-plane CMU walls, and the line element representing the veneer wythe must do the same for the veneer.

c) The right-hand pair (in-plane wythes) represents the 4-ft long wall segment. It is handled identically in concept to the center pair. The base

of the CMU wythe (Point B) is connected to the foundation by a rotational spring whose stiffness represents the combined in-plane moment-rotation behavior of the reinforced CMU wythe, plus the geometric stiffness associated with that wythe's rigid-body rotation. The base of the veneer wythe (Point B′) is connected to the foundation by a rotational spring whose stiffness represents the geometric stiffness associated with that wythe's right-body rotation. The lower end of the rotational (rocking) spring at the base of the veneer wythe (Point B′) is constrained to have the same in-plane rotation as the base of the CMU wythe, because in the real structure the veneer rests on a shelf angle attached to the base of the CMU wythe (Point B). The linear spring connecting Points B and B′ represents the hysteretic relationship between frictional resistance and relative displacement of the base of the veneer wythe with respect to the flashing-covered shelf angle. The right-hand pair is inter-connected by nonlinear springs, whose hysteretic force-deformation behavior represents the horizontal and vertical shearing responses of the in-plane connectors. The line element representing the reinforced CMU wythe must have moment-rotation behavior representing that of the in-plane CMU walls, and the line element representing the veneer wythe must do the same for the veneer.

d) The tops of the veneer wythes of the center and the right-hand pairs are connected by axial elements whose hysteretic responses represent axial constraints produced between those veneer segments by the loose lintel (described in Section 10.3.2).

10.3 DETAILS OF OPENSEES MODELING OF CMU BUILDING SPECIMEN

Details of the OpenSees model of the CMU building specimen are described in Figure 10-3 (representing the roof diaphragm and the out-of-plane wall segments) and

Figure 10-4 (representing each of the two in-plane wall segments, plus the connecting veneer lintel).

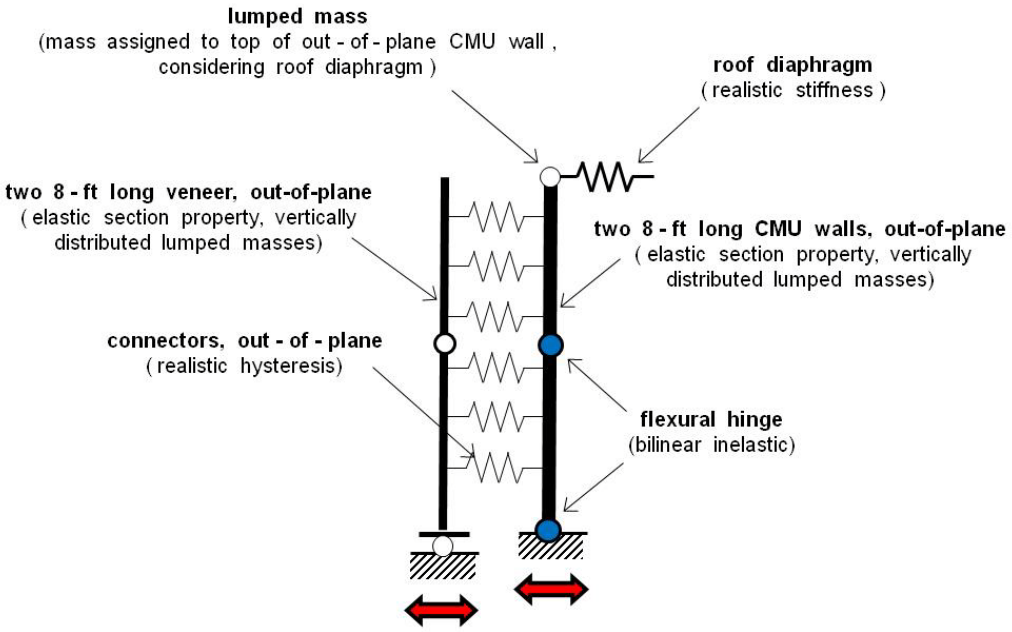

Figure 10-3 OpenSees model for CMU building specimen, out-of-plane portion

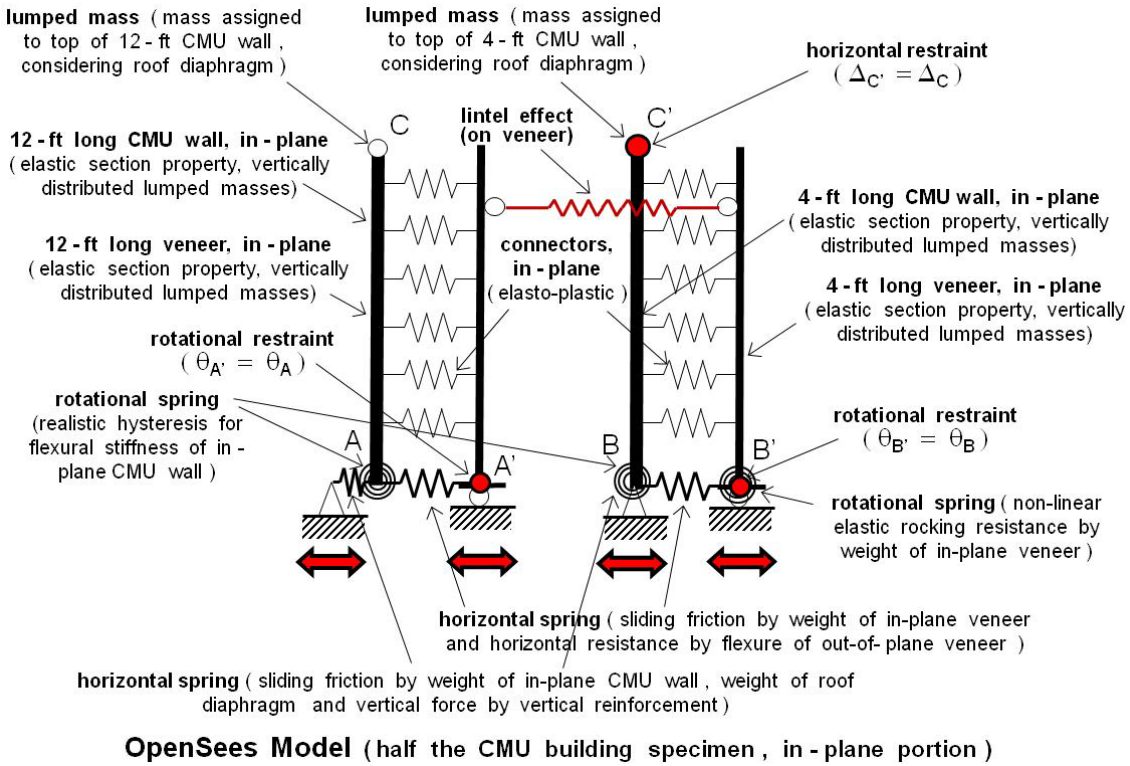

Figure 10-4 OpenSees model for CMU building specimen, in-plane portion

10.3.1 Modeling of Roof Diaphragm and Out-of-plane Wall Segments

The model shown in Figure 10-3 includes two 8-ft long out-of-plane CMU wall segments with clay masonry veneer. The out-of-plane CMU walls, clay masonry veneer, and connectors are modeled as described in Section 9.1.4 (out-of-plane CMU wall specimens). The calculated moment-curvature diagrams for a single 8-ft long out-of-plane CMU wall segment in the CMU building specimen are shown in Figure 10-5 (at the base) and Figure 10-6 (at the mid-height), assuming reinforcement with an expected yield strength of 65 ksi, 1 % strain hardening, and masonry with a compressive strength equal to the specified value of 1500 psi. Since the effects of self-weight are negligible, from Figure 10-5 and Figure 10-6 a single value of 16 kip-ft is used for simplicity as the yield moment strength both at the base and at the mid-height in the OpenSees model. To

account for the fact that there are two CMU wall segments, this yield moment strength (16 kip-ft) is multiplied by two in the OpenSees model. The total mass of the out-of-plane CMU wall in the OpenSees model is taken as twice the mass of a single 8-ft long CMU wall segment.

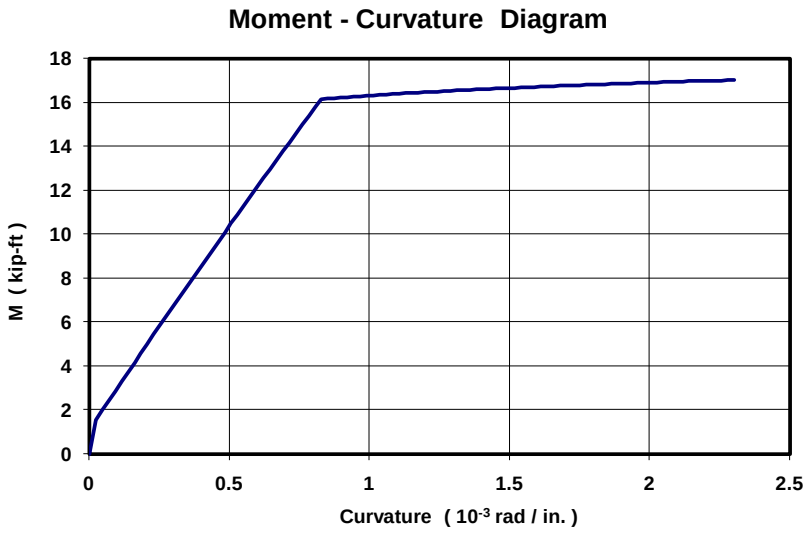

Figure 10-5 Moment-curvature diagram of 8-ft CMU wall at the base

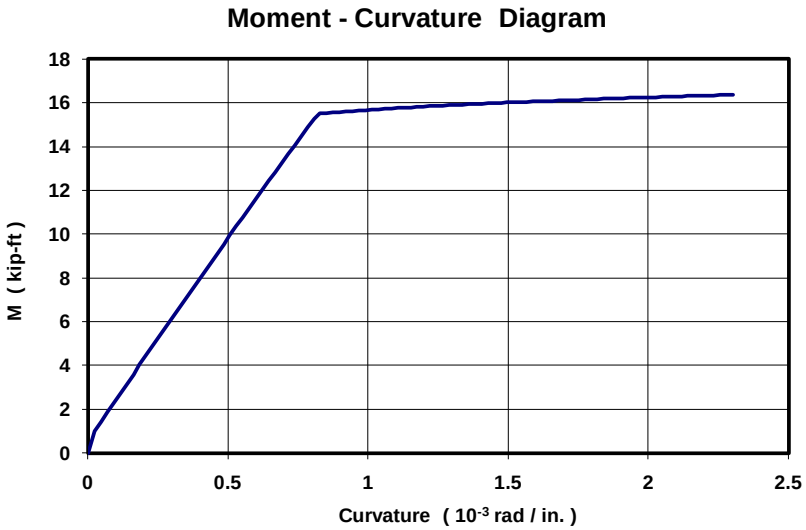

Figure 10-6 Moment-curvature diagram of 8-ft CMU wall at the mid-height

The roof diaphragm is modeled as an equivalent axial elastic rod. One-quarter the mass of the entire roof diaphragm is assigned to the top of the out-of-plane CMU walls and another quarter to the top of the in-plane CMU walls. The equivalent axial stiffness (13650 kip/in.) used in the OpenSees modeling was calculated using beam theory including flexural and shearing deformations. This stiffness represents half the stiffness of the entire roof diaphragm. In calculating shearing deformations, the variation of shear stress over the cross-section was considered, and an effective shear area equal to 5/6 of the gross area was used.

10.3.2 Modeling of In-plane Wall Segments and Connecting Veneer Lintel

The in-plane CMU walls, clay masonry veneer, and connectors are modeled essentially as described in Section 9.2.5 (in-plane CMU wall specimens). The moment-curvature diagrams at the base of each CMU wall, calculated using a spreadsheet program, are shown in Figure 10-7 and Figure 10-8 for the 12-ft long in-plane CMU wall segments, and in Figure 10-9 and Figure 10-10 for the 4-ft long in-plane CMU wall

segments. Based on these moment-curvature diagrams (Figure 10-7 through Figure 10-10), the yield, the ultimate and residual flexural strengths used in the OpenSees modeling are listed in Table 10-1.

In the spreadsheet program, the expected yield strength of 65 ksi, 1 % strain hardening, and 9 % elongation at fracture were used for reinforcement; and the specified compressive strength of 1500 psi was used for masonry. The vertical reinforcing bars were placed in the spreadsheet as designed for each CMU wall segment (12-ft long and 4-ft long). The effective flange section was taken as that prescribed by Section 1.9.4 of the 2008 MSJC Code. The self-weights of the CMU walls, clay masonry veneer and roof diaphragm were considered. The weight of the prestressed concrete planks with 3.5-in. concrete topping was assigned to the 12-ft long wall and the 4-ft long wall based on their plan lengths plus half the length of door opening. The additional weight on the roof diaphragm (19.5 kips) was assigned only to the 12-ft long CMU wall because it better represents the location of the additional weight on the CMU building specimen.

The in-plane rotation at the base of the 4-ft long CMU wall segment at flexural yield was taken as 0.0005 rad, and the corresponding value for the 12-ft long CMU wall segment was taken as 0.00017 rad. The value of 0.0005 rad is that used in OpenSees modeling of the in-plane CMU wall specimens (4-ft long in plan), and the value of 0.00017 rad, corresponding to the same extreme-fiber crack width, is 0.0005 rad divided by 3.0 (the ratio of the plan lengths of the 12-ft segment and the 4-ft segment). The rotation at ultimate flexural strength is taken as 10 times the rotation at flexural yielding. The hysteretic relationships are as determined in OpenSees modeling of the in-plane CMU wall specimens. The hysteretic relationships follow the envelope curves of Figure 10-7 through Figure 10-10, and includes pinching as shown in Figure 9-30.

Table 10-1 Flexural strengths of in-plane CMU walls used in OpenSees modeling of CMU building specimen

Flange	in tension			in compression		
flexural strength	M_y (yield)	M_u (ultimate)	M_r (residual)	M_y (yield)	M_u (ultimate)	M_r (residual)
12-ft CMU wall	850 kip-ft	1000 kip-ft	230 kip-ft	650 kip-ft	800 kip-ft	200 kip-ft
4-ft CMU wall	170 kip-ft	200 kip-ft	30 kip-ft	120 kip-ft	160 kip-ft	25 kip-ft

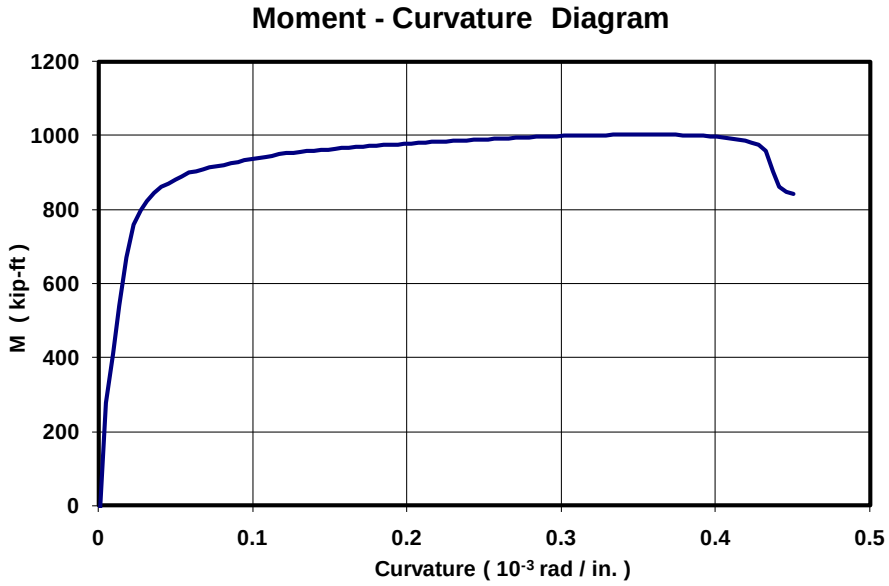

Figure 10-7 In-plane moment-curvature diagram for 12-ft CMU wall (flange in tension)

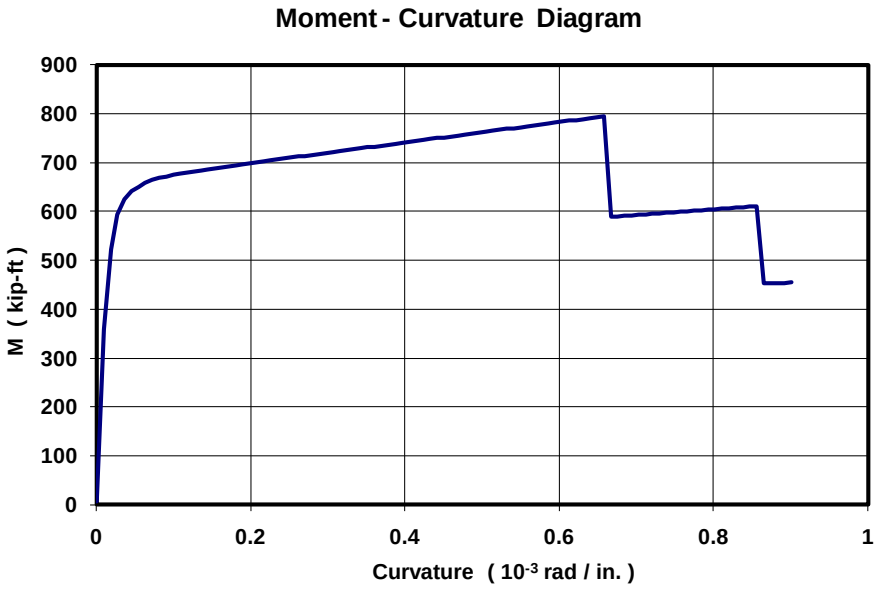

Figure 10-8 In-plane moment-curvature diagram for 12-ft CMU wall (flange in compression)

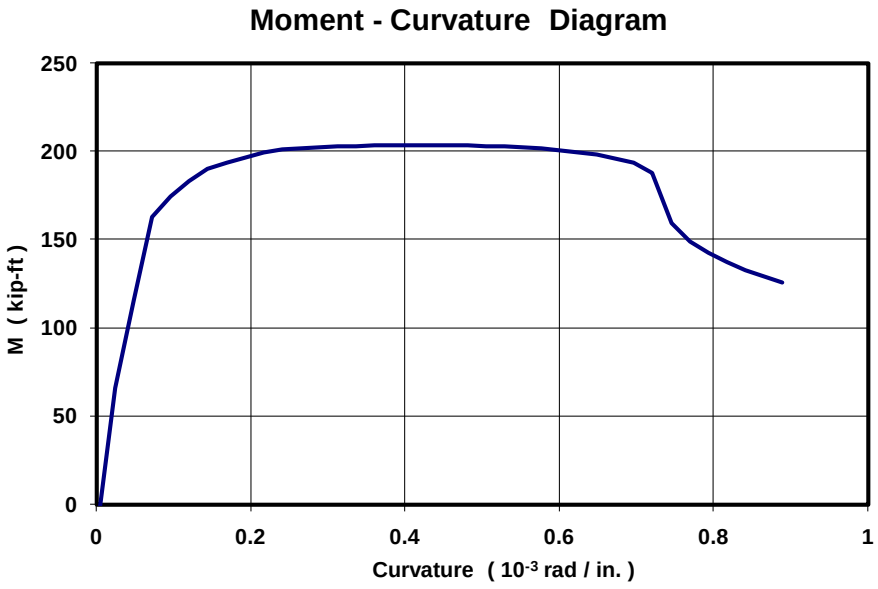

Figure 10-9 In-plane moment-curvature diagram for 4-ft CMU wall (flange in tension)

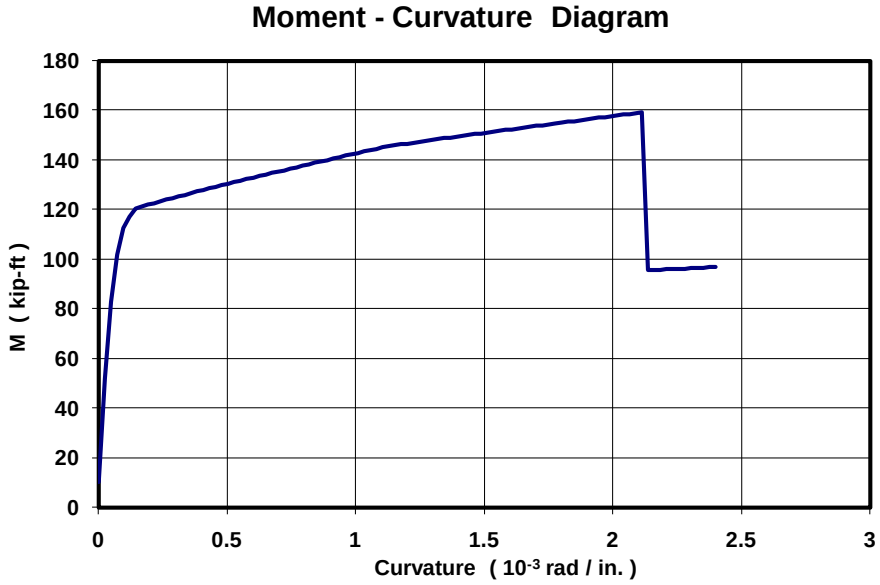

Figure 10-10 In-plane moment-curvature diagram for 4-ft CMU wall (flange in compression)

The base sliding resistance (88.8 kips) of the 12-ft long in-plane CMU wall segment is calculated using the weight of the CMU wall, clay masonry veneer, roof diaphragm, and additional weight on the roof diaphragm. The coefficient of friction between CMU walls and the concrete foundation was initially set at 1.0, but was changed to 0.8 based on calibration using shake-table test results. To avoid convergence failures in analysis, the stiffness for base sliding (up to the onset of base sliding) was set as large but finite, so that inelastic base sliding would start at 0.01 in. No analytical failure criterion for base sliding was inserted into the OpenSees model. In evaluating the OpenSees results, however, sliding failure could be assumed to have occurred at 0.20 in. of base sliding of the in-plane CMU wall segments of the CMU building specimen, as suggested in Section 7.4.4. During calibration, the effective flange was found not to help in preventing base sliding due to low out-of-plane flexural stiffness of the flange, although it does increase flexural resistance. Therefore, the flange is disregarded when calculating the sliding resistance of the 12-ft long in-plane CMU wall. The base sliding

of 4-ft long CMU walls is ignored in OpenSees modeling of the CMU building specimen because the OpenSees model does not consider the coupled rocking and sliding behavior, observed in quasi-static testing of the in-plane CMU wall specimens. Without this coupled behavior, the 4-ft long CMU walls do not slide at the base in OpenSees analysis.

The base sliding resistance of the 12-ft long in-plane veneer segment (2.12 kip) and the 4-ft long in-plane veneer segment (0.89 kip) are based on the weight of clay masonry veneer, considering the lintel and the additional length of about 0.5 ft at the corner. After calibrating the OpenSees model for the CMU building specimen, the continuous corner of the veneer was found to help considerably in preventing the in-plane veneer from sliding. Since sufficient data or research is not available on this issue, the sliding resistance of the 12-ft veneer is increased by 3.5 kips, calculated assuming 200 psi of modulus of rupture (f_r) for clay masonry and a 1-ft long cantilever (the distance from the in-plane veneer to the first row of out-of-plane connectors).

The ratio (b/h) for the 12-ft long veneer segment is (12 ft / 8 ft), or 1.5, which exceeds the expected coefficient of friction (μ) of about 0.6. As noted in Section 9.2.2, the segment is expected to slide only, without rocking, and rocking is therefore not included in the OpenSees model for this segment. The 4-ft long in-plane veneer is modeled as for the shake-table in-plane CMU wall specimens, including sliding and rocking. Due to the presence of lintel and additional effective length of veneer at the corner, the rocking resistance of the 4-ft long in-plane veneer due to self-weight is set as 3.2 kip-ft when the veneer rocks away from the lintel, and as 2.8 kip-ft toward the lintel.

After calibration of the OpenSees model for the CMU building specimen, two additional corrections were made to represent the presence of the lintel in the in-plane veneer. The corrections involved two additional analytical elements, described below and combined for simplicity in Figure 10-2 and Figure 10-4.

- The first element is intended to reproduce the connectivity (in the real building) between the in-plane veneer segments through axial compression in the lintel, due to the compressive stiffness and strength of the sealant placed in the expansion

joints at each end of the lintel. That connectivity is modeled using what was in effect a compression-only axial element with an initial stiffness of 10 kip/in. and a compressive yield strength of 10 kip. Those values are believed representative for the sealant and backer rod used in the expansion joints, and were confirmed by against the analytical response of the CMU building specimen.

- The second element is intended to reproduce the connectivity (in the real building) between the in-plane veneer segments through axial tension and compression in the lintel, due to the frictional resistance between the loose lintel and the two veneer segments. The maximum frictional resistance is calculated as 69 lbs, based on half the weight of the lintel (including clay masonry and shelf angle) multiplied by an assumed static coefficient of friction of 0.6. This amount of friction helps prevent the rocking of the 4-ft long veneer, but has only a negligible effect on the sliding resistance of the 4-ft long and the 12-ft long veneer segments.

10.4 OBSERVATIONS FROM CALIBRATION OF OPENSEES MODEL FOR CMU BUILDING SPECIMEN

The observations on the CMU building specimen, made while calibrating the OpenSees model for that specimen in Section 10.2, are summarized below. These observations supply information about the CMU building specimen, not directly available from test results.

- The coefficient of friction between CMU walls and the concrete foundation was found to be about 0.8.
- The effective flange contribution to the in-plane CMU walls was found not to help in preventing base sliding, due to low out-of-plane flexural stiffness of the flange.

- The continuous corner of the veneer was found to help considerably in preventing the in-plane veneer from sliding.
- The lintel can transfer compressive force (in the real building) between the in-plane veneer segments.
- The lintel can transfer force between the in-plane veneer, through friction between the lintel and the clay masonry veneer. This force transfer due to friction is especially helpful in preventing or decreasing the rocking of the short veneer segment.

10.5 COMPARISON OF TEST RESULTS WITH OPENSEES ANALYSIS

Primary responses of concern from the OpenSees model for the CMU building specimen, listed below, are also key seismic responses in the low-rise concrete masonry building with clay masonry veneer. In this section, shake-table test results of the CMU building specimen is compared with analytical results using the OpenSees model described in Section 10.2, focusing on these responses.

- overall response of the entire building (peak response accelerations and displacements);
- flexural yielding and base sliding of in-plane CMU walls;
- rocking, base sliding and collapse of in-plane clay masonry veneer;
- flexural yielding of out-of-plane CMU walls; and
- collapse of out-of-plane clay masonry veneer.

For the comparison, the recorded ground motion for each shake-table testing is used. The positive values from OpenSees analysis and shake-table test results indicate displacements or accelerations to the east in Figure 10-1, while negative values indicate responses to the west.

10.5.1 Comparison for Overall Response, Flexural Yielding, and Base Sliding of In-plane CMU Walls

Peak accelerations and displacements at roof diaphragm are used to represent the overall behavior in OpenSees analysis. As in the shake-table test results, these peak responses are governed primarily by in-plane response (flexural yielding and base sliding) of the analytical elements representing the CMU shear walls, and secondarily by in-plane deformation of the analytical element representing the roof diaphragm.

In the OpenSees analysis as well as the shake-table test results, the axial deformation of the analytical element representing the roof diaphragm was negligible. Accordingly, the analytical response of the CMU building specimen (predicted using the OpenSees model) was governed by the response (flexural yielding and base sliding) of the analytical elements representing the in-plane CMU walls.

In Table 7-9 are listed the peak response accelerations and displacements at the roof diaphragm from OpenSees analysis. These peak accelerations and displacements are obtained at the top of the analytical element for out-of-plane CMU walls, to include the deformation of the analytical element representing the roof diaphragm. Table 7-9 includes the responses only for Sylmar 200 %, Tarzana 100 % and 1st Tarzana 150 %. Before Sylmar 200 %, the peak displacements were negligible. At 2nd Tarzana 150 %, the OpenSees model does not represent the CMU building specimen because the vertical reinforcement of the CMU building specimen essentially fractured due to base sliding during 1st Tarzana 150 %.

The results in Table 7-9 were obtained by using tri-wire connectors for both in-plane and out-of-plane veneer. In OpenSees analysis, the overall response of the OpenSees model was by the type of connectors (tri-wire and double eye-and-pintle) used to connect the veneer to the CMU wall.

*Table 10-2 Peak responses at roof diaphragm from OpenSees analysis **

ground motion			PGA (g), measured	peak responses at roof diaphragm	
				acceleration (g)	displacement (in.)
Sylmar	200 %	max	2.03	2.17	0.03
		min	-1.62	-1.84	-0.03
Tarzana	100 %	max	1.55	1.86	0.07
		min	-2.40	-2.55	-0.02
	150 % (1st)	max	2.27	2.37	0.38
		min	-3.48	-3.09	-0.03

** tri-wire connectors were used for in-plane and out-of-plane veneer*

In Figure 10-11 and Figure 10-12, the peak response accelerations or displacements at the roof diaphragm from OpenSees analysis (Table 7-9) are compared with those from shake-table test results (Table 7-9). In these figures, the horizontal axis is the absolute peak ground acceleration, while the vertical axis is the peak response acceleration or displacement. The positive and negative responses imply the response to the east and to the west on the shake table, respectively.

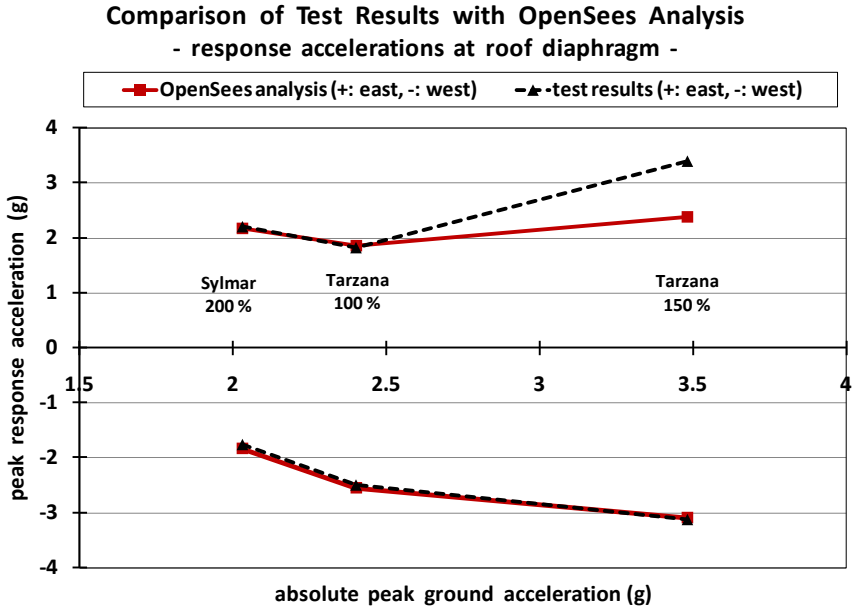

Figure 10-11 Comparison of test results with OpenSees analysis for response accelerations at roof diaphragm

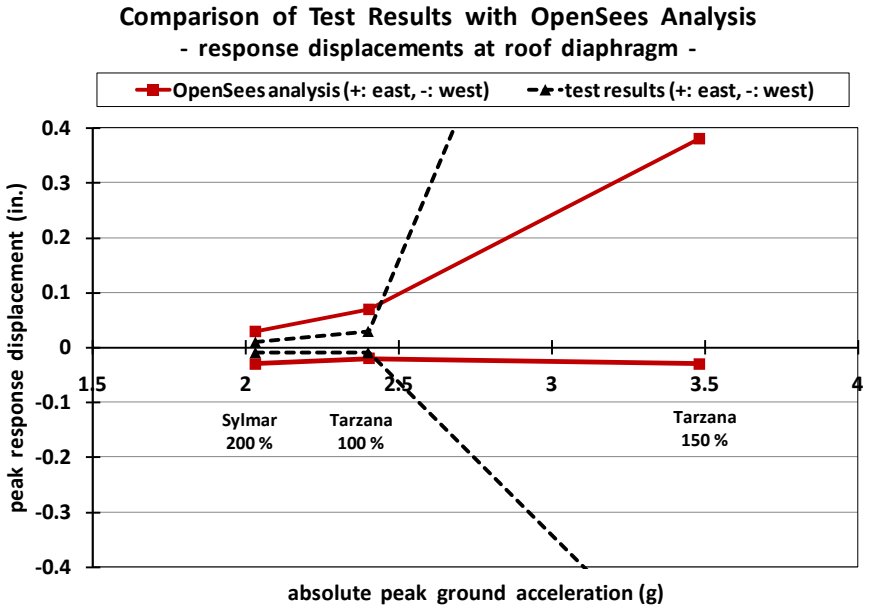

Figure 10-12 Comparison of test results with OpenSees analysis for response displacements at roof diaphragm

The comparison for response accelerations (Figure 10-11) shows good prediction using OpenSees analysis. The apparent difference for peak response acceleration (positive) at Tarzana 150 % exists because the vertical reinforcement in the CMU building specimen fractured during 1st Tarzana 150 %. The OpenSees model does not account for this fracture. This is addressed in the comparison for the response displacements at the roof diaphragm below.

In Figure 10-12, OpenSees analysis does not at first seem to provide a satisfactory estimate of peak response displacements at the roof diaphragm. Closer examination, however, shows that the predicted peak displacements are nevertheless useful. The justifications for this statement are related to the properties of the OpenSees model and the CMU building specimen, and are described below.

- First, the OpenSees model should be assumed to overestimate the displacement response before flexural cracking or base sliding of the in-plane CMU walls. The main concern in OpenSees modeling in this dissertation is inelastic deformation of the low-rise concrete masonry building with clay masonry veneer, because the elastic deformation is negligible due to huge in-plane elastic stiffness inherent in this kind of building (low-rise, shear-wall structural system). Accordingly, the OpenSees model assumes, for simplicity, that the in-plane CMU walls are initially cracked in flexure at the base. Also, to avoid convergence problems in analysis, the stiffness for base sliding (up to the onset of base sliding) in the OpenSees model was set finite so that inelastic base sliding starts at 0.01 in. In real structures, the stiffness for base sliding is infinite until the onset of base sliding.

- Second, the measured response of the in-plane CMU walls in the CMU building specimen has inherent scatter associated with base sliding. Comparing the results in Table 7-14 and Table 7-15 for Tarzana 100 %, the peak displacement near the top of the 12-ft long in-plane CMU wall is 0.05 in. on the north side and 0.03 in.

on the south side, both of which essentially came from base sliding only. This scatter is not caused by differences in connector type. Even though different connectors were used on the north side and on the south side to anchor the veneer to the CMU walls, the effect of the type of connectors (tri-wire and double eye-and-pintle) on the overall response of the entire building was negligible in the OpenSees analysis.

- Third, as a failure criterion for base sliding of in-plane CMU walls, 0.20 in. of base sliding was suggested in Section 7.4.4. Using that failure criterion, OpenSees analysis predicts the failure of the CMU building specimen by base sliding at Tarzana 150 % (Figure 10-12). Due to lack of information on base sliding, the OpenSees model established in this research cannot predict the amount of base sliding of the CMU building specimen after sliding failure (due to fracture of vertical reinforcement).

As described above, OpenSees analysis provides good estimation of peak response accelerations and displacements at the roof diaphragm until sliding failure occurs. This implies that the OpenSees model for the CMU building specimen well represents base sliding and flexural yielding of the in-plane CMU walls. These base sliding and flexural yielding are directly compared and confirmed in Table 10-3 and Table 10-4. As expected, OpenSees analysis generally predicts flexural yielding and base sliding well. It should be noted, however, that base sliding of the 12-ft long CMU wall is assumed to be well predicted, because the coefficient of friction between foundation and the in-plane CMU wall (0.8) was obtained by calibrating the OpenSees model for the CMU building specimen using shake-table test results for that specimen.

Table 10-3 Comparison for base sliding and flexural yielding, 12-ft CMU wall

ground motion	12-ft long in-plane CMU wall			
	base sliding		flexural yielding	
	OpenSees	test results	OpenSees	test results
Sylmar 200 %	onset of sliding	onset of sliding	none	not observed
Tarzana 100 %	sliding	sliding	none	not observed
Tarzana 150 % (1st)	sliding	sliding	onset of yielding	not observed

Table 10-4 Comparison for base sliding and flexural yielding, 4-ft CMU wall

ground motion	4-ft long in-plane CMU wall			
	base sliding		flexural yielding	
	OpenSees	test results	OpenSees	test results
Sylmar 200 %	none *	none	none	none
Tarzana 100 %	none *	none	none	onset of yielding
Tarzana 150 % (1st)	none *	sliding	yielding	yielding

** base sliding is not included in OpenSees modeling of 4-ft long CMU wall (refer to Section 10.2)*

10.5.2 Comparison for Rocking, Sliding and Collapse of In-plane Veneer

Analytical prediction of rocking, sliding and collapse of the in-plane veneer is compared with shake-table test results of the CMU building specimen, which has two in-plane veneer segments, 4-ft long and 12-ft long. In both the CMU building specimen and its OpenSees model, the 12-ft long veneer segment essentially only slides with respect to its corresponding CMU wall, while the 4-ft long in-plane veneer segment rocks with respect to its corresponding CMU wall, and possibly slides as well.

Peak displacements near the base are used to evaluate OpenSees prediction of sliding of the 12-ft veneer segment (with respect to its corresponding CMU wall), and peak displacements near the top are used to evaluate OpenSees prediction of rocking and sliding of the 4-ft long veneer segment (with respect to its corresponding CMU wall). In OpenSees analysis, collapse of the in-plane veneer is determined by failure of in-plane connectors, which is in turn determined by relative sliding or rocking of the in-plane veneer with respect to its corresponding CMU wall.

Peak relative displacements of the in-plane veneer are listed in Table 7-16 for tri-wire connectors and in Table 7-17 for double eye-and-pintle connectors. In the CMU building specimen, tri-wire connectors were used on the north side, while double eye-and-pintle connectors were used on the south side. In Figure 10-13 through Figure 10-16, the displacements in Table 7-16 and Table 7-17 from OpenSees analysis are compared with those in Table 7-16 and Table 7-17 from test results. In those figures, the displacements at 1st Tarzana 150 % are not plotted; comparison at that ground motion is not meaningful because the overall response of the entire building was not well predicted. Considering the level of scatter inherent in real structures (discussed in Section 9.2.7), analytical results using the simple OpenSees model (described in Section 10.2) provide good estimate of peak displacements of in-plane veneer by sliding or rocking.

Collapse of the in-plane veneer is equivalent to failure of connectors that anchor that veneer to the CMU wall. In Section 9.2.7, in-plane deformation capacity of connectors (2-in. long) was suggested for connector failure criteria: 1.8 in. for tri-wire connectors and 2.0 in. for double eye-and-pintle connectors. Based on those connector failure criteria, no collapse of the in-plane veneer is predicted up to Tarzana 100 %, which is consistent with test results.

Table 10-5 Peak relative displacements of in-plane veneer with respect to CMU walls (north, tri-wire connectors)

ground motion			PGA (g), measured	12-ft long veneer (sliding only)	4-ft long veneer (rocking and sliding)
				displacement near the base (in.)	displacement near the top (in.)
Sylmar	80 %	max	0.71	0.00	0.00
		min	-0.79	-0.00	-0.00
	120 %	max	1.11	0.00	0.02
		min	-1.18	-0.00	-0.04
	200 %	max	1.62	0.01	0.02
		min	-2.03	-0.03	-0.63
Tarzana	100 %	max	2.40	0.12	0.20
		min	-1.55	-0.00	-0.09
	150 % (1st)	max	3.48	0.54	0.64
		min	-2.27	-0.14	-0.29

Table 10-6 Peak relative displacements of in-plane veneer with respect to CMU walls (south, double eye-and-pintle connectors)

ground motion			PGA (g), measured	12-ft long veneer (sliding only)	4-ft long veneer (rocking and sliding)
				displacement near the base (in.)	displacement near the top (in.)
Sylmar	80 %	max	0.71	0.00	0.00
		min	-0.79	0.00	-0.00
	120 %	max	1.11	0.00	0.02
		min	-1.18	0.00	-0.03
	200 %	max	1.62	0.01	0.05
		min	-2.03	-0.02	-0.12
Tarzana	100 %	max	2.40	0.04	0.09
		min	-1.55	-0.01	-0.03
	150 % (1st)	max	3.48	0.08	0.17
		min	-2.27	-0.03	-0.09

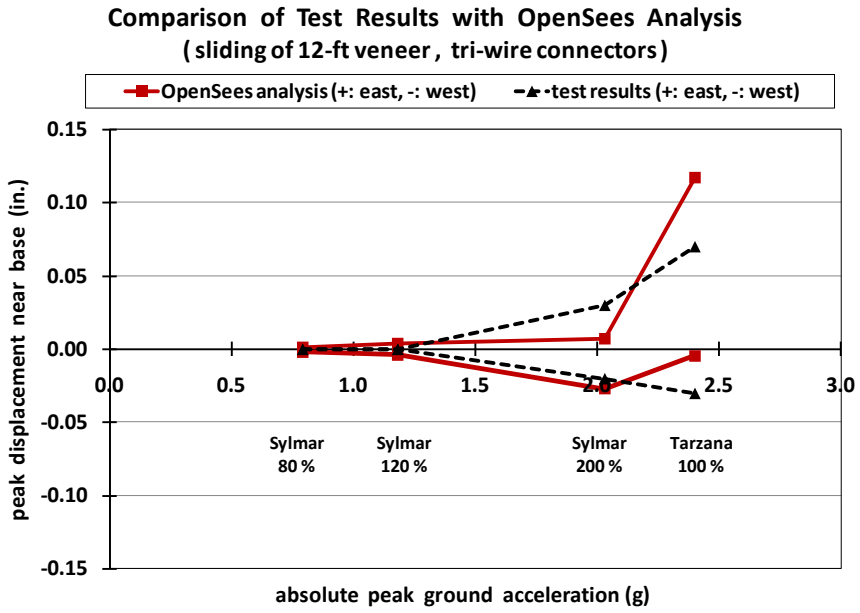

Figure 10-13 Comparison of test results with OpenSees analysis for sliding of 12-ft long veneer, tri-wire connectors

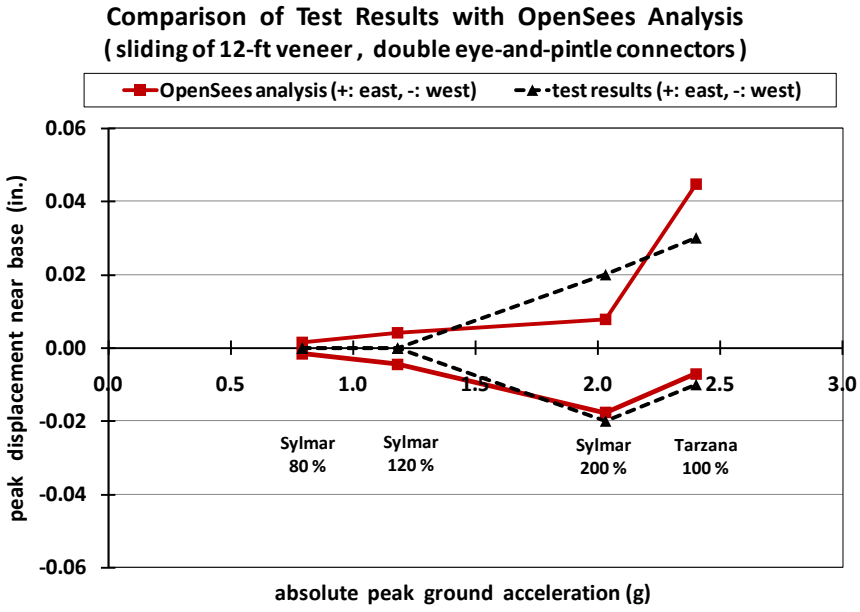

Figure 10-14 Comparison of test results with OpenSees analysis for sliding of 12-ft long veneer, double-eye-and pintle connectors

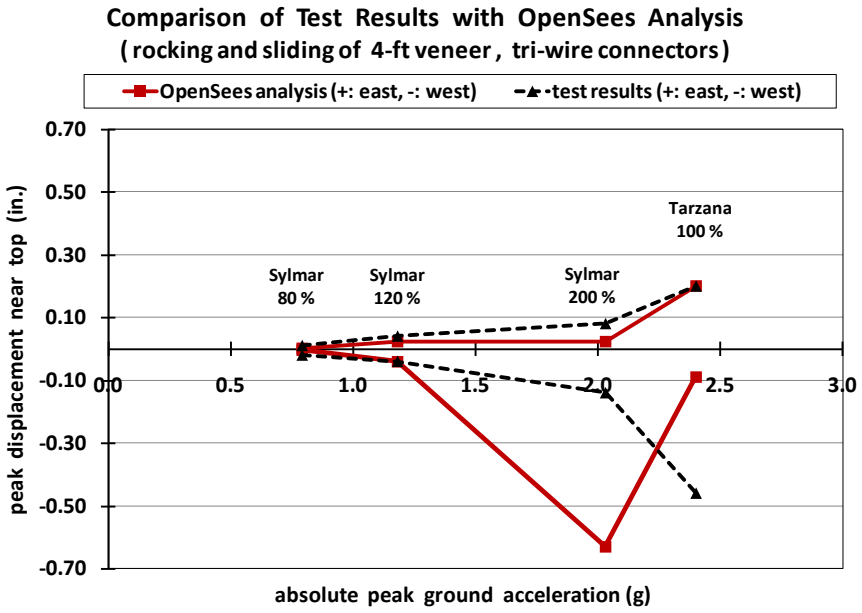

Figure 10-15 Comparison of test results with OpenSees analysis for rocking and sliding of 4-ft long veneer, tri-wire connectors

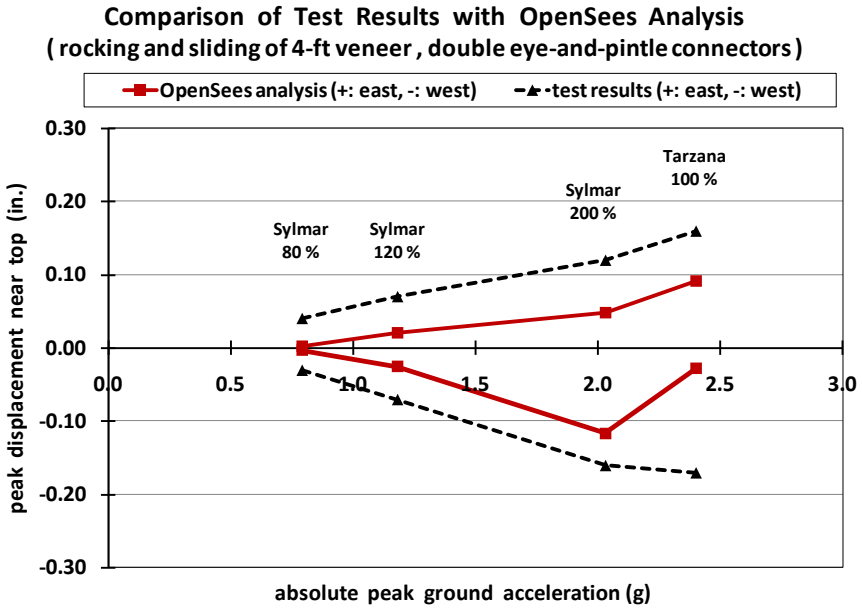

Figure 10-16 Comparison of test results with OpenSees analysis for rocking and sliding of 4-ft long veneer, double eye-and-pintle connectors

10.5.3 Comparison for Flexural Yielding of Out-of-plane CMU Walls and Collapse of Out-of-plane Veneer

In shake-table testing of the CMU building specimen, flexural yielding of the out-of-plane CMU walls was checked at the base and at the mid-height. This flexural yielding is compared with analytical results from OpenSees analysis in Table 10-7, where OpenSees analysis accurately predicts flexural yielding of the out-of-plane CMU walls. The comparison at 1st Tarzana 150 % might not be meaningful, because the overall response of the entire building was not well predicted. In the CMU building specimen and its OpenSees model, however, the flexural yielding of the out-of-plane CMU walls at the base suggests that some displacement (due to inelastic movement of the in-plane CMU walls) was imposed to the top of the out-of-plane CMU walls, as discussed in Section 7.4.6. The occurrence of flexural yielding in the out-of-plane CMU walls was not affected by the type of connectors used to anchor the clay masonry veneer to the CMU walls, either in test results or in OpenSees analysis.

Table 10-7 Comparison for flexural yielding of out-of-plane CMU walls

ground motion	flexural yielding of out-of-plane CMU walls			
	at base		at mid-height	
	OpenSees analysis	test results	OpenSees analysis	test results
Sylmar 200 %	none	none	none	none
Tarzana 100 %	none	none	none	none
Tarzana 150 % (1st)	flexural yielding	flexural yielding	none	none

Collapse of the out-of-plane veneer is equivalent to failure of connectors that anchor the veneer to the CMU walls. In Section 9.1.5, axial deformation capacity of connectors (2-in. long) was suggested for connector failure criteria, and is summarized in

Table 10-8. Based on those connector failure criteria, collapse of the out-of-plane veneer is predicted using OpenSees analysis. The prediction is compared with shake-table test results of the CMU building specimen in Table 10-9. No comparison is made at Tarzana 150 %, because the comparison is not meaningful if the overall response of the entire building is not well predicted.

For tri-wire connectors, OpenSees analysis well predicts collapse of the out-of-plane veneer up to Tarzana 100 %. For double eye-and-pintle connectors, OpenSees analysis predicts collapse of the out-of-plane veneer at lower levels of ground motion than in the test results. This seems to be due to underestimation or inherent scatter of deformation capacity of double eye-and-pintle connectors. Note that the deformation capacity of double eye-and-pintel connectors was suggested in Section 9.1.2, assuming slip between double eyes and double pintles. In Table 10-9, the maximum tensile deformation of double eye-and-pintle connectors is about 0.12 in. at Tarzana 100 %, while the failure criterion used is 0.1 in.

Table 10-8 Deformation capacity of connectors (2-in. long) for connector failure criteria

deformation capacity of connectors (2-in. long) for connector failure criteria			
double eye-and-pintle connectors		**tri-wire connectors**	
tension	**compression**	**tension**	**compression**
0.1 in.	none	0.09 in.	1 in.

Table 10-9 Collapse of out-of-plane veneer

ground motion	collapse of out-of-plane veneer			
	double eye-and-pintle connectors		tri-wire connectors	
	OpenSees analysis *	test results	OpenSees analysis *	test results
Sylmar 200 %	none	none	none	none
Tarzana 100 %	collapse	none	none	none

** based on suggested connector failure criteria (Section 9.1.2 and 9.1.5)*

10.6 RESULTS OF PARAMETER STUDY

In this section, the established OpenSees model for the CMU building specimen (Section 10.2) is used for parameter study. The primary purpose of this parameter study is to supply general information about the seismic response of this low-rise concrete masonry building with clay masonry veneer, by investigating the effect of different model parameters. In contrast to the calibrations described previously, there was no need to compare the analytical results of the parameter studies with shake-table results. Also, the input ground motions are readily available, while the recorded table motions from the tests are less readily available. For these reasons, the input ground motions used in the OpenSees parameter study are the scaled Sylmar and Tarzana input records (described in Section 6.2).

Model parameters and their effects to be examined through parameter study are as follows:

- effect of ground motion scaling (scaled PGA) on overall response (for the Sylmar and Tarzana records);
- effect of presence of veneer (in-plane and out-of-plane) on overall response;

- effect of continuous corner (veneer) and coefficient of friction (μ) on veneer response, in-plane;
- effect of lintel on veneer response, in-plane; and
- effect of connectors (strength, stiffness and type) on veneer response, in-plane and out-of-plane.

10.6.1 Effect of Ground Motion Scaling on Overall Response

To examine the effect of ground motion scaling (for the Sylmar and Tarzana records) on the overall response of the entire building, peak displacements at roof diaphragm and response amplification for acceleration are examined.

Peak displacement at roof diaphragm versus peak ground acceleration (PGA) is plotted in Figure 10-17, for the Sylmar and Tarzana ground motions. As shown by this figure, when overall response (displacement) of the entire building is in the elastic range, the overall response is proportional to PGA. We can also find that the overall response (displacement) is not sensitive to the type of ground motion in the elastic range (Tarzana record is atypically rich in high-frequency content), and becomes sensitive in inelastic range.

Response amplification for acceleration versus PGA is plotted in Figure 10-18, for Sylmar and Tarzana ground motions. We can find in Figure 10-18 that the response amplification for acceleration becomes constant or even decreases as PGA increases, as overall response of the building goes into the inelastic range. This confirms that the force transferred from ground to the building is limited by the strength of the building.

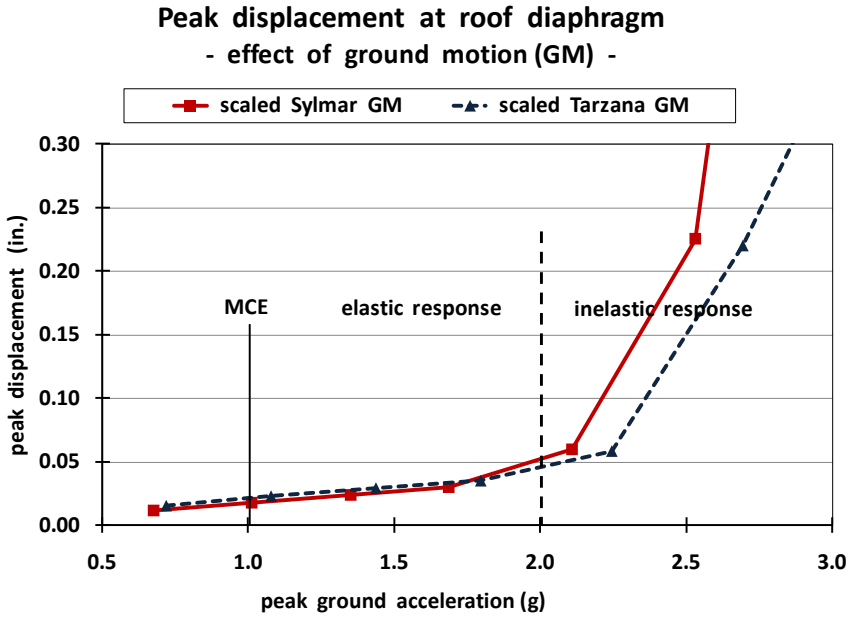

Figure 10-17 Peak displacement at roof diaphragm versus peak ground acceleration

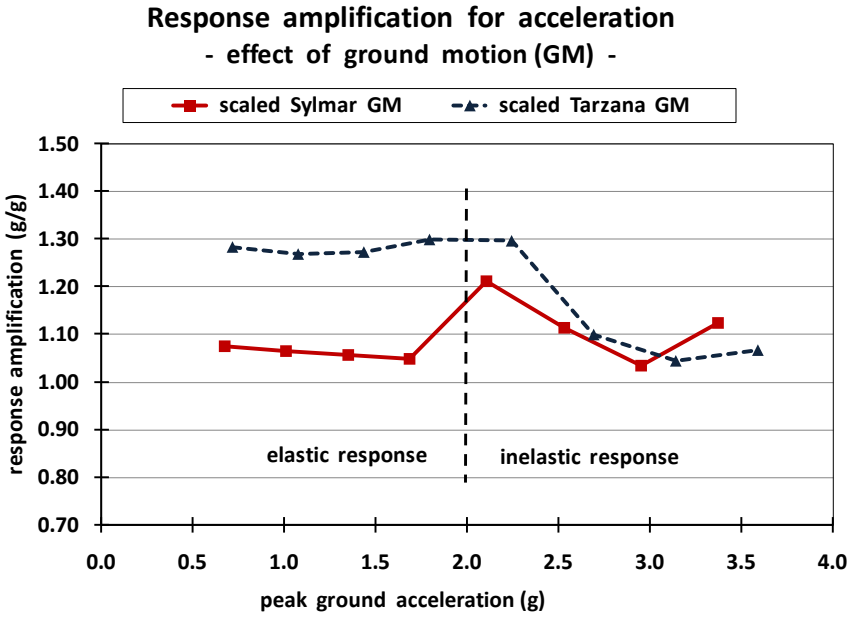

Figure 10-18 Response amplification for acceleration versus peak ground acceleration

10.6.2 Effect of Presence of Veneer on Overall Response

To examine the effect of presence of clay masonry veneer (in-plane and out-of-plane) on the overall response of the entire building, peak displacements at roof diaphragm are examined, using the scaled Sylmar record.

Peak displacement at roof diaphragm versus peak ground acceleration (PGA) is plotted in Figure 10-19, with and without clay masonry veneer. The effect of the presence of veneer on overall response is negligible in the elastic range, but large in the inelastic range. When the effect of the veneer's presence is large, in-plane veneer has more effect than out-of-plane veneer in Figure 10-19 at about 3.0 g of PGA. This is true even though the in-plane veneer and out-of-plane veneer have identical masses (the building is square, with equal-sized openings on all four sides). The in-plane veneer has a greater effect because the mass of the entire in-plane veneer is resisted by the in-plane CMU walls (governing overall response). In contrast, only the mass of about the upper half of the out-of-plane veneer is resisted by in-plane CMU walls, with the force developed by the lower half of the out-of-plane veneer being transferred to the foundation through the out-of-plane CMU walls. At higher levels of shaking, however, this difference in effective mass can be less important, because yielding of in-plane connectors or corner cracking of veneer can limit the inertial forces that can be transferred from the in-plane veneer to the in-plane shear walls.

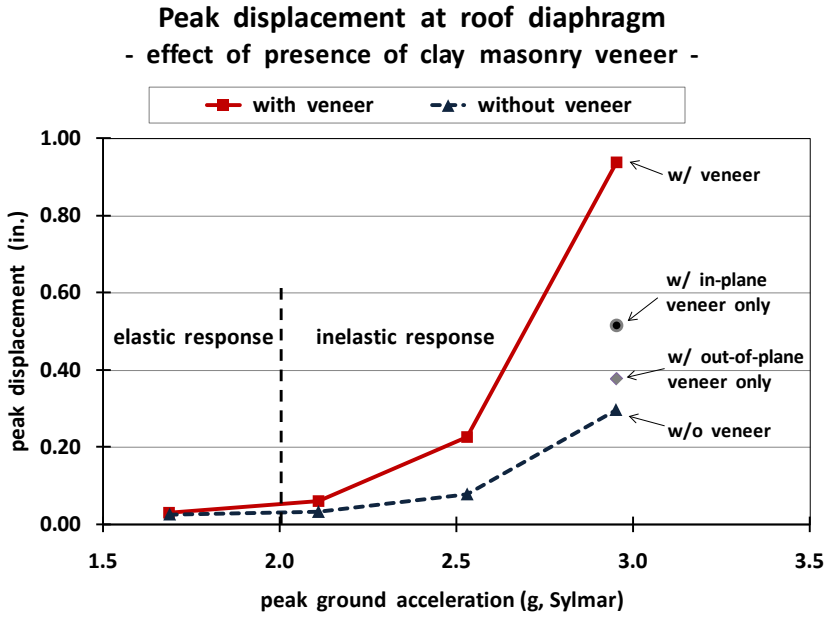

Figure 10-19 Peak displacement at roof diaphragm, with veneer and without veneer

10.6.3 Effect of Continuous Corner and Coefficient of Friction on Veneer Response, In-plane

The effect of continuous corner (veneer) and coefficient of friction (μ) on veneer response, in-plane, is examined using the criterion of peak sliding of the 12-ft long veneer segment. In the OpenSees model (Section 10.2), sliding only is permitted in 12-ft long veneer (no rocking). The scaled Sylmar record is used for input ground motion.

First, sliding of 12-ft long veneer is examined, with and without a continuous corner. The analytical results are plotted in Figure 10-20, where the veneer with discontinuous corner practically begins to slide at about 0.7 g of PGA while the veneer with continuous corner begins to slide at about 1.7 g of PGA. This implies that continuous corner of veneer can help substantially in preventing movement of in-plane veneer.

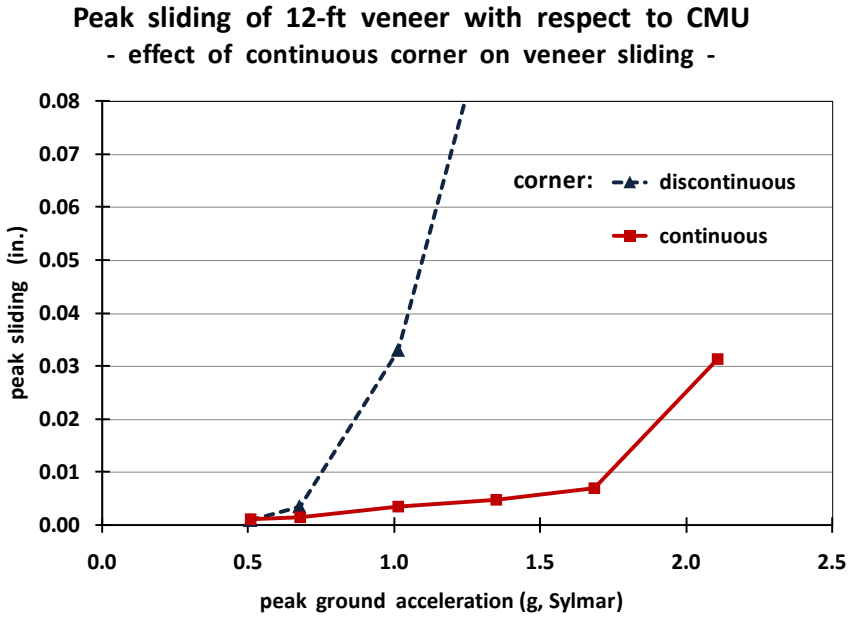

Figure 10-20 Peak sliding of veneer with respect to CMU wall, effect of continuous corner of veneer

Second, sliding of 12-ft long veneer is examined by varying the assumed coefficient of friction μ between the veneer and the flashing-covered shelf angle, using values of 0.4, 0.6 and 0.9. In OpenSees modeling for the CMU building specimen, 0.6 was used based on calibration of the OpenSees model for the CMU wall specimens. The analytical results for each μ are plotted in Figure 10-21, where sliding of veneer with higher μ starts at higher PGA. The PGA at onset of sliding is, however, not linearly proportional to μ, due to the in-plane resistance from the continuous corner of veneer.

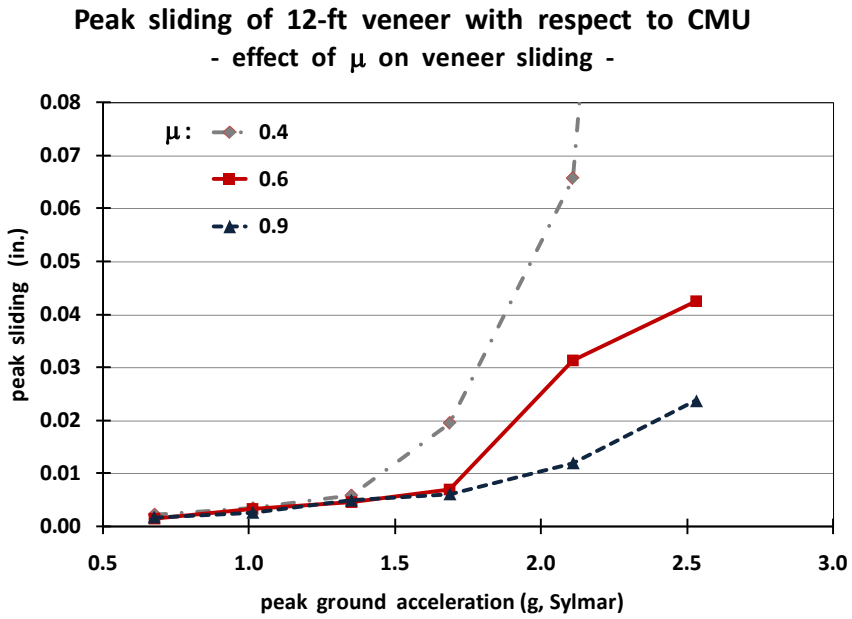

Figure 10-21 Peak sliding of veneer with respect to CMU wall, effect of μ

10.6.4 Effect of Lintel on Veneer Response, In-plane

The effect of lintel on veneer response, in-plane, is examined using peak movement of the 4-ft long veneer segment near the top, with respect to CMU walls. In OpenSees analysis, both rocking and sliding are permitted in the 4-ft long veneer segment, and the lintel is located between the 4-ft long and the 12-ft long veneer segments. The scaled Sylmar record is used for input ground motion.

The analytical results with and without the lintel are plotted in Figure 10-22 as a function of PGA. As shown in this figure, the more the 4-ft long veneer moves, the more the lintel helps in restraining veneer movement. It should be noted, however, that the 12-ft long veneer (at the other end of the lintel) had less movement near top than the 4-ft long veneer, when the lintel was not included in OpenSees modeling. Therefore, we can confirm our expectation that the lintel helps redistribute in-plane force between the veneer segments it connects.

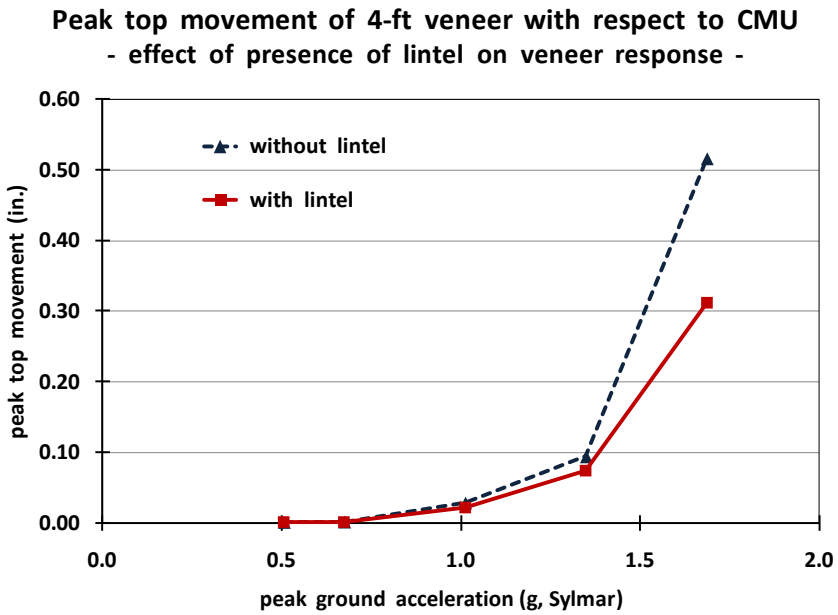

Figure 10-22 Peak movement of 4-ft veneer near top (with respect to CMU), with and without lintel

10.6.5 Effect of Connectors on Veneer Response, In-plane

To examine the effect of connectors (strength, stiffness and type) on in-plane response of clay masonry veneer, peak sliding of 12-ft long veneer with respect to the CMU is examined. In the OpenSees model (Section 10.2), sliding only is permitted in 12-ft long veneer (no rocking). The scaled Sylmar record is used for input ground motion.

First, tri-wire connectors are used for reference in OpenSees analysis, and their in-plane stiffness and strength are varied (multiplied by 0.5 and 1.5). The analytical results are plotted in Figure 10-23, where peak sliding of the veneer (with respect to CMU walls) is shown for various PGA. In this figure, onset of veneer sliding is essentially not affected by connector strength or stiffness, because the onset of sliding is dominated by coefficient of friction and the effect of continuous corner. After sliding starts, the amount of sliding is affected by connector strength and stiffness. From the figure, it is obvious that sliding increases faster as a result of decreases in connector strength than of

decreases in connector stiffness (compare 0.5 x reference strength and 0.5 x reference stiffness in Figure 10-23). The effect is not clear when strength or stiffness is increased. Therefore, we can conclude that after sliding starts, the amount of sliding is more affected by differences in connector strength than by differences in connector stiffness.

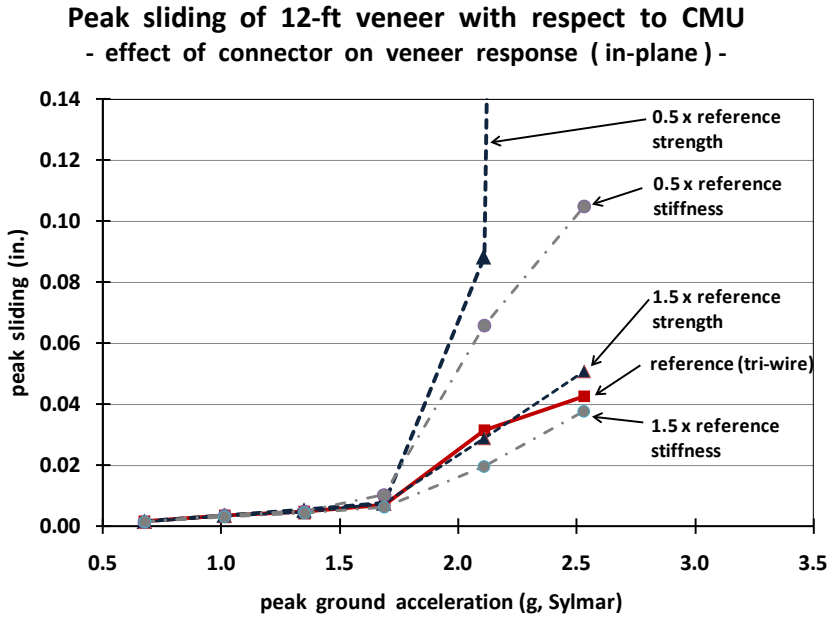

Figure 10-23 Peak sliding of veneer with respect to CMU wall, effect of connectors' strength and stiffness

Second, double eye-and-pintle connectors were used in OpenSees analysis, and the results were compared with those of tri-wire connectors. The analytical results are compared in Figure 10-24, where peak sliding of veneer (with respect to CMU walls) is shown for various PGA. In this figure, the same scale for the vertical axis was used as in Figure 10-23. The in-plane strength and stiffness of double eye-and-pintle connectors is about 2 times and about 1.3 times those of tri-wire connectors, respectively, resulting in more restraint on veneer sliding by double eye-and-pintle connectors. This is consistent with shake-table test results in Table 7-16 and Table 7-17 (compare sliding of 12-ft veneer at Sylmar 200 % and Tarzana 100%).

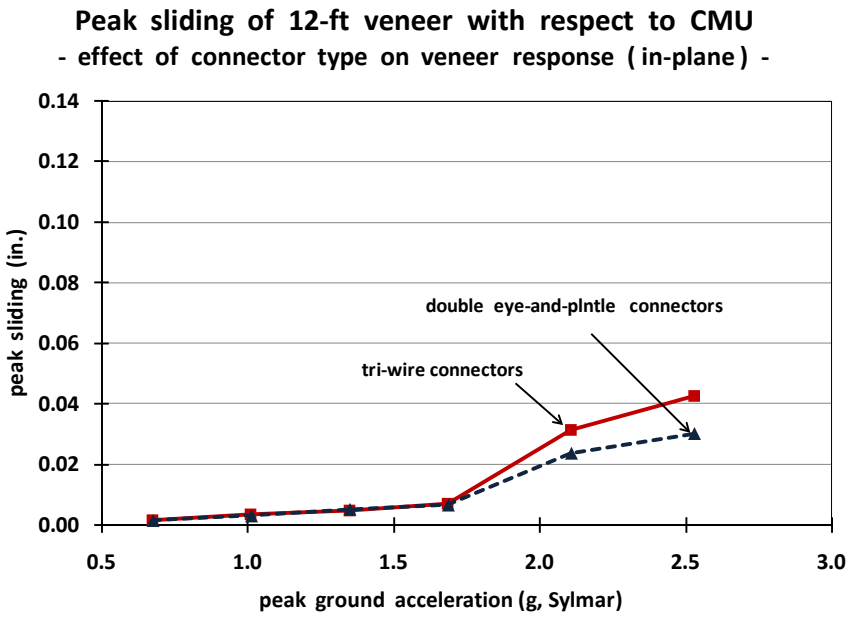

Figure 10-24 Peak sliding of veneer with respect to CMU wall, effect of type of connectors

10.6.6 Effect of Connectors on Veneer Response, Out-of-plane

To examine the effect of connectors (strength, stiffness and type) on out-of-plane response of clay masonry veneer, peak movement of out-of-plane veneer near top (with respect to CMU walls) is examined. Relative movement of out-of-plane veneer near top is generally effective in determining failure of connectors, which in turn determines collapse of clay masonry veneer. In the OpenSees analyses, the scaled Sylmar record is used for input ground motion.

First, tri-wire connectors are used for reference in OpenSees analysis, and their out-of-plane (axial) stiffness and strength are varied (multiplied by 0.5 and 1.5). The analytical results are plotted in Figure 10-25, where peak out-of-plane movement of veneer near top (with respect to CMU walls) is shown for various PGA. In this figure, it is obvious that veneer movement is much affected by differences in connector strength, but almost unaffected by differences in connector stiffness.

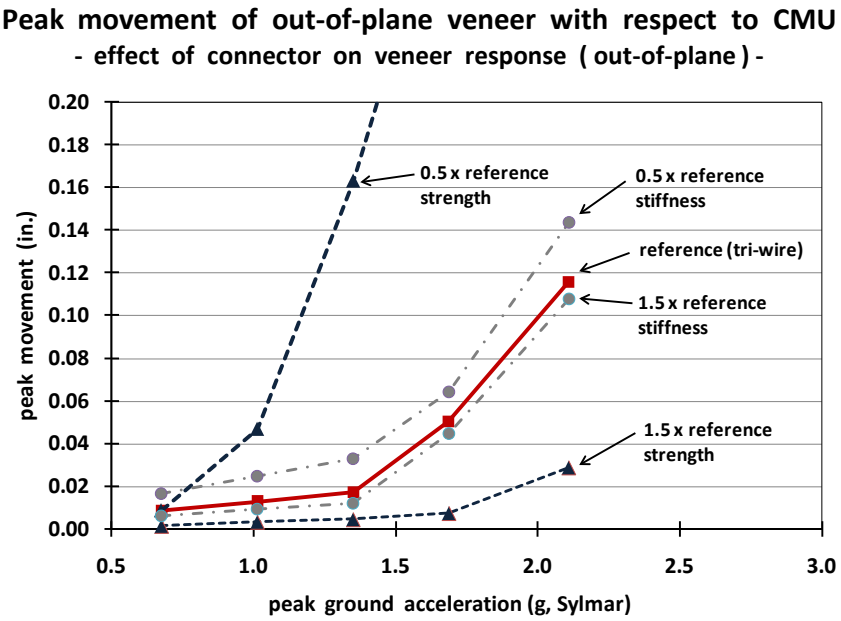

Figure 10-25 Peak movement of out-of-plane veneer near top (with respect to CMU walls), effect of connectors' strength and stiffness

Second, double eye-and-pintle connectors are used in OpenSees analysis, and the results are compared with those with tri-wire connectors. The analytical results are compared in Figure 10-26, where peak out-of-plane movement of veneer (with respect to CMU walls) is shown for various PGA. In this figure, the same scale for the vertical axis was used as in Figure 10-25. In OpenSees analysis in this research, differences in structural characteristics of double eye-and-pintle connectors vis-à-vis tri-wire connectors are complex, as illustrated in Figure 9-5 and Figure 9-8. Using information from Figure 10-25, however, the graphs shown in Figure 10-26 indicate that the most important structural difference of double eye-and-pintle connectors vis-à-vis tri-wire connectors is lower average stiffness (up to their maximum strengths).

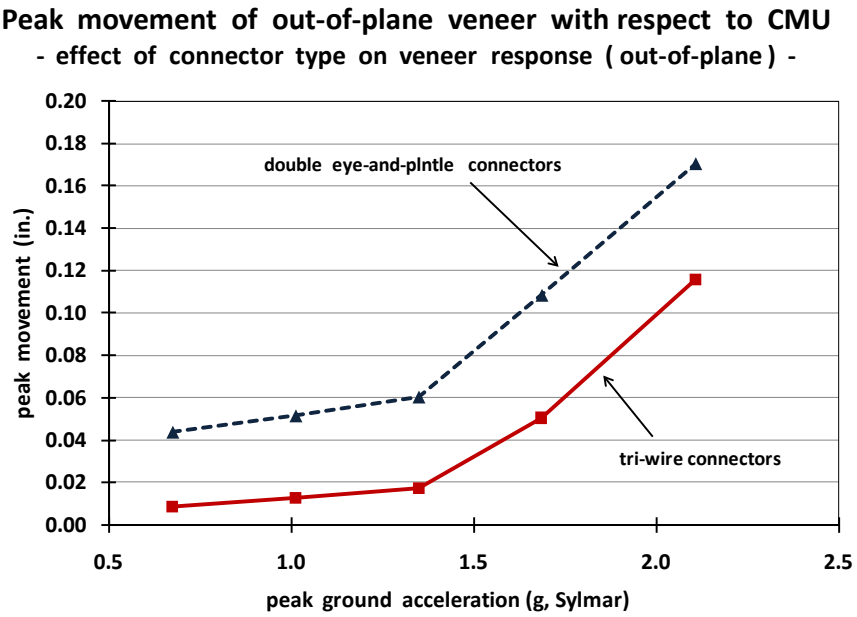

Figure 10-26 Peak movement of out-of-plane veneer near top (with respect to CMU walls), effect of type of connectors

10.7 SUMMARY OF RESULTS OF PARAMETER STUDY

Key results of parameter study in Section 10.6 are summarized below.

- In the elastic range, overall response (displacement) is proportional to peak ground acceleration (PGA) (Figure 10-17).
- In the inelastic range, overall response (displacement) is no longer proportional to peak ground acceleration (PGA), but rather increases rapidly with PGA (Figure 10-17).
- As the overall response of the building goes into the inelastic range, the response amplification for acceleration becomes constant or even decreases as PGA increases, indicating that the force transferred from ground to the building is limited by the strength of the building (Figure 10-18).

- The veneer has a negligible effect on overall response (displacement) in the elastic range, but a significant effect in the inelastic range (Figure 10-19).
- Continuity at veneer corners can substantially reduce the sliding of the in-plane veneer (Figure 10-20).
- The PGA required to initiate veneer sliding is not linearly proportional to μ, due to in-plane resistance by continuous corner of veneer (Figure 10-21).
- The force transfer through the veneer lintel helps in preventing or decreasing the movement (due to rocking and sliding) of the relatively flexible veneer segment at one end (Figure 10-22).
- After veneer sliding (in-plane) starts, the amount of sliding is more affected by difference in connectors' strength than in their stiffness (Figure 10-23).
- In reducing veneer sliding (in-plane), double eye-and-pintle connectors perform better than tri-wire connectors, due to their higher strength and stiffness (Figure 10-24).
- Out-of-plane movement of veneer is greatly affected by differences in connectors' axial strength, but little by differences in their axial stiffness (Figure 10-25).
- The primary structural difference between double eye-and-pintle connectors and tri-wire connectors is the lower average axial stiffness of the former, up to their maximum strengths (Figure 10-25 and Figure 10-26).

CHAPTER 11
Summary, Conclusions and Recommendations

11.1 SUMMARY

As a part of NSF NEES Project "Performance Based Design of New Masonry Structures," the seismic behavior and design of concrete masonry with clay masonry veneer were studied. Six concrete masonry wall specimens (CMU wall specimens) were designed, constructed and quasi-statically tested at The University of Texas at Austin (UT Austin); three were tested in-plane, and three out-of-plane. Six analogous specimens were constructed at the University of California at San Diego (UCSD) and tested on the NEES outdoor shake table there, three in-plane and three out-of-plane. A full-scale, one-story masonry building specimen (CMU building specimen) was also designed by UT Austin and tested by UCSD on the NEES outdoor shake table.

The seismic response of low-rise masonry structures is governed by the in-plane response of the masonry shear walls, which control the horizontal displacement of the roof diaphragm. The out-of-plane walls are excited at the base by the ground motion, and at the top by the roof diaphragm. In the research reported here, the flexural and base sliding behaviors of the in-plane CMU walls were studied using quasi-static testing of in-plane CMU wall specimens. The rocking and base sliding behaviors of the in-plane veneer, and the in-plane behavior of the veneer connectors, were examined using shake-table testing of in-plane CMU wall specimens. The behavior of CMU walls, veneer and veneer connectors loaded out-of-plane was studied using quasi-static testing and shake-table testing of out-of-plane CMU wall specimens. Finally, the global and local performance of low-rise concrete masonry buildings with clay masonry veneer was studied using shake-table testing of a full-scale, one-story CMU building specimen, synthesized with the results of quasi-static and shake-table test results of CMU wall specimens.

The CMU building specimen, designed and constructed according to the requirements of the 2008 MSJC Code and Specification for Seismic Design Category (SDC) D/E, resisted repeated earthquakes above the maximum considered earthquake (MCE) without collapse. In this specimen and in the quasi-static CMU wall specimens, the in-plane CMU walls responded essentially as rigid bodies, rotating and sliding at their bases. Their behavior was governed by flexural hinging, base sliding, or combinations thereof.

The in-plane veneer had a negligible effect on the global response of the CMU building specimen. In the CMU building specimen and the shake-table CMU wall specimens, the in-plane veneer and its connectors performed well under repeated earthquakes above MCE without falling off the in-plane CMU. The in-plane veneer rocked or slid (sometimes both), accompanied by yielding of the in-plane connectors. The in-plane veneer with a low aspect ratio (height to plan length), 12 ft long and 8 ft high, slid only, and the in-plane veneer with an intermediate aspect ratio, 4 ft long and 8 ft high, slid and rocked. In-plane veneer with a high aspect ratio is likely to rock only. The sliding resistance of the veneer depended on the coefficient of friction between the veneer and the shelf angle on which the veneer was laid on, and on the in-plane resistance of the connectors. The rocking resistance of the veneer was affected by the in-plane resistance of the veneer connectors.

The response of the out-of-plane CMU walls with clay masonry veneer is governed by the ground motion and by the response of the roof diaphragm. For a range of lateral stiffnesses of the roof diaphragm (or of the setup element simulating the roof diaphragm), all out-of-plane CMU walls with clay masonry veneer in the CMU building specimen and the shake-table CMU wall specimens performed well under repeated earthquakes above MCE. As the level of shaking increased, the out-of-plane CMU walls developed flexural hinges at the base and then around mid-height. When the roof diaphragm was laterally flexible enough, flexural hinges formed at the base only. In out-of-plane veneer, flexural resistance becomes zero once flexural cracking occurs in bed joints. Since the flexural stiffness of the veneer before cracking is small compared to the

flexural stiffness of the out-of-plane CMU walls, the out-of-plane veneer essentially acts as attached mass only, provided that the out-of-plane connectors continue to securely connect the CMU wall and the veneer. In all shake-table testing conducted in this research, the out-of-plane connectors securely connected the CMU wall and the veneer up to well above MCE.

Detailing of the CMU walls and the veneer in the CMU building specimen helped prevent local damage around the lintels and around the corners until above MCE. The vertically oriented control joints in the CMU walls at the ends of the lintels delayed the onset of damage to the CMU walls at the lintel ends. Vertically oriented expansion joints in the veneer at the ends of the lintels permitted the underlying masonry to rock without damage to the veneer above the lintels. Vertical expansion joints in the veneer at the corners prevented damage there. Without vertical expansion joints at the corners, the differential movement of the out-of-plane veneer and the in-plane veneer can cause local damage around the corners.

Using the OpenSees analytical framework, nonlinear analytical models were developed for each of the specimens discussed above, and were calibrated using test results from those specimens. The models capture the essential behavior of the in-plane and out-of-plane wall segments, and also the essential behavior of the CMU building specimen. They are suitable for further research studies of the detailed response of concrete masonry with clay masonry veneer. The developed OpenSees model for the CMU building specimen was also used for parameter studies, whose primary purpose was to supply general information about the seismic response of low-rise concrete masonry buildings with clay masonry veneer.

Based on the observed experimental results and comparison with analytical models, many current design and construction requirements (MSJC 2008a,b) are reaffirmed, and others are singled out for possible refinement.

11.2 CONCLUSIONS

1) The shake-table tests of the CMU building specimen have demonstrated that low-rise reinforced concrete masonry buildings with clay masonry veneer, designed and constructed according to the requirements of the 2008 MSJC Code and Specification for SDC E, can resist earthquakes above MCE without collapse. The observed performance of the CMU building specimen may not apply to all such buildings. In the CMU building specimen, the vertical and horizontal reinforcement in the CMU wall segments were governed by minimum prescriptive requirements, so that the ratio of flexural capacity to flexural demand was relatively high. Also, the CMU building specimen was configured very favorably in plan. Those circumstances would not apply to all low-rise reinforced concrete masonry buildings.

2) The seismic response of these buildings is generally consistent with performance expectations.

   a) Response of the buildings is controlled by the response of the in-plane CMU (flexural hinging or sliding at the base, singly or together, above MCE).

   b) Clay masonry veneer and connectors well performed (until well past MCE). The out-of-plane veneer experienced only minor cracking and stayed fully connected to the CMU walls without critical damage in the connectors. The in-plane veneer experienced some rocking and sliding but showed only minor cracking without critical damage in the connectors.

   c) Vertical control joints in the CMU at the ends of the lintels delayed the onset of damage to the CMU walls at the lintel ends (until well past MCE).

Vertical expansion joints in the veneer at the ends of the lintels permitted the underlying masonry to rock without damage to the veneer above the lintels. Vertical expansion joints in the veneer at the corners prevented damage there from movement of the in-plane walls.

3) The key seismic behaviors of the low-rise concrete masonry building with masonry veneer are predicted by nonlinear dynamic analysis well enough to provide guidelines to the designer: flexural hinging or sliding at the base of the in-plane CMU walls, rocking and sliding of the in-plane veneer along with the connectors, and flexural hinging at the base and at around the mid-height of the out-of-plane CMU walls, and tensile yielding and compressive buckling of the out-of-plane connectors.

4) During calibration of the nonlinear "macro-model" for the CMU building specimen and through parametric studies using the model, several observations were made. These apply strictly only to this model, but they are considered worth of further study.

   a) The coefficient of friction between CMU walls and the concrete foundation is about 0.8. The effective flange width of the in-plane CMU walls does not reduce base sliding much, because the flange is flexible out-of-plane.

   b) The veneer has a negligible effect on overall response (displacement) in the elastic range, but a significant effect in the inelastic range.

   c) Continuity at veneer corners can substantially reduce the sliding of the in-plane veneer.

d) In-plane sliding of veneer is more affected by differences in connector strength than by differences in connector stiffness. Both types of connectors tested here (double eye-and-pintle and tri-wire) satisfactorily controlled in-plane veneer sliding. Out-of-plane movement of veneer is much more affected by differences in connectors' axial strength, than by differences in their axial stiffness.

e) The loose veneer lintel transfers force between the in-plane veneer segments, through friction between the lintel and the clay masonry veneer, and through axial compression in the lintel. Because of this force transfer, veneer segments that are stiff in plane can restrain the in-plane response (rocking and sliding) of more flexible veneer segments.

11.3 RECOMMENDATIONS FOR DESIGN

1) The MSJC Code should include requirements to prevent base sliding of shear walls under the design basis earthquake (DBE), and to limit base sliding under the maximum considered earthquake (MCE). The 2008 MSJC Code and Specification does not directly address base sliding of shear walls. In the quasi-static, in-plane testing of the CMU wall specimens, base sliding of the CMU walls began to be significant after about 0.25 in. of flexural crack width at the base, even though the specimens had higher design shear strength at the base than required by the 2008 MSJC Code and Specification. That crack width corresponds to a story drift of about 0.5 % when the aspect ratio (height to plan length) is 2.0. To prevent base sliding of shear walls, short dowels or shear keys could be used at the base. Some limit on base sliding at MCE is probably useful to prevent fracture of the vertical reinforcement. Because the sliding, at which vertical bars would fracture, depends on the detailing of the bars at the interface, no single sliding limit is appropriate. Also, sliding is expected to be significant

only to low-rise structures. Higher-rise structures are expected to show more rocking behavior by flexural yielding.

2) The MSJC Code should address the in-plane response of anchored veneer, and not consider it as added mass only. This is essentially correct for out-of-plane response, but incorrect for in-plane response. For in-plane response, the veneer rocks, slides and helps dissipating energy by sliding.

3) 2008 MSJC Code and Specification requirements for joint reinforcement in anchored veneer in Seismic Design Category (SDC) E and F could be eliminated. In the shake-table testing of the CMU building specimen, the presence or absence of joint reinforcement caused no observable differences in response.

11.4 RECOMMENDATIONS FOR FUTURE RESEARCH

1) Additional research is recommended to study the bi-directional response of low-rise concrete masonry structures with clay masonry veneer. In this research, the concrete masonry walls with veneer were excited either out-of-plane or in-plane. In reality, such walls are likely to be excited simultaneously out-of-plane and in-plane.

2) Further research could be conducted to extend the results of this research to multi-story concrete masonry structures with clay masonry veneer. This research is directly related to one-story buildings only, and should be extended to multi-story buildings.

APPENDIX A

Design Drawings of CMU Wall Specimens

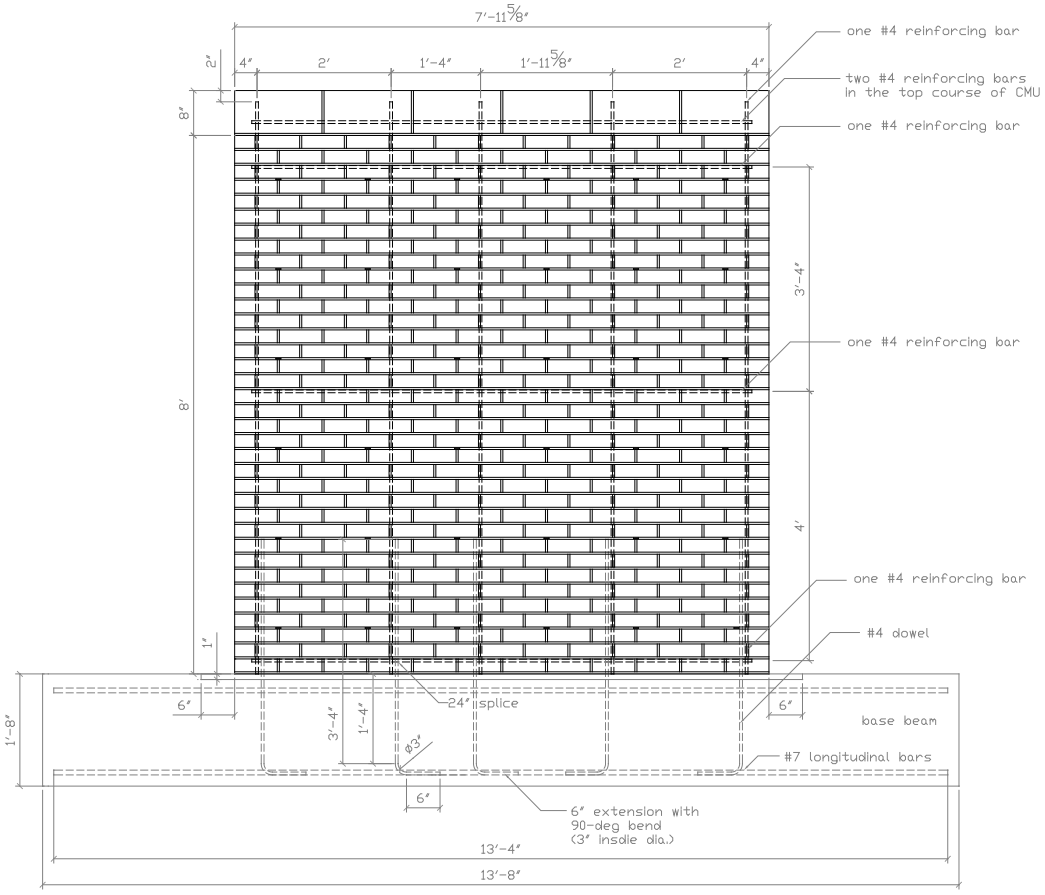

Figure A-1 Front view of specimen UT CMU 1 and UCSD CMU 1

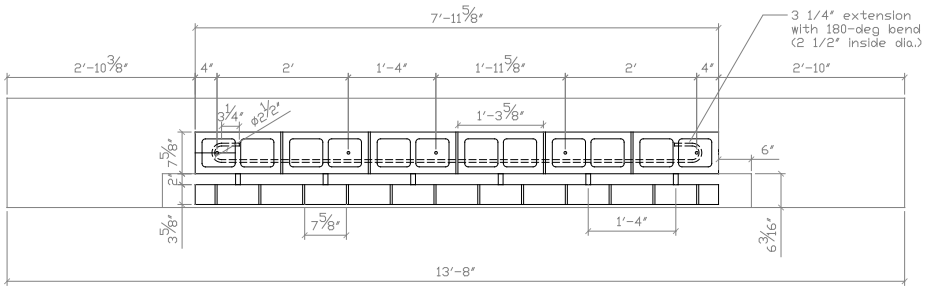

Figure A-2 Top view of specimen UT CMU 1 and UCSD CMU1

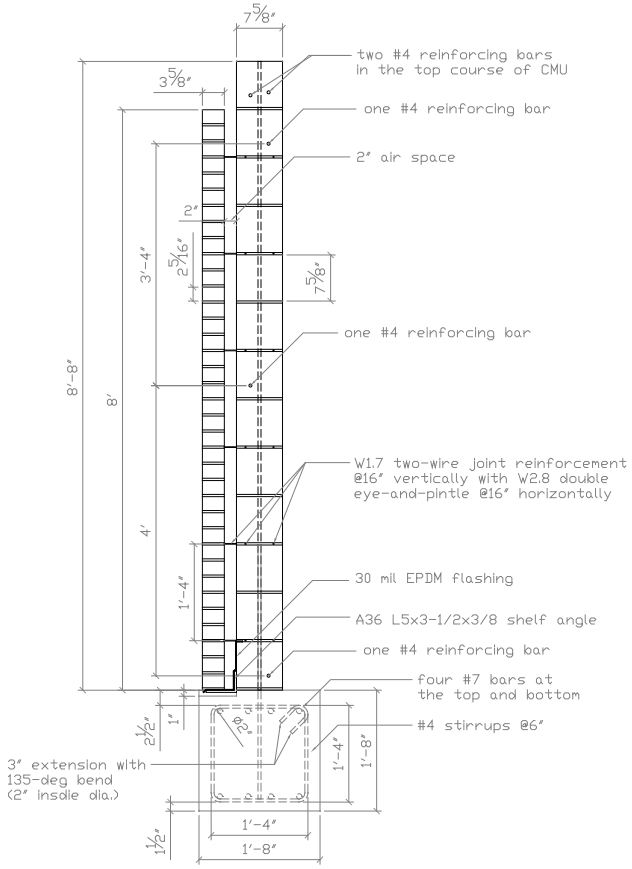

Figure A-3 Side view of specimen UT CMU 1 and UCSD CMU1

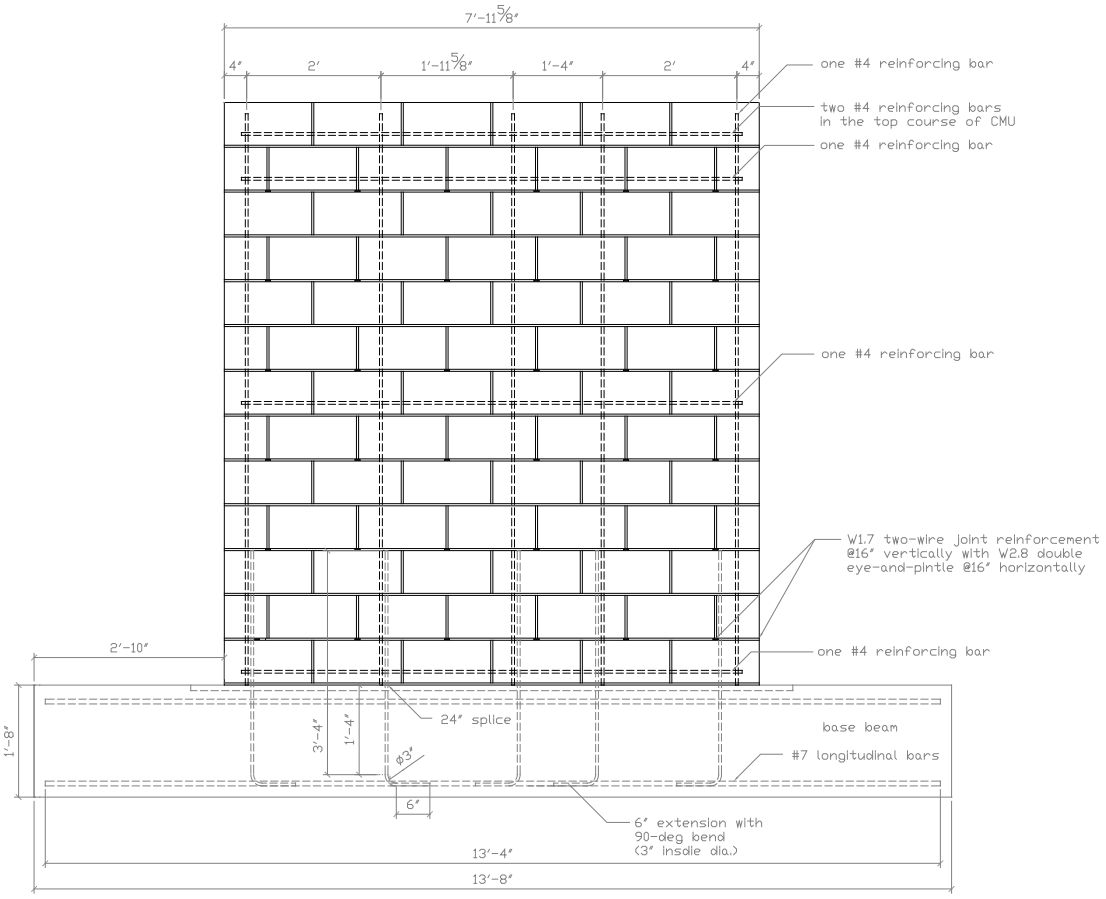

Figure A-4 Rear view of specimen UT CMU 1 and UCSD CMU1

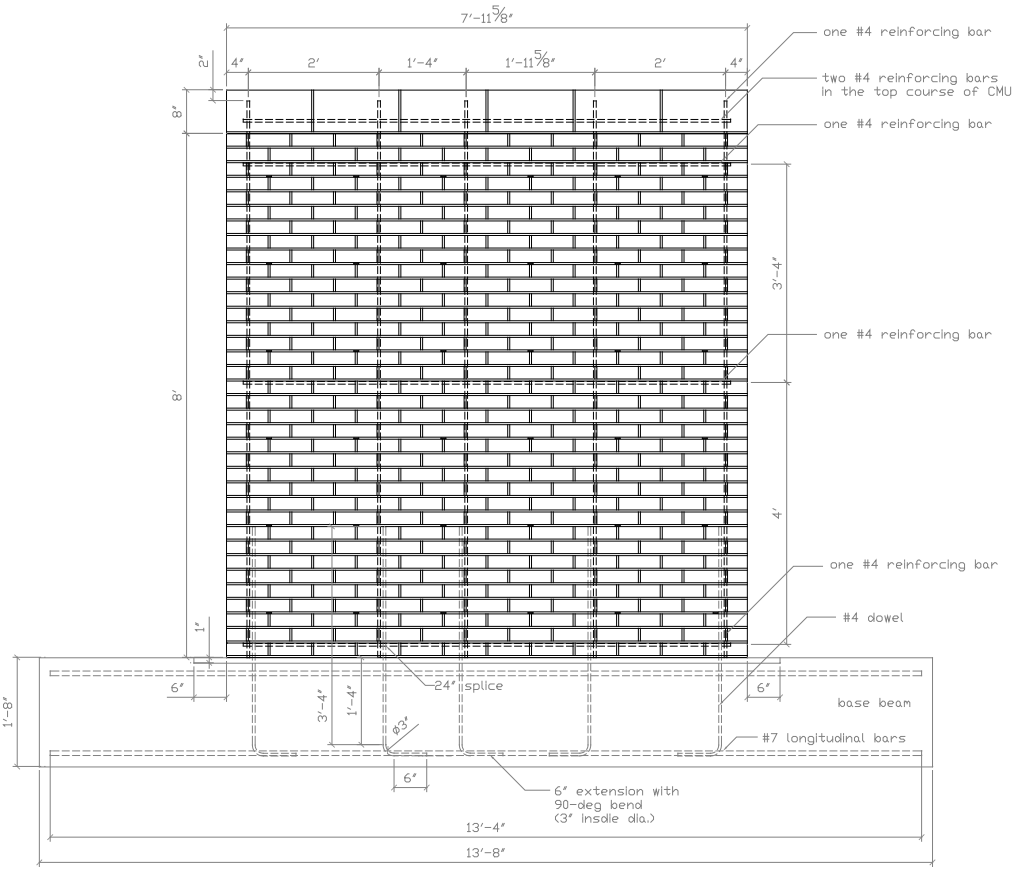

Figure A-5 Front view of specimens UT CMU 2, UT CMU 2 MC, UCSD CMU 2 and UCSD CMU 2 MC

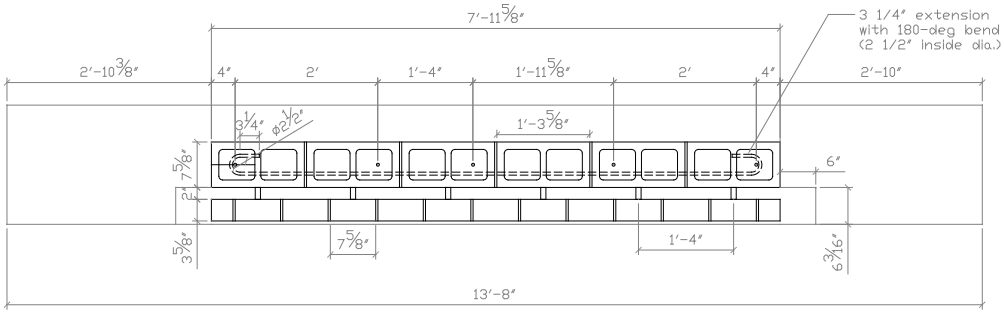

Figure A-6 Top view of specimens UT CMU 2, UT CMU 2 MC, UCSD CMU 2 and UCSD CMU 2 MC

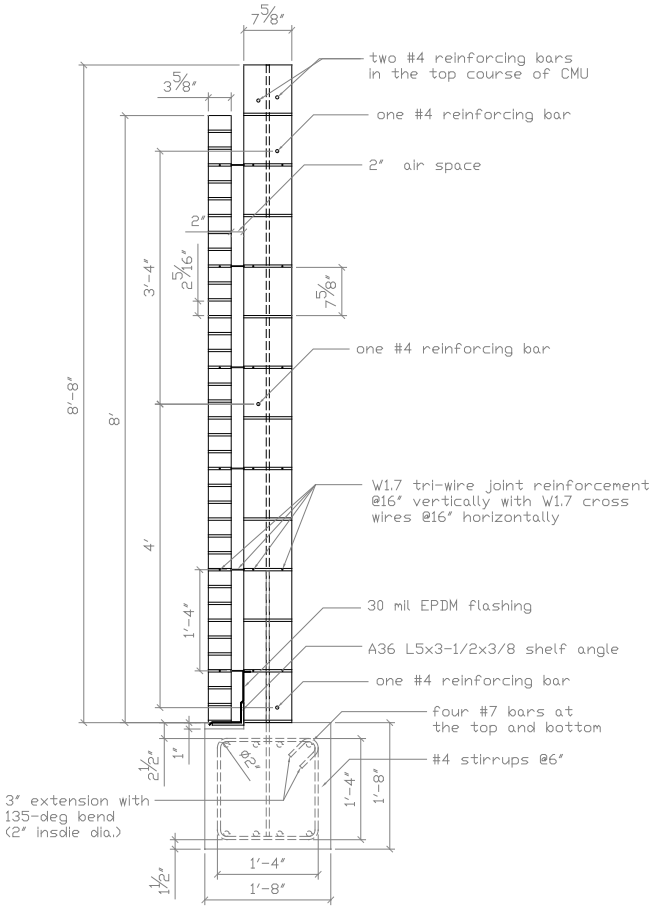

Figure A-7 Side view of specimens UT CMU 2, UT CMU 2 MC, UCSD CMU 2 and UCSD CMU 2 MC

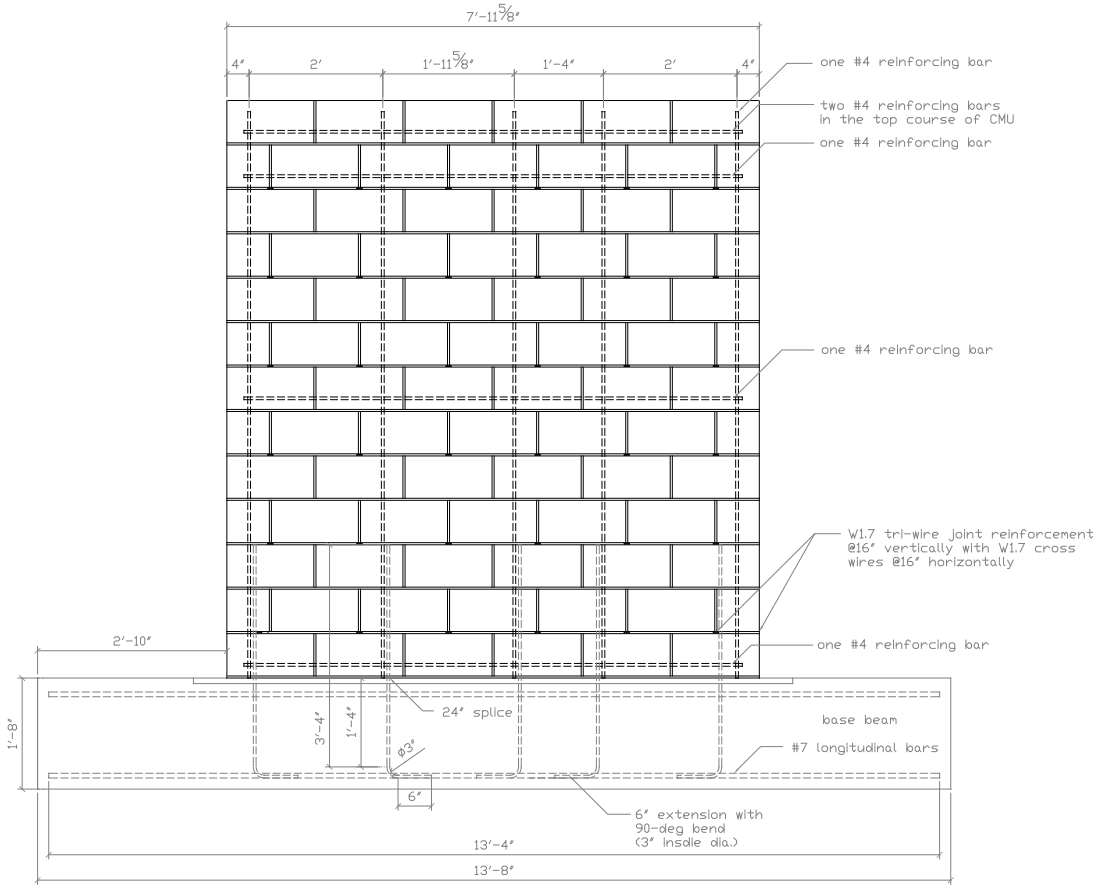

Figure A-8 Rear view of specimens UT CMU 2, UT CMU 2 MC, UCSD CMU 2 and UCSD CMU 2 MC

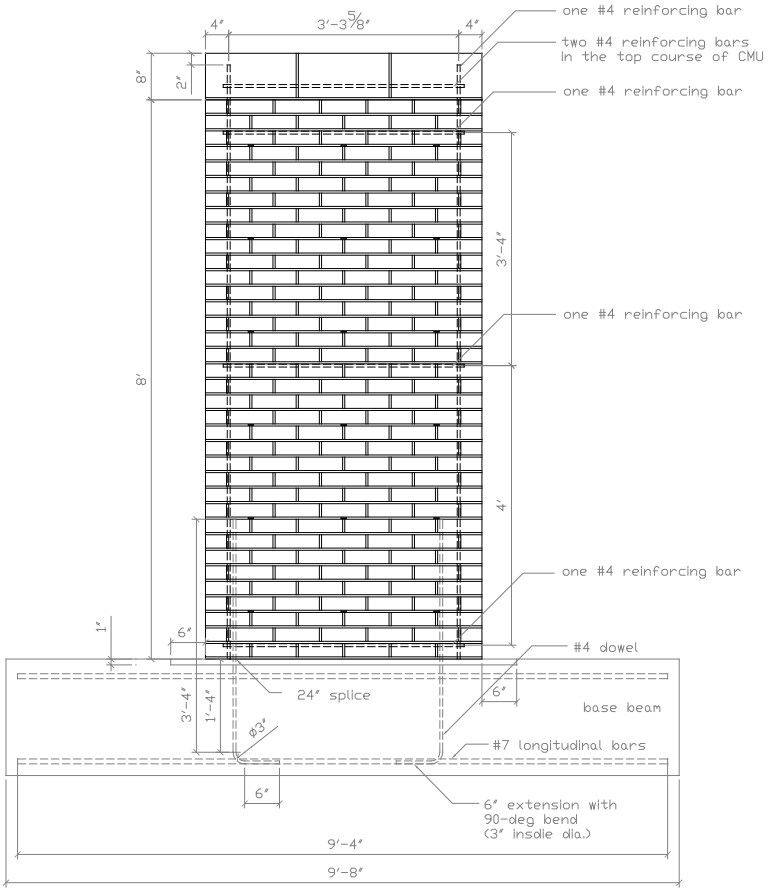

Figure A-9 Front view of specimen UT CMU 3 and UCSD CMU 3

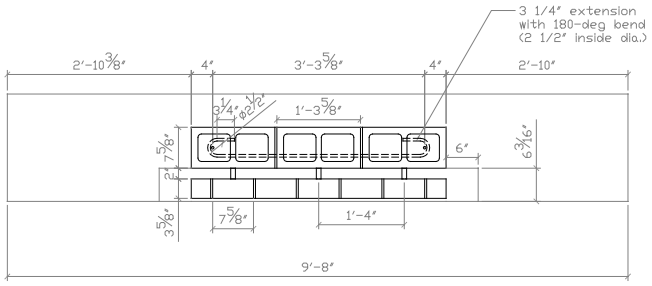

Figure A-10 Top view of specimen UT CMU 3 and UCSD CMU 3

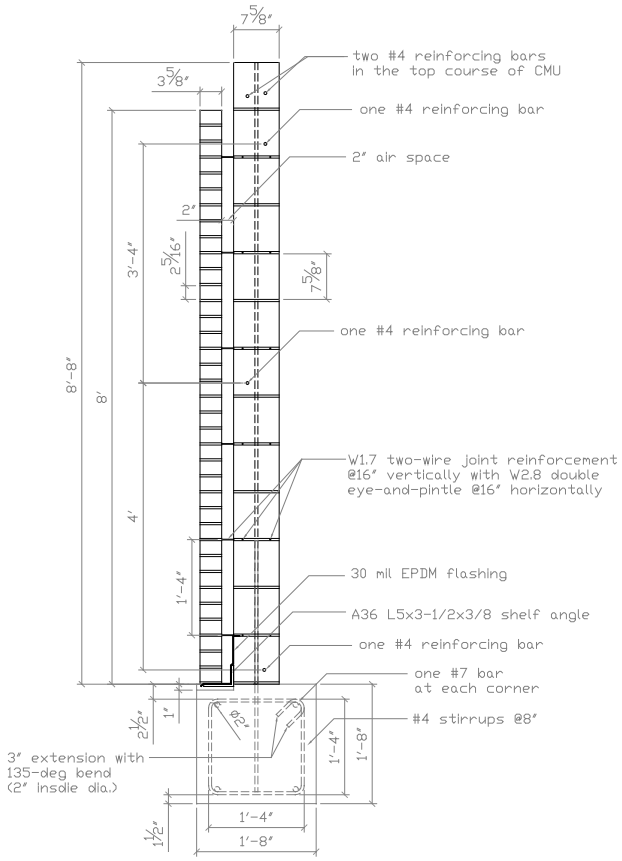

Figure A-11 Side view of specimen UT CMU 3 and UCSD CMU 3

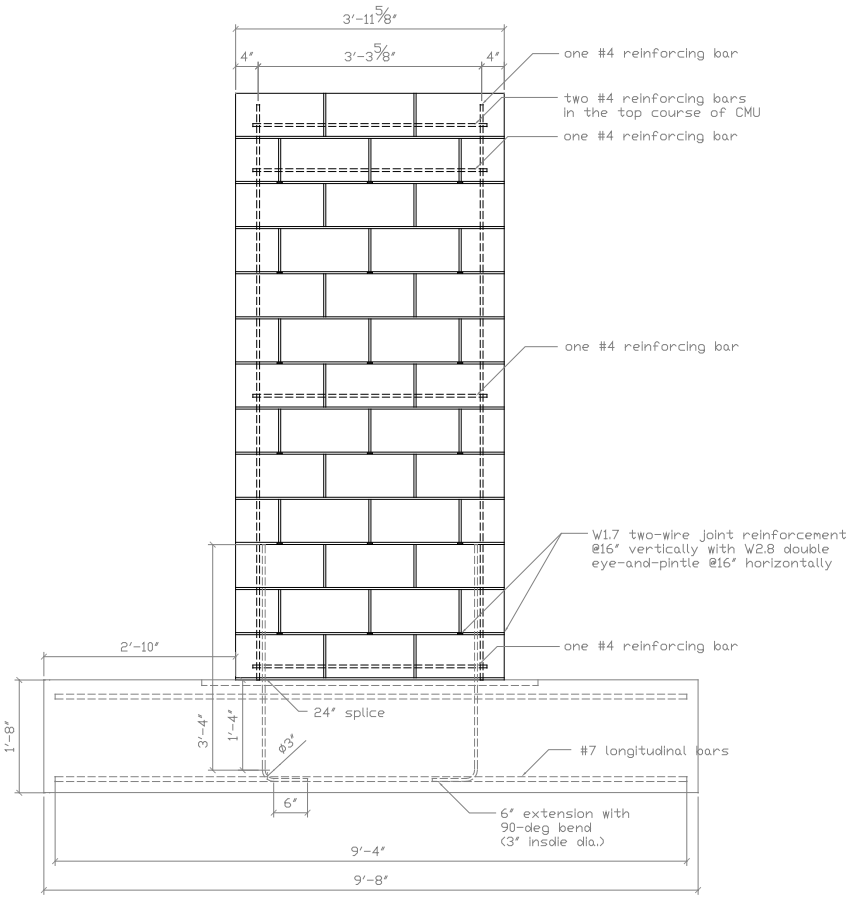

Figure A-12 Rear view of specimen UT CMU 3 and UCSD CMU 3

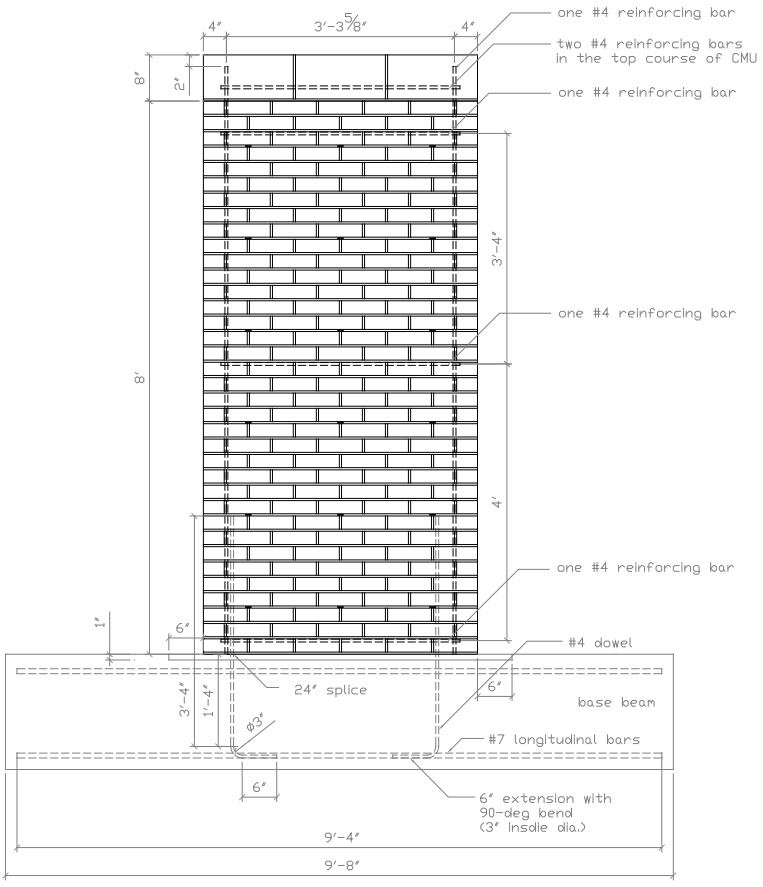

Figure A-13 Front view of specimens UT CMU 4, UT CMU 4 MC, UCSD CMU 4 and UCSD CMU 4 MC

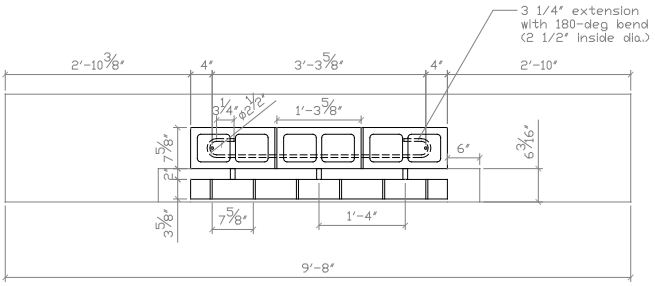

Figure A-14 Top view of specimens UT CMU 4, UT CMU 4 MC, UCSD CMU 4 and UCSD CMU 4 MC

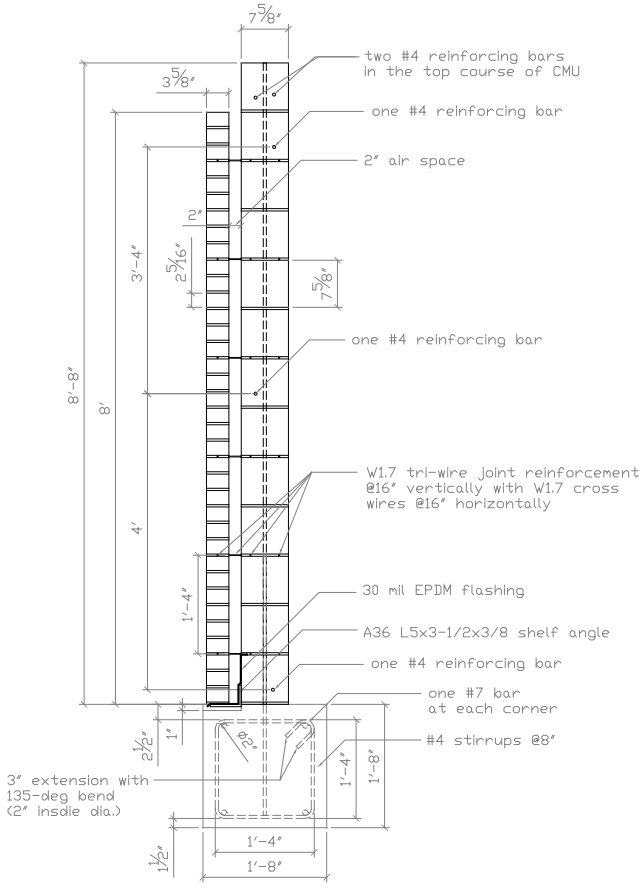

Figure A-15 Side view of specimens UT CMU 4, UT CMU 4 MC, UCSD CMU 4 and UCSD CMU 4 MC

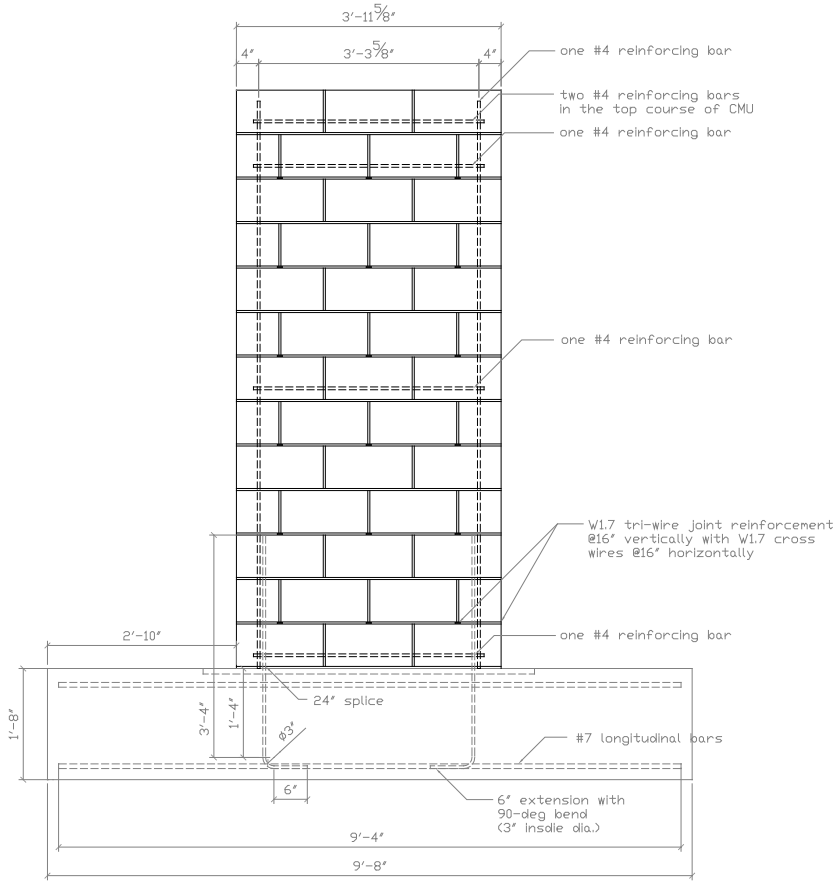

Figure A-16 Rear view of specimens UT CMU 4, UT CMU 4 MC, UCSD CMU 4 and UCSD CMU 4 MC

APPENDIX B

Design Drawings of CMU Building Specimen

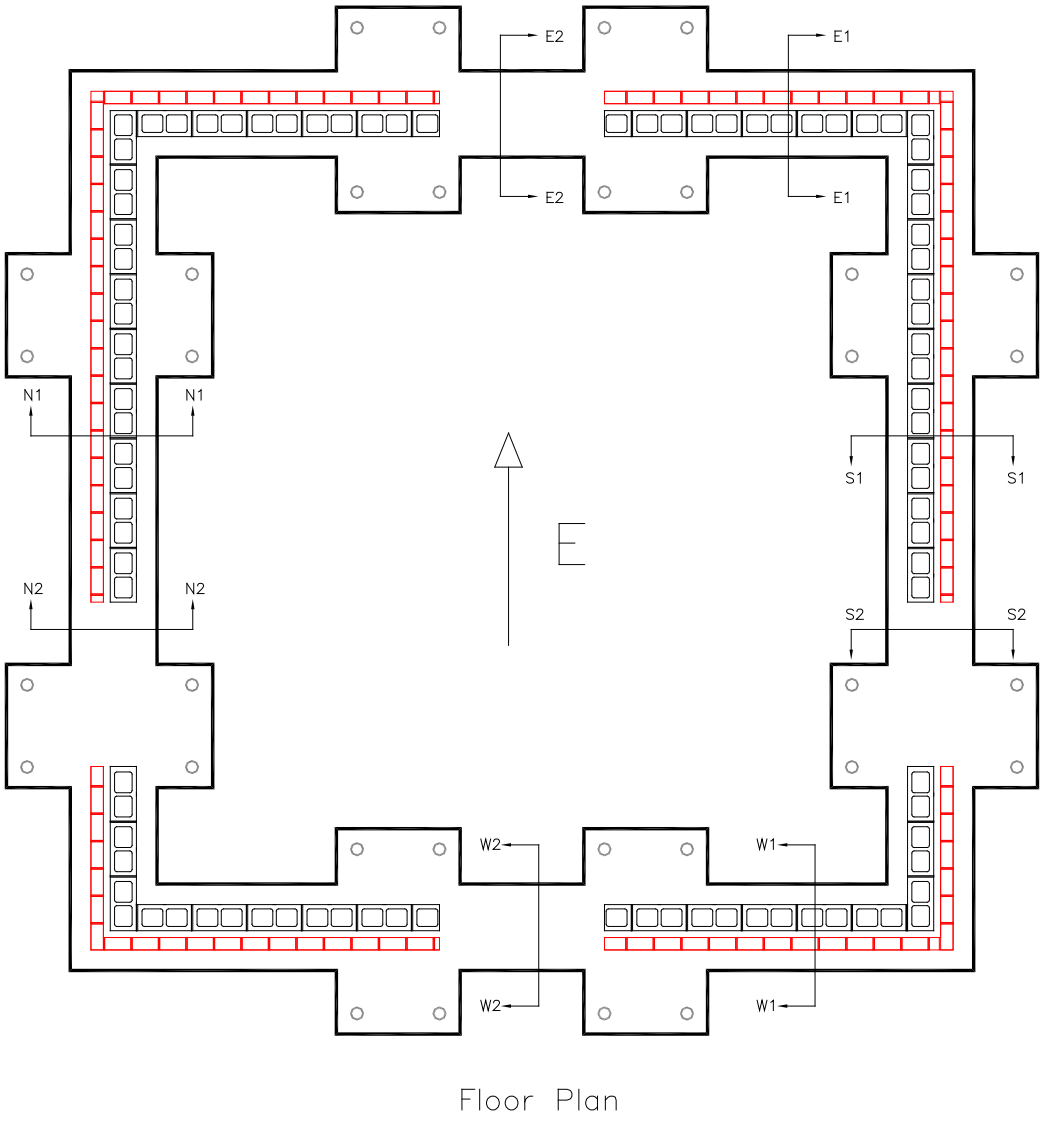

Figure B-1 Floor plan of CMU building specimen

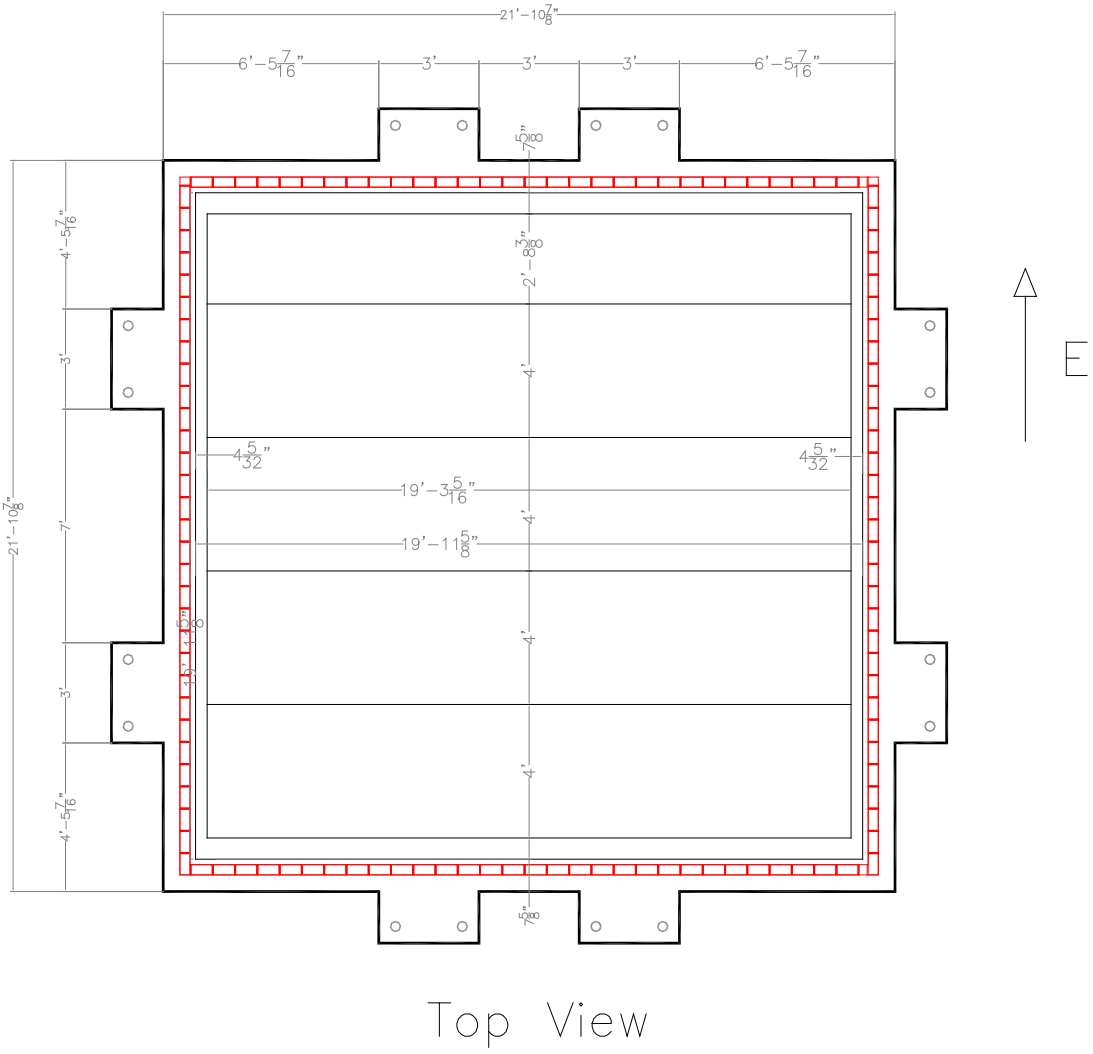

Figure B-2 Top view of CMU building specimen

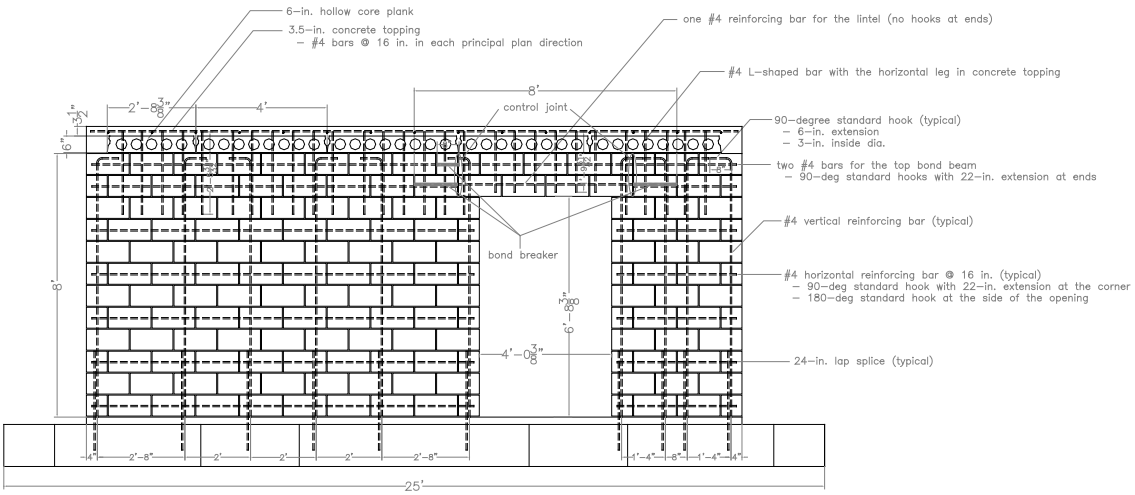

North Elevation – CMU

In the north CMU wall only, horizontal reinforcing bars start at the first course from the bottom. (in other walls at the second course)

Figure B-3 North elevation of CMU of CMU building specimen

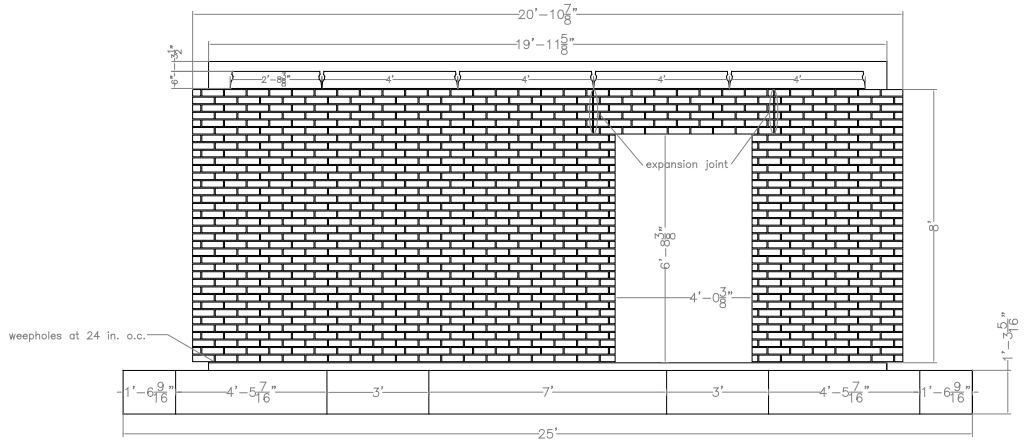

Nnorth Elevation – Veneer

Figure B-4 North elevation of veneer of CMU building specimen

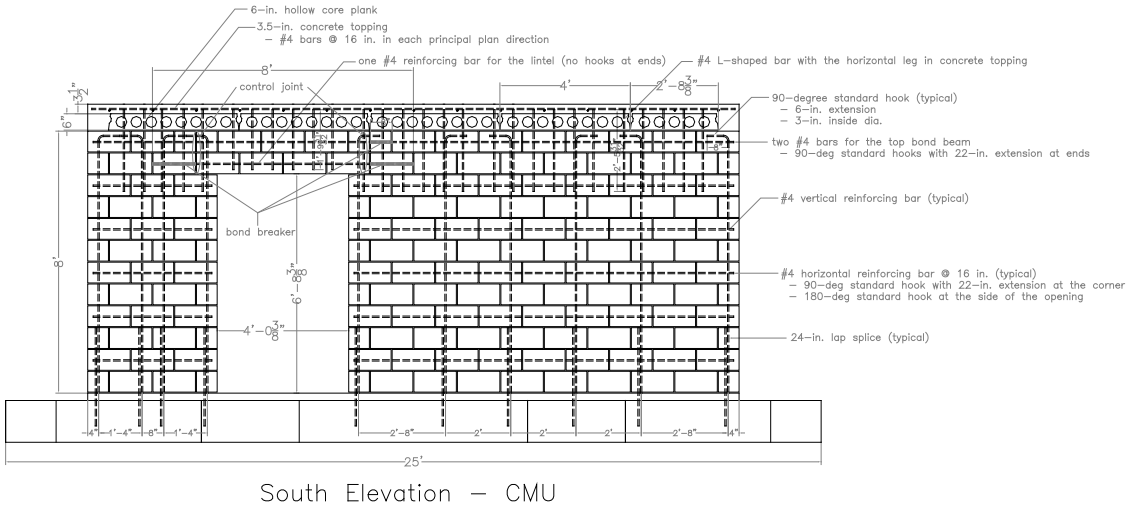

Figure B-5 South elevation of CMU of CMU building specimen

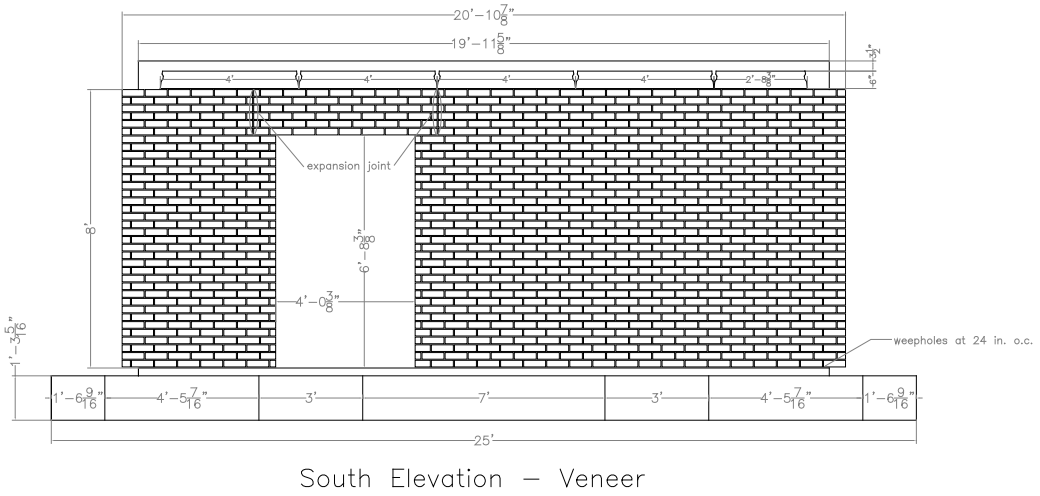

Figure B-6 South elevation of veneer of CMU building specimen

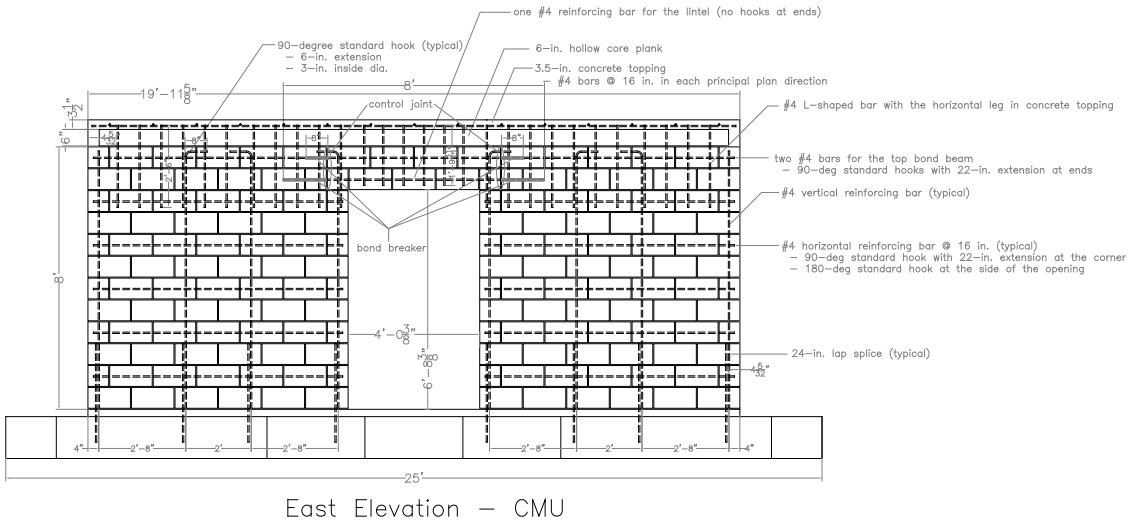

East Elevation – CMU

Figure B-7 East elevation of CMU of CMU building specimen

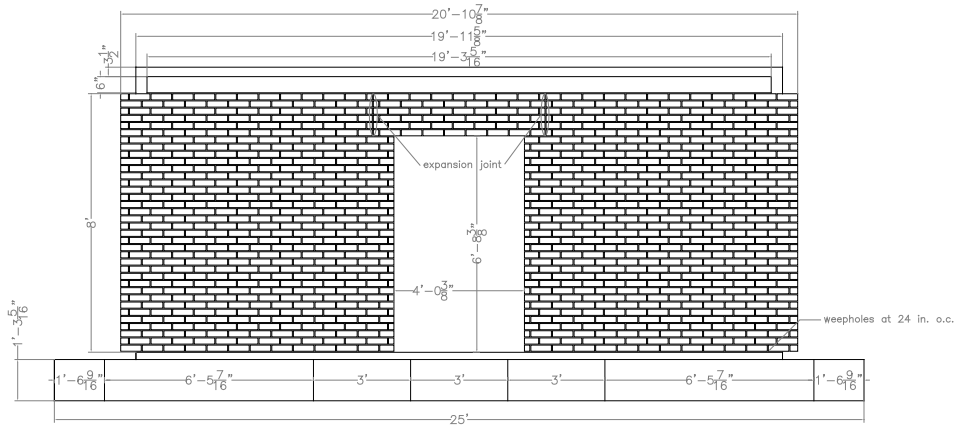

East Elevation – Veneer

Figure B-8 East elevation of veneer of CMU building specimen

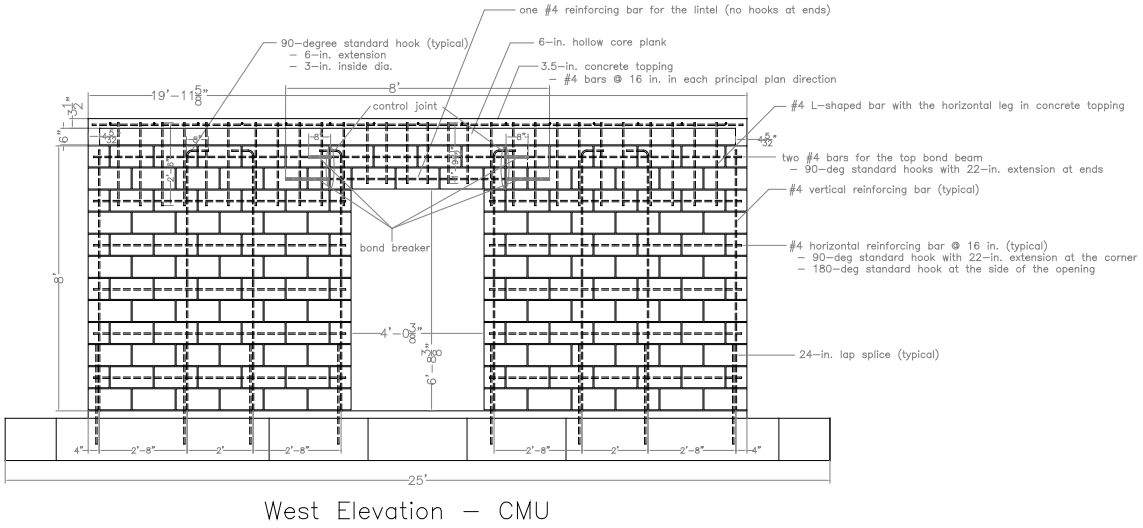

Figure B-9 West elevation of CMU of CMU building specimen

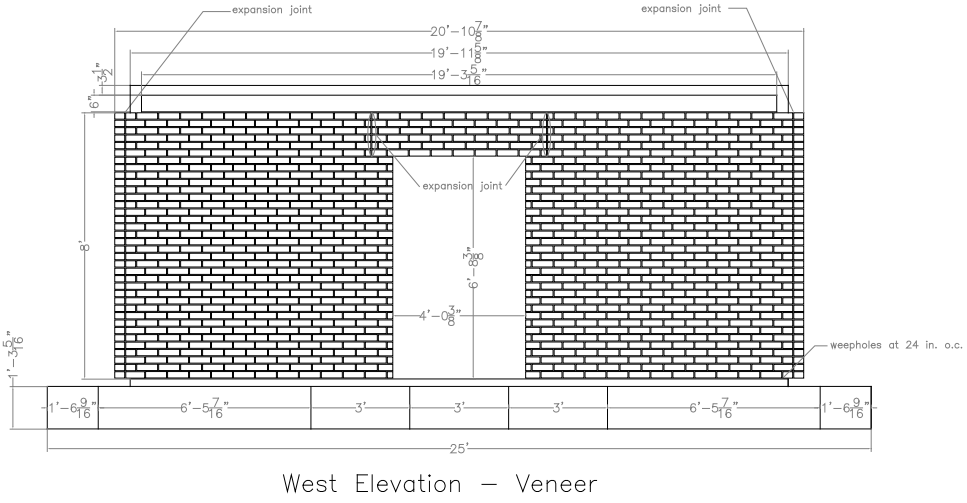

Figure B-10 West elevation of veneer of CMU building specimen

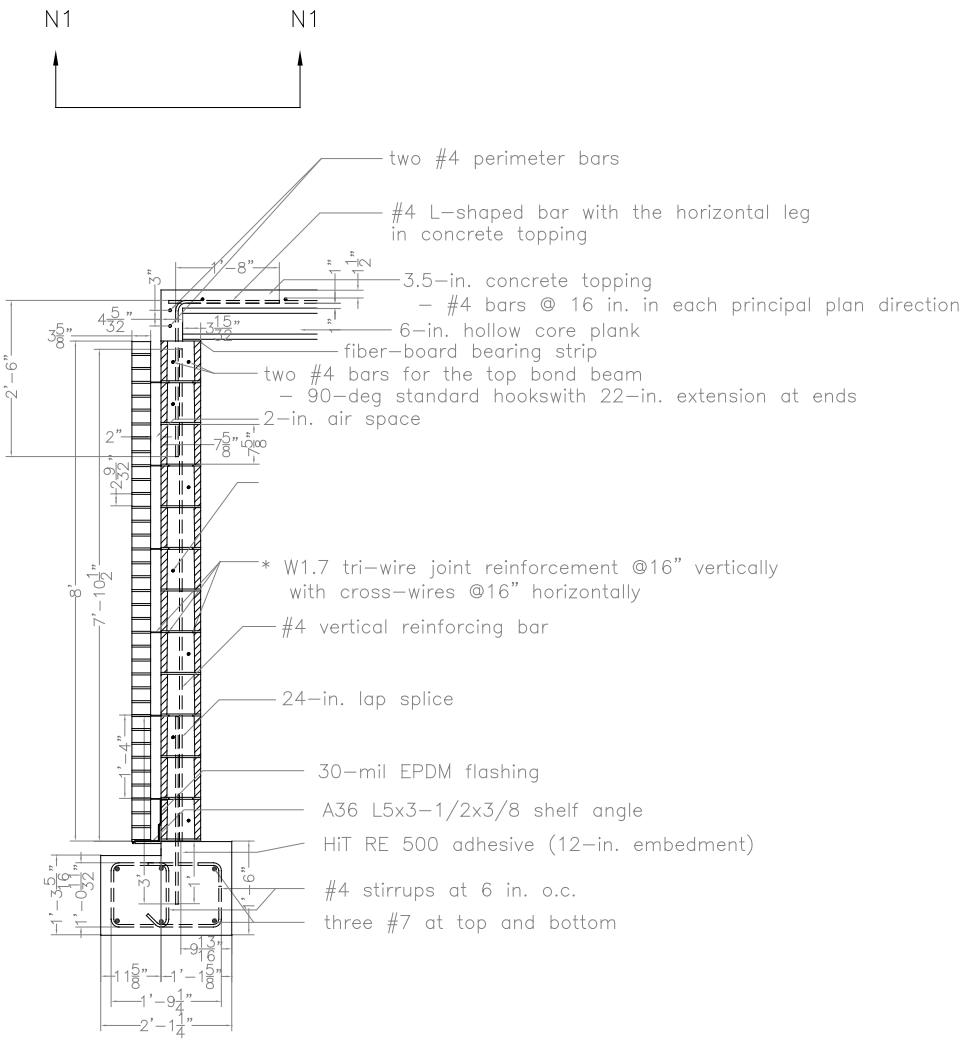

Section N1–N1

* N1–N1, N2–N2: W1.7 tri–wire connectors
* S1–S1, S2–S2: W2.8 double eye–and–pintle connectors
* Horizontal reinforcing bars start at the first course from the bottom In the north CMU wall, and at the second course In other CMU walls

Figure B-11 Section N1-N1 of CMU building specimen

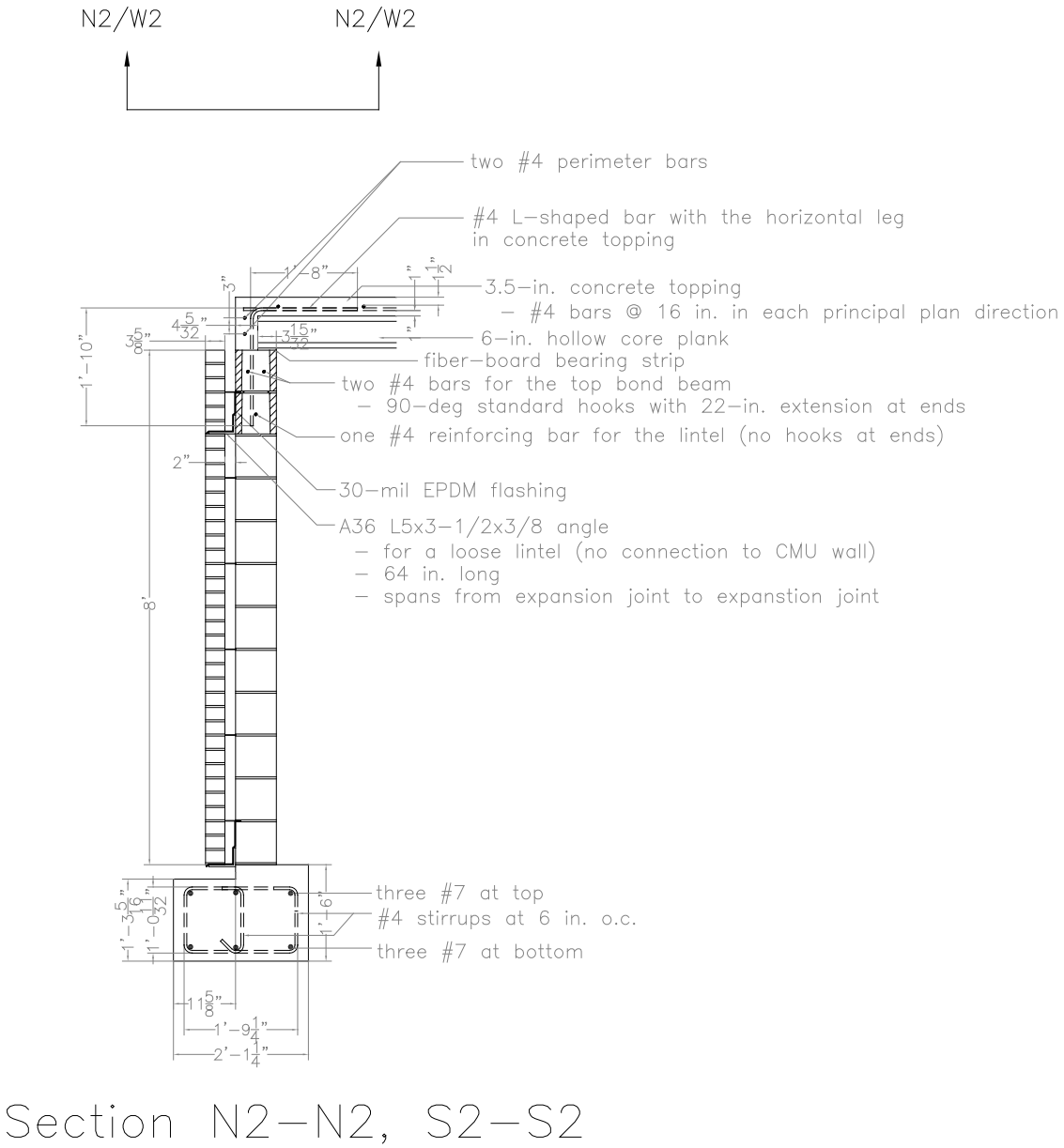

Section N2-N2, S2-S2

Figure B-12 Section N2-N2 and S2-S2 of CMU building specimen

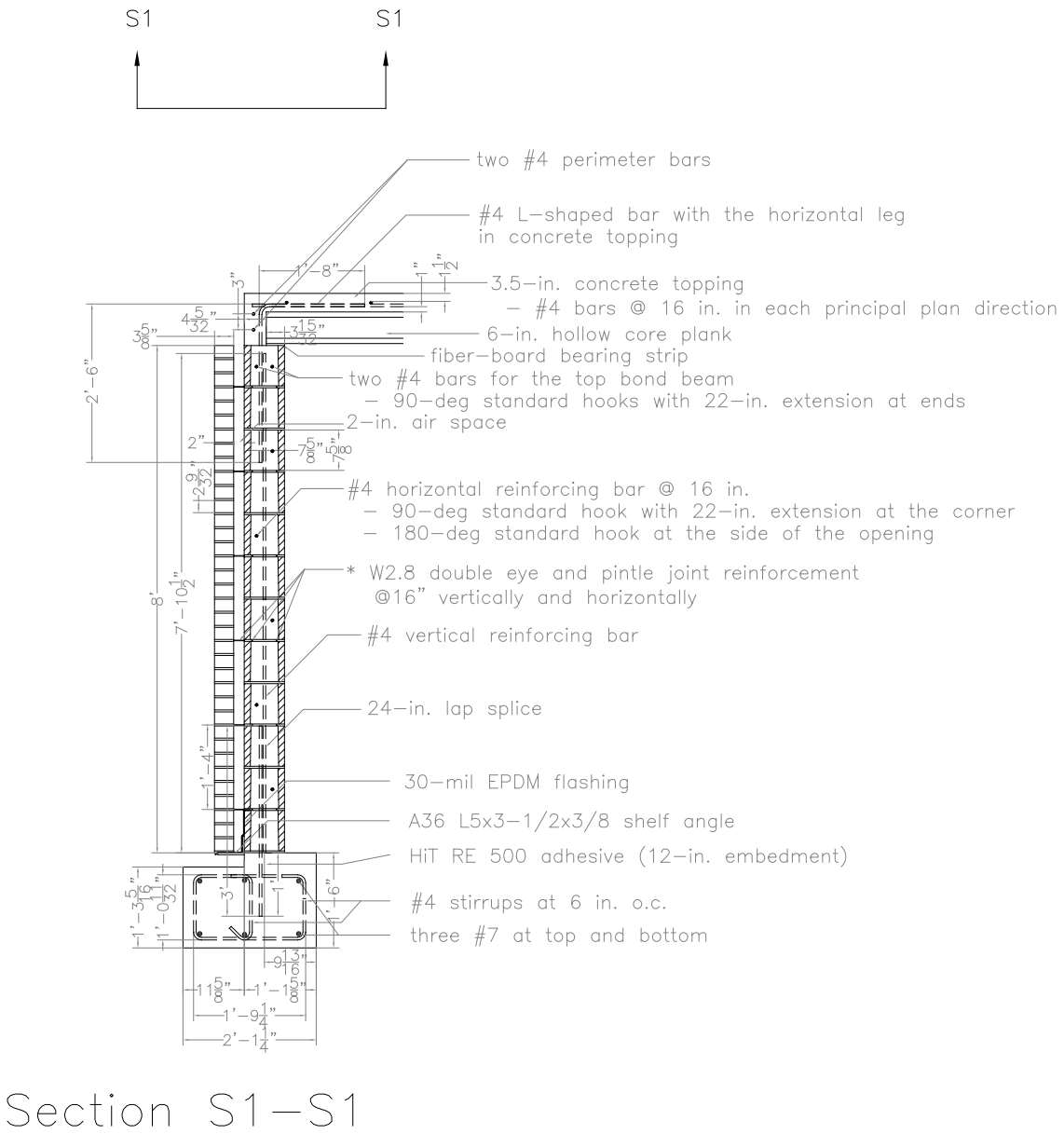

Figure B-13 Section S1-S1 of CMU building specimen

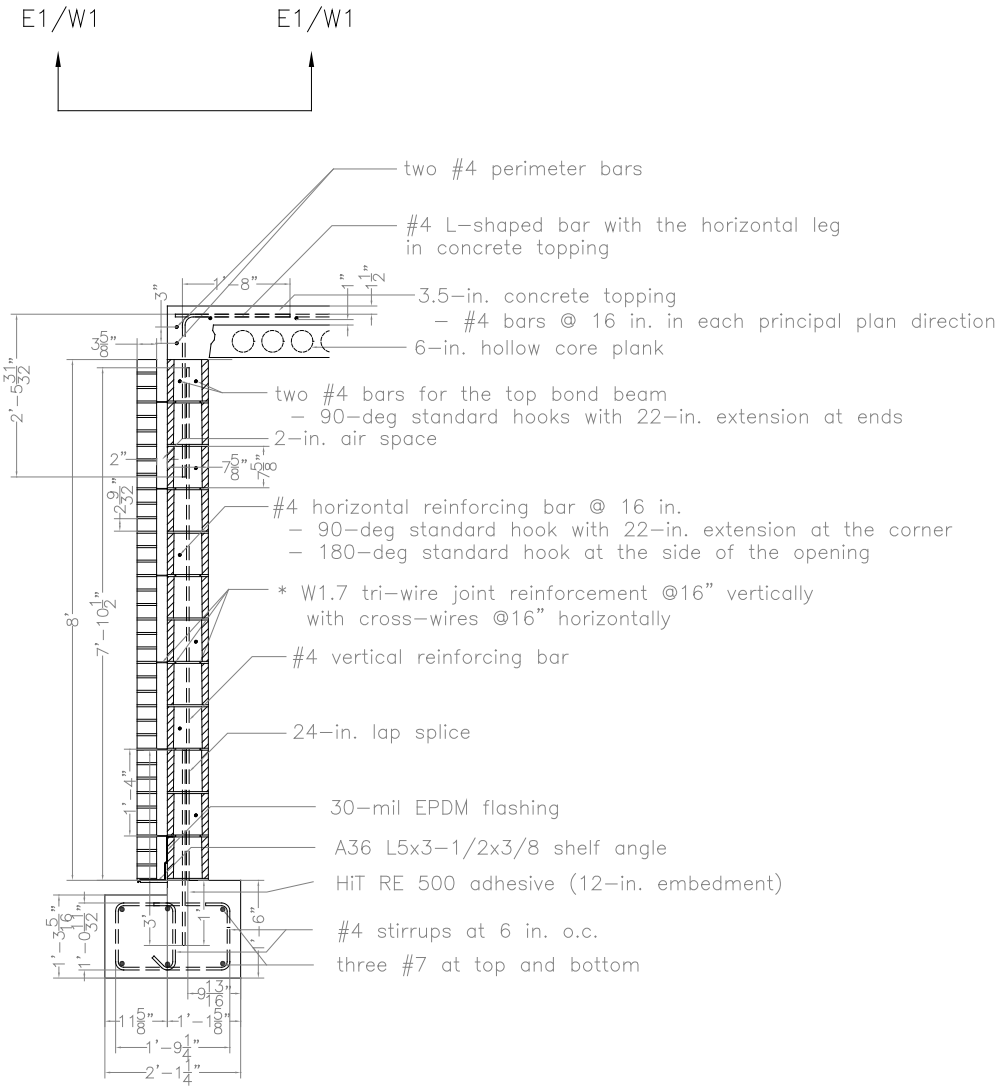

Section E1–E1, W1–W1

* E1–E1, E2–E2: W1.7 tri–wire connectors
* W1–W1, W2–W2: W2.8 double eye–and–pintle connectors

Figure B-14 Section E1-E1 and W1-W1 of CMU building specimen

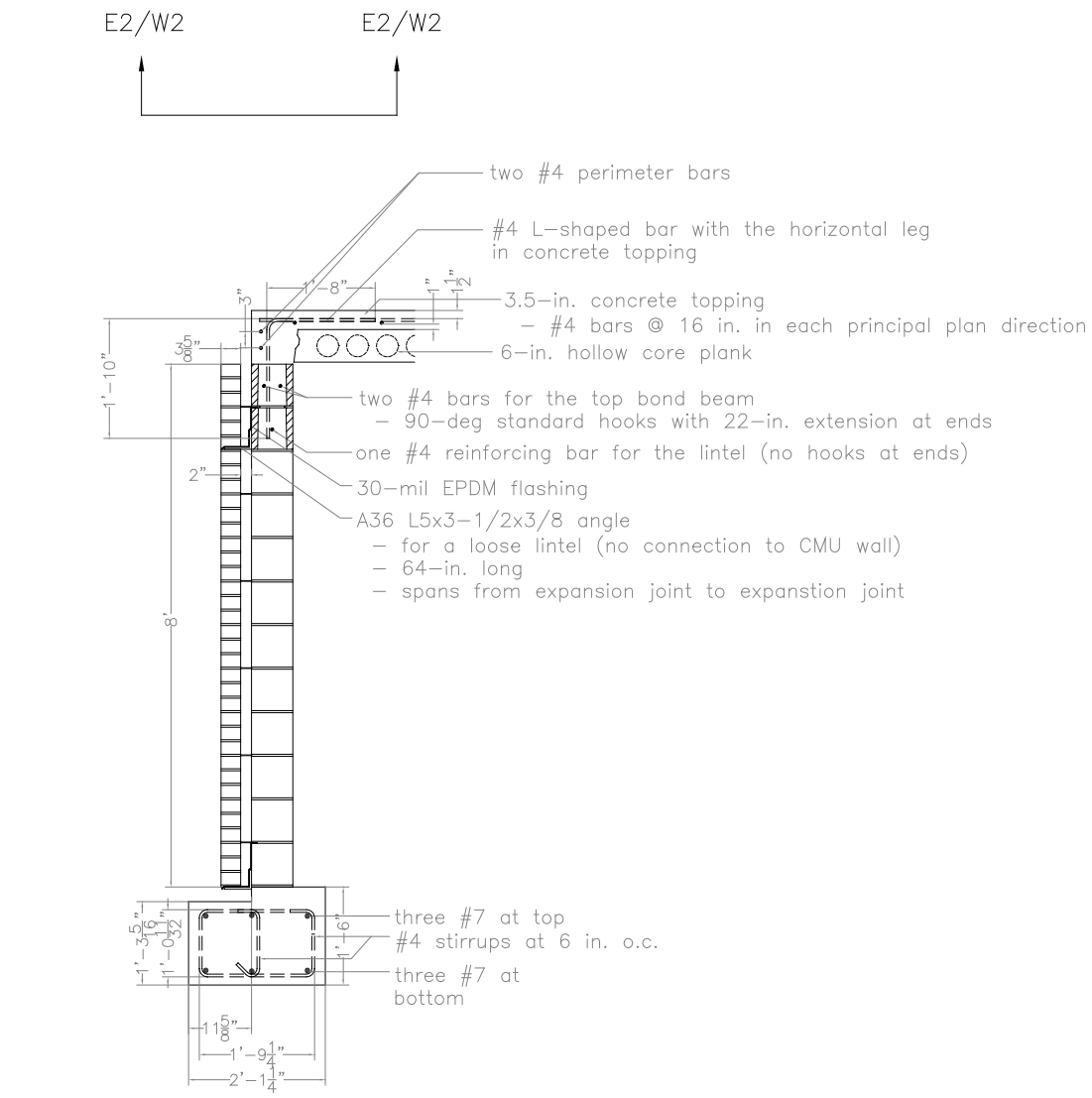

Figure B-15 Section E2-E2 and W2-W2 of CMU building specimen

Construction paper will be placed
– at control joints
– between concrete topping and CMU walls

Bond breaker around control joints
– indicated by a hatched rectangle as below

V–tooling
– at concrete topping above control joints

Expansion Joint (horizontal section)

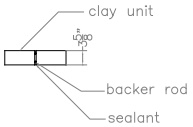

Foundation

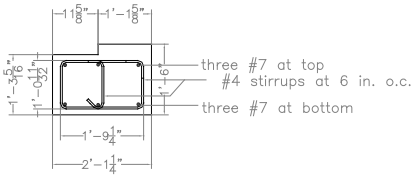

East and West

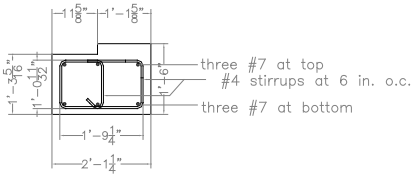

North and South

Figure B-16 Additional details of CMU building specimen

APPENDIX C
Detailed Design Calculations for CMU Building Specimen

In this chapter are presented the detailed calculations used in the design of the CMU building specimen discussed in Section 7.2. First, the in-plane strengths of each wall segment and the entire CMU building specimen are calculated with no additional roof weight, and with 19.5 kips of additional roof weight. Next, the in-plane stiffnesses of the 12-ft and 4-ft wall segments are calculated. Finally, the moment-axial force interaction diagrams used to calculate flexural strengths are shown.

The CMU building specimen is symmetrical about the direction of shaking. The north side and the south side of the specimen are composed of a 12-ft long wall, and a 4-foot long wall. Each of those walls is an L-shaped flanged wall, whose web consists of the 12-foot or 4-foot plan length (parallel to the direction of shaking), and whose flange consists of a portion of the perpendicular wall, whose effective plan length (effective flange width) is prescribed by the 2008 MSJC Code, and is different in tension and compression (MSJC 2008a). In calculating the flexural strength of each of those L-shaped walls, the axial load at the base of each L-shaped wall was assumed (for simplicity) to act at the plan center of the web of that L-shaped wall. This location is very close to that calculated including the effects of the lintel region, the flange self-weight, and any additional roof mass. During this preliminary design, any additional roof mass was assumed to be uniformly distributed over the roof. The additional roof masses were in fact placed so that additional axial forces due to them would act through the plan centers of the 12-foot long walls. This slight difference is addressed in analytical comparisons, but is not here.

In determining effective flange widths for the flexural strength, the nominal flange thickness and the floor-to-floor wall height are taken as 8 in. and 8 ft 9 in.,

respectively. The effective flange widths are therefore 8 in. multiplied by 6 when the flange is in compression, and 8 ft 9 in. multiplied by 0.75 when the flange is in tension.

C.1 DETAILED CALCULATIONS FOR IN-PLANE STRENGTHS OF WALL SEGMENTS AND CMU BUILDING SPECIMEN, NO ADDITIONAL ROOF WEIGHT

The sequence of calculations used to produce the values for Table 7.2 and Table 7.3 is traced in Table C.1, for the case of no additional roof weight. Immediately below Table C.1, are given, line by line, the calculations used to produce the values in Table C.1. The moment-axial force interaction diagrams used to calculate flexural strengths are given in Section C.4.

Table C.1 In-plane strengths of wall segments and CMU building specimen (no additional roof weight)

design strengths							
wall segment		**12-ft long wall**		**4-ft long wall**		**8-ft long wall**	
load direction (to)		**east**	**west**	**east**	**west**	**when flange is in tension**	
roof weight		87.75 psf (6-in. planks with 3.5-in. concrete topping, no additional weight)					
P	kips	22.3[(1)]	23.8[(2)]	11.9[(3)]	10.4[(4)]	7.4[(5)]	
ϕM_n	kips-ft	518.5[(6)]	724.3[(7)]	162.0[(8)]	107.9[(9)]	420.4[(10)]	
$V(\phi M_n)$	kips	64.8[(11)]	90.5[(12)]	20.3[(13)]	13.5[(14)]	52.5[(15)]	
$V(M_n)$	kips	72.0[(16)]	100.6[(17)]	22.5[(18)]	15.0[(19)]	58.4[(20)]	
ϕV_{nm}	kips	100.9[(21)]	101.2[(22)]	27.9[(23)]	27.6[(24)]	52.5[(25)]	
ϕV_n	kips	129.7[(26)]	130.0[(27)]	42.3[(28)]	42.0[(29)]	81.3[(30)]	
$\phi V_{n\_sliding}$	kips	85.0[(31)]	95.9[(32)]	67.1[(33)]	56.3[(34)]	73.1[(35)]	
expected strengths *							
wall segment		**12-ft long wall**		**4-ft long wall**		**Sum (two 12-ft and two 4-ft)**	
load direction (to)		**east**	**west**	**east**	**west**	**east**	**west**
$V(M_{n\_\exp})$	kips	103.2[(36)]	144.2[(37)]	32.3[(38)]	21.5[(39)]	271.0	331.3
$V_{n\_\exp}$	kips	177.7[(40)]	178.1[(41)]	60.7[(42)]	60.3[(43)]	476.9	476.9
$V_{n\_sliding\_\exp}$	kips	142.7[(44)]	161.4[(45)]	115.1[(46)]	96.4[(47)]	515.5	515.5
required table (base) acceleration $\ddot{u}_{g\_required} = \frac{V(M_{n\_\exp})}{1.5 \times W_{eff}}$		without veneer $W_{eff} = 52.1 kips$ [(48)]				3.31 g[(49)]	4.04 g[(50)]
		with veneer $W_{eff} = 61.4 kips$ [(51)]				2.83 g[(52)]	3.46 g[(53)]

** specified material strengths for masonry (1500 psi) and expected material strengths for vertical and horizontal reinforcement (86 ksi) were used.*

[(1)] $P_{east} = W_{roof} + W_{CMU} = 87.75 psf \times (12\,ft + 2\,ft) \times 10\,ft + 120\,pcf \times (12\,ft \times 8\,ft + 2\,ft \times 1.33\,ft + 4\,ft \times 8\,ft)$

$$\times \frac{7.63}{12}\, ft = 12.3 kips + 10.0 kips = 22.3 kips$$

(2) $P_{west} = W_{roof} + W_{CMU} = 87.75\, psf \times (12\, ft + 2\, ft) \times 10\, ft + 120\, pcf \times (12\, ft \times 8\, ft + 2\, ft \times 1.33\, ft$

$$+ 0.75 \times 8.75\, ft \times 8\, ft) \times \frac{7.63}{12}\, ft = 12.3 kips + 11.5 kips = 23.8 kips$$

(3) $P_{east} = W_{roof} + W_{CMU} = 87.75\, psf \times (4\, ft + 2\, ft) \times 10\, ft + 120\, pcf \times (4\, ft \times 8\, ft + 2\, ft \times 1.33\, ftt$

$$+ 0.75 \times 8.75\, f \times 8\, ft) \times \frac{7.63}{12}\, ft = 5.3 kips + 6.7 kips = 11.5 kips$$

(4) $P_{west} = W_{roof} + W_{CMU} = 87.75\, psf \times (4\, ft + 2\, ft) \times 10\, ft + 120\, pcf \times (4\, ft \times 8\, ft + 2\, ft \times 1.33\, ft + 4\, ft \times 8\, ft)$

$$\times \frac{7.63}{12}\, ft = 5.3 kips + 5.1 kips = 10.4 kips$$

(5) $P = W_{CMU} = 120\, pcf \times (4\, ft \times 8\, ft) \times \frac{7.63}{12}\, ft = 7.4\, kips$

(6) From Figure C-1, $\phi M_{n\_east} = 387 kips \cdot ft + \frac{22.3 kips}{56 kips} \times (718 - 387) kips \cdot ft = 518.5 kips \cdot ft$

(7) From Figure C-2, $\phi M_{n\_west} = 610 kips \cdot ft + \frac{23.8 kips}{69 kips} \times (941 - 610) kips \cdot ft = 724.3 kips \cdot ft$

(8) From Figure C-4, $\phi M_{n\_east} = 147 kips \cdot ft + \frac{11.9 kips}{27 kips} \times (181 - 147) kips \cdot ft = 162.0 kips \cdot ft$

(9) From Figure C-3, $\phi M_{n\_west} = 88 kips \cdot ft + \frac{10.4 kips}{38 kips} \times (161 - 88) kips \cdot ft = 107.9 kips \cdot ft$

(10) From Figure C-6, $\phi M_{n} = 397 kips \cdot ft + \frac{7.4 kips}{30 kips} \times (492 - 397) kips \cdot ft = 420.4 kips \cdot ft$

(11) $V(\phi M_{n\_east}) = \frac{\phi M_{n\_east}}{height} = \frac{518.5 kips \cdot ft}{8\, ft} = 64.8 kips$

(12) $V(\phi M_{n\_west}) = \frac{\phi M_{n\_west}}{height} = \frac{724.3 kips \cdot ft}{8\, ft} = 90.5 kips$

(13) $V(\phi M_{n\_east}) = \frac{\phi M_{n\_east}}{height} = \frac{162.0 kips \cdot ft}{8\, ft} = 20.3 kips$

(14) $V\left(\phi M_{n\_west}\right)=\dfrac{\phi M_{n\_west}}{height}=\dfrac{107.9kips\cdot ft}{8\,ft}=13.5kips$

(15) $V\left(\phi M_{n}\right)=\dfrac{\phi M_{n}}{height}=\dfrac{420.4kips\cdot ft}{8\,ft}=52.5kips$

(16) $V\left(M_{n\_east}\right)=\dfrac{V\left(\phi M_{n\_east}\right)}{0.9}=\dfrac{64.8kips}{0.9}=72.0kips$

(17) $V\left(M_{n\_west}\right)=\dfrac{V\left(\phi M_{n\_west}\right)}{0.9}=\dfrac{90.5kips}{0.9}=100.6kips$

(18) $V\left(M_{n\_east}\right)=\dfrac{V\left(\phi M_{n\_east}\right)}{0.9}=\dfrac{20.3kips}{0.9}=22.5kips$

(19) $V\left(M_{n\_west}\right)=\dfrac{V\left(\phi M_{n\_west}\right)}{0.9}=\dfrac{13.5kips}{0.9}=15.0kips$

(20) $V\left(M_{n}\right)=\dfrac{V\left(\phi M_{n}\right)}{0.9}=\dfrac{52.5kips}{0.9}=58.4kips$

(21) $\phi V_{nm\_east}=0.8\times\left[\left\{4.0-1.75\left(\dfrac{M_u}{V_u}\times\dfrac{1}{d_v}\right)\right\}\times A_n\times\sqrt{f'_m}+0.25P_u\right]$ * $\dfrac{M_u}{V_u\times d_v}\le 1$

$=0.8\times\left[\left\{4.0-1.75\left(8\,ft\times\dfrac{1}{12\,ft}\right)\right\}\times(144\times 7.63)in^2\times\sqrt{1500}\,psi+0.25\times 22.3kips\right]=100.9kips$

(22) $\phi V_{nm\_west}=0.8\times\left[\{2.83\}\times(144\times 7.63)in^2\times\sqrt{1500}\,psi+0.25\times 23.8kips\right]=101.2kips$

(23) $\phi V_{nm\_east}=0.8\times\left[\left\{4.0-1.75\left(\dfrac{M_u}{V_u}\times\dfrac{1}{d_v}\right)\right\}\times A_n\times\sqrt{f'_m}+0.25P_u\right]$ * $\dfrac{M_u}{V_u\times d_v}\le 1$

$=0.8\times\left[\{2.25\}\times(48\times 7.63)in^2\times\sqrt{1500}\,psi+0.25\times 11.9kips\right]=27.9kips$

(24) $\phi V_{nm\_west}=0.8\times\left[\{2.25\}\times(48\times 7.63)in^2\times\sqrt{1500}\,psi+0.25\times 10.4kips\right]=27.6kips$

(25) $\phi V_{nm}=0.8\times\left[\left\{4.0-1.75\left(\dfrac{M_u}{V_u}\times\dfrac{1}{d_v}\right)\right\}\times A_n\times\sqrt{f'_m}+0.25P_u\right]$ * $\dfrac{M_u}{V_u\times d_v}\le 1$

$=0.8\times\left[\{2.25\}\times(96\times 7.63)in^2\times\sqrt{1500}\,psi+0.25\times 7.4kips\right]=52.5kips$

(26) $\phi V_{n\_east} = \phi V_{nm\_east} + \phi V_{ns} = 100.9kips + 0.8 \times 0.5 A_v f_y \left(\frac{d_v}{s} \right)$ * $d_v \le height$

$= 100.9kips + 0.4 \times 0.2in^2 \times 60ksi \times \left(\frac{96in.}{16in.} \right) = 100.9kips + 28.8kips = 129.7kips$

(27) $\phi V_{n\_west} = \phi V_{nm\_west} + \phi V_{ns} = 101.2kips + 28.8kips = 130.0kips$

(28) $\phi V_{n\_east} = \phi V_{nm\_east} + \phi V_{ns} = 27.9kips + 0.8 \times 0.5 A_v f_y \left(\frac{d_v}{s} \right)$ * $d_v \le height$

$= 27.9kips + 0.4 \times 0.2in^2 \times 60ksi \times \left(\frac{48in.}{16in.} \right) = 27.9kips + 14.4kips = 42.3kips$

(29) $\phi V_{n\_west} = \phi V_{nm\_west} + \phi V_{ns} = 27.6kips + 14.4kips = 42.0kips$

(30) $\phi V_n = \phi V_{nm} + \phi V_{ns} = 52.5kips + 0.8 \times 0.5 A_v f_y \left(\frac{d_v}{s} \right)$ * $d_v \le height$

$= 52.5kips + 0.4 \times 0.2in^2 \times 60ksi \times \left(\frac{96in.}{16in.} \right) = 52.5kips + 28.8kips = 81.3kips$

(31) $\phi V_{n\_sliding\_east} = 0.8 \times \left\{ \mu \times \left(N_{weight} + N_{bars} \right) \right\} = 0.8 \times 1.0 \times \left(22.3kips + 7 \times 60ksi \times 0.2in^2 \right)$

$= 85.0kips$

(32) $\phi V_{n\_sliding\_west} = 0.8 \times \left\{ \mu \times \left(N_{weight} + N_{bars} \right) \right\} = 0.8 \times 1.0 \times \left(23.8kips + 8 \times 60ksi \times 0.2in^2 \right)$

$= 95.9kips$

(33) $\phi V_{n\_sliding\_east} = 0.8 \times \left\{ \mu \times \left(N_{weight} + N_{bars} \right) \right\} = 0.8 \times 1.0 \times \left(11.9kips + 6 \times 60ksi \times 0.2in^2 \right)$

$= 67.1kips$

(34) $\phi V_{n\_sliding\_west} = 0.8 \times \left\{ \mu \times \left(N_{weight} + N_{bars} \right) \right\} = 0.8 \times 1.0 \times \left(10.4kips + 5 \times 60ksi \times 0.2in^2 \right)$

$= 56.3kips$

(35) $\phi V_{n\_sliding} = 0.8 \times \left\{ \mu \times \left(N_{weight} + N_{bars} \right) \right\} = 0.8 \times 1.0 \times \left(7.4kips + 7 \times 60ksi \times 0.2in^2 \right) = 73.1kips$

(36) $V\left(M_{n\_\exp\_east} \right) = V\left(M_n \right) \times \frac{86ksi}{60ksi} = 72.0kips \times 1.43 = 103.2kips$

(37) $V\left(M_{n\_\exp\_west} \right) = V\left(M_n \right) \times \frac{86ksi}{60ksi} = 100.6kips \times 1.43 = 144.2kips$

(38) $V\left(M_{n\_\exp\_east}\right) = V\left(M_n\right) \times \frac{86ksi}{60ksi} = 22.5kips \times 1.43 = 32.3kips$

(39) $V\left(M_{n\_\exp\_west}\right) = V\left(M_n\right) \times \frac{86ksi}{60ksi} = 15.0kips \times 1.43 = 21.5kips$

(40) $V_{n\_\exp\_east} = \frac{\phi V_{nm\_east}}{\phi} + \frac{\phi V_{ns}}{\phi} \times \frac{86ksi}{60ksi} = \frac{100.9kips}{0.8} + \frac{28.8kips}{0.8} \times 1.43 = 177.7kips$

(41) $V_{n\_\exp\_west} = \frac{\phi V_{nm\_west}}{\phi} + \frac{\phi V_{ns}}{\phi} \times \frac{86ksi}{60ksi} = \frac{101.2kips}{0.8} + \frac{28.8kips}{0.8} \times 1.43 = 178.1kips$

(42) $V_{n\_\exp\_east} = \frac{\phi V_{nm\_east}}{\phi} + \frac{\phi V_{ns}}{\phi} \times \frac{86ksi}{60ksi} = \frac{27.9kips}{0.8} + \frac{14.4kips}{0.8} \times 1.43 = 60.7kips$

(43) $V_{n\_\exp\_west} = \frac{\phi V_{nm\_west}}{\phi} + \frac{\phi V_{ns}}{\phi} \times \frac{86ksi}{60ksi} = \frac{27.6kips}{0.8} + \frac{14.4kips}{0.8} \times 1.43 = 60.3kips$

(44) $V_{n\_sliding\_\exp\_east} = \mu \times \left(N_{weight} + N_{bars}\right) = 1.0 \times \left(22.3kips + 7 \times 86ksi \times 0.2in^2\right) = 142.7kips$

(45) $V_{n\_sliding\_\exp\_west} = \mu \times \left(N_{weight} + N_{bars}\right) = 1.0 \times \left(23.8kips + 8 \times 86ksi \times 0.2in^2\right) = 161.4kips$

(46) $V_{n\_sliding\_\exp\_east} = \mu \times \left(N_{weight} + N_{bars}\right) = 1.0 \times \left(11.9kips + 6 \times 86ksi \times 0.2in^2\right) = 115.1kips$

(47) $V_{n\_sliding\_\exp\_west} = \mu \times \left(N_{weight} + N_{bars}\right) = 1.0 \times \left(10.4kips + 5 \times 86ksi \times 0.2in^2\right) = 96.4kips$

(48) $W_{eff} = W_{roof} + W_{CMU\_eff} = \left(87.75psf \times 20ft \times 20ft\right) + \frac{1}{2} \times \left\{120pcf \times \left(80ft - 4 \times 4ft\right) \times 8ft \times \frac{7.63}{12}ft\right\}$

$= 35.1kips + 19.5kips = 54.6kips$

(49) $\ddot{u}_{g\_required\_east} = \frac{V\left(M_{n\_\exp\_east}\right)}{1.5 \times W_{eff}} = \frac{2 \times \left(103.2kips + 32.3kips\right)}{1.5 \times 54.6kips} = \frac{271.0kips}{1.5 \times 54.6kips} = 3.31g$

(50) $\ddot{u}_{g\_required\_west} = \frac{V\left(M_{n\_\exp\_west}\right)}{1.5 \times W_{eff}} = \frac{2 \times \left(144.2kips + 21.5kips\right)}{1.5 \times 54.6kips} = \frac{331.3kips}{1.5 \times 54.6kips} = 4.04g$

(51) $W_{eff} = W_{roof} + W_{CMU\_eff} = \left(87.75psf \times 20ft \times 20ft\right)$

$+ \frac{1}{2} \times \left\{120pcf \times \left(80ft - 4 \times 4ft\right) \times 8ft \times \frac{7.63 + 3.63}{12}ft\right\} = 35.1kips + 28.8kips = 63.9kips$

(52) $$\ddot{u}_{g\_required\_east} = \frac{V\left(M_{n\_\exp\_east}\right)}{1.5 \times W_{eff}} = \frac{2 \times \left(103.2kips + 32.3kips\right)}{1.5 \times 63.9kips} = \frac{271.0kips}{1.5 \times 63.9kips} = 2.83g$$

(53) $$\ddot{u}_{g\_required\_west} = \frac{V\left(M_{n\_\exp\_west}\right)}{1.5 \times W_{eff}} = \frac{2 \times \left(144.2kips + 21.5kips\right)}{1.5 \times 63.9kips} = \frac{331.3kips}{1.5 \times 63.9kips} = 3.46g$$

C.2 DETAILED CALCULATIONS FOR IN-PLANE STRENGTHS OF WALL SEGMENTS AND CMU BUILDING SPECIMEN, 19.5-KIP ADDITIONAL ROOF WEIGHT

The sequence of calculations used to produce the values for Table 7.4 and Table 7.5 is traced in Table C.2, for the case of 19.5-kip additional weight. Immediately below Table C.2 are given, line by line, the calculations used to produce the values in Table C.2. The moment-axial force interaction diagrams used to calculate flexural strengths are given in Section C.4.

Table C.2 In-plane strengths of wall segments and CMU building specimen (19.5-kip additional roof weight)

design strengths						
wall segment		**12-ft long wall**		**4-ft long wall**		**8-ft long wall**
load direction (to)		**east**	**west**	**east**	**west**	**when flange is in tension**
roof weight		136.5 psf (6-in. planks with 3.5-in. concrete topping, 19.5-kip additional weight)				
P	kips	29.1[(1)]	30.6[(2)]	14.8[(3)]	13.3[(4)]	7.4[(5)]
ϕM_n	kips-ft	558.9[(6)]	757.0[(7)]	165.7[(8)]	113.5[(9)]	420.4[(10)]
$V(\phi M_n)$	kips	69.9[(11)]	94.6[(12)]	20.7[(13)]	14.2[(14)]	52.5[(15)]
$V(M_n)$	kips	77.6[(16)]	105.1[(17)]	23.0[(18)]	15.8[(19)]	58.4[(20)]
ϕV_{nm}	kips	102.3[(21)]	102.6[(22)]	28.5[(23)]	28.2[(24)]	52.5[(25)]
ϕV_n	kips	131.1[(26)]	131.4[(27)]	42.9[(28)]	42.6[(29)]	81.3[(30)]
$\phi V_{n\_sliding}$	kips	90.5[(31)]	101.3[(32)]	69.5[(33)]	58.6[(34)]	73.1[(35)]

expected strengths *							
wall segment		**12-ft long wall**		**4-ft long wall**		**Sum (two 12-ft and two 4-ft)**	
load direction (to)		**east**	**west**	**east**	**west**	**east**	**west**
$V(M_{n\_\exp})$	kips	111.3[(36)]	150.7[(37)]	33.0[(38)]	22.6[(39)]	288.5	346.6
$V_{n\_\exp}$	kips	179.4[(40)]	179.8[(41)]	61.4[(42)]	61.0[(43)]	481.7	481.7
$V_{n\_sliding\_\exp}$	kips	149.5[(44)]	168.2[(45)]	118.0[(46)]	99.3[(47)]	535.0	535.0
Required table (base) acceleration $\ddot{u}_{g\_required} = \frac{V(M_{n\_\exp})}{1.5 \times W_{eff}}$			Without Veneer $W_{eff} = 74.1 kips$ [(48)]			2.59 g[(49)]	3.12 g[(50)]
			With Veneer $W_{eff} = 83.4 kips$ [(51)]			2.31 g[(52)]	2.77 g[(53)]

** specified material strengths for masonry (1500 psi) and expected material strengths for vertical and horizontal reinforcement (86 ksi) were used.*

[(1)] $P_{east} = W_{roof} + W_{CMU} = 136.5 psf \times (12 ft + 2 ft) \times 10 ft + 120 pcf \times (12 ft \times 8 ft + 2 ft \times 1.33 ft$

$$+ 4\,ft \times 8\,ft) \times \frac{7.63}{12}\,ft = 19.1kips + 10.0kips = 29.1kips$$

(2) $P_{west} = W_{roof} + W_{CMU} = 136.5\,psf \times (12\,ft + 2\,ft) \times 10\,ft + 120\,pcf \times (12\,ft \times 8\,ft + 2\,ft \times 1.33\,ft$

$$+ 0.75 \times 8.75\,ft \times 8\,ft) \times \frac{7.63}{12}\,ft = 19.1kips + 11.5kips = 30.6kips$$

(3) $P_{east} = W_{roof} + W_{CMU} = 136.5\,psf \times (4\,ft + 2\,ft) \times 10\,ft + 120\,pcf \times (4\,ft \times 8\,ft + 2\,ft \times 1.33\,ftt$

$$+ 0.75 \times 8.75\,f \times 8\,ft) \times \frac{7.63}{12}\,ft = 8.2kips + 6.7kips = 14.8kips$$

(4) $P_{west} = W_{roof} + W_{CMU} = 136.5\,psf \times (4\,ft + 2\,ft) \times 10\,ft + 120\,pcf \times (4\,ft \times 8\,ft + 2\,ft \times 1.33\,ft$

$$+ 4\,ft \times 8\,ft) \times \frac{7.63}{12}\,ft = 8.2kips + 5.1kips = 13.3kips$$

(5) $P = W_{CMU} = 120\,pcf \times (4\,ft \times 8\,ft) \times \frac{7.63}{12}\,ft = 7.4\,kips$

(6) From Figure C-1, $\phi M_{n\_east} = 387kips \cdot ft + \frac{29.1kips}{56kips} \times (718 - 387)kips \cdot ft = 558.9kips \cdot ft$

(7) From Figure C-2, $\phi M_{n\_west} = 610kips \cdot ft + \frac{30.6kips}{69kips} \times (941 - 610)kips \cdot ft = 757.0kips \cdot ft$

(8) From Figure C-4, $\phi M_{n\_east} = 147kips \cdot ft + \frac{14.8kips}{27kips} \times (181 - 147)kips \cdot ft = 165.7kips \cdot ft$

(9) From Figure C-3, $\phi M_{n\_west} = 88kips \cdot ft + \frac{13.3kips}{38kips} \times (161 - 88)kips \cdot ft = 113.5kips \cdot ft$

(10) From Figure C-6, $\phi M_n = 397kips \cdot ft + \frac{7.4kips}{30kips} \times (492 - 397)kips \cdot ft = 420.4kips \cdot ft$

(11) $V(\phi M_{n\_east}) = \frac{\phi M_{n\_east}}{height} = \frac{558.9kips \cdot ft}{8\,ft} = 69.9kips$

(12) $V(\phi M_{n\_west}) = \frac{\phi M_{n\_west}}{height} = \frac{757.0kips \cdot ft}{8\,ft} = 94.6kips$

(13) $V(\phi M_{n\_east}) = \frac{\phi M_{n\_east}}{height} = \frac{165.7kips \cdot ft}{8\,ft} = 20.7kips$

(14) $V\left(\phi M_{n\_west}\right)=\dfrac{\phi M_{n\_west}}{height}=\dfrac{113.5kips\cdot ft}{8\,ft}=14.2kips$

(15) $V\left(\phi M_{n}\right)=\dfrac{\phi M_{n}}{height}=\dfrac{420.4kips\cdot ft}{8\,ft}=52.5kips$

(16) $V\left(M_{n\_east}\right)=\dfrac{V\left(\phi M_{n\_east}\right)}{0.9}=\dfrac{69.9kips}{0.9}=77.6kips$

(17) $V\left(M_{n\_west}\right)=\dfrac{V\left(\phi M_{n\_west}\right)}{0.9}=\dfrac{94.6kips}{0.9}=105.1kips$

(18) $V\left(M_{n\_east}\right)=\dfrac{V\left(\phi M_{n\_east}\right)}{0.9}=\dfrac{20.7kips}{0.9}=23.0kips$

(19) $V\left(M_{n\_west}\right)=\dfrac{V\left(\phi M_{n\_west}\right)}{0.9}=\dfrac{14.2kips}{0.9}=15.8kips$

(20) $V\left(M_{n}\right)=\dfrac{V\left(\phi M_{n}\right)}{0.9}=\dfrac{52.5kips}{0.9}=58.4kips$

(21) $\phi V_{nm\_east}=0.8\times\left[\left\{4.0-1.75\left(\dfrac{M_u}{V_u}\times\dfrac{1}{d_v}\right)\right\}\times A_n\times\sqrt{f'_m}+0.25P_u\right]$ * $\dfrac{M_u}{V_u\times d_v}\le 1$

$=0.8\times\left[\left\{4.0-1.75\left(8\,ft\times\dfrac{1}{12\,ft}\right)\right\}\times(144\times 7.63)in^2\times\sqrt{1500}\,psi+0.25\times 29.1kips\right]=102.3kips$

(22) $\phi V_{nm\_west}=0.8\times\left[\{2.83\}\times(144\times 7.63)in^2\times\sqrt{1500}\,psi+0.25\times 30.6kips\right]=102.6kips$

(23) $\phi V_{nm\_east}=0.8\times\left[\left\{4.0-1.75\left(\dfrac{M_u}{V_u}\times\dfrac{1}{d_v}\right)\right\}\times A_n\times\sqrt{f'_m}+0.25P_u\right]$ * $\dfrac{M_u}{V_u\times d_v}\le 1$

$=0.8\times\left[\{2.25\}\times(48\times 7.63)in^2\times\sqrt{1500}\,psi+0.25\times 14.8kips\right]=28.5kips$

(24) $\phi V_{nm\_west}=0.8\times\left[\{2.25\}\times(48\times 7.63)in^2\times\sqrt{1500}\,psi+0.25\times 13.3kips\right]=28.2kips$

(25) $\phi V_{nm}=0.8\times\left[\left\{4.0-1.75\left(\dfrac{M_u}{V_u}\times\dfrac{1}{d_v}\right)\right\}\times A_n\times\sqrt{f'_m}+0.25P_u\right]$ * $\dfrac{M_u}{V_u\times d_v}\le 1$

$$= 0.8 \times \left[\{2.25\} \times (96 \times 7.63) in^2 \times \sqrt{1500}\, psi + 0.25 \times 7.4 kips \right] = 52.5 kips$$

(26) $\phi V_{n\_east} = \phi V_{nm\_east} + \phi V_{ns} = 102.3 kips + 0.8 \times 0.5 A_v f_y \left(\frac{d_v}{s} \right)$ * $d_v \le height$

$$= 102.3 kips + 0.4 \times 0.2 in^2 \times 60 ksi \times \left(\frac{96 in.}{16 in.} \right) = 102.3 kips + 28.8 kips = 131.1 kips$$

(27) $\phi V_{n\_west} = \phi V_{nm\_west} + \phi V_{ns} = 102.6 kips + 28.8 kips = 131.4 kips$

(28) $\phi V_{n\_east} = \phi V_{nm\_east} + \phi V_{ns} = 28.5 kips + 0.8 \times 0.5 A_v f_y \left(\frac{d_v}{s} \right)$ * $d_v \le height$

$$= 28.5 kips + 0.4 \times 0.2 in^2 \times 60 ksi \times \left(\frac{48 in.}{16 in.} \right) = 28.5 kips + 14.4 kips = 42.9 kips$$

(29) $\phi V_{n\_west} = \phi V_{nm\_west} + \phi V_{ns} = 28.2 kips + 14.4 kips = 42.6 kips$

(30) $\phi V_n = \phi V_{nm} + \phi V_{ns} = 52.5 kips + 0.8 \times 0.5 A_v f_y \left(\frac{d_v}{s} \right)$ * $d_v \le height$

$$= 52.5 kips + 0.4 \times 0.2 in^2 \times 60 ksi \times \left(\frac{96 in.}{16 in.} \right) = 52.5 kips + 28.8 kips = 81.3 kips$$

(31) $\phi V_{n\_sliding\_east} = 0.8 \times \mu \times \left(N_{weight} + N_{bars} \right) = 0.8 \times 1.0 \times \left(29.1 kips + 7 \times 60 ksi \times 0.2 in^2 \right) = 90.5 kips$

(32) $\phi V_{n\_sliding\_west} = 0.8 \times \mu \times \left(N_{weight} + N_{bars} \right) = 0.8 \times 1.0 \times \left(30.6 kips + 8 \times 60 ksi \times 0.2 in^2 \right) = 101.3 kips$

(33) $\phi V_{n\_sliding\_east} = 0.8 \times \mu \times \left(N_{weight} + N_{bars} \right) = 0.8 \times 1.0 \times \left(14.8 kips + 6 \times 60 ksi \times 0.2 in^2 \right) = 69.5 kips$

(34) $\phi V_{n\_sliding\_west} = 0.8 \times \mu \times \left(N_{weight} + N_{bars} \right) = 0.8 \times 1.0 \times \left(13.3 kips + 5 \times 60 ksi \times 0.2 in^2 \right) = 58.6 kips$

(35) $\phi V_{n\_sliding} = 0.8 \times \mu \times \left(N_{weight} + N_{bars} \right) = 0.8 \times 1.0 \times \left(7.4 kips + 7 \times 60 ksi \times 0.2 in^2 \right) = 73.1 kips$

(36) $V\left(M_{n\_\exp\_east} \right) = V\left(M_n \right) \times \frac{86 ksi}{60 ksi} = 77.6 kips \times 1.43 = 111.3 kips$

(37) $V\left(M_{n\_\exp\_east} \right) = V\left(M_n \right) \times \frac{86 ksi}{60 ksi} = 105.1 kips \times 1.43 = 150.7 kips$

(38) $V\left(M_{n\_\exp\_east} \right) = V\left(M_n \right) \times \frac{86 ksi}{60 ksi} = 23.0 kips \times 1.43 = 33.0 kips$

(39) $V\left(M_{n\_\exp\_west} \right) = V\left(M_n \right) \times \frac{86 ksi}{60 ksi} = 15.8 kips \times 1.43 = 22.6 kips$

(40) $$V_{n\_\exp\_east} = \frac{\phi V_{nm\_east}}{\phi} + \frac{\phi V_{ns}}{\phi} \times \frac{86ksi}{60ksi} = \frac{102.3kips}{0.8} + \frac{28.8kips}{0.8} \times 1.43 = 179.4kips$$

(41) $$V_{n\_\exp\_west} = \frac{\phi V_{nm\_west}}{\phi} + \frac{\phi V_{ns}}{\phi} \times \frac{86ksi}{60ksi} = \frac{102.6kips}{0.8} + \frac{28.8kips}{0.8} \times 1.43 = 179.8kips$$

(42) $$V_{n\_\exp\_east} = \frac{\phi V_{nm\_east}}{\phi} + \frac{\phi V_{ns}}{\phi} \times \frac{86ksi}{60ksi} = \frac{28.5kips}{0.8} + \frac{14.4kips}{0.8} \times 1.43 = 61.4kips$$

(43) $$V_{n\_\exp\_west} = \frac{\phi V_{nm\_west}}{\phi} + \frac{\phi V_{ns}}{\phi} \times \frac{86ksi}{60ksi} = \frac{28.2kips}{0.8} + \frac{14.4kips}{0.8} \times 1.43 = 61.0kips$$

(44) $$V_{n\_sliding\_\exp\_east} = \mu \times \left(N_{weight} + N_{bars}\right) = 1.0 \times \left(29.1kips + 7 \times 86ksi \times 0.2in^2\right) = 149.5kips$$

(45) $$V_{n\_sliding\_\exp\_west} = \mu \times \left(N_{weight} + N_{bars}\right) = 1.0 \times \left(30.6kips + 8 \times 86ksi \times 0.2in^2\right) = 168.2kips$$

(46) $$V_{n\_sliding\_\exp\_east} = \mu \times \left(N_{weight} + N_{bars}\right) = 1.0 \times \left(14.8kips + 6 \times 86ksi \times 0.2in^2\right) = 118.0kips$$

(47) $$V_{n\_sliding\_\exp\_west} = \mu \times \left(N_{weight} + N_{bars}\right) = 1.0 \times \left(13.3kips + 5 \times 86ksi \times 0.2in^2\right) = 99.3kips$$

(48) $$W_{eff} = W_{roof} + W_{CMU\_eff} = \left(136.5psf \times 20ft \times 20ft\right) + \frac{1}{2} \times \left\{120pcf \times \left(80ft - 4 \times 4ft\right) \times 8ft \times \frac{7.63}{12}ft\right\}$$

$$= 54.6kips + 19.5kips = 74.1kips$$

(49) $$\ddot{u}_{g\_required\_east} = \frac{V\left(M_{n\_\exp\_east}\right)}{1.5 \times W_{eff}} = \frac{2 \times \left(111.3kips + 33.0kips\right)}{1.5 \times 74.1kips} = \frac{288.5kips}{1.5 \times 74.1kips} = 2.59g$$

(50) $$\ddot{u}_{g\_required\_west} = \frac{V\left(M_{n\_\exp\_west}\right)}{1.5 \times W_{eff}} = \frac{2 \times \left(150.7kips + 22.6kips\right)}{1.5 \times 74.1kips} = \frac{346.6kips}{1.5 \times 74.1kips} = 3.12g$$

(51) $$W_{eff} = W_{roof} + W_{CMU\_eff} = \left(136.5psf \times 20ft \times 20ft\right) + \frac{1}{2} \times \left\{120pcf \times \left(80ft - 4 \times 4ft\right) \times 8ft \times \frac{7.63 + 3.63}{12}ft\right\}$$

$$= 54.6kips + 28.8kips = 83.4kips$$

(52) $$\ddot{u}_{g\_required\_east} = \frac{V\left(M_{n\_\exp\_east}\right)}{1.5 \times W_{eff}} = \frac{2 \times \left(111.3kips + 33.0kips\right)}{1.5 \times 83.4kips} = \frac{288.5kips}{1.5 \times 83.4kips} = 2.31g$$

(53) $$\ddot{u}_{g\_required\_west} = \frac{V\left(M_{n\_\exp\_west}\right)}{1.5 \times W_{eff}} = \frac{2 \times \left(150.7kips + 22.6kips\right)}{1.5 \times 83.4kips} = \frac{346.6kips}{1.5 \times 83.4kips} = 2.77g$$

C.3 IN-PLANE STIFFNESS CALCULATIONS FOR 12-FT AND 4-FT WALLS

The in-plane stiffnesses of the 12-ft long and 4-ft long CMU walls are calculated based on elastic theory. Both flexural stiffness and shear stiffness are considered. To be consistent with the calculation of flexural and shear strengths, the effective flange is considered for flexural stiffness but disregarded for shear stiffness. For the flexural stiffness, the effective flange width of 48 in. is used whether the flange is in tension or compression. In the 2008 MSJC Code, the effective flange width depends on whether the flange is in tension or compression. In this section, however, only one effective flange width (48 in. from the flange under compression) is used for simplicity, because the purpose of this section is to simply and approximately evaluate the in-plane stiffness of the wall segments. For shear stiffness, the effective flange is ignored, and accordingly the web area only is considered. The calculations for the in-plane stiffness of each wall segment are described below step by step.

$l = 96\,in.$

$E_m = 0.5 \times 900\ f'_m = 450 \times 1500\,psi = 675\,ksi$ * 0.5: factor for cracked section

$G = E_v = 0.4\,E_v = 0.4 \times 675\,ksi = 270\,ksi$

$$\bar{x}_{12\,ft} = \frac{7.63\,in. \times 144\,in. \times \frac{144\,in.}{2} + 48\,in. \times 7.63\,in. \times \frac{7.63\,in.}{2}}{7.63\,in. \times 144\,in. + 48\,in. \times 7.63\,in.} = 54.0\,in.$$

* $\bar{x}$: center of gravity of section measured from the flanged edge

$$I_{12\,ft} = \sum\left(\frac{bh^3}{12} + Ad^2\right) = \left\{\frac{7.63\,in. \times (144\,in.)^3}{12} + (7.63\,in. \times 144\,in.) \times \left(\frac{144\,in.}{2} - 54.0\,in.\right)^2\right\}$$

$$+ \left\{\frac{48\,in. \times (7.63\,in.)^3}{12} + (48\,in. \times 7.63\,in.) \times \left(\frac{7.63\,in.}{2} - 54.0\,in.\right)^2\right\} = 3.18 \times 10^6\,in.^4$$

$$k_{m\_12\,ft} = \frac{3\,E\,I_{12\,ft}}{l^3} = 7.28 \times 10^3\ kips/in.$$

$$A_{v\_12\,ft} = 7.63\,in. \times 144\,in. = 1099\,in.^2$$

$$k_{v\_12\,ft} = \frac{A_{v\_12\,ft}\,G}{1.2\,l} = 2.58 \times 10^3 \; kips/in.$$ * 1.2: form factor for rectangular section

$$K_{12\,ft} = \frac{k_{m\_12\,ft} \times k_{v\_12\,ft}}{k_{m\_12\,ft} + k_{v\_12\,ft}} = 1.90 \times 10^3 \; kips/in.$$

$$\bar{x}_{4\,ft} = \frac{7.63\,in. \times 48\,in. \times \frac{144\,in.}{2} + 48\,in. \times 7.63\,in. \times \frac{7.63\,in.}{2}}{7.63\,in. \times 48\,in. + 48\,in. \times 7.63\,in.} = 12.0\,in.$$

* $\bar{x}$: center of gravity of section measured from the flanged edge

$$I_{4\,ft} = \sum\left(\frac{bh^3}{12} + Ad^2\right) = \left\{\frac{7.63\,in. \times (48\,in.)^3}{12} + (7.63\,in. \times 48\,in.) \times \left(\frac{48\,in.}{2} - 12.0\,in.\right)^2\right\}$$

$$+ \left\{\frac{48\,in. \times (7.63\,in.)^3}{12} + (48\,in. \times 7.63\,in.) \times \left(\frac{7.63\,in.}{2} - 12.0\,in.\right)^2\right\} = 0.571 \times 10^6\,in.^4$$

$$k_{m\_4\,ft} = \frac{3\,E\,I_{4\,ft}}{l^3} = 1.31 \times 10^3 \; kips/in.$$

$$A_{v\_4\,ft} = 7.63\,in. \times 48\,in. = 366\,in.^2$$

$$k_{v\_4\,ft} = \frac{A_{v\_4\,ft}\,G}{1.2\,l} = 0.86 \times 10^3 \; kips/in.$$ * 1.2: form factor for rectangular section

$$K_{4\,ft} = \frac{k_{m\_4\,ft} \times k_{v\_4\,ft}}{k_{m\_4\,ft} + k_{v\_4\,ft}} = 0.52 \times 10^3 \; kips/in.$$

$$\frac{K_{12\,ft}}{K_{4\,ft}} = \frac{1.90 \times 10^3 \; kips/in.}{0.52 \times 10^3 \; kips/in.} = 3.67$$

C.4 STRENGTH INTERACTION DIAGRAMS FOR WALL SEGMENTS

In Figure C-1 is given the in-plane interaction diagram for the 12-ft wall segment, loaded with the flange in compression (that is, loaded to the east). The curve gives

combinations of design axial and flexural capacities, without the flange and with the flange. The straight lines give the moment associated with the design shear capacity from masonry, and the design shear capacity from masonry plus horizontal reinforcement. As the axial load increases from zero to about 100 kips, the design flexural capacity including the flange becomes greater than the moment associated with the design shear capacity including horizontal reinforcement, indicating that shear-dominated failure becomes more likely. This is consistent with but not identical to the capacity-design approach of the 2008 MSJC Code.

In Figure C-2 is given the corresponding in-plane interaction diagram for the 12-ft wall segment, loaded with the flange in tension (that is, loaded to the west); in Figure C-3 is given the in-plane interaction diagram for the 4-ft wall segment, loaded with the flange in compression (that is, loaded to the west); in Figure C-4 is given the corresponding in-plane interaction diagram for the 4-ft wall segment, loaded with the flange in tension (that is, loaded to the east); in Figure C-5 is given the out-of-plane interaction diagram for the 8-ft wall segment; and in Figure C-6 is given the in-plane interaction diagram for the 8-ft wall segment, loaded with the flange in tension.

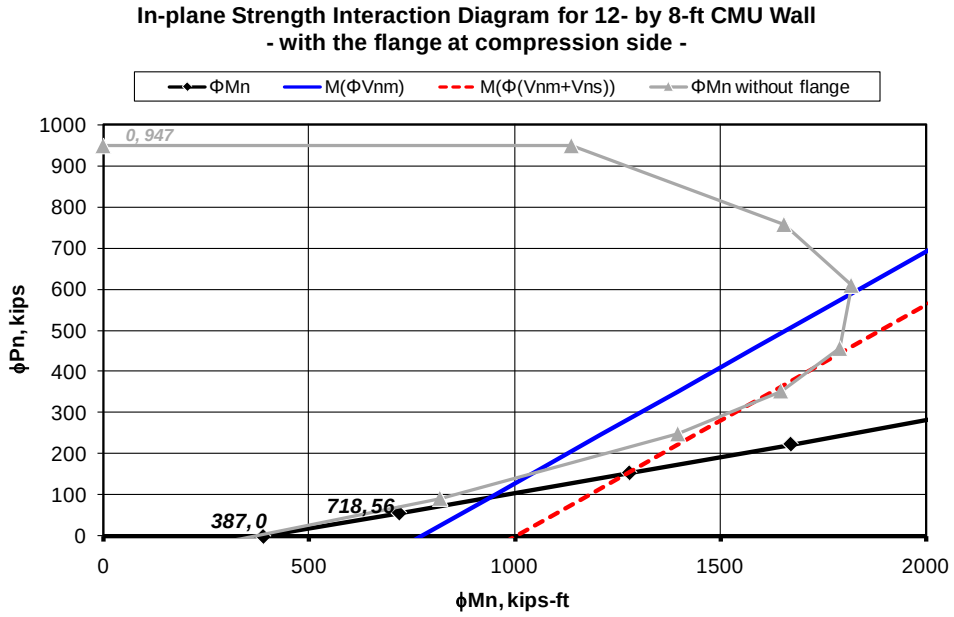

Figure C-1 In-plane strength interaction diagram of a 12-ft long wall with the flange in compression (loaded to east)

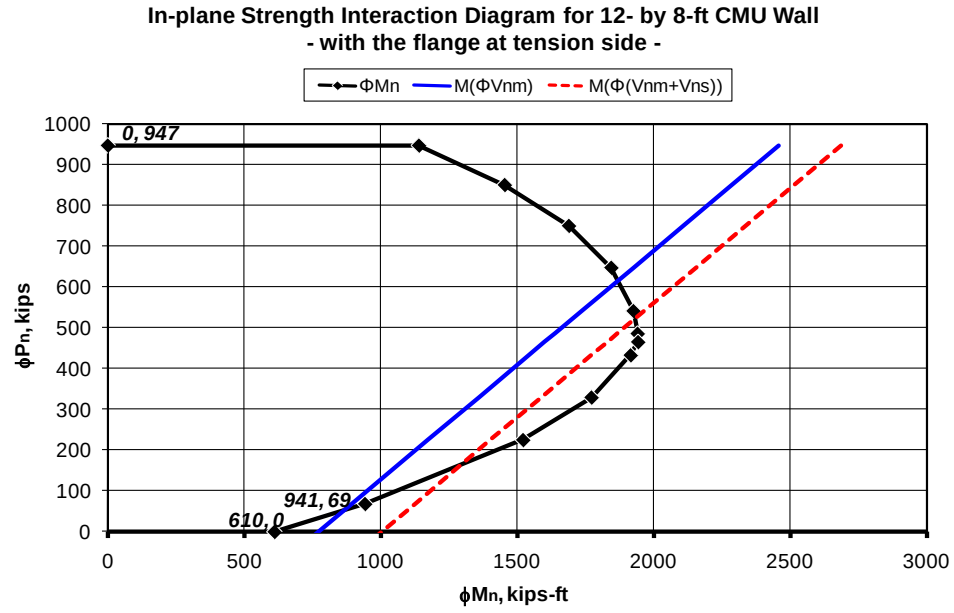

Figure C-2 In-plane strength interaction diagram of a 12-ft long wall with the flange in tension (loaded to west)

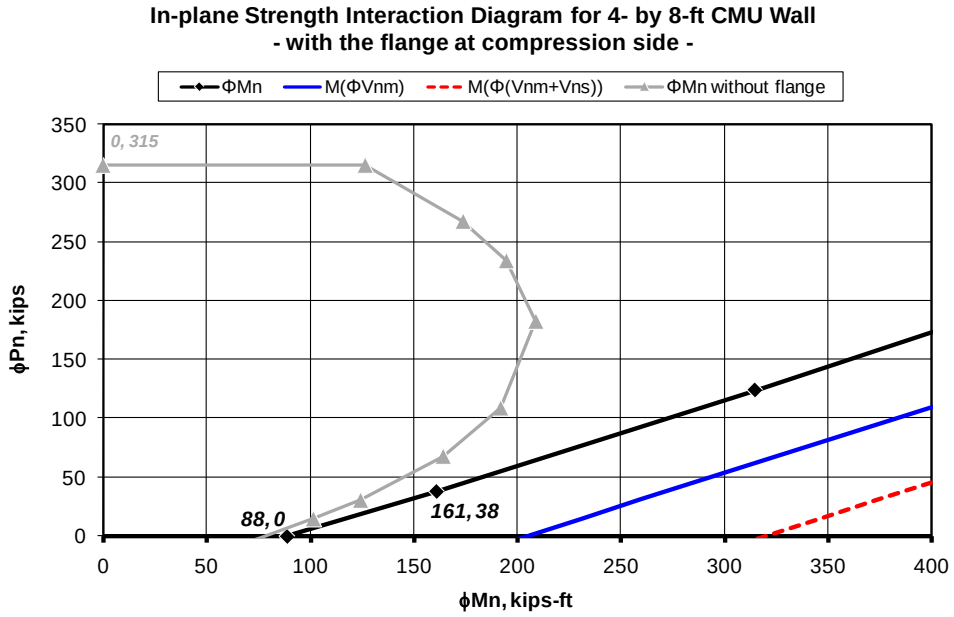

Figure C-3 In-plane strength interaction diagram of a 4-ft long wall with the flange in compression (loaded to west)

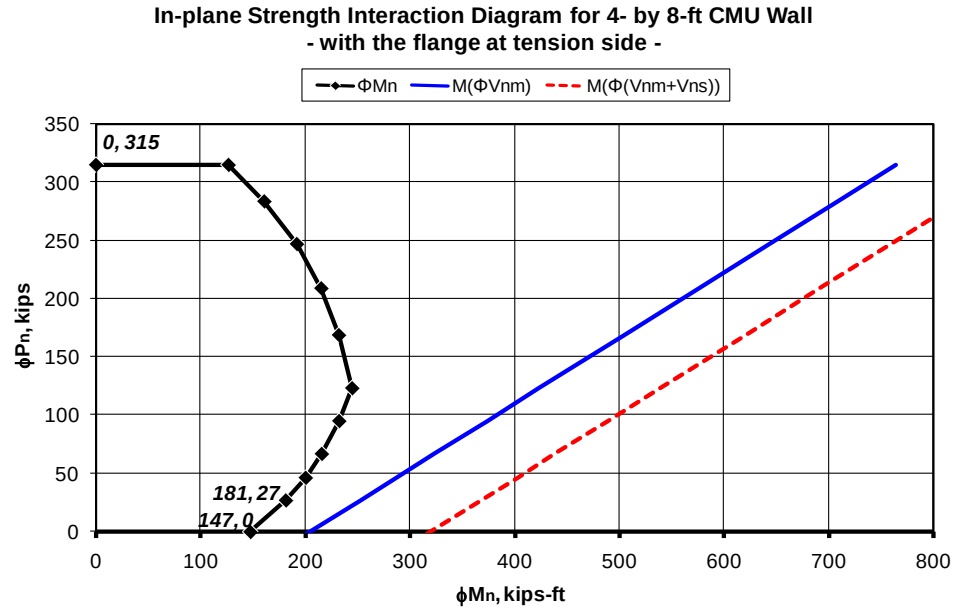

Figure C-4 In-plane strength interaction diagram of a 4-ft long wall with the flange in tension (loaded to east)

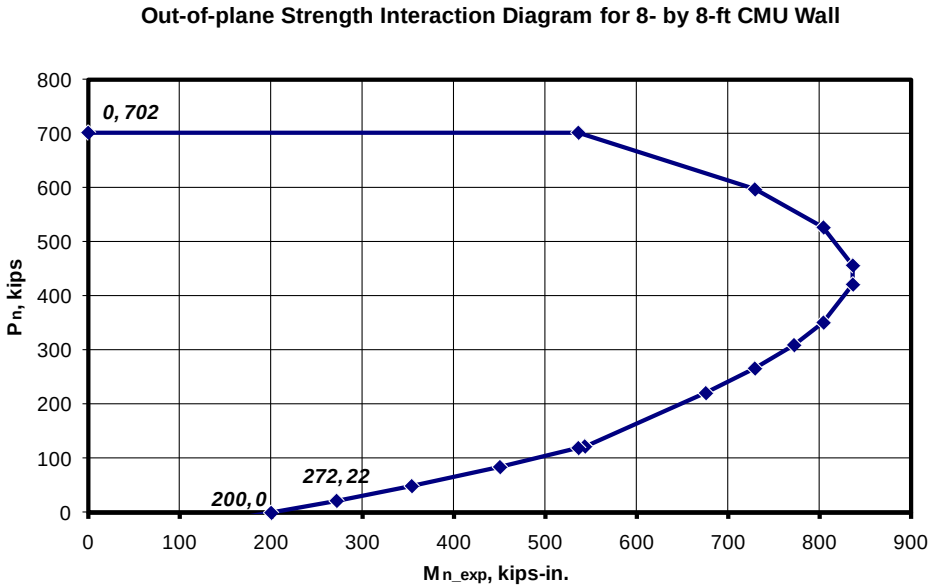

Figure C-5 Out-of-plane strength interaction diagram of an 8-ft long wall

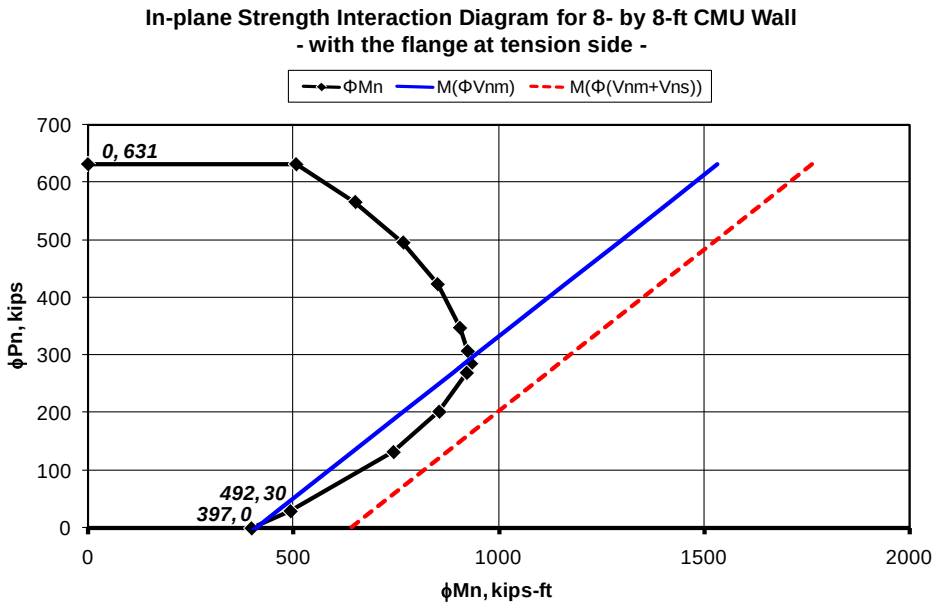

Figure C-6 In-plane strength interaction diagram of an 8-ft long wall with flange in tension

APPENDIX D

Instrumentation for CMU Building Specimen

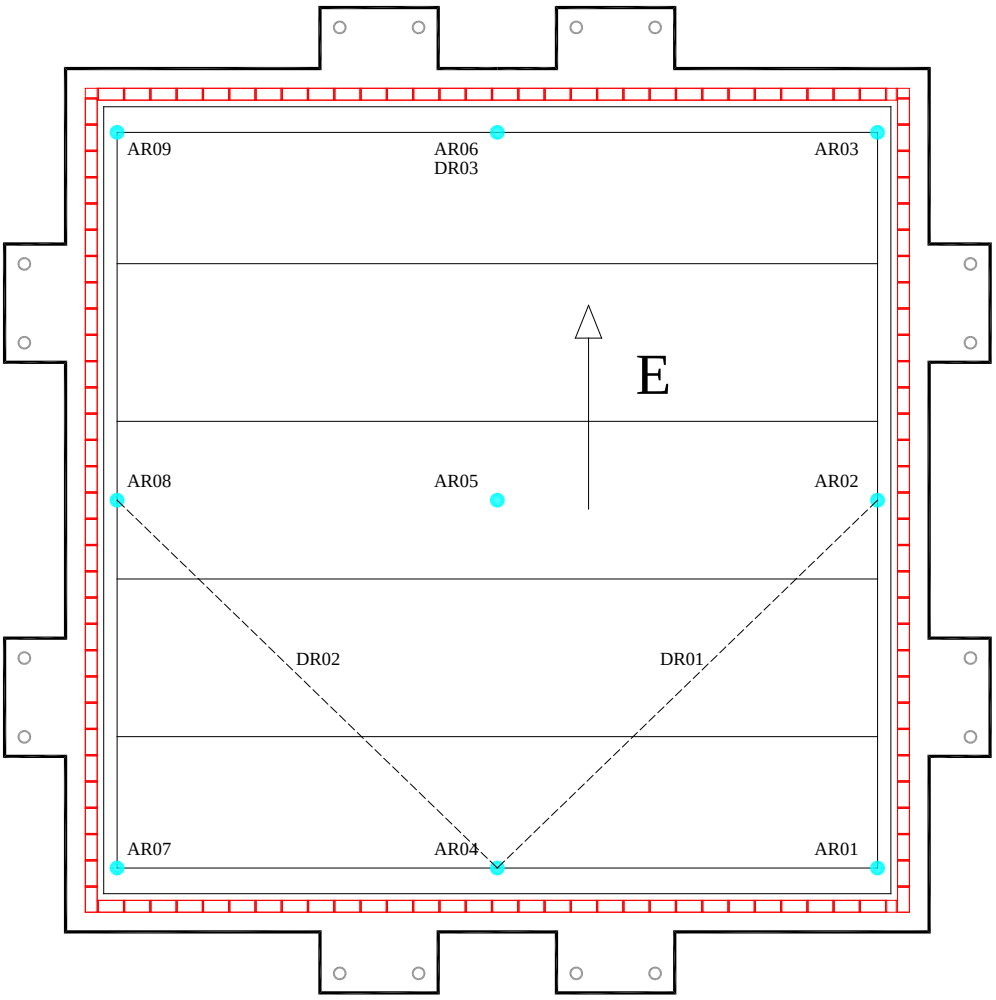

Figure D-1 Instrumentation for CMU building specimen (roof diaphragm)

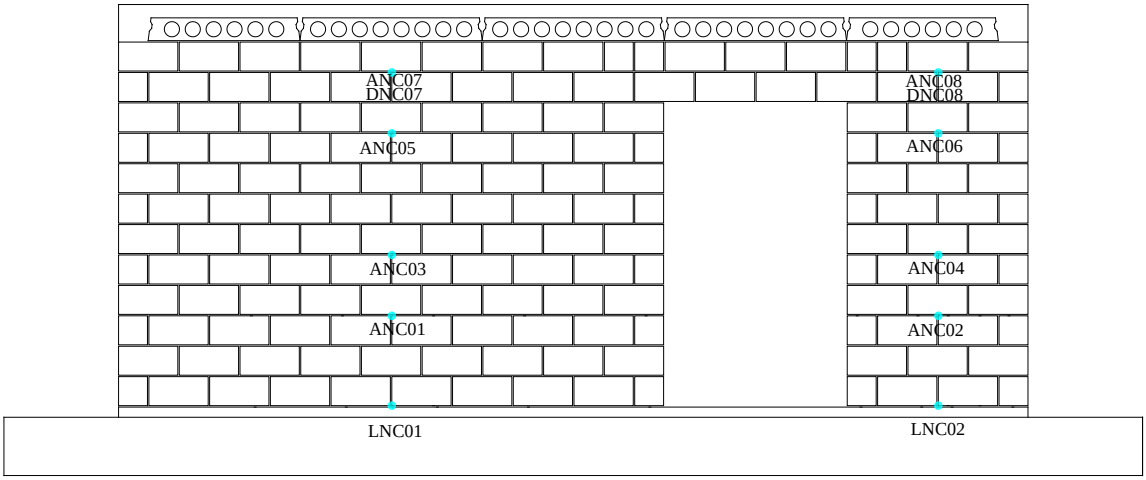

North Elevation - CMU

Figure D-2 Instrumentation for CMU building specimen (north, CMU)

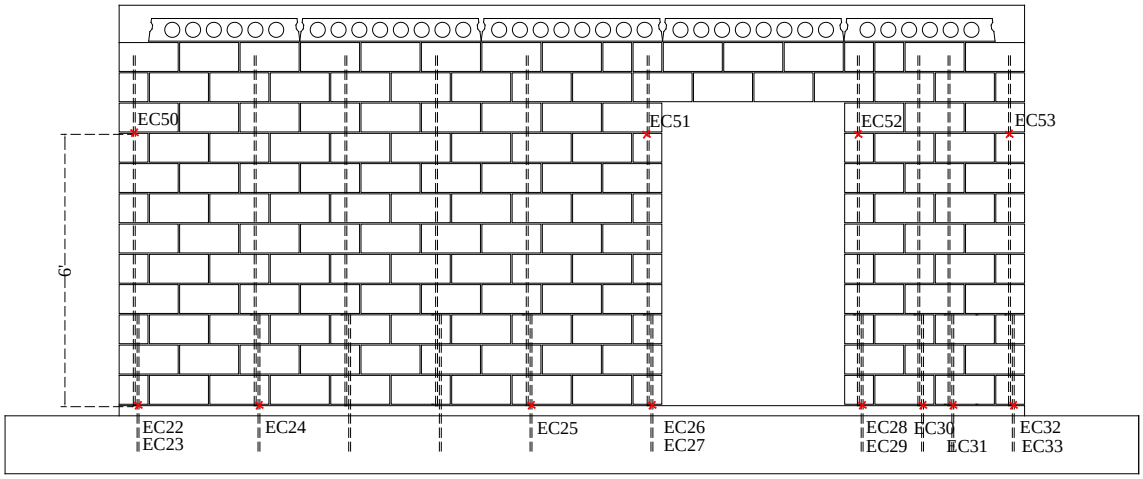

North Elevation - CMU

Figure D-3 Instrumentation for CMU building specimen (north, reinforcement)

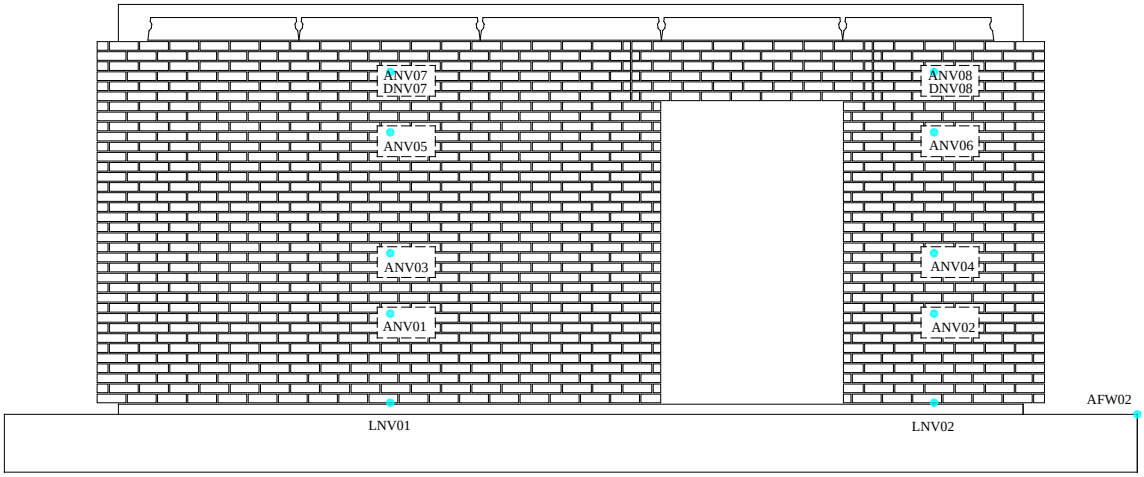

North Elevation - Veneer

Figure D-4 Instrumentation for CMU building specimen (north, veneer)

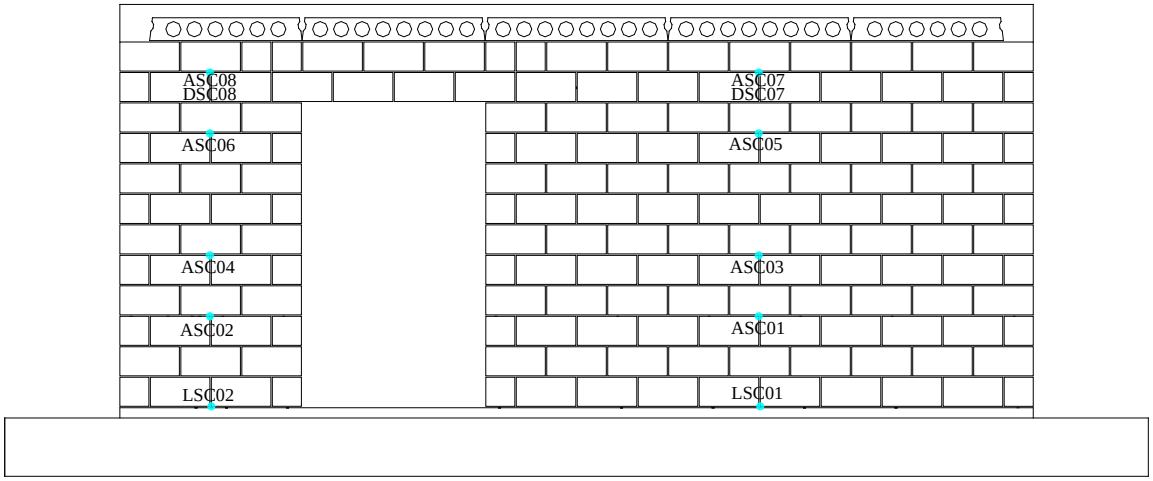

South Elevation - CMU

Figure D-5 Instrumentation for CMU building specimen (south, CMU)

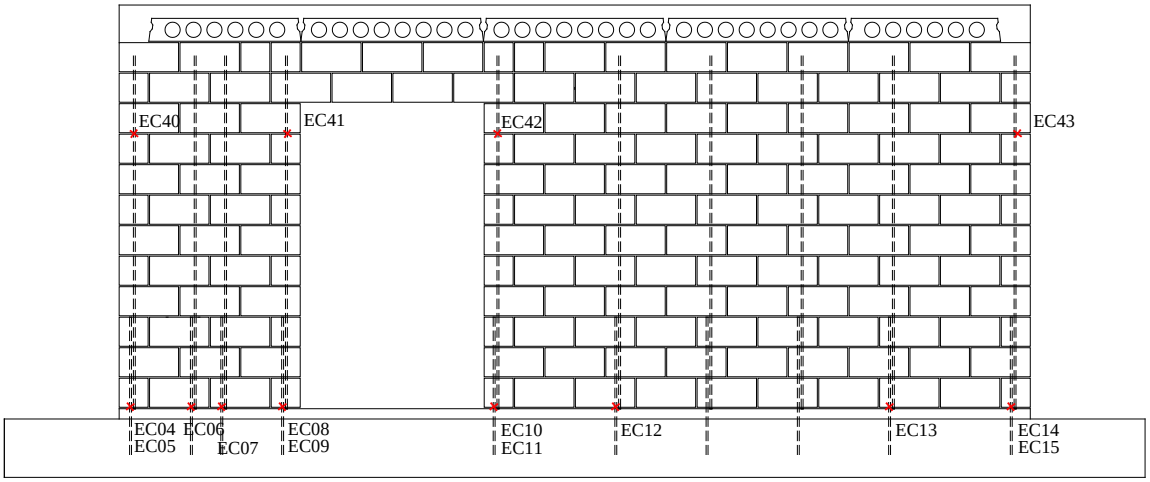

South Elevation - CMU

Figure D-6 Instrumentation for CMU building specimen (south, reinforcement)

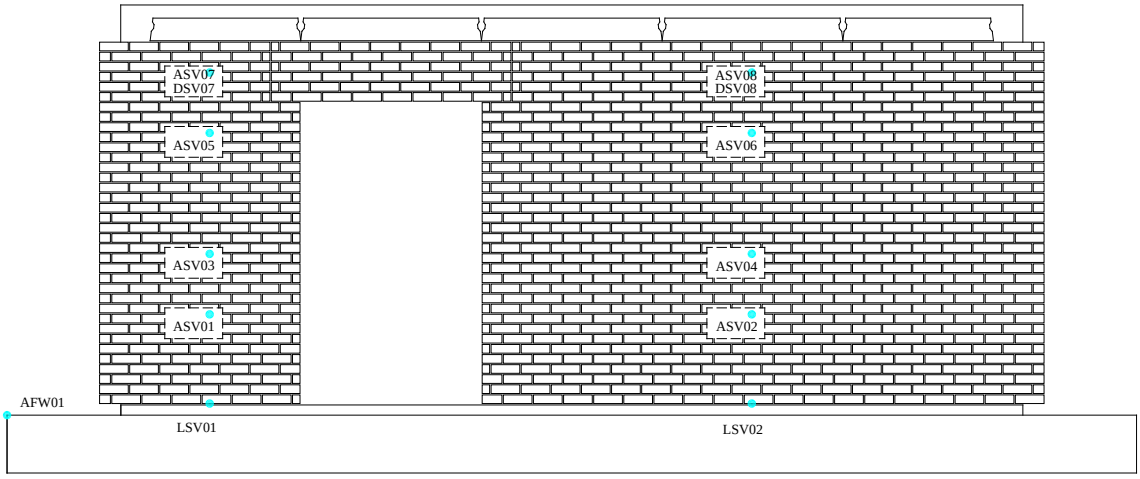

South Elevation - Veneer

Figure D-7 Instrumentation for CMU building specimen (south, veneer)

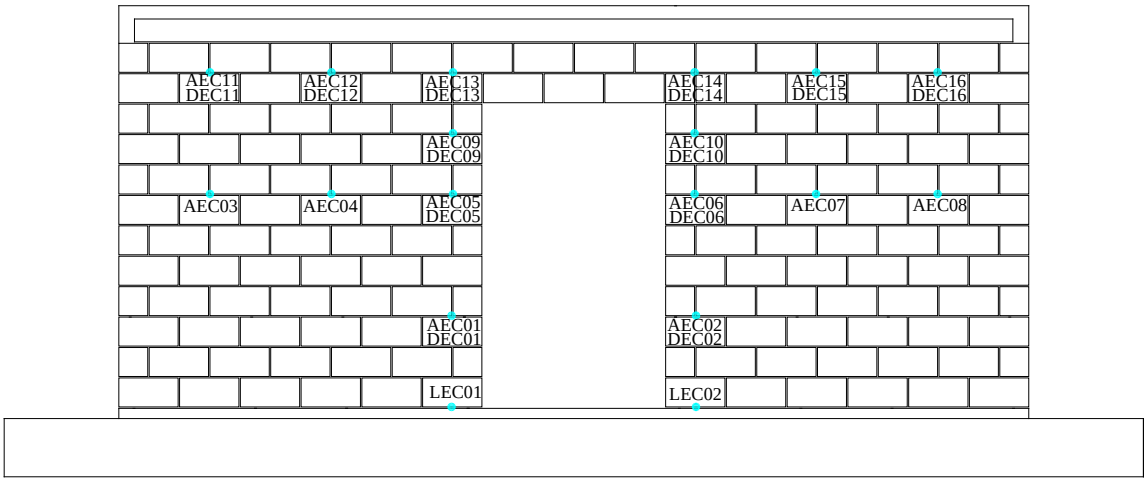

East Elevation - CMU

Figure D-8 Instrumentation for CMU building specimen (east, CMU)

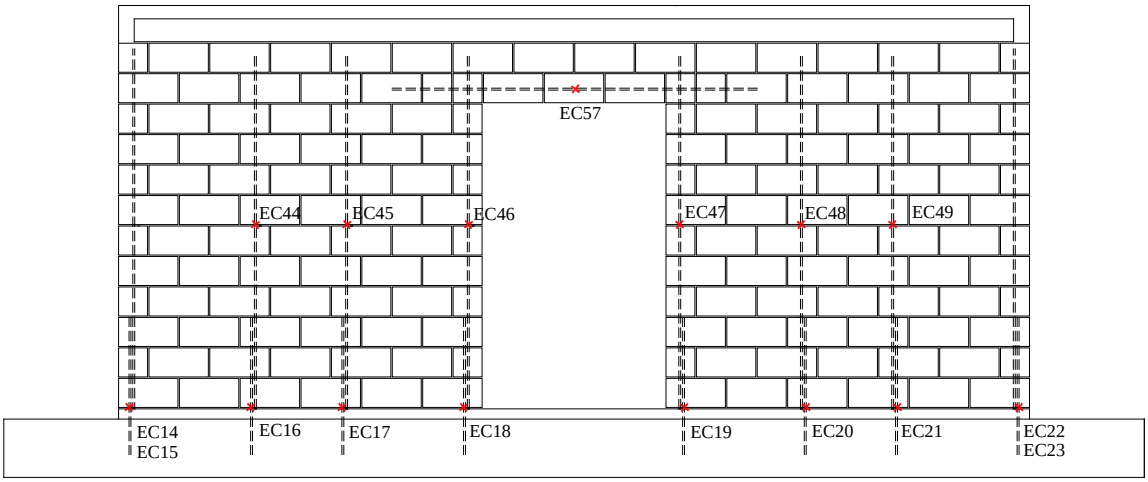

East Elevation - CMU

Figure D-9 Instrumentation for CMU building Specimen (east, reinforcement)

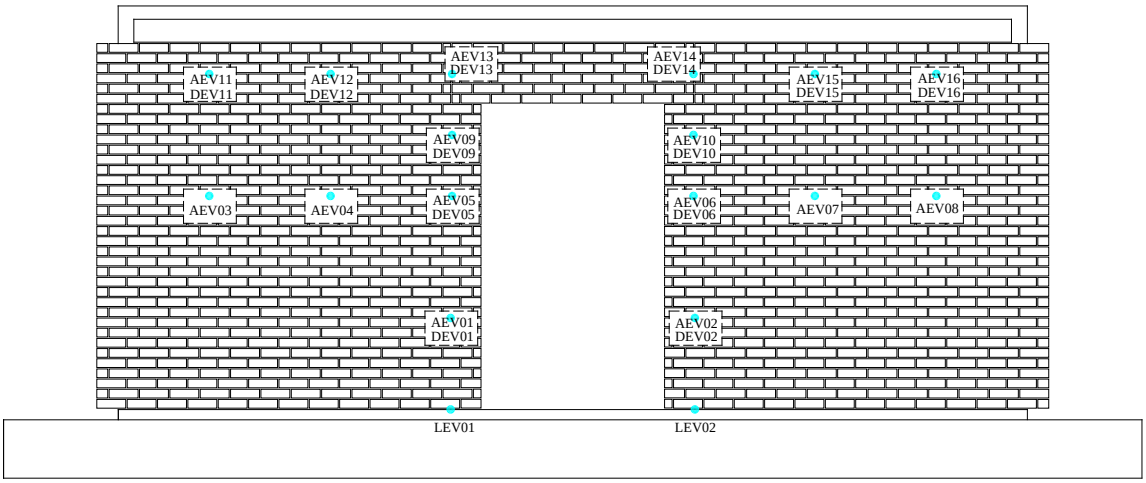

East Elevation - Veneer

Figure D-10 Instrumentation for CMU building specimen (east, veneer)

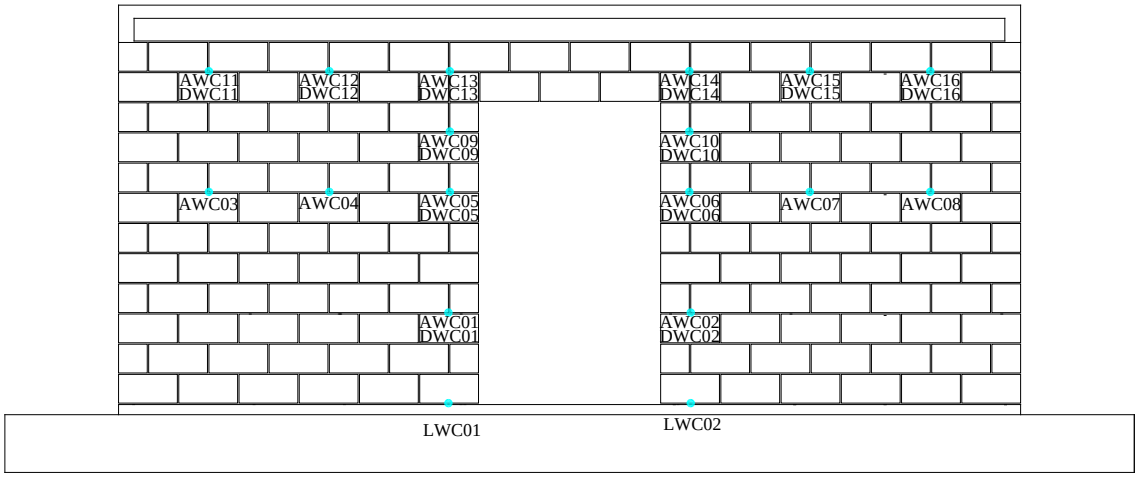

West Elevation - CMU

Figure D-11 Instrumentation for CMU building specimen (west, CMU)

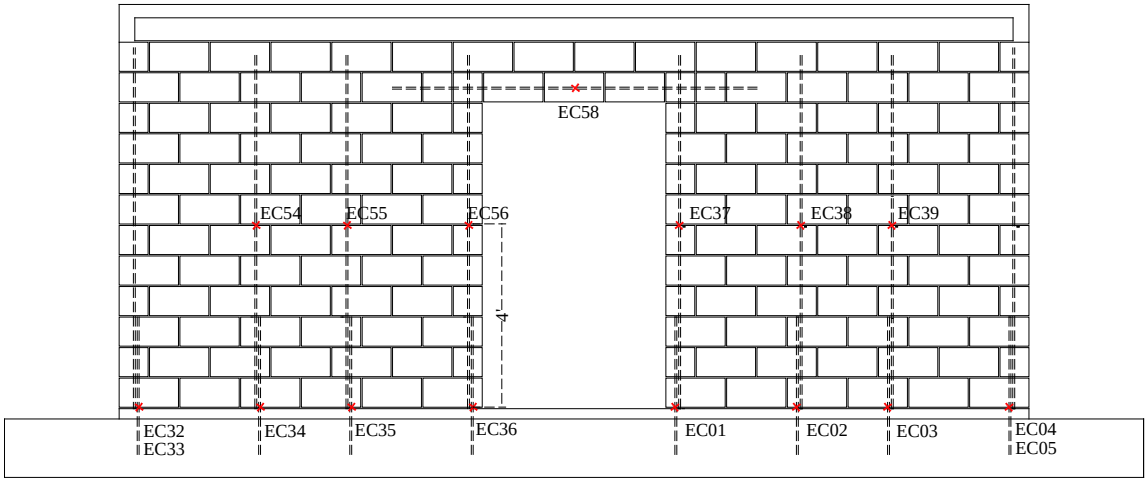

West Elevation - CMU

Figure D-12 Instrumentation for CMU building specimen (west, reinforcement)

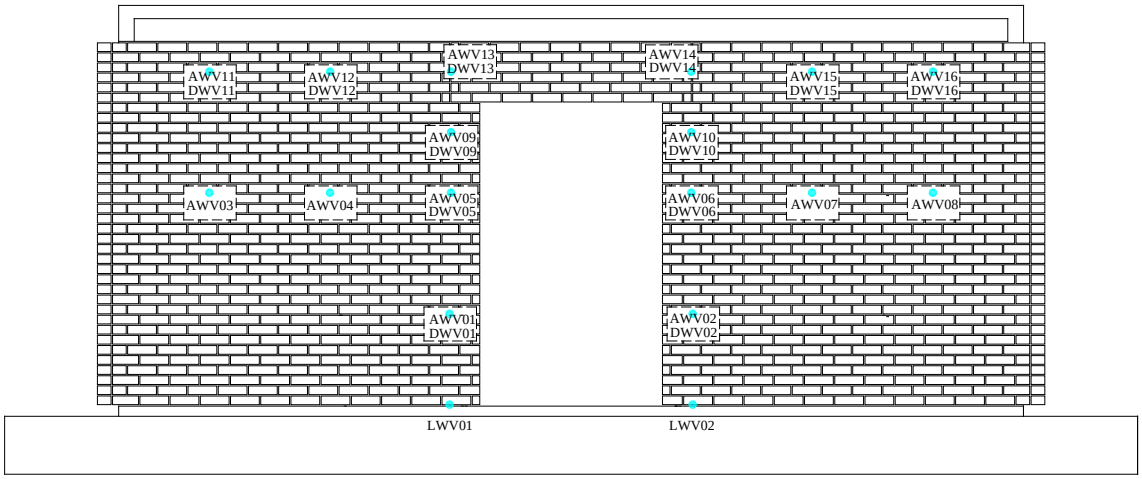

West Elevation - Veneer

Figure D-13 Instrumentation for CMU building specimen (west, veneer)

REFERENCES

1. ACI 318-08 (2008): “Building Code Requirements for Structural Concrete (ACI 318-08) and Commentary (ACI 318R-08),” American Concrete Institute, Farmington Hills, Michigan.

2. ASCE 7-05 (2005): “Minimum Design Loads for Buildings and Other Structures (ASCE 7-05) (with Supplement),” American Society of Civil Engineers, Reston, Virginia.

3. Assis, G. F., Hamid, A. A., and Harry, H. G. (1989): "Material Models for Grouted Block Masonry," U.S.-Japan Coordinated Program for Masonry Building Research Report No. 1.2(a)-2, Drexel University, Philadelphia, Pennsylvania.

4. ASTM A370-05 (2005): “Standard Test Methods and Definitions for Mechanical Testing of Steel Products,” American Society for Testing and Materials, West Conshohocken, PA.

5. ASTM C109-05 (2005): “Standard Test Method for Compressive Strength of Hydraulic Cement Mortars (Using 2-in. or [50-mm] Cube Specimens),” American Society for Testing and Materials, West Conshohocken, PA.

6. ASTM C140-07 (2007): “Standard Test Methods for Sampling and Testing Concrete Masonry Units and Related Units,” American Society for Testing and Materials, West Conshohocken, PA.

7. ASTM C780-06 (2006): “Standard Test Method for Preconstruction and Construction Evaluation of Mortars for Plain and Reinforced Unit Masonry,” American Society for Testing and Materials, West Conshohocken, PA.

8. ASTM C1019-07 (2007): “Standard Test Method for Sampling and Testing Grout,” American Society for Testing and Materials, West Conshohocken, PA.

9. ASTM C1072-06 (2006): “Standard Test Method for Measurement of Masonry Flexural Bond Strength,” American Society for Testing and Materials, West Conshohocken, PA.

10. ASTM C1314-07 (2007): “Standard Test Method for Compressive Strength of Masonry Prisms,” American Society for Testing and Materials, West Conshohocken, PA.

11. ASTM C1357-05 (2005): "Standard Test Methods for Evaluating Masonry Bond Strength," American Society for Testing and Materials, West Conshohocken, PA.

12. ASTM C1552-03a (2003): "Standard Practice for Capping Concrete Masonry Units, Related Units and Masonry Prisms for Compression Testing," American Society for Testing and Materials, West Conshohocken, PA.

13. Chopra, A. K. (2001): "Dynamics of Structures: Theory and Applications to Earthquake Engineering," 2nd Ed., New Jersey, Prentice Hall.

14. FEMA 461 (2007): "Interim Testing Protocols for Determining the Seismic Performance Characteristics of Structural and Nonstructural Components," Applied Technology Council, Redwood City, California.

15. Ghobarah, Ahmed (2001): "Performance-based design in earthquake engineering: State of development," Engineering Structures, Vol. 23, No. 8, 878-884.

16. He, L. and Priestley, M. J. N. (1992): "Seismic Behavior of Flanged Masonry Walls," University of California, San Diego, Department of Applied Mechanics and Engineering Sciences, Report No. SSRP-92/09.

17. Leiva, G., Klingner, R. E. (1991): "In-Plane Seismic Resistance of Two-Story Concrete Masonry Shear Walls with Openings," U.S.-Japan Coordinated Program for Masonry Building Research Report No. 3.1(c)-2, PMFSEL Report No. 91-2, The University of Texas at Austin, Austin, Texas.

18. Merryman, K. M., et al. (1990): "In-Plane Seismic Resistance of Two-Story Concrete Masonry Coupled Shear Walls," U.S.-Japan Coordinated Program for Masonry Building Research Report No. 3.1.(c)-1, PMFSEL Report No. 89-3, The University of Texas at Austin, Austin, Texas.

19. MSJC 2008a (2008): "Building Code Requirements for Masonry Structures (TMS 402-08 / ACI 530-08 / ASCE 5-08)," The Masonry Society, Boulder, Colorado, the American Concrete Institute, Farmington Hills, Michigan, and the American Society of Civil Engineers, Reston, Virginia.

20. MSJC 2008b (2008): "Specification for Masonry Structures (TMS 602-08 / ACI 530.1-08 / ASCE 6-08)," The Masonry Society, Boulder, Colorado, the American Concrete Institute, Farmington Hills, Michigan, and the American Society of Civil Engineers, Reston, Virginia.

21. Reneckis D., LaFave J. M., and Clarke W. M. (2004): "Out-of-plane performance of masonry veneer walls on wood frames." Engineering Structures, Vol. 26, 1027-1042.

22. Seible, F., et al. (1992): "The U.S.-TCCMAR 5-Story Full Scale Masonry Research Building Test - Preliminary Report," University of California, San Diego, Department of Applied Mechanics and Engineering Sciences, Report No. TR-92/01.

23. Seible, F., et al. (1994): “The U.S.-TCCMAR Full-scale Five-story Masonry Research Building Test: Part I - Executive Summary,” University of California, San Diego, Department of Applied Mechanics and Engineering Sciences, Report No. SSRP-94/01.

24. Shing, P. B., et al. (1991): "Response of Single-Story Reinforced Masonry Shear Walls to In-Plane Lateral Loads," U.S.-Japan Coordinated Program for Masonry Building Research Report No. 3.1(1)-2, University of Colorado at Boulder, Boulder, Colorado.

25. Yi, J., et al. (2003): “Analysis of load in ties in masonry veneer walls,” Canadian Journal of Civil Engineering, Vol. 30, No. 5, 850-860.

VITA

Seongwoo Jo was born in Gyeongnam, South Korea on February 18, 1979, the son of Taegyu Jo and Geumok Park. After graduating from Chang-Sin High School, Gyeongnam, South Korea, in 1997, he entered Seoul National University in Seoul, South Korea. From February in 1999 to August in 2001, he serviced in the Republic of Korea Air Force. In February of 2004, he received the degree of Bachelor of Science. In August, 2004, he entered The Graduate School at The University of Texas at Austin, and completed his Master of Science degree in Engineering in December of 2006. While completing his work on the thesis, he entered Ph.D. program in the same graduate school in fall 2006.

Permanent address: 44-5 Banji
Changwon, Gyeongnam, 641-170
South Korea

This dissertation was typed by the author.